Wood fuel from British Columbia: multi-scale assessment of the economic, energetic and environmental efficiencies of the supply chains of conventional and torrefied wood pellets

by

Huimin Yun

B.Sc., Dalian Nationalities University, 2010

M. Sc., Beijing University of Chemical Technology, 2013

A THESIS SUBMITTED IN PARTIAL FULFILLMENT OF

THE REQUIREMENTS FOR THE DEGREE OF

DOCTOR OF PHILOSOPHY

in

THE FACULTY OF GRADUATE AND POSTDOCTORAL STUDIES

(Chemical and Biological Engineering)

THE UNIVERSITY OF BRITISH COLUMBIA

(Vancouver)

December 2018

© Huimin Yun, 2018

The following individuals certify that they have read, and recommend to the Faculty of Graduate and Postdoctoral Studies for acceptance, the dissertation entitled:

Wood fuel from British Columbia: multi-scale assessment of the economic, energetic and environmental efficiencies of the supply chains of conventional and torrefied wood pellets

submitted by Huimin Yun in partial fulfillment of the requirements for

the degree of Doctor of Philosophy

in Chemical and Biological Engineering

Examining Committee:

Prof. Xiaotao Bi

Supervisor

Prof. Roland Clift

Co-supervisor

Prof. Bhushan Gopaluni

Supervisory Committee Member

Prof. Hadi Dowlatabadi

Supervisory Committee Member

Prof. Shahab Sokhansanj

University Examiner

Prof. Guangyu Wang

University Examiner

Additional Supervisory Committee Members:

Supervisory Committee Member

Supervisory Committee Member

Abstract

This thesis investigates several key aspects of the supply systems of torrefied and conventional wood pellet (TWP/CWP) from British Columbia (BC): what are the economic, environmental, and energetic ("3E") performances of TWPs and CWPs supplied from BC into different markets? What is the best pathway for making TWPs? Can the TWPs production process be operated auto-thermally? If so, under what operating conditions?

A simulation platform is developed, including models for rotary and fluidized bed dryers, directly and indirectly heated rotary and fluidized bed torrefiers, and integrating heat and mass transfer, kinetics, particle hydrodynamics, thermodynamics and element evolutions.

The auto-thermal operation boundaries are identified for the torrefaction system. The boundaries are influenced by drying technology, N_2 flowrate, biomass properties and torrefaction conditions. A heat and mass integration scheme is proposed to avoid the use of N_2 for torrefaction by recycling flue gases and to expand the auto-thermal operation boundaries.

CWP and TWP production processes are analyzed, revealing that torrefying the biomass before grinding can reduce the "3E" impacts significantly. Due to auto-thermal operation, electricity is the main energy consumption and contributor to greenhouse gas (GHG) emissions. Capital costs contribute about 10% of the total production costs, with the remaining 90% being the operating cost, within which raw material, electricity, and labor are the major components. The minimum selling price at which BC TWPs is estimated as ~$6.7/GJ, equivalent to 140$/t.

The "3E" performances of BC CWP/TWPs supply chains to the UK, Japan, Ontario and Alberta are quantified with uncertainties considered. TWPs can reduce "3E" impacts by

about 25% in comparison with CWPs. Transportation is the main energy consumer and GHG emission contributor, while transportation and production are the major cost stages. There is significant potential to replace coal with BC TWPs domestically and overseas, particularly in the UK, EU and Pacific Asia, due to the comparative advantages of BC's clean electricity system and rich biomass resources.

Lay Summary

British Columbia (BC) is a major producer and exporter of wood pellets, accounting for more than 66% of Canadian capacity. This thesis investigates the economic, energetic, and environmental ("3E") performances of the BC conventional and torrefied wood pellets (CWP/TWP) supply chains. Several potential CWP/TWP production pathways are compared in terms of the "3E" impacts to identify the best pathway and critical stages along the supply chain. The minimum selling price and potential GDP contribution of BC TWPs are also quantified. Strategies to improve the production and supply chain efficiencies are proposed, which are useful to decision makers from government and companies.

Preface

This dissertation is original, unpublished, independent work by the author, Huimin Yun under supervision of Prof. Xiaotao Bi and Prof. Roland Clift. I developed the models, carried out all the simulations to generate data. The analysis was done by me with input from Prof. Bi and Prof. Clift.

Table of Contents

List of Tables

List of Figures

List of symbols

A	m^2	Area of tube wall
C′	-	Constant
Cap	MW	Power plant electricity generation capacity
c_m	kg/cum	Mass concentration of biomass
C_p	kJ/kg-K	Specific heat capacity
CDF	-	Cumulative distribution function
CF	$/year	Cash flow
CWP	-	Conventional wood pellet
d	km	Transportation distance
db	-	Dry basis
d_p	m	Effective diameter of the particle
dt	tonne	Dry tonne, without moisture
D	m	Effective diameter
DC	$/year	Depreciation cost
DCF	$/year	Discounted cash flow
DFC	$/t	Distance fixed cost
DVC	$/t-km	Distance variable cost
e	GJ electricity/GJ wood pellet	Electricity consumption
E	-	Energetic, environmental, or economic index
EF		Emission factor
EI	kJ/t-km	Energy intensity of transportation vehicle
EM	t material/GJ pellet	Amount of raw material to construct the equipment to produce per GJ of wood pellet
EM′	t material/unit	Amount of material to construct the equipment
F		Fuel consumption
g	9.8 m/s^2	gravitational acceleration
GDP	$/year	Gross domestic product
GSR	$/year	gross sales revenue
h	kW/sqm-K	Heat transfer coefficient
H	$/hr	Transportation hourly rate

IRR	%	Internal rate of return
k	m/s	Mass transfer coefficient
k_{tor}	1/s	Torrefaction reaction constant
k_{wood}	1/s	Drying rate constant for wood
L	m	Total length of the drum
M	kg water/kg dry matter	Moisture content
$\dot{M}$	kg water/kg dry matter - sec	Evaporation rate of one particle
MF		Mass fraction
MSP	$/t	Minimum sale price of wood pellet
N	-	Numbers of equipment
N_P	-	Total number of particles in the dryer
Nu	-	Nusselt number
NPV	$/year	Net present value
PI	%	Profitability index
PO	year	Payout period
Pr	-	Prandtl number
PVI	$/year	Cumulative Cash Inflows
PVO	$/year	Cumulative Cash Outflows
Q	kJ/hr	Enthalpy
$\dot{Q}$	kW	Heat flow rate
Q'	kJ/hr	Enthalpy endowed in flue gases that available for heat transfer
Ra	-	Rayleigh number
RDP	g CO_2eq/kWh electricity generated	GHG emissions reduction potential by replacing coal with wood pellet for electricity generation
ROR	%	Desired rate of return
Re	-	Reynolds number
Sh	-	Sherwood number
spe	kJ/kg biomass	Specific heat capacity
t	tonne	tonne
t_c	sec	Average solid contact time with hot surface per cascaded

		cycle
T	K	Temperature of the combustion gas in the shell side of the torrefier
TWP		Torrefied wood pellet
u	m/sec	Velocity
$\dot{v}(\eta)$	-	Normalized drying rate of one particle
w		The value determined for weight fraction
w_{ij}	-	Mass fraction of the jth constituent in component i
wb		Wet basis
wl		Biomass weight loss
wt		Weight basis
W	KW	Mechanically power
WC		Wood chips
WP		Wood pellet
x_C^d		Mass fraction of carbon on dry basis
x_C^{dm}		Mass fraction of carbon on dry and matter free basis
Y	kg water/kg dry matter	Moisture content of gas
Y^* (T_{GS})	kg water/kg dry matter	Saturated moisture content of gas
Y^* (T_{GS}) $-$ Y]	kg water/kg dry matter	Drying potential for evaporation
z	m	Horizontal length location of the drum
Z	gCO_2eq/kWh electricity generated	Emission intensity of electricity generation

Superscript

c	convection
d	Dry basis
m	Mineral-matter-free basis
r	Radiation
v	vapor
*	Overall transfer coefficient

Subscript

A	ash
A-B	Transportation point A to B
bed	Fluidized bed
bs	Bulk solid
C	carbon
cargo	Biomass cargo
char	Char/torrefied biomass
Cl	chlorine
coal	Electricity generation by coal
com	Combustion
cw – cb	Covered wall to covered solid bed
db	Dry biomass
DP	Driven power
dry	Drying/dry
eco	Economic impact
ele	electricity
eg – ep	gas to solid particle
endo	endothermic
ene	Energy consumption
end	Power plant stage
env	Environmental impact
eq	Equilibrium
ew – eb	Exposed wall to exposed bed
ew – eg	Exposed wall to exposed gas
exo	exothermic
FC	Fixed carbon
fluegas	Flue gases
ff	Filling fraction
fuel	Different types of fuel energy
G	Gas phase
grinding	Grinding process

gw	Gas to wall
H	hydrogen
Ham/hammer	Hammer mill
harvesting	Harvesting stage
H-P	harvesting, sawmilling, production
H_2O	Moisture
i	Component
j	Constituent C, H, O, N, and ash
LC	Life cycle
m	Stage harvesting, sawmilling, production, port operation, storage and end-use
M	Material used for equipment constuction
MM	Mineral matter
max	maximum
marine	Marine transportation
MC	Biomass moisture content
n	Primary fuel type
N	Nitrogen
N_2	Nitrogen
NP	Output work
O	oxygen
P	particle
pelleting	Pelleting process
production	Production stage
Prod	product
port	Port operation stage
power	Power plant
raw	Raw material
react	reactant
rail	Railway transportation
s	Solid phase
sawmill	Sawmilling stage
sel	Selected equipment
storage	Storage stage

So	Organic sulfur
St	Total sulfur
Sp	Pyritic sulfur
S	Other sulfur
t	transportation
trans	transportation
tor	Torrefaction/torrefied
torgas	torgas
truck	Truck transportatopm
U	Unit operation in the production stage, including drying ,torrefaction, combustion, grinding, pelleting and auxilary equipment i.e. air blower and heat exchanger
v	vehicle
V	volatile
VM	Volatile matter
WC	Wood chips
water	water
0	Initial
θ	Wood pellet and coal co-firing ratio

List of Greek Letters

α	-	Biomass weight loss during torrefaction
β_{char}	kg char/kg biomass	Mass fraction of char in the torrefaction product
δ	m^2/s	Diffusivity
Δh^V	kJ/kg water evaporated	Enthalpy of evaporation
$\Delta_c h^d$	kJ/kg	Standard combustion heat of biomass
$\Delta_f h^d$	kJ/kg	Standard formation heat of biomass
$\Delta H_{tor,N_2}(T_{tor})$	kJ/kg	Heat requirement of the torrefaction process accounting with sensible heat of N_2
$\Delta H_{tor}(T_{tor})$	kJ/kg	Torrefaction reaction heat at temperature T
$\Delta H^o(25°C)$	kJ/kg	Standard heat of reaction
Δw^d		Correction factor for other losses, such as the loss of carbon in carbonates and the loss of hydrogen present in the water of clays
ε_b		Volumetric fraction of the bubble phase in the total reactor volume element
η	-	Normalized moisture content
θ	%	Wood pellet and coal co-firing ratio
ϑ_d	-	Average fraction of the wall area covered by the solids
λ	w/m-K	Thermal conductivity
μ	m^2/s	Dynamic viscosity
v	Km/hr	Speed of vehicle
ξ	%	efficiency
ξ_v	1/K	Volumetric expansion coefficient of gas
ρ	kg/cum	Density
σ	-	Stefan-Boltzmann constant
τ	sec	Mean residence time
ϵ	m	Thickness of the tube wall
ϕ_s	o	Solid half filling angle of the solid inside reactor
ψ	-	Thickness of the gas film as the fraction of particle diameter
ω	Rad/sec	Angular speed of reactor

Acknowledgements

Foremost, I would like to express my sincere gratitude to my supervisors, Prof. Xiaotao Bi and Prof. Roland Clift, for their continuous supports, tremendous efforts and great guidance during my PhD studies. Their diligence, genuineness, and enthusiasm and curiosity to new things always inspire me. I have learned a lot through discussions and communications with Prof. Bi and Prof. Clift, not only in the scientific arena, but also on a personal level.

I would also like to thank the rest of my thesis committee: Prof. Dowlatabadi and Prof. Gopaluni for their constructive criticisms and insightful comments which incented me to widen my research from various perspectives.

Thanks to all the CHBE faculty and staff, who had been very friendly and supportive. I enjoyed the days at CHBE.

My sincere thanks to all my friends and colleagues at UBC, your precious friendship made my life colorful. They sent me to VGH and took care of me when I was sick.

Last but not least, I would like to thank my family for their selfless love and unconditional support. Especially thanks to my boyfriend Tenghu Wu, who provided me with incredible encouragement and support throughout all the good and bad time.

Chapter 1: Introduction

1.1 Background

1.1.1 BC wood pellet industry

British Columbia (BC) has significant forest resources, with about 60% of its land (55 million hectares) being productive forest land, providing rich, diverse, and abundant wood fiber [1]. These forests contain approximately 11 billion m^3 of standing timber [2]. In addition to the notable resources, BC claims to have the most sustainable forest policies and practices in the world [3]. BC owns over 52 million hectares third-party-certified forests which accounts for 14% of the world's total and contributes more than any other province to Canada's certified forests [4]. This makes BC's forestry-related industry the cornerstone of the provincial economy. In 2016, the forest industry contributed $12.9 billion to the total provincial Gross Domestic Product (GDP), exported $13.7 billion worth of forest products, accounting for 34% of all provincial exports; 140,728 jobs in BC rely on forest sector, 1 in 17 jobs in the province was created due to the BC forest industry, and 1 in 4 of provincial manufacturing jobs in BC was in forestry [2].

However, the forest in the BC interior region was infested by the mountain pine beetle epidemics in the 1990's which peaked in 2005 [5]. During these epidemics, over 18 million hectares of forest were impacted, resulting in a loss of approximately 723 million cubic meters (53%) of merchantable pine volume through 2012 [6]. It is projected that by 2017 the total merchantable pine volume affected was 752 million cubic meters (58%) [2]. The annual allowable cuts are now being reduced as the majority of the beetle-damaged timber has been salvaged. Non-merchantable woody biomass is piled and burnt at the roadside to remove a source of fuel for forest fires [6]. These waste wood residues are

potentially an enormous alternative energy source, as a natural stable carbon energy carrier capable of storing and releasing energy on demand, also with a short life cycle in comparison with coal. The wood pellet industry has therefore developed to exploit the opportunity opened up on one hand by the growing demand for renewable energy sources, and on the other hand by the creation of significant long-term value for the BC bio-economy. Due to the damages and defects, production of lumber results in considerable wastes: only about 47% of the volume in every log that reaches sawmills is converted to saleable lumber, and the rests are residues that must be disposed or used for other purposes, including 33% of wood chips, 7% of sawdust, 8% of shavings, and 5% of barks [7]. These residues are the current main sources of raw material for wood pellets in BC. Cocchi et al. [8] estimated that biomass energy in BC can provide more than 1600 MW of heat and/power generation capacity and 3.2 million t (tonne) of wood pellet capacity. In 2017, the total production capacity of BC wood pellets was 2.4 million t, representing 66% of total Canadian wood pellet capacity [9]. Thus, there is still space to expand the BC wood pellet production capacity if the demand keeps growing.

Domestic usage of wood pellets in BC is limited due to the abundant and cheap hydropower and natural gas in the province, with no coal-fired power plants. The primary destinations of BC wood pellets are the United Kingdom (UK) (71% by weight), Japan (14%), Belgium (7.4%), and Italy (3.1%) in 2017 [10]. In the UK, the BC wood pellets are mostly fed to the Drax power plant, which produces about 17% of UK's renewable electricity [11]. In September 2018, Drax finished converting four of its six power plants from coal to biomass [12]. When all units are converted, Drax will use 7 to 8 million t of wood pellets annually [13]. The wood pellet market in EU is driven by the greenhouse gas (GHG)

reduction mandates to achieve at least 40% cuts from 1990 levels by year 2030 [14]. The Japanese wood pellet market is driven by the policies (e.g. feed-in-tariff (FIT)) and regulations that require all power companies to reduce GHG intensity by 35% (a reduction from 0.57 kg CO_2eq/kWh to 0.37 kg CO_2eq/kWh) from 2013 levels by 2030. To achieve this goal, Japan will have to consume about 7.4 million t of pellets per year [15]. In Canada, the provincial governments have enacted regulations to close coal-fired power generation stations. For example, the Ontario government is the first in North American to eliminate coal-fired electricity generation [16]. The 205 MW Atikokan GS is now the largest 100 percent biomass facility in North America. The Alberta government has also decided to phase out coal-fired electricity generation by 2030 [17].

Currently, up to 50% wood pellets are traded globally [14]. To improve the competitiveness of BC wood pellets, and also for the purpose of reducing the carbon footprint associated with the global trade, it is essential to improve the efficiencies of pellet production and the overall supply chains.

1.1.2 Torrefied wood pellet production pathways

Although conventional wood pellets (CWPs) have better and more consistent quality than wood chips, and are therefore generally more attractive as traded fuel, CWP still has some characteristics that are undesirable for storage, transport and end-use. The principal disadvantages are relatively low caloric value and energy density, low grindability, and tendency to absorb moisture. Torrefaction, a form of mild pyrolysis at relatively low temperature, is an effective treatment to improve the calorific value, grindability, and shelf-life of biomass materials. The properties of the CWP, TWP, and coal are summarized as shown in Table 1.1.

Table 1.1 Properties of wood chips, torrefied biomass, CWPs, TWPs and coal [18]

Parameter	Wood chips	Torrefied biomass	CWP	TWP	Coal
Moisture content (MC) (wt%)	30–60	3	7–10	1-5	5-10
Lower calorific value (CV)	6-13	19.9	15–16	20-24	>25
Mass density (kg/m^3)	250–400	230	600–650	750-850	800-1000
Calorific value (MWh/t)	1.7-3.6	5.5	4.5	5.2-6.2	7
Energy Density (MWh/m^3)	0.7-0.9	3	3	4.2-5	5.6-7
Grindability (kW h/t)	237	23	237	23-78	23-78
Hygroscopic nature	Hydrophilic	Hydrophobic	Hydrophilic	Hydrophobic	Hydrophobic
Milling requirements	Special	Classic	Special	Classic	Classic

The energy density of bulk pellets can be increased from 17 GJ/t to approximately 20-22 GJ/t by torrefaction [19]. Thus, transportation costs of TWPs can potentially be 20% to 40% lower than for CWPs [20], if the bulk density of the TWPs remains the same as the CWPs. It should be noted that torrefaction increases heating value, grindability, and hydrophobicity of wood, but it also makes it more difficult to densify torrefied biomass into pellets, resulting in pellets of lower mass density, with inferior strength or durability [21].

The CWP production process consists of drying, grinding, pelleting, and cooling in sequence. There are several potential configurations/pathways to produce TWPs by placing the torrefaction unit at different positions in the overall flowsheet, as shown in Figure 1.1.

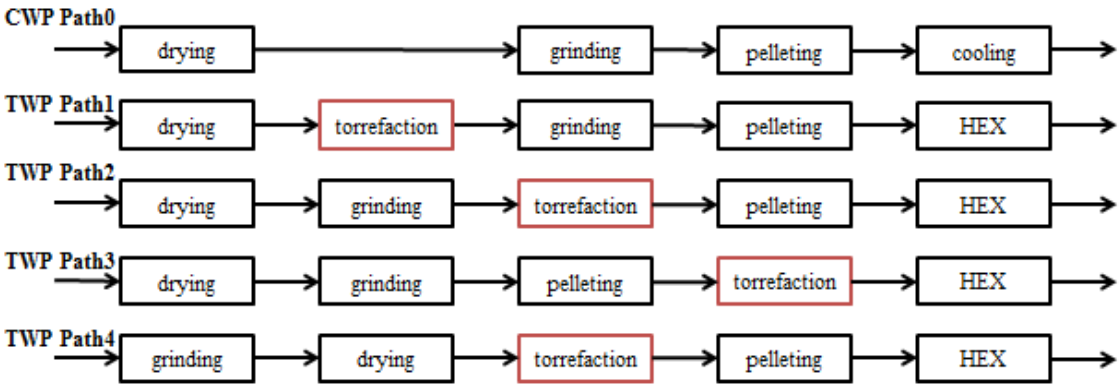

Figure 1.1 Configurations of conventional and torrefied wood pellet production pathways

1. Path 1 performs torrefaction immediately following drying, followed by grinding. This exploits the advantage of improved grindability of the torrefied biomass to lower the grinding power usage. However, long residence times are needed to torrefy large wood chips and it is difficult to densify torrefied sawdust into strong pellets, leading to higher thermal energy use for torrefaction and higher power use in pelletization. Ghiasi et al. [22] reported that inter-particle bonding of biomass particles was significantly reduced after torrefaction, making it difficult to densify biomass into pellets. Often, binder or steam conditioning is required to make pellets with sufficient strength [21], [22], [23]. Applicable binders include starch, lignin, plastic, minerals and food-based binders e.g. wheat flour, or vegetable oil, but all these binders are expensive. Peng et al. [24] investigated the performances of sawdust (< 1mm particle size) as a binder and found that it could be an effective and low-cost binder for making strong pellets from torrefied powders. Thus, in this study, sawdust is considered as the binder in the pathways when binders are required. The fraction of

the added binders normally ranges from 5 to 20 wt% [24], with a typical value around 8wt% [24].

2. Path 2 places torrefaction after the grinding operation, taking advantage of the reduced biomass particle size to improve the heat and mass transfer rates in the torrefaction process. Thus, the shorter particle residence time requires smaller reactor size in this configuration. Similar to Path 1, sawdust binders is required to make strong torrefied pellets [21], [22], [23], [25], at a fraction of 8wt%.
3. Path 3 represents the simplest modification of the conventional pellet process: torrefaction is added as a new step immediately following pelletization, thus has the merit of retrofitting the existing pellet plant without substantially alerting its existing operation. In doing so, difficulties in densifying torrefied sawdust into pellets are avoided, so that, no binders are used in this pathway. However, torrefaction of regular pellets will lead to reduced pellet strength and density, lowering the quality of the torrefied pellets in comparison with the products in Paths 1, 2, and 4 [21], [25]. To compensate for the reduction in strength and density, one may increase the compression pressure to make denser and stronger conventional pellets before subjecting them to torrefaction [22]. Another possible operation of Path 3 is to operate torrefaction at the power plant, i.e. transport CWP to the power plant gate and then torrefy it. But this way will be low efficient because some of the transported fuel (from biomass) is lost during torrefaction. In the current analysis, therefore, torrefaction is only considered to take place at the pellet plant as an integrated part of the plant operation.

4. Path 4 is a modification of Path 2 in which biomass is first ground so that the heat and mass transfer rates can be improved in both drying and torrefaction processes. It should be noted that in order to avoid damaging the hammer mill, Path 4 is only suggested for biomass feedstock with low moisture contents (<50wt%db). As in Paths 1 and 2, sawdust binder is used at fraction of 8wt%.

Different types of equipment will be needed for the different pathways due to the differences in the biomass thermal and physical properties caused by the process sequences. For example, for wood chips, rotary drums are often applied for drying and torrefaction, while for small biomass particles around 1 mm in size, the fluidized bed is more efficient. The TWP production pathways can be integrated by incorporating a combustion process to burn the gases and liquids released during torrefaction, called torgas, to provide heat for drying and torrefaction. Process synthesis in the wood pellet production systems is therefore explored, involving equipment design and heat and mass integration, to reduce energy consumption, production costs and air emissions. By energy integration, it may be possible to avoid additional fuel usage completely through auto-thermal operation of the drying, torrefaction, and combustion units. This topic will be further discussed in section 1.1.3.

The additional production investments and emissions associated with torrefaction and heat integration of the process are major concerns. Although extensive laboratory research has been conducted to investigate torrefaction, grinding, and densification of different biomass species, torrefaction has not progressed beyond pilot and demonstration plants to commercial scale [25]. Therefore, the comparisons of CWP and TWP production processes are mainly based on process simulation as summarized in Table 1.2 [23], [26], [27], [28], [29], [30]. Opposite views have been expressed regarding the economic and environmental

performances of conventional and torrefied wood pellets. For example, Bergman and Veringa [31] identified clear economic benefits for TWPs, whereas Agar [32] concluded that the production cost of TWPs (3.02 €/GJ) is higher than CWPs (2.23 €/GJ). However, there is general agreement that TWP shows advantages for long distance transportation. For example, Agar [32] estimated that the CIF (Cost, Insurance and Freight) costs of shipping over 11,450 km, corresponding to shipping from BC to Asia Pacific i.e. Vietnam, are 5.22€/GJ and 5.58 €/GJ for TWP and CWP, respectively; Beets [20] also drew a similar conclusion for a pellet supply chain from Georgia, US, to Geertruidenberg, Netherland, in which the FOB costs for conventional and torrefied wood pellets are 7.6 €/GJ and 6.4 to 7 €/GJ, respectively.

So far, there has been no published research comparing different torrefied wood pellet production pathways. This is thus one of the topics of this thesis.

Table 1.2 Literature on wood pellet economic evaluation

Reference	Pellet type	Capacity	Country	Raw material	Raw material Cost	Pellet cost	
[26]	CWP	24,000t/year	Austrian	sawdust		95.56$/t	5.62$/GJ
[27]	CWP	case1	Finland	shavings (MC10wt%db)	95 €/dt	141 €/t	8.29 €/GJ
		20,000t/year;		wet sawdust	83 €/dt	145 €/t	8.53 €/GJ
		case 2		Round wood chips	92 €/dt		
		120,000t/year	Germany	shavings (MC10wt%db)	101 €/dt	150 €/t	8.82 €/GJ
				wet sawdust	90 €/dt	158 €/t	9.29 €/GJ
				Round wood chips	90 €/dt		
			Norway	shavings (MC10wt%db)	110 €/dt	160 €/t	9.41 €/GJ
				wet sawdust	90 €/dt	158 €/t	9.29 €/GJ
				Round wood chips	88 €/dt		
			Sweden	shavings (MC10wt%db)	101 €/dt	150 €/t	8.82 €/GJ
				wet sawdust	90 €/dt	155 €/t	9.12 €/GJ
				Round wood chips	92 €/dt		
			US	shavings (MC10wt%db)	79 €/dt	122 €/t	7.18 €/GJ
				wet sawdust	63 €/dt	119 €/t	7.00 €/GJ
				Round wood chips	65 €/dt		
[33]	CWP	45,000t/year	Canada (Prince George)	sawdust		51$/t	3.00 $/GJ
[34]	CWP	20t/hr	Canada (Prince George)	sawdust	25$/dt	69.29 $/t	4.08$/GJ
[29]	CWP	190,000t/year	Canada (Prince George)	forest residues	65$/dr	95$/t	5.59$/GJ
		250,000t/year					
	steam CWP					146$/t	8.59$/GJ
[32]	CWP		Port to Port			35.17 €/t	2.23 €/GJ
	TWP		(shipping 11450km)		13.28 €/dt	55.21 €/t	3.02 €/GJ
[35]	TWP				35.11$/dt	163.36$/t	7.41$/GJ
[36]	TWP				49.6$/dt	171.74$/t	7.79$/GJ
[6]	TWP				76.63$/dt	174.17$/t	7.90$/GJ
[37], [36]	TWP				55.12$/dt	183.87$/t	8.34$/GJ
[20]	CWP	750,000t/year	Georgia, US to	pine pulpwood	74$/dt	119 €/t	7.00 €/GJ
	TWP		Geertruidenberg, NL		74$/dt	136 €/t	6.47 €/GJ

Raw material cost (raw material + harvesting + transportation); dt: dry tonne

1.1.3 Auto-thermal operation of wood pellet production process

As a mild pyrolysis process, torrefaction is usually carried out at 250°C to 300°C, at atmospheric pressure in an oxygen-free or low oxygen environment. N_2 is commonly used to provide the anoxic environment in laboratory studies, but combustion flue gases can be used in pilot and commercial operations. During torrefaction, biomass is decomposed and condensable and non-condensable volatiles are released. Those volatiles, called torgas, can be combusted to provide heat for torrefaction and drying. When the high heating value (HHV) of the torgas is equal to or higher than the heat required for drying and torrefaction, the process is considered auto-thermal, as shown in Figure 1.2. The heart of the auto-thermal process is the torrefaction unit because it determines the amount and HHV of the torgas and the heat required for torrefaction. Besides, heat integration strategies, drying heat requirement, biomass moisture content, and the carrying gas (e.g. N_2) flowrate also influence the heat balance over the process.

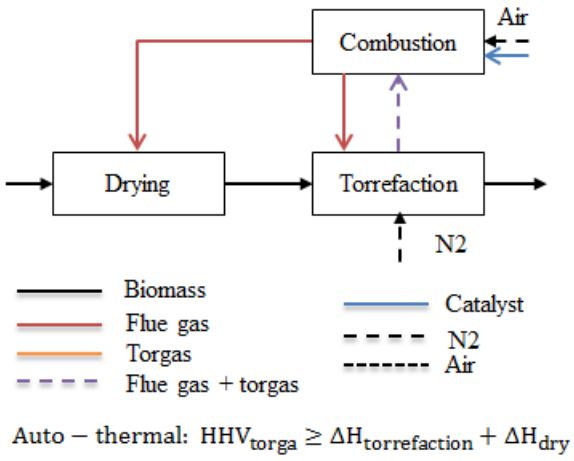

Figure 1.2 Auto-thermal operation definition of the thermal system (including drying, torrefaction, and torgas combustion)

Theoretically, there are various strategies to integrate the thermal system, leading to a number of possible flowsheets. However, it is not necessary to analyze all possible heat integration configurations. This work focusses on two of the possible configurations which offer the best performance in terms of production costs, emissions and energy efficiency. The first is shown Figure 1.3 (a), where the high-temperature flue gases are first used to provide heat to the torrefaction unit and then for the dryer. In this configuration, N_2 is supplied as the carrying gas for torrefaction, without recycle of combustion flue gases, and a catalyst may be involved depending on the combustion temperature. Case 2, shown in Figure 1.3 (b), is designed to avoid the use of N_2: flue gases are recycled, so that both direct and indirect heat transfer are involved.

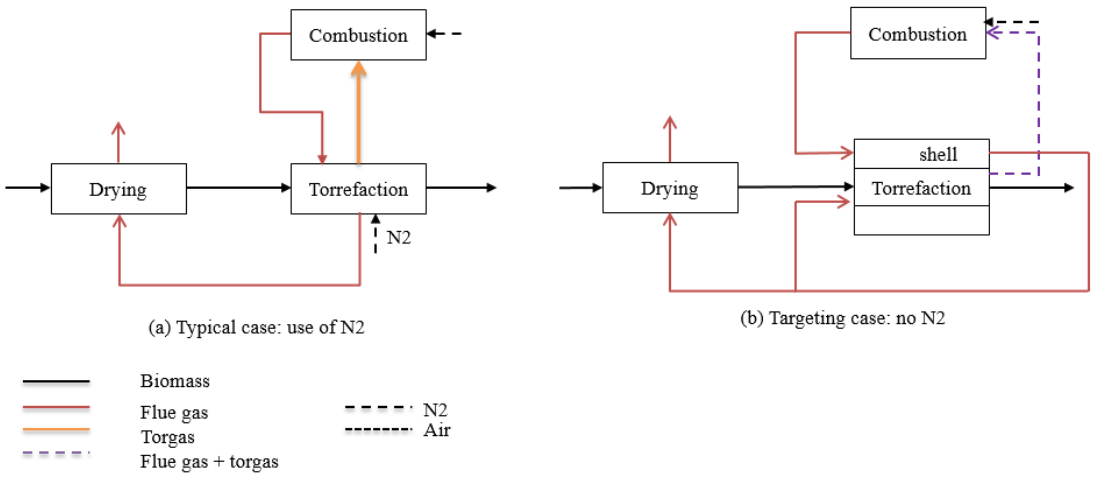

Figure 1.3 Illustration of auto-thermal operation: (a) Typical heat integration strategy of the torrefaction system using N_2 as the carrying gas; (b) Target heat integration strategy of the commercial torrefaction system, with flue gases used as the carrying gas.

The conditions for auto-thermal operation are examined based on process modeling. There is little published work on auto-thermal operation of the torrefaction system, and all

the published studies are based on the configuration in Figure 1.3 (a). For example, Bergman et al. [29] carried out process simulation of the torrefaction process with the default assumptions of 30% biomass weight loss and an initial biomass moisture content of 50wt%db (on dry basis). They concluded that auto-thermal operation is possible when the torrefaction is carried out (a) above 270℃ with a reaction time longer than 20min; (b) above 280℃ at short reaction times (5 to 20 min), and (c) at 300℃ with 10 min residence time. Shah et al. [39] also carried out process simulation with thermal integration of combustion and drying process without considering torrefaction heat requirement, assuming constant drying heat consumption and constant HHV of the torgas. They concluded that the torrefaction system could be operated auto-thermally at 300°C for all considered moisture levels up to 60wt%wb (on wet basis), but auto-thermal operation is not possible at 200℃–220°C. Syu and Chiueh [40] performed process simulation for torrefaction at 250°C with residence time of 30min, with the simplified assumptions of reaction heat as 0.8 MJ/kg biomass and constant torrefaction conditions at 250℃ with 30 min residence time and 21.8% of biomass weight loss. They concluded that the process can be auto-thermal if the biomass moisture content is less than 12wt%db.

The simulations summarized above identified different auto-thermal operation conditions based on different simulation assumptions. However, all of them made some crucial assumptions in their simulation which may not be realistic and could lead to large errors in predicting auto-thermal conditions. The neglected factors include:

(1) dependence of heat evolution during torrefaction on reaction conditions;

(2) efficiency differences between different drying technologies;

(3) variation of N_2 flow rate on the torrefaction reaction heat requirement;

(4) heat and mass transfer, reaction kinetics.

The current study will take the above neglected factors into considerations in determining the boundaries of auto-thermal operation.

1.2 Motivation and objectives of this thesis

It is still debatable whether TWPs are economically and environmentally advantageous over CWPs because of the additional investments and emissions, and, if so, what are the best process pathways and sequences to make TWPs. This research tries to answer those questions. The questions are inherently multi-scale, as shown in Figure 1.4.

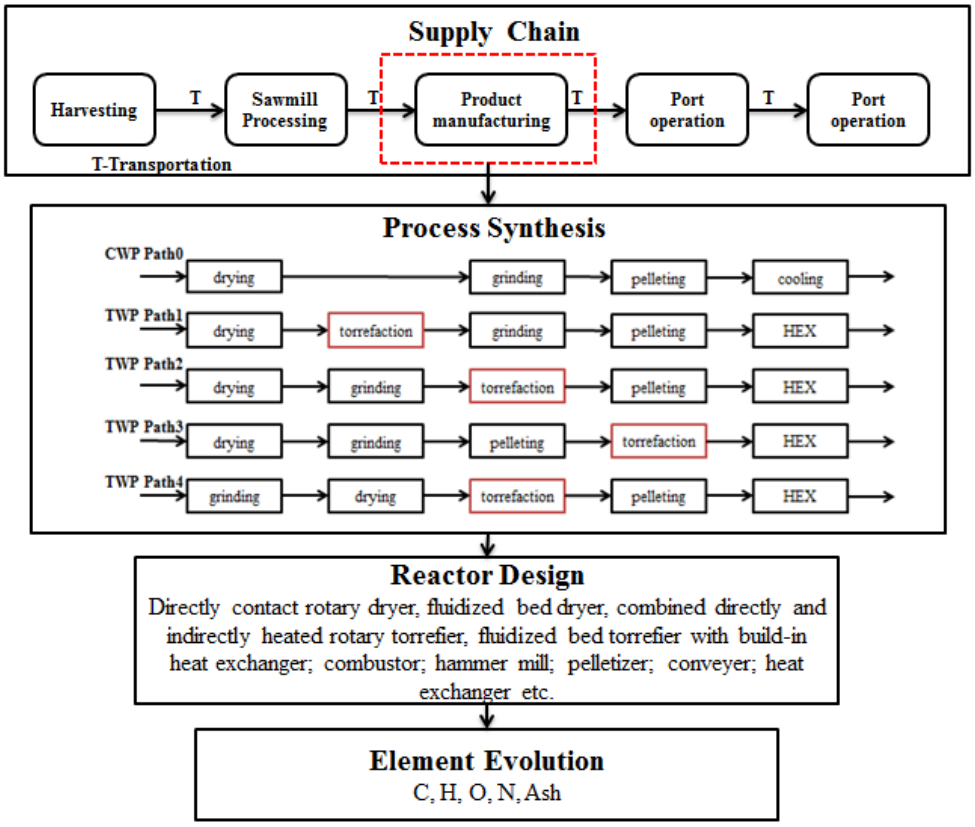

Figure 1.4 Multi-scale research questions in the current study

The specific questions to be addressed are:

- **Supply chain level**

(1) What are the supply chain energy consumption, GHG emissions, and costs of BC CWP and TWP delivered to different destinations?

Metrics for the direction of sustainable development need to cover all three dimensions: techno-economic, ecological and social [41]. Indicators of these dimensions are well reviewed and discussed by Clift [41] and Azapagic and Perdan [42]: economic indicators include value-added, contribution to GDP, expenditure on environmental protection etc.; environmental impacts cover global warming, acidification, health impacts etc.; and social indicator involves labor conditions, work satisfaction, preservation of cultural values etc. In this study, among all these indicators, we selected energy consumption, greenhouse gas emission and total cost as the indicators because: (a) primary energy consumption reflects the depletion of energy sourses which is a major resource concern; (b) GHG emission creates global warming impact which is a matter of the greatest concern and should be addressed immediately. In comparison, other environmental impacts, such as water use and human toxicity are local, sensitive to population density, topography, and weather conditions etc., and therefore should be analyzed specifically in different regions; (c) economic metrics in this study include production costs, investment return, GDP contribution, and supply chain delivered costs, which cover both micro and macro-economic activities and these metrics are of the greatest concern to decision makers from government and industry.

(2) What are the hotspots or key stages and parameters in the supply chains?

The suitable markets for BC wood pellets can be identified by answering the above two questions. To answer those supply chain questions needs a quantified analysis of the production of CWP and TWP, addressing the following process level questions:

- **Process level**

(1) How to achieve auto-thermal operation by heat integration to avoid the use of additional fuel for drying and torrefaction?

(2) How to recycle combustion flue gases to avoid the use of N_2?

(3) What are the best pathways to make TWPs?

(4) What are the minimum selling prices and the potential GDP contributions of the BC TWPs?

Torrefaction needs inert gas like N_2 to provide an anoxic environment. This is very expensive, so that using flue gases (combusted torgas) to replace N_2 is desirable for commercial torrefaction processes. However, the integration should be carefully performed to (a) avoid biomass ignition caused by residual oxygen in the flue gases, (b) achieve efficient heat and mass transfer, and (c) satisfy operating constraints e.g. maintain fluidization. Thus, the following questions need to be addressed:

- **Unit level**

For each unit operation, the suitable unit and its operating conditions need to be specified based on simulations. Specifically, the questions for different unit operations in each pathway are shown in Figure 1.5.

- **Element level**

The reactor design involves thermal and physical properties of the material (biomass and gases in this system), which are determined by their compositions. Thus, for the torrefaction reaction, the following questions are also required to be answered:

(1) How do the elemental compositions of the biomass and torgas evolve?

(2) How does the torrefaction reaction change with torrefaction operation conditions?

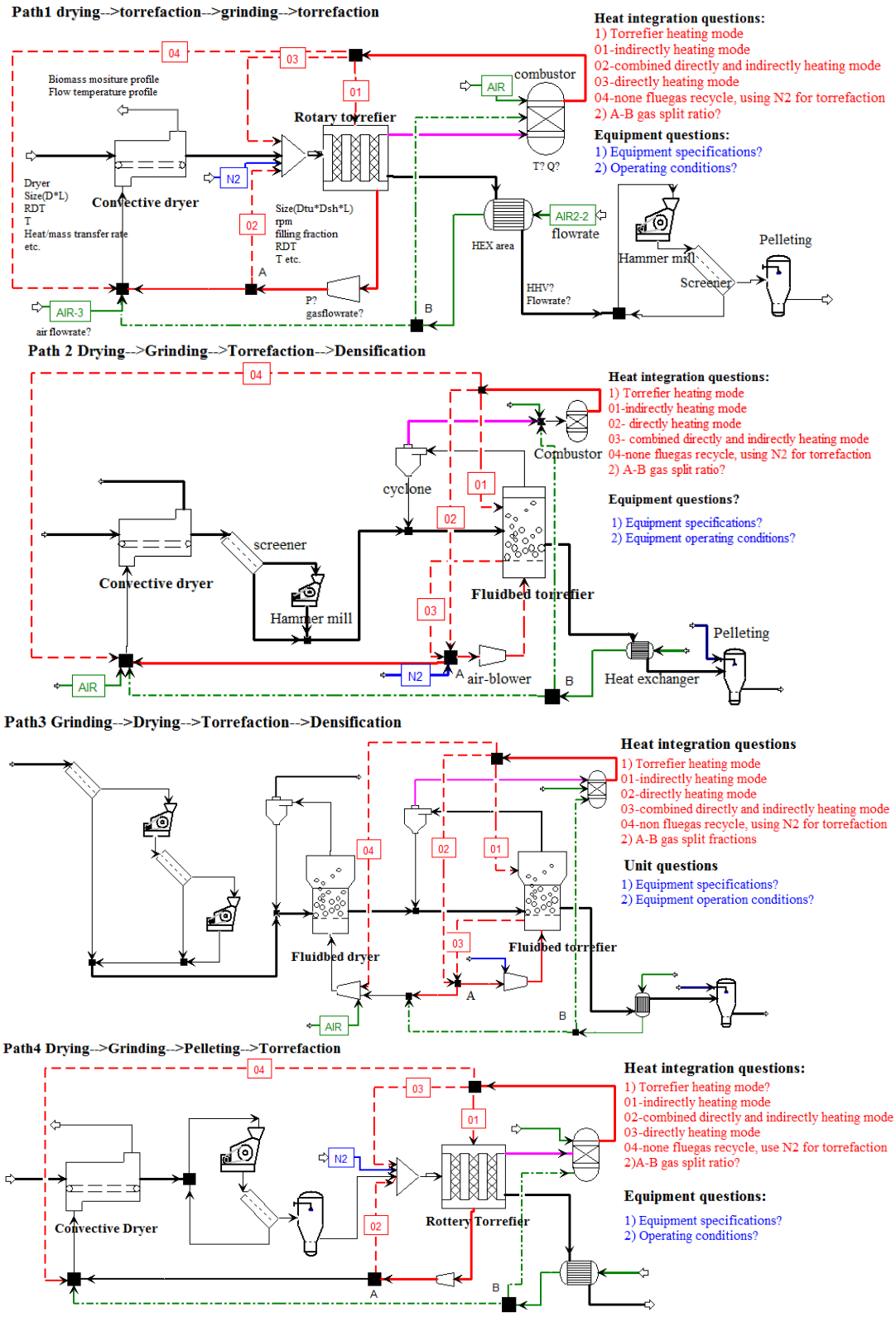

Figure 1.5 Conceptual design of the four possible TWP production pathways

1.3 Approach adopted in thesis

A hybrid method is proposed in Figure 1.6 to solve the research questions identified. Inventory data of harvesting, sawmilling, port operation, and storage will be adopted from literature and government report. Transportation cost models in different ways, truck, railway, and marine, will be developed based on quoted price from website.

Specifically, this study will focus on the production stage. A simulation platform will be developed to link the upper-level supply chain performance with the performances of unit operations at lower level. The platform contains elemental models which are used to quantify the thermal and physical properties of material in the system, unit operations models based on heat and mass transfer, kinetics, thermodynamics, and hydrodynamics models, process mass balance, heat integration and analysis, and supply chain performances. The simulation platform is developed based on Aspen Plus 8.4 and FORTRAN programming. When the production process simulation platform is developed for different CWP and TWP production pathways, we can then carry out unit operation analysis to search for optimum operation conditions, sensitivity analysis, scale up/down analysis and process integration to identify auto-thermal operation conditions. Process simulation results will be the input data to Aspen Economic Analyzer to map the equipment and carry out techno-economic evaluations and investment analysis.

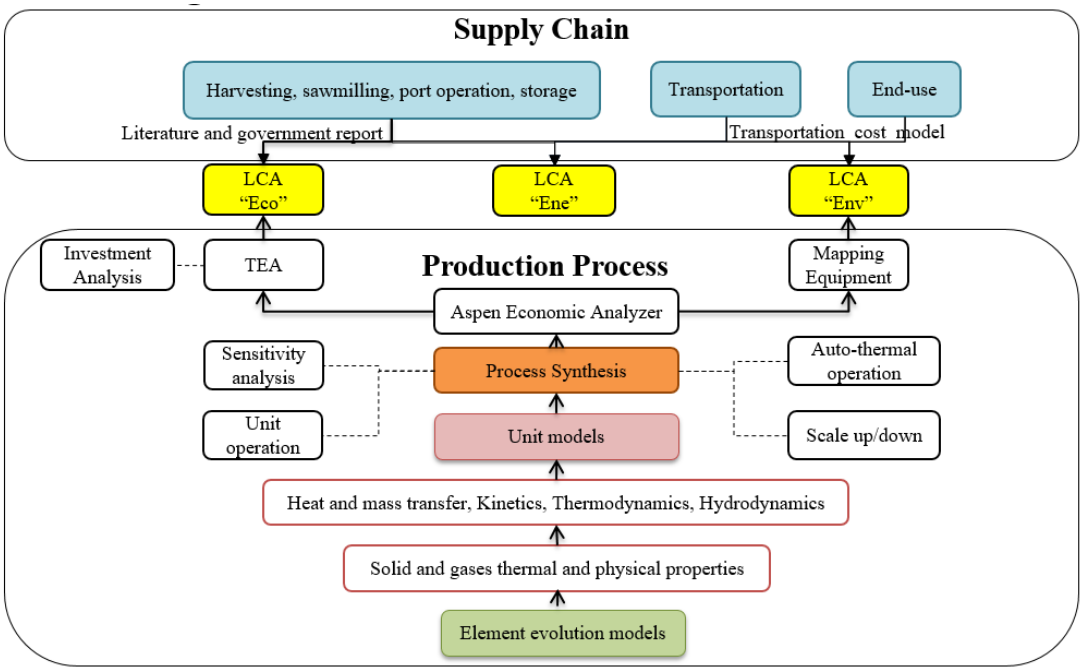

Figure 1.6 Illustration of the methodologies used to solve the multi-scale research questions

Three metrics are used to compare the performances of different wood pellet production pathways: economic index expressed as $/GJ delivered to different users; environmental index expressed as GHG emissions, reported as CO_2 equivalent based on 100-year global warming potentials and gCO_2eq/kWh-electricity delivered to the power plant gate; and energy consumption index in GJ primary energy input/GJ pellet delivered. The information required to quantify the three metrics is summarized in Table 1.3. Equipment sizes and heat and mass balances are the input data for carrying out a techno-economic evaluation in Aspen Economic Analyzer to quantify the production costs of the wood pellet, and for quantifying the production energy consumptions and GHG emissions of different pathways. These "3E" (energy, environmental, and economics) indicators are the input data for the supply chain analysis, combined with data from other stages along the supply chain.

The inventories of other stages are simplified by using secondary data from literature and government reports.

Table 1.3 Required characteristic parameters to quantify the "3E" indicators for different equipment

Equipment		Economic index	Energy index	Environmental index
Dryer	Fluidized bed	S (D, H), EM	E	EM, E
	Rotary (directly heated)	S (L, D), EM	E	
Torrefier	Fluidized bed with a built-in heat exchanger	S (D, H), EM	E	EM, E
	Combined directly and indirectly heated rotary reactor	S (L, Dtu, Dsh), EM	E	
Combustor		H, EM	E	EM, E
Heat exchanger		S (A), EM	E	EM, E
Hammermill		W_{DP}, EM	E	EM, E
Pelleting machine		W_{DP}, EM	E	EM, E
Air Blower		W_{DP}, EM	E	EM, E

S: size; L: length; D: diameter; Dtu: tube diameter; Dsh: shell diameter; H: height; A: area
EM: equipment material
H: heat duty of combustor
E: energy consumption
W_{DP}: driving power

1.4 Structure of the thesis

Figure 1.7 shows the layout of this thesis. Chapter 1 gives an introduction, setting out the research objectives and approaches. Chapter 2 presents the modeling and simulation of unit operations making up the different pathways. Chapter 3 to chapter 5 will present the results and discussions at unit level, process level and supply chain level, respectively. Specifically, Chapter 3 investigates the conditions for auto-thermal operation of the torrefied wood pellet production processes, which provides the targeted auto-thermal operation envelop of the torrefaction process, and macro-level observations of the thermal system based on element evolutions. Chapter 4 will investigate the wood pellet plant "3E"

performances under different configurations, in order to propose strategies for pellet production to reduce emissions, increase energy efficiency, and reduce costs. Chapter 5 will compare the wood pellet production pathways on a supply chain level - specifically, BC wood pellet supply chains to different markets - based on the "3E" metrics. Through life cycle analysis (LCA), the supply chain hotspots will be revealed. Strategies will also be proposed in this chapter to help enhance the sustainable development of the BC wood pellet sector.

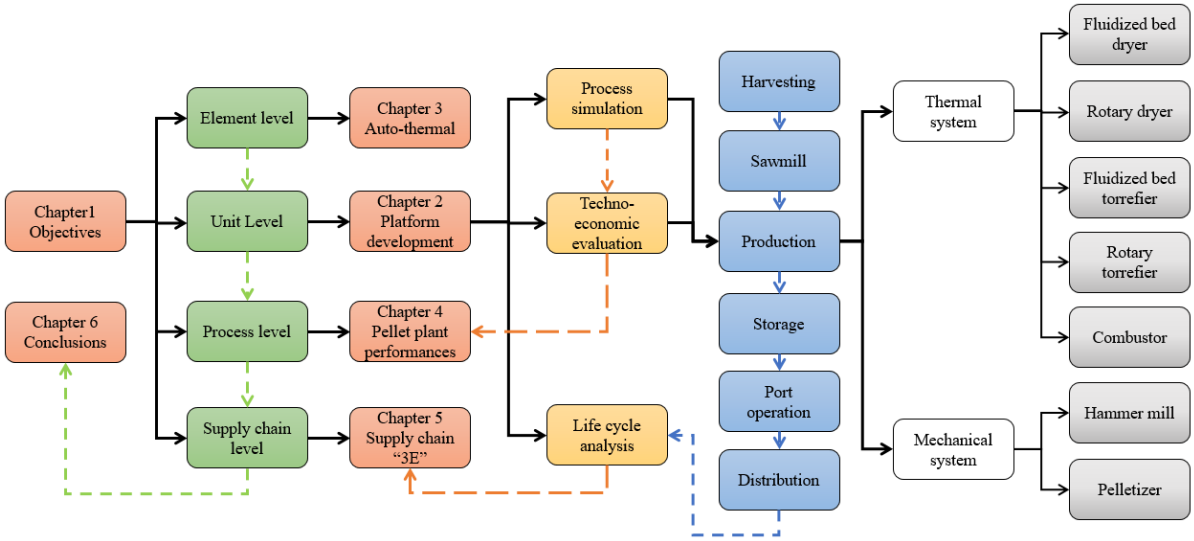

Figure 1.7 Layout of the thesis

Chapter 2: Development of models for wood pellet production processes

2.1 Introduction

This chapter presents the development of a simulation platform for different wood pellet production pathways. The objectives of developing such a platform are to: (a) size the equipment, which is the required information to quantify the "3E" (energetic, environmental, and economic) metrics of the wood pellet production processes; (b) carry out heat and mass integration of the overall production processes to achieve auto-thermal operation, or at least to recover heat to increase energetic efficiency if auto-thermal conditions are not achievable; and (c) identify suitable or optimal unit operation conditions. Given these three purposes, the flowsheet is simulated on a steady-state basis, rather than using dynamic modeling, which would be appropriate if the focus were on the operability and controllability of the plant but which is more detailed and time-consuming. The sequential modular method is used to solve the overall flowsheet balances.

2.1.1 Thermal and mechanical systems

The wood pellet production processes are divided into two separate systems, distinguishing between thermal and mechanical processes, as shown in Figure 2.1. The thermal processes include drying, torrefaction, and combustion. These units represent the main consumers of sources of thermal energy; therefore, heat integration will be carried out in this system. Due to the different operation sequences in the different pathways, the equipment types are different: rotary dryer is used in Paths 0, 1, 2, and 4, fluidized bed dryer is used in Path 3; combined direct and indirect rotary torrefier is used for Paths 1 and 4, while fluidized bed torrefier with build-in heat exchanger is used in Paths 2 and 3. A single combustor type is used in all pathways. The mechanical system involves two major units,

grinding and pelleting, powered by electricity work. These two units are also involved in all pathways.

Simulation of the thermal system is based on strict mathematical modeling, while quantification of the mechanical system is based on experimental data and empirical correlations.

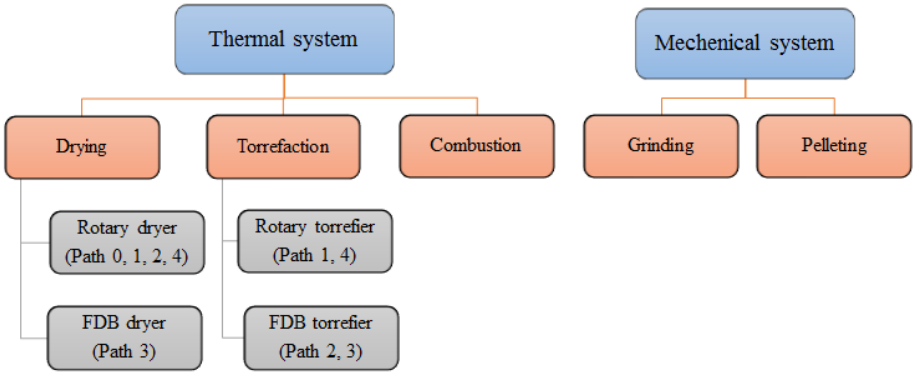

Figure 2.1 Thermal and mechanical systems of the TWP production processes

2.1.2 Solid phase approaches

Three phases are involved in the thermal system: biomass in the solid phase; water and other liquid components entrained in the torgas; and air, non-condensable torgas components, and N_2 in the gas phase. The introduction of solids to a physical or chemical process can affect the process in many ways. Three aspects are crucial for the one-dimensional solid phase modeling and simulation:

(a) How the properties of the single particles are related to the average properties of the bulk solids;

(b) The thermal properties of the solid particles, including the enthalpy changes associated with reaction (in this case torrefaction) and drying;

(c) Heat and mass transfer between the solid phase and the other phases.

In this study, modeling of the solid phase is based on the discrete element method, which essentially quantifies the overall solid-fluid properties by quantifying the properties of individual particles. Since the purpose of this analysis is to develop approximate estimates of capital and operating costs, rather than more precise cost estimates. Therefore, detailed modelling is therefore not justified. To keep the analysis as simple as possible, distributions of particle size and processing time are not considered: the development of the solid phase properties is represented by the history of the average biomass particle.

Biomass thermal properties influence the energy balances of the process. Unlike liquid and gases, whose properties can be quantified through pure component properties, biomass is usually characterized by its element analysis through its Ultimate Analysis (ULTANAL: i.e. moisture (wet basis), fixed carbon (dry basis), volatile matter (dry basis) and ash (dry basis)) Proximate Analysis (PROXIMAL: i.e. ash, carbon, hydrogen, nitrogen, chlorine, sulfur and oxygen contents, all on dry basis) and Sulphur Analysis (SULFANAL: i.e. pyritic, sulfate and organic Sulphur, all on dry basis). Therefore, the element evolution of biomass through chemical and physical changes should be captured; this topic will be discussed in detail later.

Heat and mass transfer between the solid phase and the surrounding gas phase and surfaces such as walls are determined by the behaviors of the solid and gas phases in the different types of process equipment. This will be discussed in the context of specific equipment types. The physical and chemical properties of the particles are changed in the drying and torrefaction processes; this will also be discussed in detail in the sections devoted to these processes.

2.1.3 Multi-level model structure

Figure 2.2 shows how modelling at the element and particle level are built into the structure of the simulation platform for the thermal system. Element evolution models (indicated as 1st stage in Figure 2.2) are used to calculate the thermal properties of the materials (both biomass solid and torgas, in 2nd stage), which are then involved in the hydrodynamic, thermodynamic, kinetic, and heat and mass transfer models (3rd stage). The results from these models are used in the energy and mass balances of the dryer and torrefier models (4th stage) in which the equipment sizes and operating conditions are determined for each of the different pathways. Lastly, heat and mass integration is carried out to increase the energy and mass efficiencies of the thermal process, to achieve auto-thermal operation of the thermal system (6th stage).

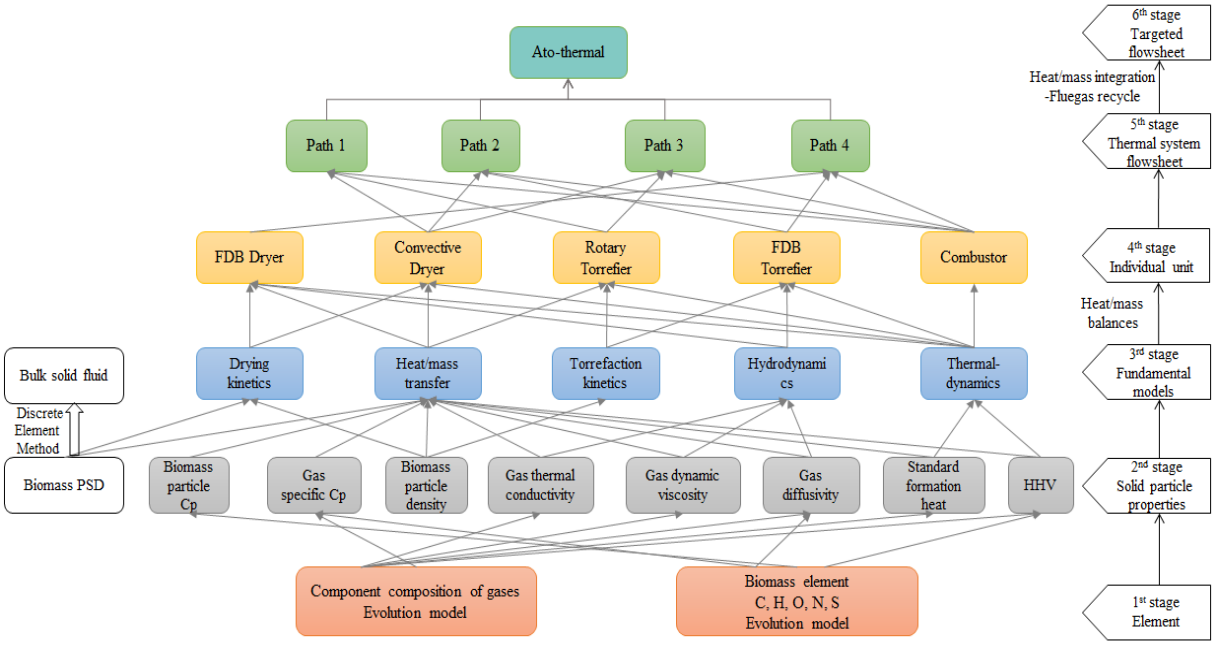

Figure 2.2 Structure of the multi-scale research methods

2.2 Development of the models in the simulation platform

The ensuing sections will present the models incorporated in the platform. The element evolution and material thermal properties models will be presented first, to establish the basis for the individual unit process models, followed by the individual process models.

2.2.1 Element evolution models and biomass physical and thermal properties

2.2.1.1 Quantification of material properties

Gas and liquid phase materials are characterized as mixtures of discrete components. Thus, the mixture properties (enthalpy, conductivity, diffusivity etc.) involved in the mass and energy balances can be estimated from the pure component properties and mixture composition. For example, the standard heat of formation and specific heat capacity of the torgas are involved in estimating the heat of torrefaction. Similarly, the gas viscosity and diffusivity are critical in determining the heat and mass transfer coefficients between particle and gas in the dryer and torrefier. Those properties change as the reaction proceeds. Therefore, the simulation must calculate how the compositions of the gas and liquid evolve during the thermal treatment processes.

By contrast, the properties of the solid biomass are characterized by the elemental composition rather than a chemical formula; see section 2.1.2 above. Important biomass particle properties involved in the energy balances include density, which influences the mechanics of the particle movement, HHV, heat of formation, and specific heat capacity. Biomass particle density can be quantified by the DCOALIGT model [43], which is based on biomass ULTANAL and SULFANAL analysis. The thermal properties of the biomass (HHV, standard heat of formation, and specific heat capacity) can be quantified according to

its ULTANAL, PROXANAL, and SULFANAL analysis. The HHV of the biomass particles can be calculated according to the correlations proposed by Boie, Dulong, Grummel and Davis, Mott and Spooner, and IGT [44]. Rönsch and Wagner [44] compared these correlations and concluded that the correlation developed by Mott and Spooner is the most reliable for wood. Therefore, the Mott and Spooner correlation is used here to estimate the HHV of the solid biomass. The standard heat of formation of the biomass particle is calculated according to the HCOALGEN model [43] and the specific heat capacity of the biomass and char by the Kirov correlation [46]. Details of those models can be found in Appendix A [43].

2.2.1.2 Evolution of gas and liquid compositions

The gases in the drying process, serving as moisture carrier, can be air, a mixture of air and flue gases, and flue gases, depending on the heat integration strategy. The composition of the flue gases is determined by the combustion conditions, primarily the air/fuel ratio which determines whether combustion is complete or incomplete and by the composition of the torgas.

The torgas composition is complex, including dozens and even hundreds of individual components, too many to be detected by current gas phase analysis; only the most abundant compounds can be identified. Few experimental studies have been carried out to evaluate the chemical composition and of the torgas at different torrefaction conditions [38], [47], [48], [49], [25], [26] using Fourier-transform infrared spectroscopy (FTIR), Gas chromatography (GC), and high performance liquid chromatography (HPLC); they show high levels of water, carbon dioxide, carbon monoxide, acetic acid and methanol, and lower levels of formic acid, lactic acid and furfural.

This study is based on the torgas composition evaluated by Prins et al. [47] and shown in Table 2.1. These authors provided relatively complete composition data for the torgas under different torrefaction conditions. The biomass element evolution model developed by Bates et al. [52] is also based on the experimental data of Prins et al. Prins et al. only estimated the torgas composition at 230℃, 250℃, 270℃, 280℃, and 300℃. Interpolation has been used here to predict the torgas composition at 240℃, 260℃, and 290℃, as shown in Table 2.1.

Table 2.1 Torgas compositions at different torrefaction conditions [47]

Temperature	230 ºC	240 ºC*	250 ºC	260 ºC*	270 ºC	280 ºC	290 ºC*	300 ºC
Residence time			30min		15min	10min		10min
Weight loss			0.1		0.14	0.2		0.25
Acetic acid	0.12	0.12	0.12	0.15	0.17	0.15	0.15	0.15
Water	0.53	0.53	0.54	0.47	0.43	0.38	0.39	0.39
Formic acid	0.03	0.03	0.04	0.04	0.05	0.05	0.06	0.06
Methanol	0.02	0.03	0.03	0.05	0.06	0.09	0.10	0.11
Lactic acid	0.01	0.02	0.03	0.04	0.05	0.09	0.12	0.13
Carbon dioxide	0.27	0.24	0.23	0.22	0.22	0.20	0.15	0.12
Carbon monoxide	0.02	0.02	0.02	0.03	0.03	0.04	0.04	0.04
Total volatile yield	1.00	1.00	1.00	1.00	1.00	1.00	1.00	1.00

*calculated by interpolation

2.2.1.3 Evolution of solid phase composition

The composition of the solid biomass has been reported more frequently than that of the gas phase, usually in terms of PROXANAL, ULTANAL, and SULFANAL analysis. Changes during the drying process are straightforward, determined by the extent of moisture removal. To represent the development of the biomass composition during pyrolysis, C-H-O

ternary diagrams are commonly used [53],[54]. Peduzzi et al. [54] described a linear evolution of the C-H-O element of the torrefied solid as a function of biomass weight loss based on Prins' [47] and Nocquet's [50] experimental data as shown in Table 2.2.

Table 2.2 Literature reported solid elemental evolution models [54]

Experimental data	Coefficients	Elemental evolution correlations
[50]	$m_C = 0.0062$	$\frac{C\%_{T00}}{C\%_{B00}} = 1 + m_C \cdot wl;$
	$m_H = -0.0025$	
[55] , [31]	$m_C = 0.0058$	$\frac{H\%_{T00}}{H\%_{B00}} = 1 + m_H \cdot wl$
	$m_H = -0.003$	
		$O\%_{T00} = 100 - C\%_{T00} - H\%_{T00} - N\%_{B00}/(100 - wl)$

Note: compositions in the models are on a dry and ash free basis
Wl: biomass weight loss during torrefaction
C%: mass fraction of carbon; H% mass fraction of hydrogen; N%: mass fraction of nitrogen
B00: biomass, 0% moisture
T00: torrefied biomass, 0% moisture

The torrefied biomass element evolution model used here is adopted from Bates et al. [52], in which the elemental composition of the biomass was related to the torgas composition and the biomass weight loss reported by Prins et al. [47], as shown in (2.1).

$$MF_{j,Char} = (MF_{j,biomass} - \alpha * MF_{j,torgas})/(1 - \alpha) \quad (2.1)$$

Where j indicates elements of C, H, O, N, and ash, $MF_{j,biomass}$ is the mass fraction of element j in the dry biomass, and α is the biomass weight loss. $MF_{j,torgas}$ is the mass fraction of element j in the torgas, with the values of 18%, 7%, 75%, 0%, and 0% respectively, obtained by a least-square regression of 18 sets of experimental data from Prins et al. [47] and Bates et al. [52].

2.2.2 Unit operation models

Modeling of the individual process units covers the following three aspects:

1. The chemical and physical processes occurring in the unit;

2. The equations representing those processes;
3. The computer code that uses the equations;

Only the first of those three will be presented in the following sections; the latter two are presented in Appendix B .

2.2.2.1 Drying

The essence of the drying process is to remove water from the product (biomass in this case) to an acceptably low value. Water may be removed from solids mechanically, by compression or centrifugation, or thermally by evaporation. In this study, the biomass is dried by a thermal process in which the solid is contacted with a gas which transports the water vapour. Moisture can be held in varying degree of bonding: water that is loosely bound will be removed easily, whilst the remaining strongly-bound water is more difficult to remove. For every type of biomass , there is a representative curve that describes its drying characteristics at a specific temperature, relative gas velocity, humidity and pressure. This curve, referred to as the drying curve, takes the form shown in Figure 2.3 (a), which shows two product particles with the same particle diameter and dried under the same air conditions. In the first drying period, the particle surface is sufficiently wet that its surface is covered by a loosely-bound water film so that particle drys like a drop of pure liquid. In the falling rate drying period, the migration of water from inner interstices of each particle to the outer surface becomes the limiting factor determining the drying rate; this behavior is product specific, due to different particle structures.

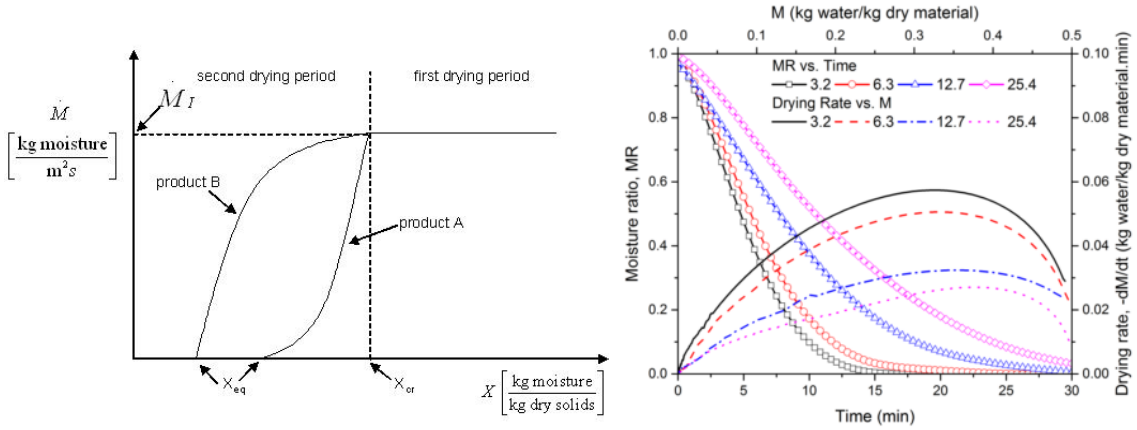

Figure 2.3 (a) Single-particle drying curves for two different products; (b) Drying rates of ground pine wood chips particles (dp=3.2, 6.3, 12.7, 25.4 mm; T(dry)=100C, carrying gas=atmospheric air) with different initial moisture content (dry basis) (Figure adopted from Razaei PhD thesis 2017)

In this study, the biomass drying kinetics is adopted from Razaei [56], who carried out thin layer drying experiments for biomass of different properties (particle size and moisture content) and investigated their drying kinetics under different drying conditions (temperature and drying gas). Figure 2.3 (b) shows drying kinetics for biomass sample with intial moisture content of 50wt% db and different particel sizes. It is observed from the dark and the dashed pink lines in Figure 2.3 (b), that the falling rate drying period starts at moisture content of 35wt%db for 25.4mm wood chips and at 40wt%db for 3.2mm wood particles, after a rising rate period and a very short constant rate period. This drying kinetics of biomass is described by the model as shown in Eq. (2.2).

$$\eta = \frac{M - M_{eq}}{M_0 - M_{eq}} = \exp\left(-k_{wood} \cdot \tau\right) \tag{2.2}$$

Where M_{eq} is the equilibrium moisture content, which is 0 in this case; M_0 is the initial moisture content; M is the instantaneous moisture content; τ is the mean residence time of

particle in the dryer; k_{wood} is the drying kinetics constant, correlated to the drying temperature, the biomass initial moisture content, as well as the biomass particle size as shown in Eq. (2.3) [56].

$$k_{wood} = \exp\left[(0.013T) - (2.372M_0) - \left(0.035d_p\right) - 2.095\right] \quad (2.3)$$

Where T is drying temperature in °C, $M_0$is the initial moisture content, d (mm) is the mean particle size.

The above biomass drying kinetics model is incorporated into a single particle evaporation model, which is incorporated into the governing heat and mass balances of the rotary and fluidized bed dryers. Detail description of the single particle evaporation model is presented in B. 1. 1.

2.2.2.1.1 Rotary dryer

In this study, a directly heated rotary dryer is used in Paths 0, 1, 2, and 4, to dry the 20mm wood chips by contact with a mixture of air and flue gases. In the dryer, drying gas flow travels cocurrently with the solid, as shown in Figure 2.4 (a). Both solids and the gas phases are in the plug flow, suggesting that there is no moisture and temperature gredient at the same vertical position. Solids are transported through the drum by the action of cascading from flights attached to the walls, with each cascade comprising the cycle of lifting on a flight and falling through the air stream as shown in Figure 2.4 (b) [57].

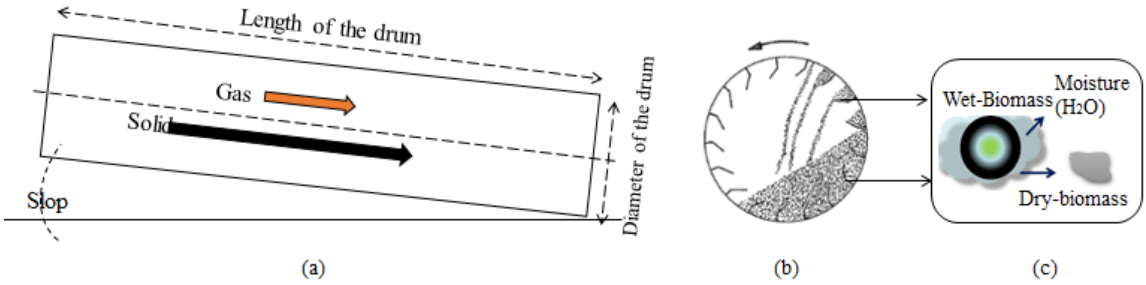

Figure 2.4 (a) Solid and gas flow traveling mechanism in a cocurrent direct heat rotary dryer; (b) solid particle cascading mechanism in a rotary dryer; (c) drying mechanism in wet biomass particle

Overall heat transfer mechanism in the directly heated rotary dryer is shown in Figure 2.5 (a), which mainly contains five terms:

(1) Heat transfer from gas to solid particle through convection Q_{eg-ep};

(2) Heat transfer from covered wall to covered bulk bed surface through conduction Q_{cw-cb};

(3) Heat transfer from exposed wall to freeboard gas through convection Q_{ew-eb};

(4) Heat transfer from exposed wall to exposed bed through radiation Q^{r}_{ew-eb};

(5) Heat loss Q_{loss}.

In this study, considering the real operation in the drum, it is assumed:

(a) the drying is carried out around or lower than 100°C;

(b) the drum wall temperature is equal to the drying gas temperature at steady state operation;

(c) in comparison with the overall particle surface area, drum wall area is neglegible;

Therefore, heat transfer from covered wall to covered bulk bed Q_{cw-cb}, from exposed wall to freeboard gas Q_{ew-eb}, as well as the radiation heat transfer from exposed wall to bulk bed

Q^{r}_{ew-eb} are negleced. Only heat transfer from flue gases to solid particles Q_{eg-ep} is considered, as shown in Figure 2.5 (b).

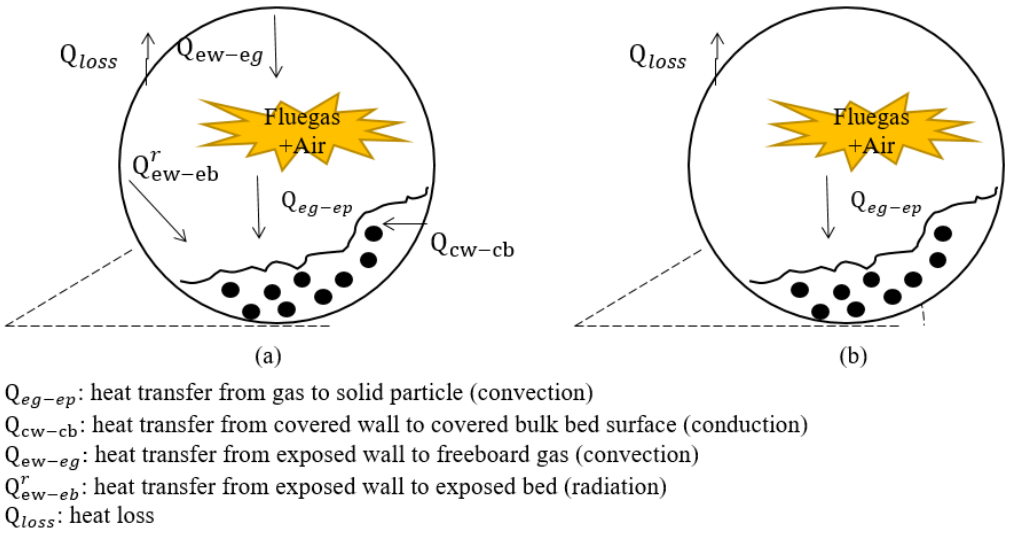

Figure 2.5 (a) Complete mechanism of the directly heated rotary dryer; (b) Mechanism of the directly heated rotary dryer in this study

Mass transfer of the solid and the gas phase is represented by a single particle and surouding gas mass transfer coefficient model because both these phases are in plug flow. Details of the mass transfer coefficient between single particle and surrounding gas are presented in B. 1. 2.

2.2.2.1.2 Fluidized bed dryer

In Path 3, the biomass solid is reduced to 1mm by a hammer mill, and subsequently dried. Fluidized bed drying is selected for these solid particles due to the excellent solid and gas contact and thus enhanced heat and mass transfer rates achieved in a fluidized bed [58]. In a fluidized bed dryer, a bed of solid particles is maintained in a fluid-like a state by an upward gas stream, as illustrated in Figure 2.6. The volumetric flow rate of the gas has to

exceed a certain limiting value (minimum fluidization velocity, u_{mf}) to maintain fluidization (diagram A). As the flow rate increases, the bed passes through a range of behaviors. At first, it expands as virtually solid-free gas bubbles form and grow (diagram B). If the bed vessel is sufficiently narrow and high, the bubbles ultimately fill the entire cross section and pass through the bed as a series of gas slugs (diagram C). As the gas velocity increases further, more and more solids are carried out of the bed, which is then described as a turbulent bed (diagram D). Solids entrained in the fluidizing gas must be collected and returned to the bed; the simplest way to do this is to use a cyclone to recycle the entrained bed materials (diagram E).

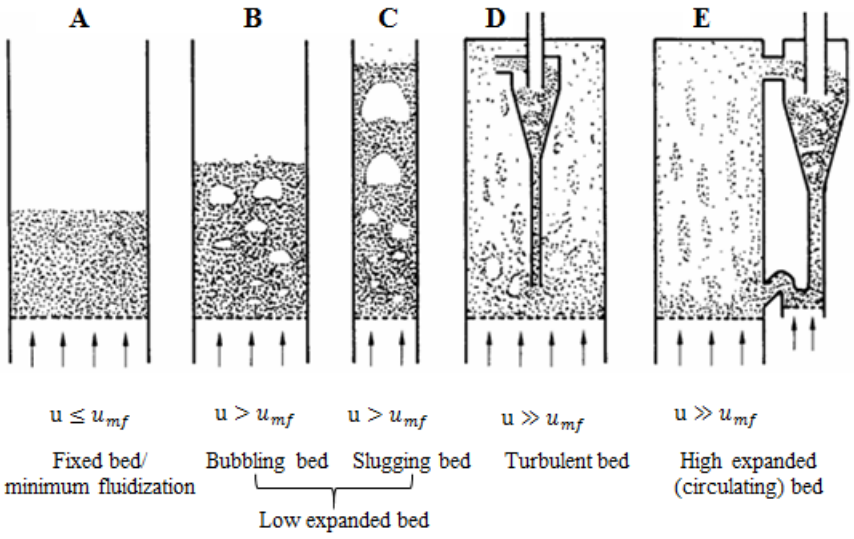

Figure 2.6 Forms of gas-solid fluidized beds

There have been two approaches in modeling the rate of mass transfer in fluidized bed dryers [59]: (a) homogeneous bed approach, which considers the fluidized bed dryer to behave like a fixed bed and correlates the fluidized bed mass transfer coefficient in a manner similar to that in a fixed bed based on a plug-flow model; and (b) bubbling bed approach,

which considers the fluidized bed to consist of two phases, a bubble phase and an emulsion phase, and the gas interchange between the two phases constitutes the rate of mass transfer. Here, homogeneous approach is applied for fluidized bed average mass transfer coefficient. In this approach, two types of the mass transfer coefficients are defined [60], [59]:

- k_{bed} the overall or effective mass transfer coefficient
- k_p the single particle or local mass transfer coefficient

The relationship of these two mass transfer coefficients in fluidized bed is shown in Figure 2.7 (a), which illustrates several groups of experiments that carried out to evaluate the overall fluidized bed mass transfer coefficient. In general, for particle Reynolds number greater than 80, the average mass transfer coefficient of the bed is higher than the single particle mass transfer coefficient, because in this case the gas phase passes through the bed solids close to plug flow, with negligible bubble cloud or cloud emulsion resistance. The trend is reversed if Reynolds number of the particle is lower than 80. One explanation is because in a bubbling fluidized bed, most of the particles stay in the emulsion phase. Many of these particles are thus considered as inert from mass-transfer point of view, because they do not contribute to significant amount of mass transfer to the bubbling gas. Another explanation is that in bubbling fluidized bed, the moisture in the particle must go from particle to emulsion gas and then further to cloud or bubble phase before it can be removed from of the bed. Therefore, the effective bed mass transfer coefficient is lower than the single particle transfer rate.

Similar to the mass transfer, Figure 2.7 (b) shows the heat transfer in gas fluidized beds. As can be seen, the average fluidized bed heat transfer is dependent on the particle and gas properties.

Therefore, bed average heat and mass transfer coefficient models of the fluidized bed are applied in this study. Details of the bed-average mass and heat transfer coefficient models are presented in B. 1. 3.

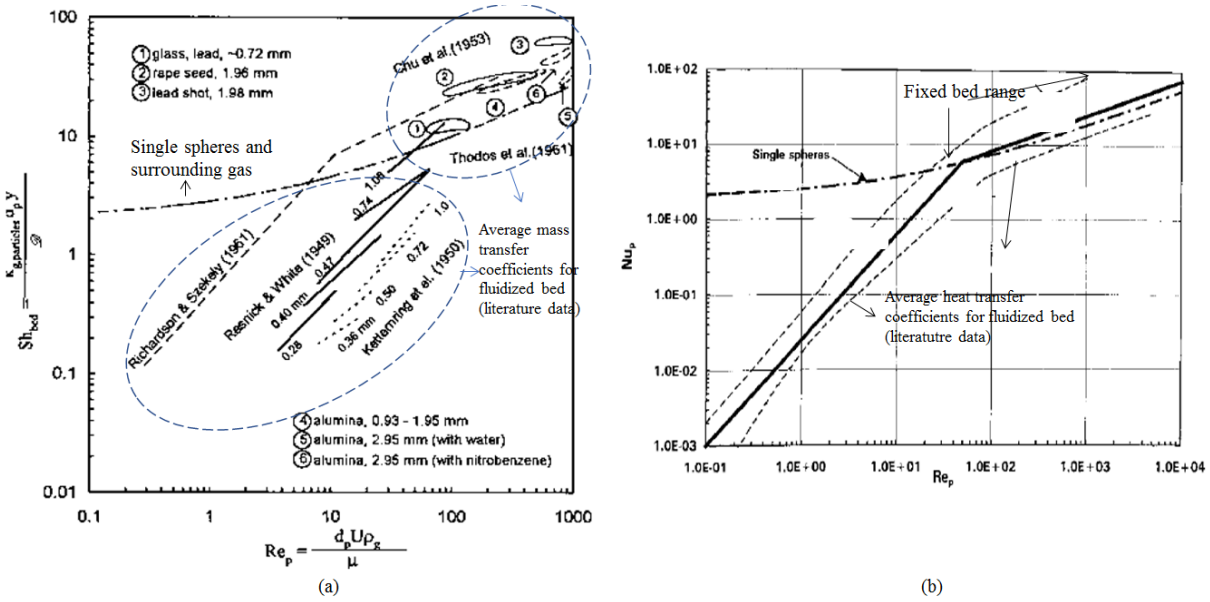

Figure 2.7 (a) Average mass transfer coefficient in fluidized bed; (b) Average heat transfer coefficient in fluidized bed (from Kunii and Levenspiel 1991)

Hydrodynamics in the bottom zone is calculated according to Werther and Wein [61], which considers the combined action of bubble coalescence and splitting. The upper zone free-board zone is calculated according to Kunii and Levenspiel [60], suggest an exponential decay of the solids volume concentration, as shown in Figure 2.7 (b). Detail description of this model is referred to [62], [63], [64], [65].

2.2.2.2 Torrefaction

Biomass torrefaction is a heterogeneous reaction process, with its reactant (dry biomass) in the solid phase and products in solid (torrefied biomass) and gas (torgas) phases.

Such kind of heterogeneous reaction modeling has been well reported [66]. The main challenges in simulating biomass torrefaction in different types of reactors are: (a) appropriate description of fluid behaviors in different phases, (b) the behavior of individual biomass particles inside the reactor, (c) the heat and mass transfer between phases, and (d) reaction kinetics. In the present work, the simplifying assumption is made that the biomass particle size is in uniform, and its diameter remains the same during torrefaction. Also, the residence time of the particles is assumed to be uniform.

Biomass torrefaction kinetics has been studied extensively both by experiments and modeling. A comprehensive review of the torrefaction kinetics can be found in [16], [25], [68], [67], [69], [70], [71]. An intrinsic one-step first order torrefaction reaction model is applied in this study, adopted from Peng et al. and shown in Eq.s **(**2.4) and **(**2.5), with $k_{tor}=2.9\times10^{8}\exp(-130{,}690/RT)$, in s^{-1} [68]. The reaction stoichiometry at different torrefaction conditions is based on the weight loss data from Table 2.3, which is adopted from [72] based on Figure 2.8.

$$\text{Biomass} \xrightarrow{k_{tor}} \alpha\text{Volatiles} + (1-\alpha)\text{Chars} \tag{2.4}$$

$$\frac{dc_m}{dt} = k_{tor}c_m \tag{2.5}$$

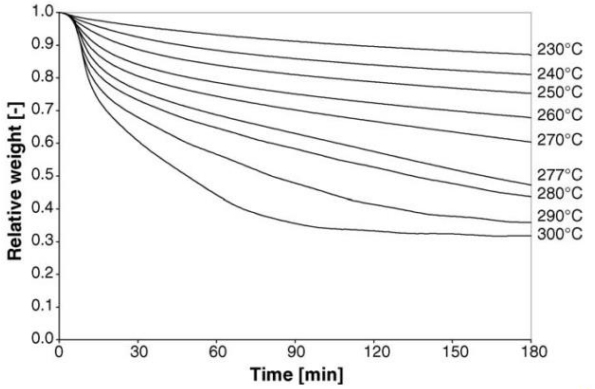

Figure 2.8 Biomass weight loss curves during torrefaction at various final temperatures (adopted from [72])

Table 2.3 Stoichiometry (α) of the pseudo-one-step torrefaction reaction based on experimental data in [72]

	300ºC	290ºC	280ºC	270ºC	260ºC	250ºC
15min	0.29	0.24	0.20	0.14	0.10	0.08
30min	0.40	0.31	0.28	0.20	0.16	0.10
60min	0.55	0.42	0.35	0.25	0.20	0.16
90min	0.64	0.51	0.40	0.30	0.25	0.18
120min	0.68	0.60	0.48	0.32	0.29	0.20

2.2.2.2.1 Rotary torrefier

In Paths 1 and 4, torrefaction is carried out in a combined direct and indirect heated rotary torrefier. The drum contains a shell outside the reactor tube as illustrated in Figure 2.9 (a): solid biomass travels through the tube, moves forward by cascading by freight as in a rotary dryer when the drum is rotated as illustrated in Figure 2.9 (b). The flue gases exiting from combustor will enter the shell side of the drum, flowing co-currently to the solid, and then enters the tube to flow counter-currently with the solid. The flue gases contain CO_2, H_2O, and O_2. Complex reactions will occur when these components contact with biomass solid at the torrefaction temperature. In addition, Wang et al. [49] reported that biomass

could burn when O_2 exceeds 9% in the gas. Therefore, flowrate of the recycled flue gases should be limited to reduce its influence on the torrefaction, with volumetric flowrate that able to fill the drum being sufficient. Torrefaction happens at the solid phase as shown in Figure 2.9 (c).

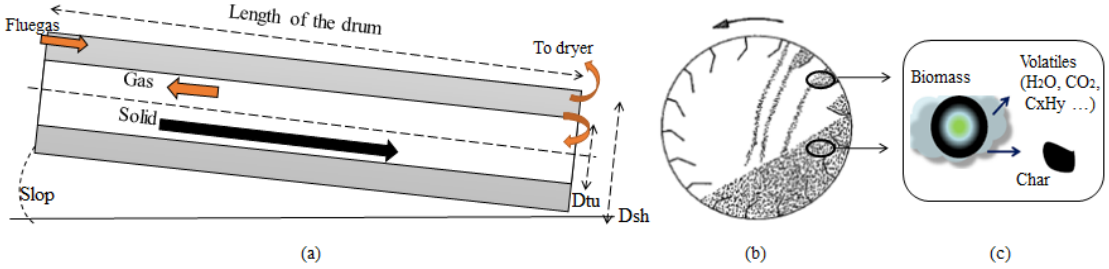

Figure 2.9 (a) Gas and solid phase travel routes in combined directly and indirectly heated rotary torrefier; (b) solid particle cascading mechanism in a rotary dryer; (c) biomass particle decomposition mechanism

The intrinsic features of heat transfer in a combined directly and indirectly heated rotary torrefier include are illustrated in Figure 2.10 (a), which contains:

I. Directly heated—tube side heat transfer

(1) from covered drum wall to covered solids through conduction $Q_{cw-cb,tu}$;

(2) between solid particle and surrounding gas phase $Q_{eg-ep,tu}$;

(3) from exposed drum wall to the gas phase above solid through natural convection $Q_{ew-eg,tu}$;

(4) from exposed wall to exposed surface of the solid bed through radiation$Q^{r}_{ew-es,tu}$;

II. Indirectly heated--shell side heat transfer

(1) From gas to shell wall through forced convection, $Q^{c}_{gw,sh}$ and radiation, $Q^{r}_{gw,sh}$.

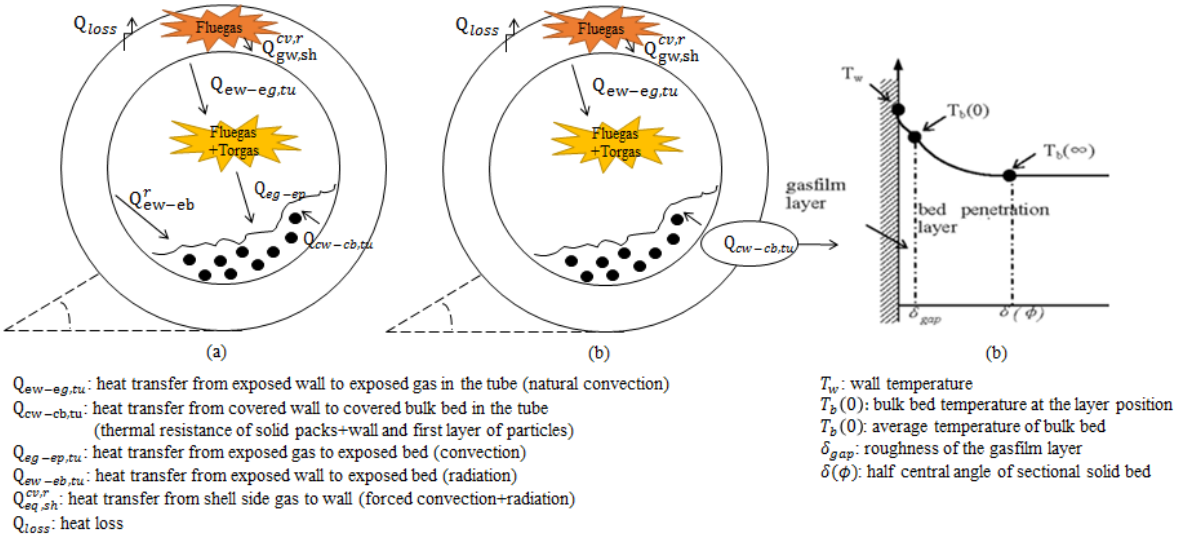

Figure 2.10 (a) Mechanism of heat transfer of directly and indirectly heated rotary torrefier; (b) mechanism of heat transfer of the directly and indirectly heated rotary torrefier in current study (c) mechanism of heat transfer between the covered wall and bulk bed in a rotary dryer

Since the gas flow in the tube side is very limited, therefore, heat transfer between the gas and solid particle, $Q_{eg-ep,tu}$, as well as the exposed wall to gas, $Q^{r}_{ew-es,tu}$ are neglected, as shown in Figure 2.10 (b).

Similar to the rotary dryer, mass transfer coefficient model between a single particle and the surrounding gas is used. Details of the heat and mass transfer coefficient models are presented in B. 2. 1.

2.2.2.2.2 Fluidized bed torrefier

Fluidized bed torrefiers with build-in heat exchanger are applied in Paths 2 and 4 for particles of 1mm in average diameter. As shown in Figure 2.11 (a), the flue gases enter the immersed heat exchanger in the fluidized bed torrefier to provide heat to solid indirectly, and then part of the flue gases will enter from the gas distributor to the bottom of the bed to

fluidize the bed particles in contact with solid directly, the left part of the flue gases will be used for the drying of biomass. Flow rate of the recycled flue gases to the torrefier is thus a design parameter, which is constrained by minimum fluidization velocity, diameter of the reactor, and energy balances in the torrefier etc.

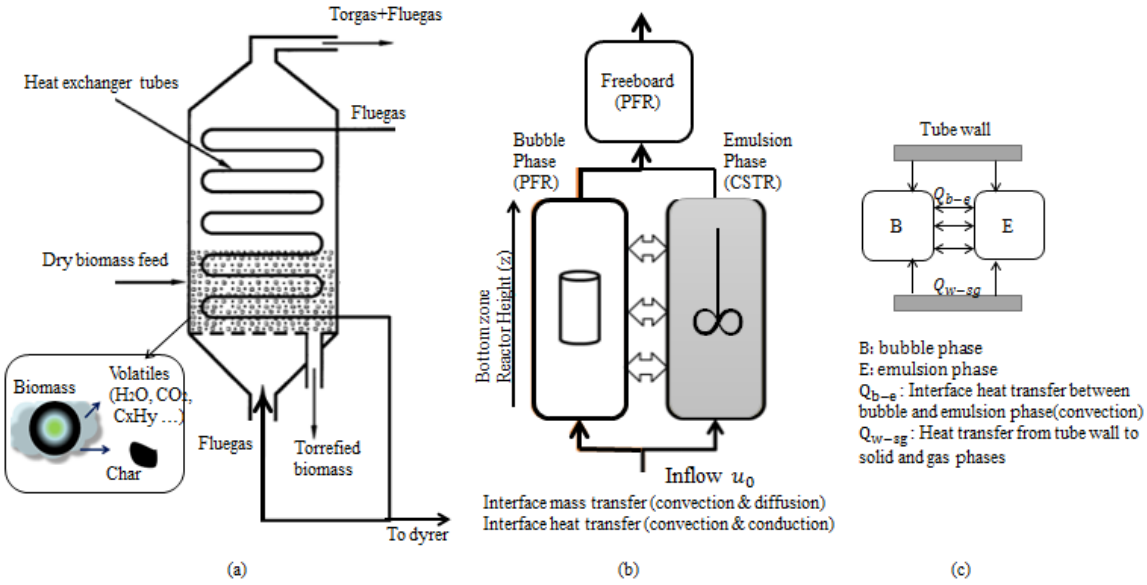

Figure 2.11 (a) Structure and flow diagram of the fluidized bed torrefier with build-in heat exchanger; (b) two phase bubbling fluidized bed model of the fluidized bed torrefier; (c) heat transfer mechanism of solid and gas phase in bubbling fluidized bed torrefier with build-in heat exchanger

Similar to the fluidized bed dryer, two-phase model is applied to simulate the bubbling bed torrefier. The model shares the same assumption of (a), (b) and (c) as the fluidized bed dryer model. In addition, biomass torrefaction happens at the solid phase. Reaction in the upper free-board zone is not considered. The decomposed volatiles travel in the emulsion and the bubble phases as illustrated in Figure 2.11 (b). According to Werther and Wein, no change in volumetric gas flow due to reaction is considered. Heat transfer between bubble and gas phases is considered. In addition, heat transfer from tube to the bed

is also included in the model. This module is available in Aspen Plus, with detail descriptions provided in [62], [63], [64], [65].

2.2.3 Combustion

The combustor is characterized by the heat released during combustion. Once the heat duty is determined, equipment sizes and costs can be quantified by Aspen Economic Analyzer [73]. The combustion heat duty is determined by the HHV of the torgas, as summarized in Table 2.4, and the equipment energy efficiency.

Table 2.4 Torgas compositions and HHVs at different torrefaction conditions [72]

Mass fraction	250 ºC (30min)	260 ºC	270 ºC (15min)	280 ºC (10min)	290 ºC	300 ºC (10min)
HHV of torgas (MJ/kg)	3.23	4.31	5.08	6.58	7.48	8.04

Note: torgas compositions refer to Table 2.1

Another important parameter of the combustion process is the combustion temperature, which influences the heat integration strategy of the thermal system as illustrated in Figure 2.12,

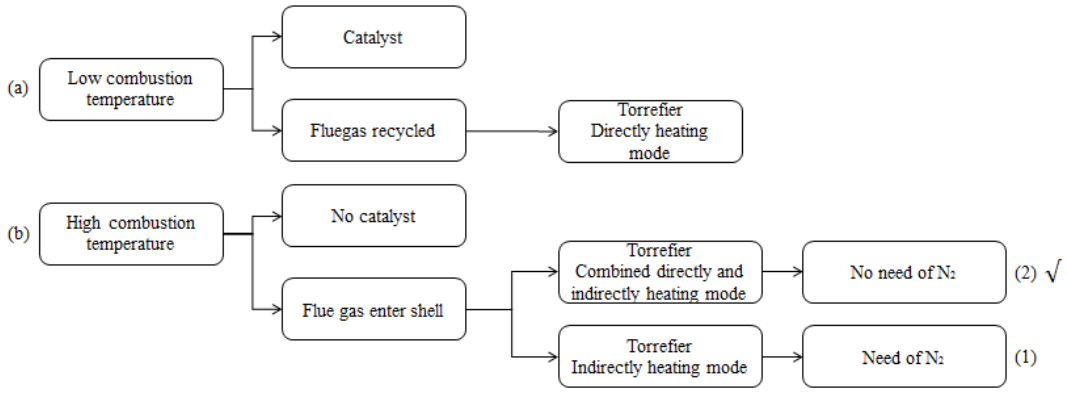

Figure 2.12 Combustion temperature influences on torrefier heating mode and flue gases recycle strategies

(a) At low combustion temperature, catalyst may be needed to ensure sustainable combustion. But the flue gases may be able to be recycled directly to the torrefier to replace N_2 without igniting the biomass;

(b) At very high combustion temperature, combustion can sustain without catalyst. But due to the high temperature, the flue gases can not contact with the biomass particle directly. In this case, the flue gases have to provide heat to the torrefier indirectly through a shell or immersed heat exchanger tubes. Two cases will occur when the flue gases travel out of the shell or the heat exchanger:

    (1) If the temperature of the flue gases is still higher than the biomass ignition temperature, it will not be able to be recycled to contact with biomass particles. In this case, N_2 will be needed to provide an anaerobic environment for torrefaction;

    (2) If the flue gases temperature is lower than the biomass ignition temperature, it then can be recycled to replace N_2. In this case, combined direct and indirect heating mode is applied, and N_2 is avoided. This is the desired heat integration strategy to avoid use of N_2 and catalyst.

The combustion temperature is determined by the air torgas ratio. It is preferred to have the combustion temperature at stoichiometry air-fuel ratio to ensure the highest combustion temperature. In the current study, a Gibbs reactor, which is based on thermodynamic first law and second law, was used to predict the adiabatic temperature and composition of the combustion flue gases.

2.2.4 Grinding

The grinding process is carried out in a commercial scale hammer mill to reduce the biomass particle size from 20mm to 1mm. The hammer mill is characterized by its mechanically driven power W_{DP} (input work/power), which is determined by its output work (W_{NP}) and mechanical efficiency (ξ) as Eq. (2.6).

$$W_{DP} = W_{NP}/\xi_{hammer} \tag{2.6}$$

The hammer mill output power W_{NP} can be calculated according to biomass hardness (specific energy consumption, $spe_{grinding,MC}$) and the biomass flowrate ($\dot{m}_{grinding}$), as expressed by Eq. (2.7).

$$W_{r,ham} = spe_{grinding,MC} \cdot \dot{m}_{grinding} \tag{2.7}$$

Usually, there is a limit to the mechanical machine driven power. Numbers of hammer mills will be required if one hammer mill is not sufficient to treat large amount of biomass. The number of the hammer mill is determined by the theoretical energy requirement and the driven power $W_{hammer,sel}$ of the selected equipment, calculated according to Eq. (2.8). Many companies provide the hammer mill machine specifications, e.g. [74].

$$N_{ham} = \frac{spe_{grinding,MC} \cdot \dot{m}_{grinding}/\xi_{hammer}}{W_{hammer,sel}} \tag{2.8}$$

In this study, three groups of biomass wood chips will be grinded:

(1) MC 50wt%db in Path 4;

(2) MC15wt%db in Path 0, 2, and 3;

(3) torrefied wood chips in Path 1.

Biomass group (2) is mostly grinded in the commercial hammer mill, with its energy consumption being correlated to many factors, including biomass type, hammer mill rotation

speed, screen size etc. A comprehensive literature review of the biomass grinding process is provided in Table B.1 and Table B.2. Esteban et al. [75] evaluated the energy consumptions of grinding pine wood chips with MC 15wt%db from 15mm to 1.5mm by using commercial hammer mill with a rotation speed of 3000 rpm, and the specific energy consumption $spe_{grinding,MC15wt\%db}$ was reported as 427 kJ/kg of biomass. Cadoche et al. [76] reported a value of 468kJ/kg biomass for a commercial hammer mill using 1.6mm screen for hard wood chips. Here, we assumed the specific energy consumption of biomass group (2) is 427 kJ/kg biomass.

Grinding of biomass groups (1) and (3) by using commercial scale hammer mill are not found through literature review. However, lab scale experiments had been carried out as summarized in Table 2.5. Colin et al. [77] evaluated grinding of wood chips with MC 50wt%wb, MC 15wt%wb, and torrefied wood chips with 20% and 15% biomass weight loss. They found out that energy consumption of grinding torrefied wood chips is about 9 (with 20% weight loss) to 15 (with 15% weight loss) times to that of biomass with MC 15wt%db. Similar observations are also reported by Cadoche et al. [76] and Wang et al. [70], as shown in Table 2.5. Energy consumption of grinding biomass with MC 50wt%db is about two times of MC 15wt%db [77]. The absolute value obtained from lab scale may not be applicable for commercial-scale operations. However, the relative ratio of grinding biomass to different conditions is considered transferable. In this study, we assume the specific energy consumptions of grinding three groups of the biomass: 427 kJ/kg for biomass wood chips with MC 15%, 854 kJ/kg for MC 50wt%db, and 38 kJ/kg (1/11 of $spe_{grinding,MC\ 15wt\%db}$) for torrefied wood chip. Variations of these values for different biomass and the influences on the "3E" metrics will be discussed in Chapter 4 and Chapter 5.

Table 2.5 Reported specific energy consumptions of grinding biomass with different properties

Reference	Biomass properties	$spe_{grinding,MC\ 15wt\%db}$ (kJ/kg biomass)	$spe_{grinding,torrefied}$ (kJ/kg biomass)	$spe_{grinding,MC\ 50wt\%db}$ (kJ/kg biomass)
Colin et al. [77]	wood chips 5-15mm	450	30-50	900
Cadoche et al. [76]	beech chips	990	90	
	spruce	880	90	
Wang et al. [70]	Stem wood	792	52	
	Stump wood	576	53	

2.2.5 Pelleting

Pelletization is carried out to densify sawdust from ~1 mm to uniform sizes of 6 mm in diameter and 40 mm in length [78]. Similar to the grinding process, the biomass pelleting process is also a mechanical process, which "3E" metrics are also characterized by its driven power and the equipment numbers. The useful work of the pelleting machine is determined by the specific energy consumption ($spe_{pelleting,MC}$) of pelleting different type of biomass material and the biomass treatment flowrate ($\dot{m}_{pelleting}$), as calculated by Eq. (2.9).

$$W_{r,pelleting} = spe_{pelleting,MC} \cdot \dot{m}_{pelleting} \tag{2.9}$$

The number of the pelleting machine is calculated according to Eq. (2.10).

$$N_{pelleting} = \frac{spe_{pelleting,MC} \cdot \dot{m}_{pelleting} / \xi_{pelleting}}{W_{pelleting,sel}} \tag{2.10}$$

Here, $W_{pelleting,sel}$ is the selected driven power of the pelleting machine which is also determined by treatment capacity and type.

Two groups of biomass particles are to be densified:

(1) biomass with MC 10wt%db in Paths 0 and 3;

(2) torrefied biomass in Paths 1, 2 and 4.

Many researches on conventional and torrefied biomass pelletization in lab scale have been carried out, as summarized in Table B.3. The specific energy consumption of biomass pelletization highly depends on biomass species, moisture content, torrefied biomass properties, and pelleting machine type and capacity etc. Thus, determination of the specific energy consumption of the above two groups of biomass should reference to those cases in similar conditions. Data summarized in Table 2.6 reveal that specific energy consumption for pelleting torrefied biomass $spe_{pelleting,twp}$, either with or without binder, is about 1.1-1.5 times of that $spe_{pelleting,cwp}$ for pelleting conventional biomass.

Jannasch et al. [79] reported a commercial scale pelleting process: switchgrass biomass particle was pelletized in capacity of 2 t/hr. The specific energy consumption was evaluated as 268 kJ/kg biomass [79]. Since this work is also in commercial scale, therefore, it is assumed that the specific energy consumption for pelleting the biomass particle with MC 10wt%db and torrefied wood particles is 270 kJ/kg [79] and 340 kJ/kg (1.25 times, mean ratio according to Table 2.6), respectively. The electricity consumption of the pelleting process is calculated by multiplying the specific energy consumption with the biomass flowrate. Uncertainties of these parameters to the "3E" metrics will be discussed in Chapter 4 and Chapter 5.

Table 2.6 Reported specific energy consumptions of the pelletization with different biomass properties

Reference	Biomass type	$spe_{pelleting,CWP}$ (kJ/kg biomass)	$spe_{pelleting,TWP}$ (kJ/kg biomass)	Binder	$spe_{pelleting,TWP}$/ $spe_{pelleting,CWP}$
[68]	Spruce	29	31	NA	1.1
	Pine	28	32	NA	1.2
	Fir	31	34	NA	1.1
	SPF	31	36	NA	1.1
	Bark	19	28	NA	1.5

Reference	Biomass type	$spe_{pelleting,CWP}$ (kJ/kg biomass)	$spe_{pelleting,TWP}$ (kJ/kg biomass)	Binder	$spe_{pelleting,TWP}$/ $spe_{pelleting,CWP}$
[24]	Pine sawdust	39.1	52.8	NA	1.4
			50.7	10wt% sawdust	1.3
			46.2	20wt% sawdust	1.2
			42.9	30wt% sawdust	1.1
[80]	Cedarwood	32	34-36	NA	1-1.1
	Camphorwood	27	31-41	NA	1.1-1.5
[81]		28	42	NA	1.5

As aforementioned that binders are usually applied for torrefied biomass densification to increase its inter-particle bonding and strength of the pellet product [22]. Peng et al. [24] reported that sawdust particles (< 1mm) could be used as an effective and low-cost binder for making strong pellets from torrefied powders. Thus, in this study, 8wt% of sawdust is used as the biner, and the sawdust moisture content is assumed to be 50wt%wb.

2.3 Heat integration

Heat integration of the thermal system is carried out for each pathway when the individual unit model is established. The desired flowsheet is to achieve auto-thermal operation and avoid the use of N_2 and catalyst, which will be discussed in Chapter 4. The key tasks of the process heat integration are to find out appropriate torrefaction operating conditions and equipment specifications to achieve the desired flowsheet.

2.4 Conclusions

In chapter 2, a simulation platform is developed based on Aspen Plus and FORTRAN programming. The production process is divided into thermal system and mechanic system. Simulation of the thermal system is based on steady state and the individual unit models are developed based on strict mathematical models which are in element and particle level,

which include a directly heated rotary dryer, a fluidized bed dryer, a combined directly and indirectly heated rotary torrefier, and a fluidized bed torrefier with build-in heat exchanger. The platform enables us to size the equipment, optimize operation conditions, perform sensitivity analysis, and carry out process heat and mass integration. Mechanical units, including grinding and pelleting, are characterized based on reported experimental data in the lab and commercial scale. This simulation platform will generate data for different operation scenarios and provide data for techno-economic evaluation and supply chain analysis.

Chapter 3: Identification of suitable torrefaction operation envelops

3.1 Introduction

This chapter investigates the overall performances of the torrefaction system, to define the boundaries of practical auto-thermal operation for the configuration shown in Figure 1.3 (a), to provide a possible range of operating conditions to guide the design of the commercial process to produce torrefied pellets. This involves elucidating (a) thermal properties changes of both solid and gas phases during the torrefaction process and (b) how the energy balance depends on torrefaction conditions such as temperature and residence time.

3.2 Definition of boundaries of auto-thermal operation

Figure 3.1 shows the process configuration for thermal integration on which the analysis is based. The flue gases are recycled to provide the heat and gas flow required, first for torrefaction and then for the drying process. A minimum temperature approach (ΔT min) of 5^{o}C is used to identify the maximum heat integration potential [82]. Thus, for heat integration with the cold flows such as air at ambient temperature 25℃, the minimum temperature for the flue gases leaving the system is assumed to be 30℃. The data required for heat integration relate to the enthalpy of the hot flue gases, the cold untorrefied biomass and the drying air.

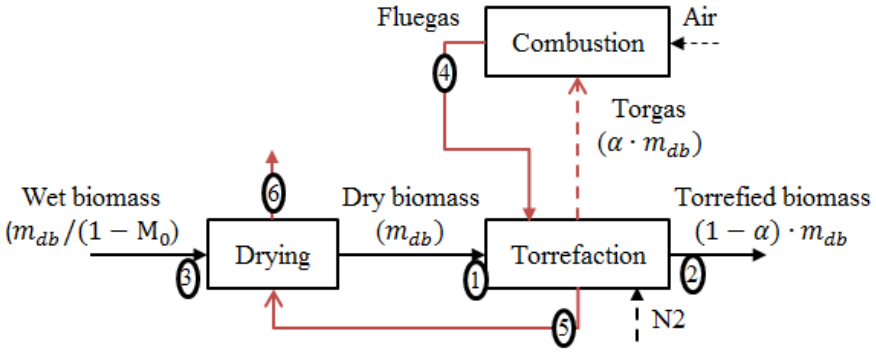

Figure 3.1 Flow chart of the thermally integrated torrefaction system

Figure 3.2 illustrates the development of enthalpy and temperature in the heat exchange network. Case A refers to auto-thermal operation with extra heat available in the system; in case B the system is just auto-thermal with no surplus heat; and in case C the system cannot be operated auto-thermally.

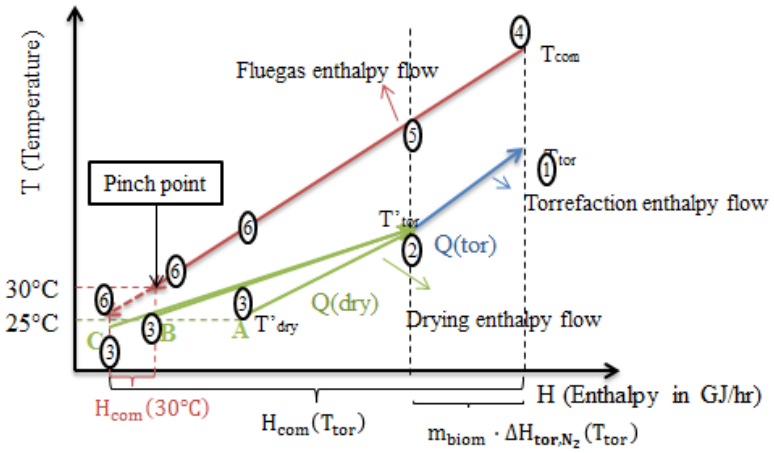

T_{com}: combustion temperature
T_{tor}: torrefaction temperature
T'_{tor}: Inlet temperature of the dry biomass into the torrefier
T'_{dry}: Drying air inlet temperature
Q(dry): drying heat
Q(tor): torrefaction heat requirement $Q(tor) = m_{biom} \cdot \Delta H_{tor,N_2}(T_{tor})$
$H_{com}(T_{tor})$: enthalpy of torgas
$H_{com}(30°C)$: enthalpy of torgas that can not used for heat exchange

Figure 3.2 Illustration of the heat exchange network of the thermal system

The enthalpy available from the flue gases (Q_{com}, measured in GJ/hr) is defined by the energy balance over the combustion process as:

$$Q_{com} = \dot{m}_{db} \cdot \alpha \cdot HHV_{tor} \cdot \xi_{com} = \dot{m}_{fluegas} \cdot C_{p,fluegas} \cdot (T_{com} - T_s) \qquad (3.1)$$

Here $\dot{m}_{db} \cdot \alpha \cdot HHV_{tor}$ represents the enthalpy flow available from combustion of the torgas, where $\dot{m}_{db}$ (t/hr) is the mass flowrate of dry biomass entering the torrefier, α is the fractional biomass weight loss in torrefaction, and HHV_{tor} (GJ/t) is the higher heating value of the torgas, and ξ_{com} is the thermal efficiency of the combustion process (i.e. the fraction of the enthalpy of combustion carried by the flue gases). The second term, $m_{fluegas} \cdot C_{p,fluegas} \cdot (T_{com} - T_s)$, relates the combustion heat released to the temperature of the exiting flue gases, T_{com} is the adiabatic combustion temperature; $m_{fluegas}$ is the mass flowrate of the flue gases (in t/hr), equal to the sum of the flows of torgas and air into the combustor; $C_{p,fluegas}$ is the specific heat capacity at constant pressure of the flue gases (in MJ/t-K); and T_s is the reference temperature (298K), which is also the temperature at which the air enters the combustor.

Allowing for a minimum temperature approach $\Delta T_{min} = 5℃$ [82], the total heat available for transfer Q'_{com} in the torrefaction and drying units is:

$$Q'_{com} = \dot{m}_{fluegas} \cdot C_{p,fluegas} \cdot (T_{com} - T_s) - \dot{m}_{fluegas} \cdot C_{p,fluegas} \cdot \Delta T_{min} \qquad (3.2)$$

To determine the heat available for thermal integration Q'_{com}, the following parameters are required: (1) torgas mass or molar flowrate, (2) composition of the torgas at different torrefaction conditions, (3) air flowrate used for combustion and (4) adiabatic combustion temperature. Torgas flowrate can be determined by biomass weight loss and the torgas composition can be determined by using experimental data, such as the case presented

in Table 2.4 but noting that such data refer to very specific reaction conditions. The air flowrate is determined by the torgas composition and flowrate. The adiabatic combustion temperature is determined by the air fuel ratio and calculated by solving energy balances. Ideally, the combustion is carried out with a stoichiometric mixture of air and torgas, so that combustion proceeds at the highest temperature to maintain combustion without catalyst.

At present, instead of determining the four parameters identified above, we make the simplifying assumption that the change in enthalpy of the flue gases from 25°C to 30°C can be neglected. This assumption is justified by the low temperature difference and the fact that the air flowrate is also relatively small because combustion is carried out at conditions close to stoichiometric. This assumption simplifies Eq. (3.2) to Eq. (3.3).

$$Q'_{com} = \dot{m}_{db} \cdot \alpha \cdot HHV_{tor} \cdot \xi_{com} \tag{3.3}$$

The enthalpy flow required for the torrefaction process is expressed as Q_{tor}:

$$Q_{tor} = \dot{m}_{db} \cdot \Delta H_{tor,N_2}(T_{tor})/\xi_{tor} = \dot{m}_{fluegas} \cdot C_{p,fluegas} \cdot (T_{com} - T'_{tor}) \tag{3.4}$$

Where $\dot{m}_{db}$ is the mass flowrate of the dry biomass entering the torrefier in t/hr. $\xi_{tor}$is the thermal efficiency of the torrefier; and $\dot{m}_{fluegas} \cdot C_{p,fluegas} \cdot (T_{com} - T'_{tor})$ is the enthalpy transferred from the flue gases to the torrefied solids, where T'_{tor} is the temperature of the flue gases leaving the torrefier. $\Delta H_{tor,N_2}(T_{tor})$ is the heat requirement for torrefaction in GJ/t biomass converted, as illustrated in Figure 3.3. Because the temperature of the dry biomass before entering the torrefier is $T_{s,dry}$ (higher than 25°C), $\Delta H_{tor,N_2}(T_{tor})$ thus can be quantified as the sum of torrefaction reaction heat at temperature T_{tor} and the sensible heat of N_2, minus the sensible heat of dry biomass from 25°C to $T_{s,dry}$, as expressed by Eq. **(**3.5).

The last term is negligible due to low specific heat of biomass (ranges 1.2-1.5 kJ/kg-K from 40 to100 °C [83]) and low drying temperature in this study (lower than 100 °C).

$$\Delta H_{tor,N_2}(T_{tor}) = \Delta H_{tor}(T_{tor}) + \dot{m}_{N_2} \cdot \int_{25℃}^{T_{tor}} C_{p,N_2} dT - \int_{25℃}^{T_{s,dry}} C_{p,db} dT \qquad (3.5)$$

Where $\dot{m}_{N2}$ in kg N_2/kg biomass, represents the mass flowrate of N2 used per kg biomass. $\Delta H_{tor}(T_{tor})$ is the torrefaction reaction heat defined as Eq. (3.6).

$$\Delta H_{tor}(T_{tor}) = \Delta H^{o}(25℃) + \Delta H_{prod} - \Delta H_{react} \qquad (3.6)$$

Here ΔH_{prod} and ΔH_{react} are the sensible heat of product and reactant from standard temperature to torrefaction temperature, respectively.

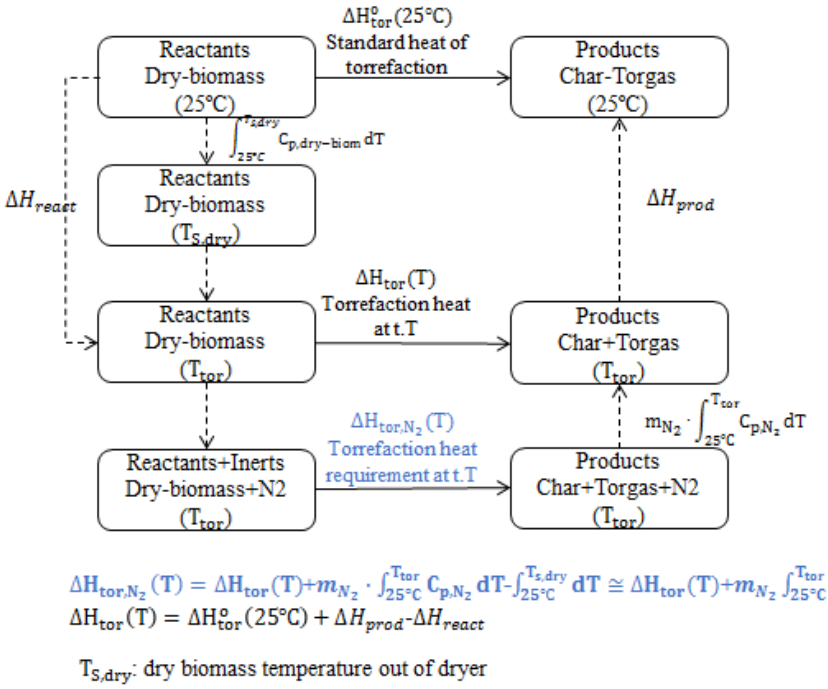

Figure 3.3 Definition of torrefaction heat requirement $\Delta H_{tor,N_2}(T_{tor})$ and torrefaction reaction heat $\Delta H_{tor}(T_{tor})$

The enthalpy flow required by the drying process is expressed as Q_{dry}:

$$Q_{dry} = \dot{m}_{water} \cdot \Delta h^{v}/\xi_{dry} = \dot{m}_{fluegas} \cdot C_{p,fluegas} \cdot (T'_{tor} - T'_{tor}) \quad (3.7)$$

Here $\dot{m}_{water} \cdot Q_{dry}/\xi_{dry}$ is the heat required for the drying process, where m_{water} is the amount of removed from the wet biomass in t/hr; Δh^{v} is the latent heat of evaporation of the water, in GJ/t; ξ_{dry} is the thermal efficiency of the dryer; and $\dot{m}_{fluegas} \cdot C_{p,fluegas} \cdot (T'_{tor} - T'_{dry})$ is the enthalpy flow exchanged from the flue gases in the dryer, where T'_{dry} is the temperature of the flue gases leaving the dryer. The water evaporated is given by:

$$\dot{m}_{water} = (\dot{m}_{db} + \dot{m}_{water}) \cdot M_0 \quad (3.8)$$

Thus,

$$\dot{m}_{water} = \dot{m}_{db} \cdot \frac{M_0}{1 - M_0} \quad (3.9)$$

where $\dot{m}_{db}$ is the flow rate of bone-dry biomass and M_0 is the fractional initial moisture content of the biomass on wet basis.

The limiting auto-thermal condition, defined by case B in Figure 3.2, can thus be expressed by equating the heat available from the hot flue gases with the heat required for torrefaction and drying, as in Eq. (3.11) where α is the fractional biomass weight loss:

$$\text{Biomass} \xrightarrow{k_{tor}} \alpha \cdot \text{Volatiles} + (1 - \alpha)\ \text{Char} \quad (3.10)$$

$$\dot{m}_{db} \cdot \alpha \cdot HHV_{tor} \cdot \xi_{com} = \dot{m}_{db} \cdot \Delta H_{tor,N_2}(T_{tor})/\xi_{tor} - \dot{m}_{db} \cdot \frac{M_0}{1 - M_0} \cdot Q_{dry}/\xi_{dry} \geq 0 \quad (3.11)$$

Eq. (3.11) can be reduced to (3.12).

$$\alpha \cdot HHV_{tor} \cdot \xi_{com} - \frac{\Delta H_{tor,N_2}(T_{tor})}{\xi_{tor}} - \frac{M_0}{1 - M_0} \cdot Q_{dry}/\xi_{dry} \geq 0 \quad (3.12)$$

3.2.1 Heat of torrefaction

The reaction heat of torrefaction has been measured experimentally and predicted by models in several studies (summarized in Table 3.1), and its value varies widely from 255kJ/kg (endothermic) to -3500kJ/kg (exothermic). The reported heat of torrefaction depends on the composition of the woody biomass, and the torrefaction conditions. The biomass usually contains around 30% hemicellulose, 50% cellulose, and 20% lignin; the proportions vary between softwood and hardwood species. Thermogravimetric (TGA) analyses have revealed that hemicellulose is the most active component, decomposing between 200℃ and 300 ℃; cellulose degrades between 275℃ and 350℃; and lignin is the least reactive and decomposes over the range from 200℃ to 600℃ [83]. Many experiments have revealed that the decomposition of hemicellulose is slightly exothermic [83], [84], [85], [86]. Cellulose decomposes via competing and overlapping endothermic volatile formation and exothermic char formation [83], [87], [85], [88], [89], [90]. Rath et al. [83] suggested that the overall heat of biomass pyrolysis depends on the competition between exothermic char formation and endothermic volatile formation, as shown in Eq. (3.13) [83]. The same observations are also reported by Milosavljevic et al. [88] and Mok and Antal [87], [90]. The trends of the char formation and volatile formation are highly dependent on operating conditions. Rath et al. reported that in a biomass pyrolysis experiment using differential scanning calorimetry (DSC), the char yield is clearly higher when a larger sample is used, and when the calorimeter sample is fitted with a cap. Possibly because the use of lid hinder the evaporation and diffusion of volatiles, thus enhancing the char formation reactions. Other operating conditions may also enhance char formation, such as rapid heating [88] and elevated pressure [87]. Many studies observed an apparent shift from endothermic to

exothermic behavior as the reaction proceeds [21], [22], [67], [92], [83], [84], suggesting that during biomass pyrolysis, volatile formation is dominant at the beginning, whereas char formation becomes stronger in the later stages.

$$H_{tor}(T_{tor}) = \Delta H_{exo}\beta_{char} + \Delta H_{endo}(1 - \beta_{char}) \quad (3.13)$$

where β_{char} is the mass fraction of char in the product with units of (kg char/kg biomass); ΔH_{exo} and ΔH_{endo} are the exothermic heat of char formation and endothermic heat of volatile formation, respectively.

Table 3.1 Experimentally measured or deduced enthalpy of reaction for torrefaction and pyrolysis

Reference	Enthalpy of reaction	Temperature range ºC	Feedstock	Method
[93]	87 kJ/kg willow at 250ºC with RDT of 30min, 12.8% wl; 124 kJ/kg at 300ºC, RDT 10min, 33.2% wl.	250, 300	Willow	ASTM bomb calorimetry
[67]	150 to1350 kJ/kg biomass with -130 kJ/kg (at 240 ℃, RDT 30 min, with 18% wl) and -230 kJ/kg (at 280 ℃, RDT 30 min and 32% wl).	230-280	Beech	Estimated through analysis of products and reactant
[92]	148 to -199 kJ/kg biomass; more exothermic behavior for increasing degree of torrefaction and a slightly lower heat consumption for a higher torrefaction temperature.	270-300	Beech	Measurement of heat consumption of lab scale continuous screw reactor
[83]	Exothermic char formation competing with endothermic volatile formation: +936 (beech) and +1277 (spruce) kJ/kg for volatile formation; -3525 (beech) and -3827 (spruce) kJ/kg for char formation	100-500	Spruce, Beech	DSC
[94]	-293 to +1673 kJ/kg mass loss	275-470	Beech	Deduced from experimental data with the single particle model
[95]	+200.8kJ/kg biomass	470	Beech	Deduced from experimental data with the single particle model
[96]	+255 to -20kJ/kg biomass	300-600	Wood Sawdust	Deduced from experimental data with the single particle model
[97]	+25 kJ/kg char, tar, gas	200-850	Various	Deduced from experimental data with the single particle model
[98]	-55.3 to +176 kJ/kg biomass	100-600	Pine, oak Sawdust	Deduced from experimental data with a model of packed sawdust reactor
[91]	+275 to +540 kJ/kg biomass	200-300	Willow	Friedl correlation modeling
	-182 to -387 kJ/kg biomass			IGT correlation modeling
	+150 to -50 kJ/kg biomass			Boie correlation modeling

DSC: differential scanning calorimetry
(-) exothermic, (+) endothermic.
RDT: mean residence time
wl: biomass weight loss

3.2.2 Drying heat

Theoretical energy consumption of the drying process can be estimated as the sum of sensible heat required to raise the temperature of wet biomass to the drying temperature from its initial temperature, and the latent heat required to evaporate the moisture content. The energy required for water evaporation ranges from 2265 (at 100°C, 1atm) to 2570 kJ/kg (25°C) water evaporated depending on the wet-bulb temperature [99].

However, the real operation typically consumes significantly more energy than the theoretical value, usually more than 1.5 times of the thermodynamic minimum value. This is due to the real barriers to moisture removal: additional heat required to break the bound and release bound moisture, unavoidable heat losses, low heat transfer rate, etc. Various measures are available to improve the energy efficiency of the dryer. One way is to improve the heat and mass transfer rates by using a device such as a fluidized bed or rotary drum. Another method is to recover the latent heat of the water. Drying technologies developed to recover the latent heat include multi-stage drying, heat pump drying, and self-heat recuperative drying technologies as shown in Table 3.2. However, applying the advanced drying technologies require additional capital investment. Therefore, there exists a trade-off between energy saving and capital cost.

Table 3.2 Energy consumption of different advanced drying technologies

References	Specific energy consumption (kJ/kg water evaporated)	Drying Technology	Recovery of latent heat of water	Recovery of sensible heat of water
[100]	3100-4000	Conventional drying	No	No
[101]	1000-2000	Heat pump drying	Yes	Part of
[102]	2480-2570	Conventional	No	No
[103]	2500-3000	Conventional heat	No	No

References	Specific energy consumption (kJ/kg water evaporated)	Drying Technology	Recovery of latent heat of water	Recovery of sensible heat of water
	500-900	Self-heat recovery with		
	100-300	Self-heat recuperative	Yes	Yes
	60-100	Self-heat recuperative	Yes	Yes
[104]	2810-3000	Hot air drying	No	No
	3000-5000	Vacuum drying	No	No
	900-3600	Heat pump drying	Yes	No

In the current study, for a preliminary analysis, we have considered two typical drying technologies for evaluating the system with auto-thermal operation: 1) conventional drying technology, assumed to have relatively low heat loss (20%) but without recovering the latent heat, with 3.0 MJ/kg water evaporated, and advanced drying technology with 1.0 MJ/kg water evaporated.

3.3 Results

3.3.1 Torgas and biomass HHVs at different torrefaction conditions

The torgas HHV, calculated based on Table 2.4, ranges from 3.23 MJ/kg to 8.04 MJ/kg, increasing with increasing torrefaction temperature and mass loss (which is determined by torrefaction temperature and residence time) due to decrease in the fraction of the noncombustible components in the gas mixture, primarily water and CO_2. The predicted values and their dependence on temperature in the current study compare well with published experimental results [47], [52], [67], [71]. Stelt et al. reported values of 1- 8MJ/kg for the LHV of volatiles produced during beech and willow torrefaction [67]. Prins et al. [47] estimated the LHV of torgas ranges from 4.9 to 10.6MJ/kg. Based on the experimental data of Prins et al., Bates and Ghoniem [52] applied the Boie's correlation for the HHV and

reported that for mass loss between 0 and 50%, the average HHV of the total volatiles ranges from 4.43 to 10.6MJ/kg. In this study, least square regression of literature HHV data has been carried out to identify the dependence of torgas HHV on torrefaction temperature and weight loss as shown in Eq. (3.14) and Figure 3.4 (a).

$$\mathrm{HHV_{torgas}} = 9.11 \times 10^{-4} \cdot \mathrm{T}^{1.76} \cdot \mathrm{wl}^{0.64} \tag{3.14}$$

where T is the temperature in ^{o}C and wl is fractional biomass weight loss during torrefaction.

Figure 3.4 (b) shows the variation of biomass HHV with torrefaction temperature and residence time (which determine the biomass weight loss). The biomass HHV ranges from 22 MJ/kg to 36 MJ/kg due to the increase in carbon content and decrease in ash content, and the biomass HHV tends to increase with increasing temperature and residence time. Temperature has a more significant effect on biomass HHV than residence time. The calculated HHV is slightly higher than the experimental value, which is usually around 15 MJ/kg for wood, 22 to 28MJ/kg for the torrefied wood and 36 MJ/kg for coal. This deviation is due to (a) the neglect of heat loss for biomass HHV calculation and (b) discrepancies between different correlations to quantify biomass HHV. The quantified biomass HHV here is based on models without heat loss of the biomass combustion taken into consideration, but the experimental evaluated biomass HHV is usually not adiabatic. If a 20% or higher heat loss is considered, the calculated HHV of torgas and biomass will be close to the reported experimental value. Boie, Dulong, Grummel and Davis, Mott and Spooner, and IGT correlations predict results significantly from each other [44]. Ohliger et al. [92] evaluated the LHV of torrefied beech wood and found that the LHV ranges from 21 to 25.6 MJ/kg and increases when biomass weight loss increases from 0.2 to 0.5.

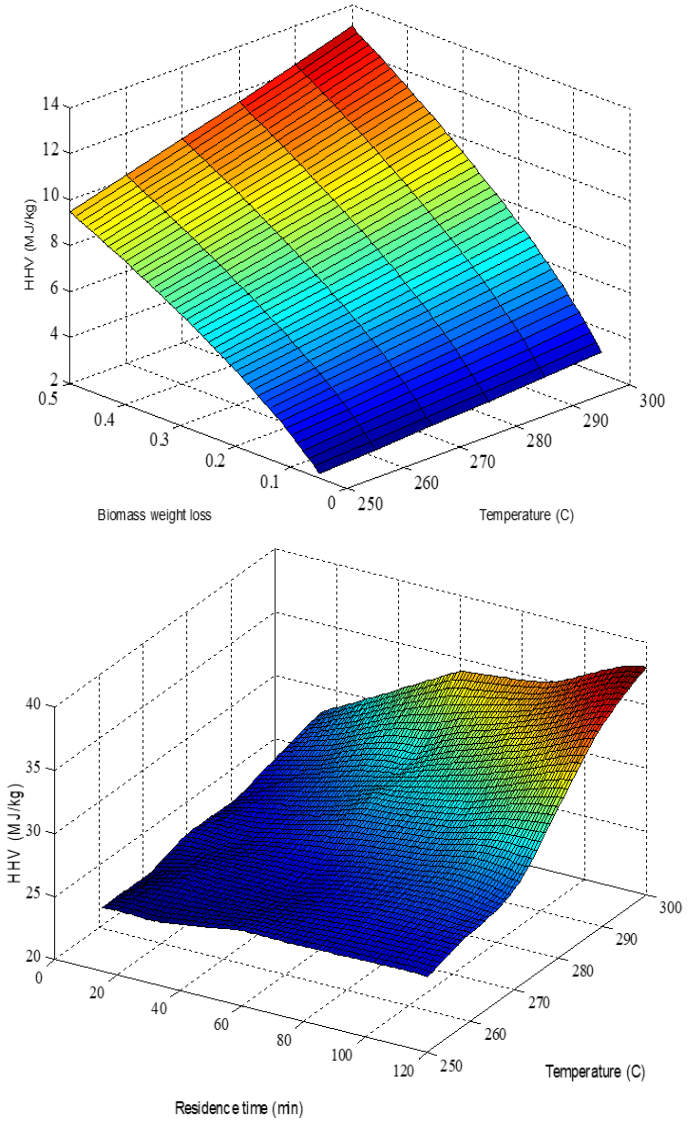

Figure 3.4 (a) Calculated torgas HHVs as a function of torrefaction temperature and biomass weight loss; (b) calculated torrefied biomass HHVs as a function of torrefaction temperature and residence time

3.3.2 Solid and volatile product energy yield

The solid product energy yield η_s and volatile product energy yield η_v are indicators of the energy efficiency of the biomass fuel production process, which are defined by Eq.s

(3.15) and (3.16). For a solid product desired process, a higher η_s is expected. Similarly, for a volatile product desired pyrolysis process, a higher η_v is expected.

$$\eta_s = (1 - \alpha) \cdot \frac{HHV_{torb}}{HHV_{db}} \tag{3.15}$$

$$\eta_v = \alpha \cdot \frac{HHV_{torgas}}{HHV_{db}} \tag{3.16}$$

Here HHV_{db} is the initial dry biomass HHV (MJ/kg), HHV_{torb} is the instantaneous HHV of torrefied biomass (MJ/kg) and HHV_{torgas} is the instantaneous HHV of torgas at different torrefaction conditions.

Figure 3.5 shows the calculated solid and volatile energy yields from this study, in comparison with other studies. The solid energy yield in the current study shows a linear decrease with increasing biomass weight loss at 250 ºC to 300ºC and appears higher than the values in other studies. Here, torrefied wood pellets are the desired product, so the lower biomass weight loss, the better. However, auto-thermal operation depends on the torgas HHV to provide the heat of torrefaction, these two parameters are determined by torrefaction conditions (temperature, T, and biomass weight loss, wl). Therefore, there should be a set of torrefaction operating boundaries, defined by temperature and weight loss (T, wl) that enable auto-thermal operation. Optimal operation corresponds to conditions within this envelope at which the highest η_s can be achieved. This topic will be investigated in later sections.

The volatile energy yield at 280 ºC is presented as an example., which increases sharply with biomass weight loss and shows a similar trend, but with lower actual values, in comparison with the work presented by Bates et al. [52].

The over-estimation of the solid HHVs and under-estimation of torgas HHVs are probably due to (a) the use of different HHV correlations (Mott and Spooner model in present study and Boie's and Friedl's model in Bate's work) and (b) composition difference of the volatile components between the current study and the others [52].

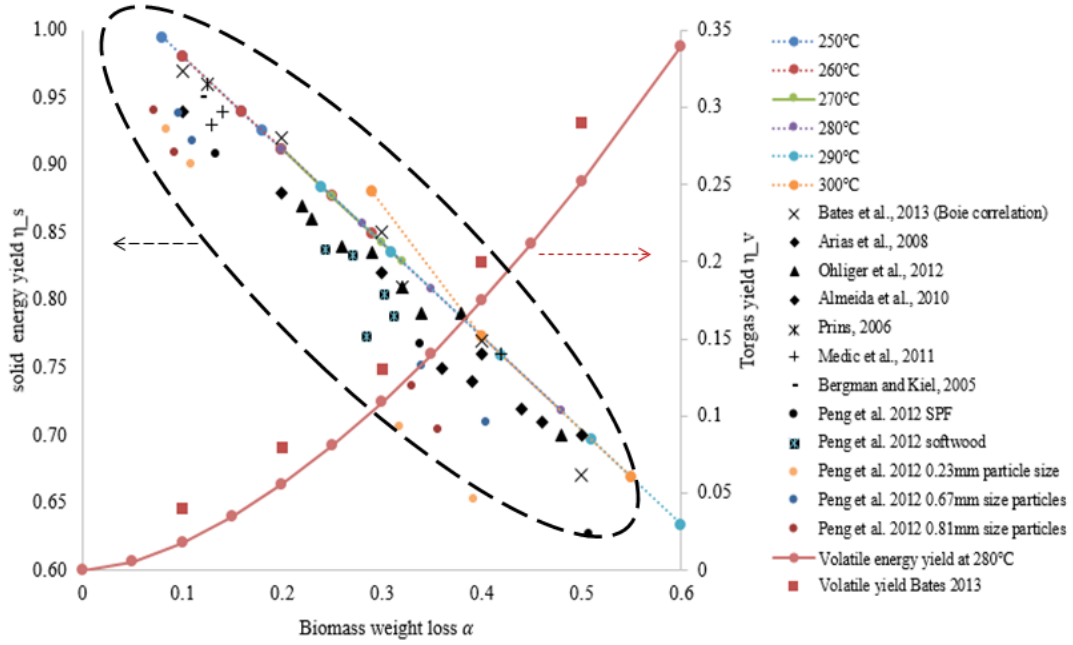

Figure 3.5 Solid and volatile energy yields at different biomass weight loss and torrefaction temperature in comparison with the literature data

3.3.3 Torrefaction reaction heat

Figure 3.6 (a) shows the torrefaction reaction heat $\Delta H_{tor}(T_{tor})$, as defined by Eq. (3.6), as a function of torrefaction temperature and biomass weight loss. Torrefaction reaction heat has a linear relationship with the biomass weight loss at different torrefaction temperatures: with a positive slope at 250℃ and 260℃ and negative slope at 270℃, 280℃, 290℃, and 300℃. In addition, the overall torrefaction heat appears endothermic when

torrefaction is operated at 250℃ to 270℃, and exothermic when torrefaction is operated at 280℃ to 300℃ with biomass weight loss higher than 23%. The phenomenon may be explained by the competition between volatile-forming (endothermic) and char-forming (exothermic) processes: the former should be dominant at the beginning of biomass decomposition, while the later dominant when the temperature and biomass weight loss increase. A similar phenomenon has been reported in [21], [22], [67], [92], [83] and [84], as aforementioned. This study differs in predicting that the shift from endothermic to exothermic reaction occurs at 23% biomass weight loss, whereas it was observed by Rath et al. at 21% of biomass weight loss when the temperature is above 280℃ and by Bates et al. [52], [91] that the shift happened above 280℃ without biomass weight loss indicated.

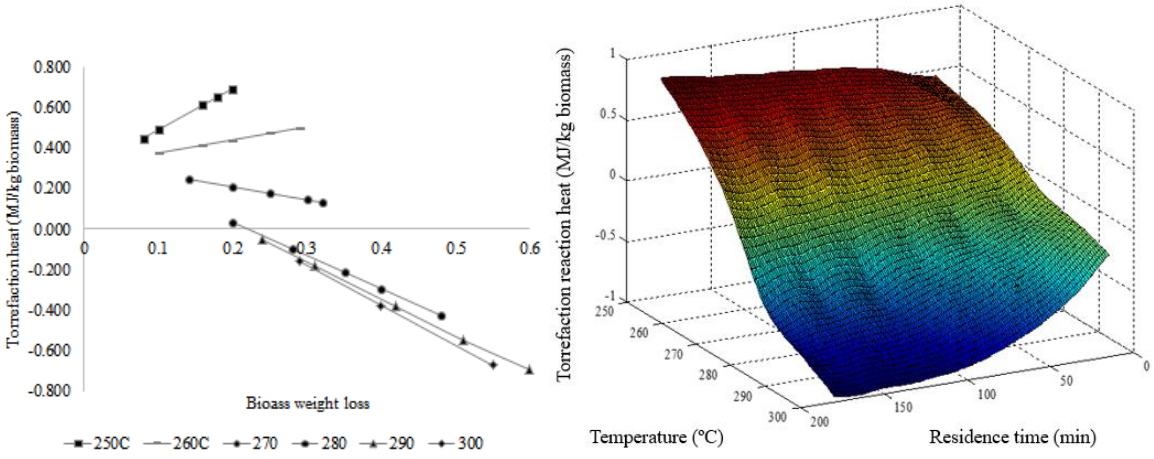

Figure 3.6 (a) torrefaction heat at different torrefaction temperature and biomass weight loss; (b) torrefaction heat at different temperature and residence time

The linear relationship between torrefaction heat and biomass weight loss at different temperatures is expressed by Eq. (3.17), with fitted a and b values summarized in Table 3.3.

Figure 3.6 (b) shows that torrefaction reaction heat decreases with increasing torrefaction temperature and residence time, as shown in Figure 3.6 (a).

$$\Delta H_{tor}(T_{tor}) = a\,(T) \cdot wl + b\,(T) \tag{3.17}$$

Table 3.3 Linear correlations between torrefaction temperature and torrefaction heat

Torrefaction temperature ℃	a(T)	b(T)
250	2.05	0.29
260	0.65	0.31
270	-0.64	0.34
280	-1.65	0.36
290	-1.80	0.38
300	-1.99	0.42

Table 3.4 Endothermic and exothermic heat of torrefaction at different temperatures in this study and literature data

	Present work				Rath et al. [21]	
	270 ºC	280 ºC	290 ºC	300 ºC	spruce	beech
ΔH_{endo} (MJ/kg biomass)	0.39	0.36	0.38	0.42	1.28	0.94
ΔH_{exo} (MJ/kg biomass)	-0.30	-1.29	-1.43	-1.57	-3.8	-3.53

3.3.4 Heat requirement of torrefaction process

In addition to the torrefaction reaction heat $\Delta H_{tor}(T_{tor})$, heat requirement of the torrfaction process $\Delta H_{tor,N_2}(T_{tor})$ also includes the sensible heat needed to raise the N_2 flow to the torrefaction temperature. Figure 3.7 shows the heat requirement of the torrefaction process with 70 kg N_2 /g as a representative value, to show the extent to which the heat requiremetns exceeds that in Figure 3.6 (b). Rath et al. [21] also analyzed the influence of N_2 flowrate on the heat required for biomass pyrolysis and observed an increased heat requirement when the N_2 flowrate is increased.

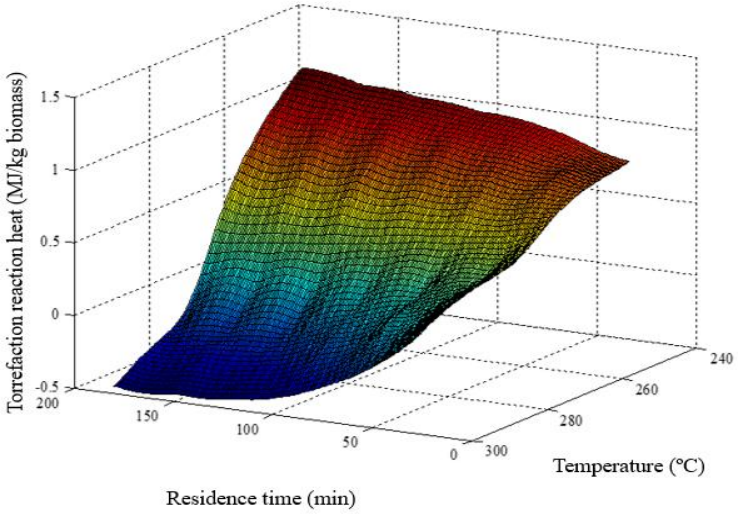

Figure 3.7 Heat requirement of torrefaction process with N_2 mass flowrate =70kg N_2/g biomass

3.3.5 System auto-thermal boundaries

The torrefaction operating conditions are the key to auto-thermal operation of the overall process. Therefore, analysis of the auto-thermal boundaries will be based on the logic of "under what torrefaction operation conditions (temperature, biomass weight loss or mean residence time), can the thermal system achieve auto-thermal operation?"

The requirement for auto-thermal operation of the system can be expressed by combining Eq. (3.12) and Eq. (3.14), leading to Eq. (3.18).

$$\alpha \cdot (9.11 \times 10^{-4} \cdot T^{1.77} \cdot wl^{0.64})/\xi_{fluegas} - (a(T) \cdot wl + b(T))/\xi_{tor} - (\frac{M_0}{1 - M_0}) \cdot Q_{dry} \geq 0 \quad (3.18)$$

Here the coefficient a(T) and b (T) at different temperature are taken from Table 3.3. 20% of heat losses are considered for the drying, torrefaction, and combustion processes.

3.3.5.1 Influence of drying heat

Two cases are carried out to investigate the influence of drying heat: case (a) with biomass initial moisture content of 50wt%wb (equivalent to 67wt%db) and case (b) with biomass initial moisture content of 33wt%wb (equivalent to 50wt%db). Both of two cases are assumed with no N_2 usage in torrefaction. Conventional (3 MJ/kg water evaporated) and advanced (1 MJ/kg water evaporated) drying technologies are applied in those two cases. Conventional drying system does not re-use the latent heat of water that evaporated from biomass, while advanced drying technology recycles the latent heat of water to improve energy efficiencies. Commonly applied advanced drying technologies include heat pump, self-recuperative drying, multi-stage drying etc.

Figure 3.8 illustrates the auto-thermal operation boundaries of the two cases. It is indicated that in comparison with the conventional drying technology, when the advanced drying technology is applied, the thermal system can achieve auto-thermal at low torrefaction temperature and low biomass weight loss. For example, in case (b), if torrefaction is operated at 300 °C, to ensure auto-thermal operation, about 15% of biomass weight loss has to be achieved when advanced drying technology is applied. However, if conventional drying technology is applied to this system, biomass weight loss has to be 23% to avoid use of additional fuel. Higher biomass weight loss will lead to a lower solid product energy yield, which is not preferred for wood pellet production. Thus, application of advanced drying technology can help achieve high product yield but needs a higher capital investment and higher electricity usage to recover latent heat of water. Thus, there is a trade-off between the use of advanced drying technology and additional fuel usage.

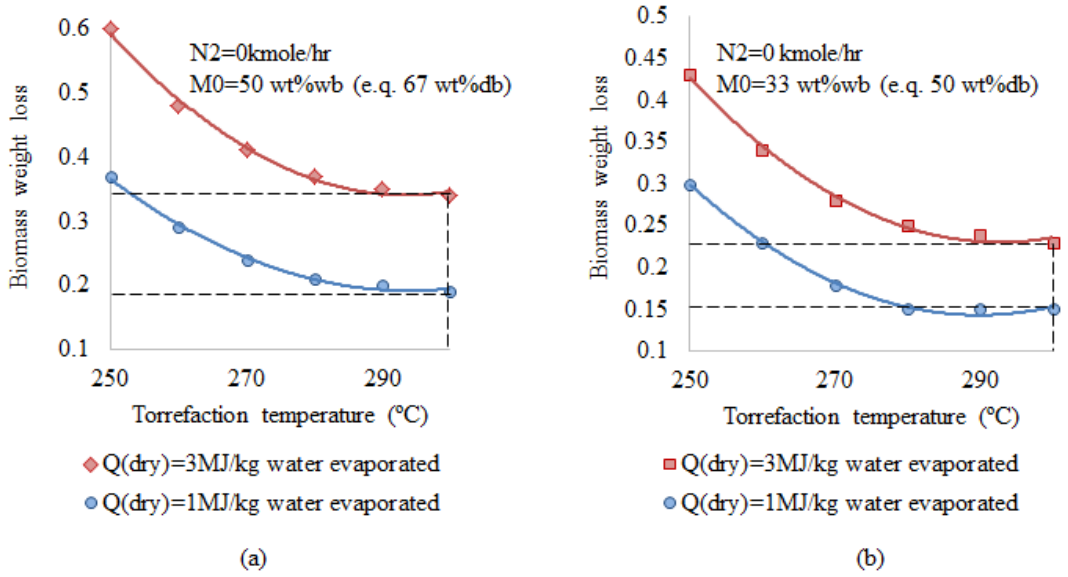

Figure 3.8 Auto-thermal operation boundaries of biomass torrefaction process using conventional drying technology and advanced drying technology: (a) case with biomass initial moisture content 50wt%wb; (b) case with biomass initial moisture content 33wt%wb

3.3.5.2 Influence of N_2 flow

Figure 3.9 shows the N_2 flowrate influences on process auto-thermal operation boundaries, with the boundaries being defined by torrefaction temperature and biomass weight loss: case (a) with biomass initial moisture content of 50wt%wb, case (b) with biomass initial moisture content of 33wt%wb, and both of two cases applied conventional drying technology. It is revealed that avoiding the use of N_2 enables the process to be auto-thermal at lower torrefaction temperature and lower biomass weight loss, hence leading to a higher solid product yield. For example, when torrefaction temperature is 300 °C, the system can achieve auto-thermal operation with 33% and 23% of biomass weight loss for case (a)

and (b) without use of N_2 and need higher levels of biomass weight loss when N_2 is involved, 38% for case (a), and 28% for case (b), respectively.

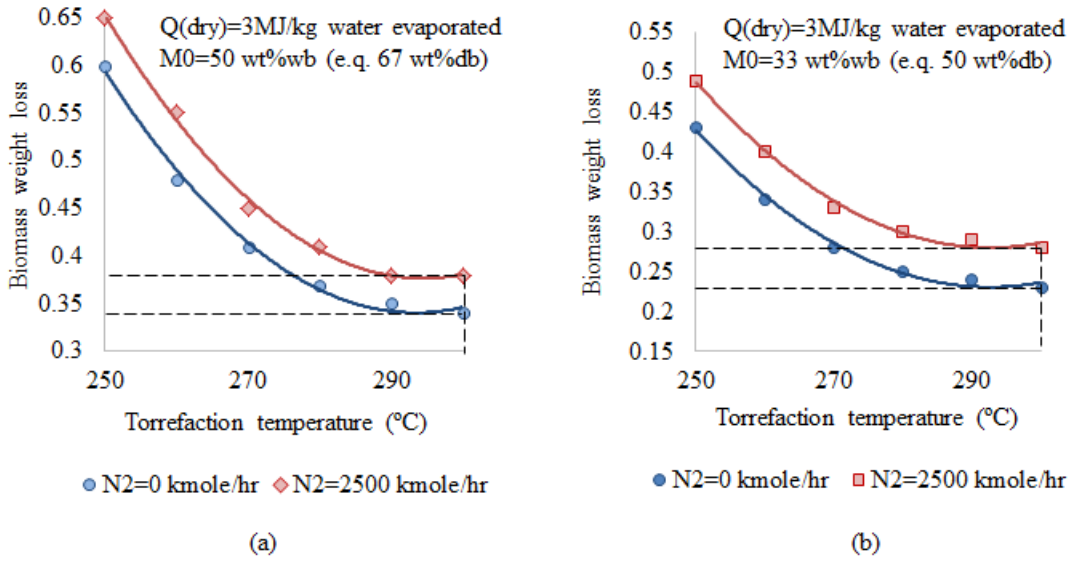

Figure 3.9 Influence of N_2 flowrate used for torrefaction on the torrefaction process auto-thermal boundary (a) case with biomass initial moisture content 50wt%wb; (b) case with biomass initial moisture content 33wt%wb

It should be noted that under the flowsheet configuration as shown in Figure 3.1, some N_2 flow is required to: (a) provide an anaerobic environment for the torrefaction, and (b) to fluidize the particles in the fluidized bed, or to increase the heat transfer rate in a rotary drum reactor, usually in the range of 2 to 10 m/s. The N_2 flow rate is related to the operating constraints as well as the reactor size.

An improved configuration is proposed to avoid the use of N_2 as shown in Figure 3.10: part of the flue gases will be recycled to the torrefier to replace N_2. To further reduce the process operating cost, catalyst should be avoided for the combustion of volatiles by maintaining a high temperature in the combustor. To avoid biomass ignition, the flue gases

should pass through the shell side of the torrefier first before to the tube side. The recycled flue gases should be controlled to minimize its influences on torrefaction. Under this configuration, the recycle ratio of the flue gases and the torrefaction operating conditions are important design parameters which determines the process energy balances, heat and mass transfer, and hydrodynamics. Process simulation of TWP production processes under this configuration is carried out in Chapter 4, including detail reactor design and heat integration included.

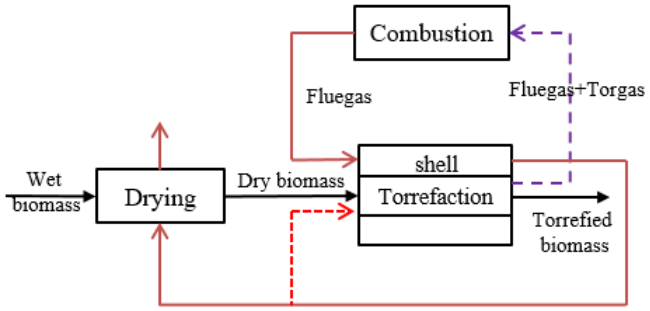

Figure 3.10 Improved flowsheet configuration of torrefaction heat integration

3.3.5.3 Impact of biomass moisture contents

Biomass initial moisture content determines the amount of water to be removed from the drying process, which in turn will influence the boundaries of auto-thermal operation. For given torrefaction conditions and drying technology, it is important to diagnose whether the system can achieve auto-thermal operation for a given biomass feedstock before real operation. The highest moisture content of the biomass M_{omax} on wet basis at which auto-thermal operation can be achieved with a given drying technology can be calculated by Eq. (3.19), which can be derived from Eq.s (3.12) and (3.18).

$$M_{omax} = \frac{1}{\frac{Q_{dry}}{\alpha \cdot HHV_{tor} * \xi_{fluegas} - \Delta H_{tor,N_2}(T_{tor})/\xi_{tor}} + 1} \quad (3.19)$$

Figure 3.11 shows values for M_{omax} for different drying technologies (a): Q (dry) =3.0 MJ/kg water evaporated; (b): Q (dry) =1.0 MJ/kg water evaporated. All the scenarios presented are assumed to use no N_2. For example, for a biomass feedstock with 50wt%wb of moisture content with the conventional drying technology, auto-thermal operation can be achieved if torrefaction is operated at 250ºC with at least 58% of biomass weight loss, or alternatively the torrefaction temperature can be increased to 280ºC with 35% weight loss. If the advanced drying technology is applied as shown in Figure 3.9 (b), the system can achieve auto-thermal operation when torrefaction is carried out at 250ºC with 38% biomass weight loss. It should be noted that the highest moisture content M_{omax} would be different for other scenarios with different biomass composition, torrefaction conditions, biomass torrefaction kinetics, drying technology, heat loss, and N_2 flowrate. The present work provides a method to pre-determine whether it is feasible to have the system operated auto-thermally, so as to select appropriate design and operation strategies.

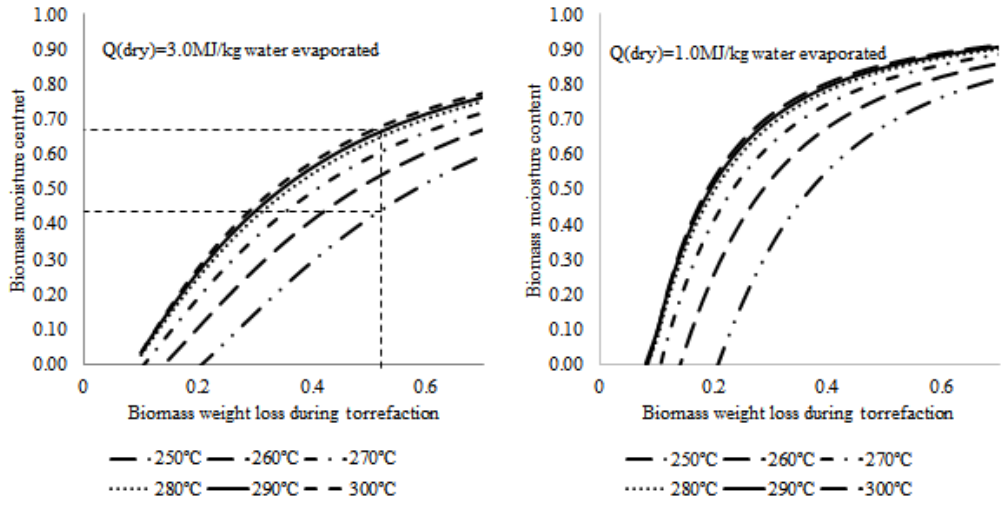

Figure 3.11 Highest biomass moisture content (on wet basis) for achieving auto-thermal operation with different drying technologies and torrefaction conditions without N_2 use: (a): Q(dry)=3.0 MJ/kg water evaporated; (b): Q(dry)=1.0 MJ/kg water evaporated

3.4 Conclusions

In this chapter, the boundaries of the auto-thermal operation of the biomass torrefaction system have been defined and investigated. Several key parameters that influence the process auto-thermal operation are analyzed, which include drying technology, biomass initial moisture content, N_2 flowrate, and torrefaction conditions. Torgas and biomass HHVs, as well as the torrefaction reaction heat, are also estimated based on elemental changes.

It is found that torgas HHV and biomass HHV increase with torrefaction temperature and biomass weight loss. During torrefaction, solid product energy yield increases with lower biomass weight loss, while conversely, the gas product energy yield increases with higher biomass weight loss. Torrefaction reaction heat has a linear relationship with the biomass weight loss, with a positive slope at 250ºC and 260ºC, and negative slope at 270ºC to 300ºC.

In addition, there is a shift from endothermic to exothermic at 23% biomass weight loss at torrefaction temperatures of 270ºC to 300ºC, suggesting that volatile formation is dominant at the beginning and char formation is surpassed in the later torrefaction.

Sensitivities analysis of auto-thermal operation revealed that the advanced drying technology can help the system achieve auto-thermal at lower torrefaction temperature and residence time, thus leading to a higher process throughput and product yield with a relatively lower product HHV. Applying inert N_2 flow narrows the auto-thermal operation boundaries. To expand the auto-thermal operating boundaries, hot combustion flue gases can be recycled to replace N_2, which will be presented in Chapter 4.

Overall, the auto-thermal operation of the TWP production system varies for different biomass species and different operation conditions. Present work provides a general method to pre-diagnose the potential of auto-thermal for different systems.

Chapter 4: Comparison of different torrefied wood pellet production pathways

4.1 Introduction

The analysis carried out in this chapter stands from a producer point of view, aims to investigate several key issues the BC wood pellet producer would care: (1) which pathway (see Figure 4.1) is the best one to produce wood pellet (CWP and TWP)? The performances of these pathways are quantified in terms of the "3E" indices, namely energy consumption in "GJ primary energy input/GJ pellet produced" (simplified to GJ/GJ WPs), environmental index of GHG equivalent emissions in "gCO_2eq/GJ-pellet-produced" (gCO_2eq/GJ-WPs), and economic index of production costs in "$/GJ pellet produced" ($/GJ-WPs). (2) What are the key parameters that influence the wood pellet production "3E" metrics. (3) What are the minimum selling prices and investment returns of a TWP plant? (4) What are the social contributions of TWPs to BC? (5) What are the comparative advantages of BC TWP manufacturing?

The system boundaries for the metrics of energy consumption, GHG emissions, and production costs in this chapter are defined below:

- Only energy consumed during the operation of the plant is accounted, i.e. electricity used for operation of mechanical items if the system achieves auto-thermal operation, or electricity used for mechanical units and additional fuels for thermal units, such as natural gas or biomass, if auto-thermal operation is not achieved. Energy consumed for building the plants and the manufacturing of the equipment are not included.

- CHG emissions from plant operation, including electricity for operation of mechanical units and additional fuels for thermal system if required, and equipment fabrications, e.g. carbon steel used for dryers, torrefiers, combustors, hammer mills, pelleting machine, heat exchangers, air blowers, and rubber for belt conveyors, are included in the assessment. Emissions from building constructions and electricity used for office lighting and heating are not included.
- Both capital and operating costs are considered. Operating costs include raw material, utilities, labor and maintenance, operating charges, plant overhead, general and administrative costs, while capital investment covers equipment purchasing and setting, piping, civil, steel, instruction, electrical, insulation, paint, contract fee and others. Detailed descriptions of these categories are provided in Table C.3.

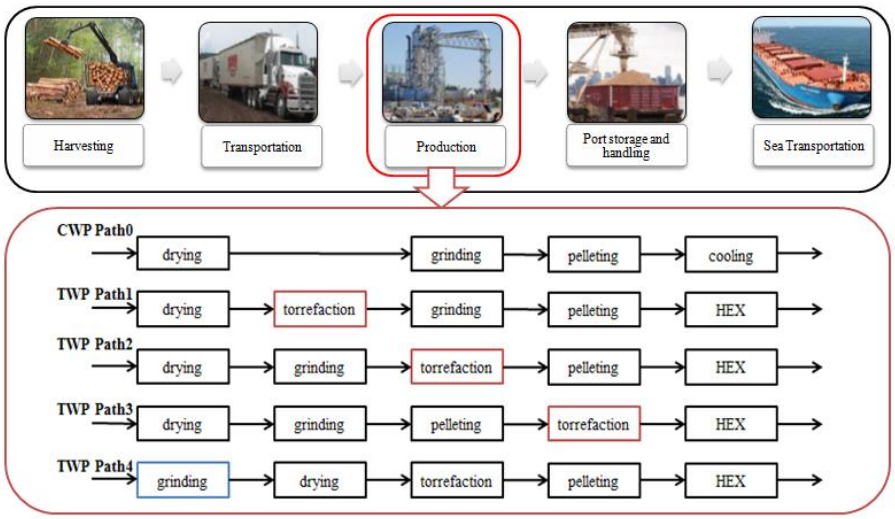

Figure 4.1 CWP and TWP production plant

4.2 Case study definition and key assumption

The case studies are based on a commercial scale wood pellet production plant located in Prince George, BC, Canada. For a fair comparison, all the pathways are determined to produce 10t/hr of wood pellet. The plant operates continuously for 24 hours per day and 333 days per year. In addition, to ensure uniform HHVs for the TWPs, torrefaction conditions are the same in Paths 1-4. Figure 4.2 shows the conceptual design of the flowsheets with information of the equipment type and mass flowrates in each unit according mass balances. Heat integration configurations are based on the "targeting case" as presented in Figure 1.3 (b) and Figure 3.10, in order to avoid the use of N_2 in the processes. As a first approximation, 80% thermal and mechanic efficiencies are considered for all the thermal and mechanics operations in the flowsheets. Table 4.1 summarizes the key assumptions for process simulations.

Table 4.1 Assumptions for techno-economic evaluation

Name	Units	Item
Plant location		Prince Gorge, BC, Canada
Life Cycle Period	Year/Days per	20/333/8000
Capacity	t wood pellet/hr	10
Heat and work efficiency		80%
Key operating cost categories		
Raw material costs (transported to pellet	$/dt	25
Operator	$/Hour	20
Supervisor	$/Hour	35
Electricity	$/KWH	0.06
Binder (sawdust)	$/dt	25

dt: dry tonne

The raw material is assumed to be pine wood chips with an initial average particle size of 20 mm and average moisture content (MC) of 50% on a dry basis (db). Table 4.2 shows the composition of the wet biomass, which is used to calculate the biomass thermal properties e.g. enthalpy and mass density as the mathematical correlations are provided in Appendix A .

Table 4.2 Composition of biomass feedstock

Description	Elements	Biomass
Proximate analysis weight % (dry basis db)	Moisture	50
	Fixed carbon	17
	Volatile Matter	82.88
	Ash	0.12
Ultimate analysis weight % (dry basis)	Ash (w_A^d)	0.12
	Carbon (w_C^d)	50.01
	Hydrogen (w_H^d)	6.07
	Nitrogen (w_N^d)	0.15
	Chlorine (w_{Cl}^d)	0
	Sulfur (w_S^d)	0
	Oxygen (w_O^d)	43.77
SULFANAL analysis Weight % (dry basis)	Pyritic (w_{Sp}^d)	0
	Sulfate (w_{St}^d)	0
	Organic (w_{So}^d)	0

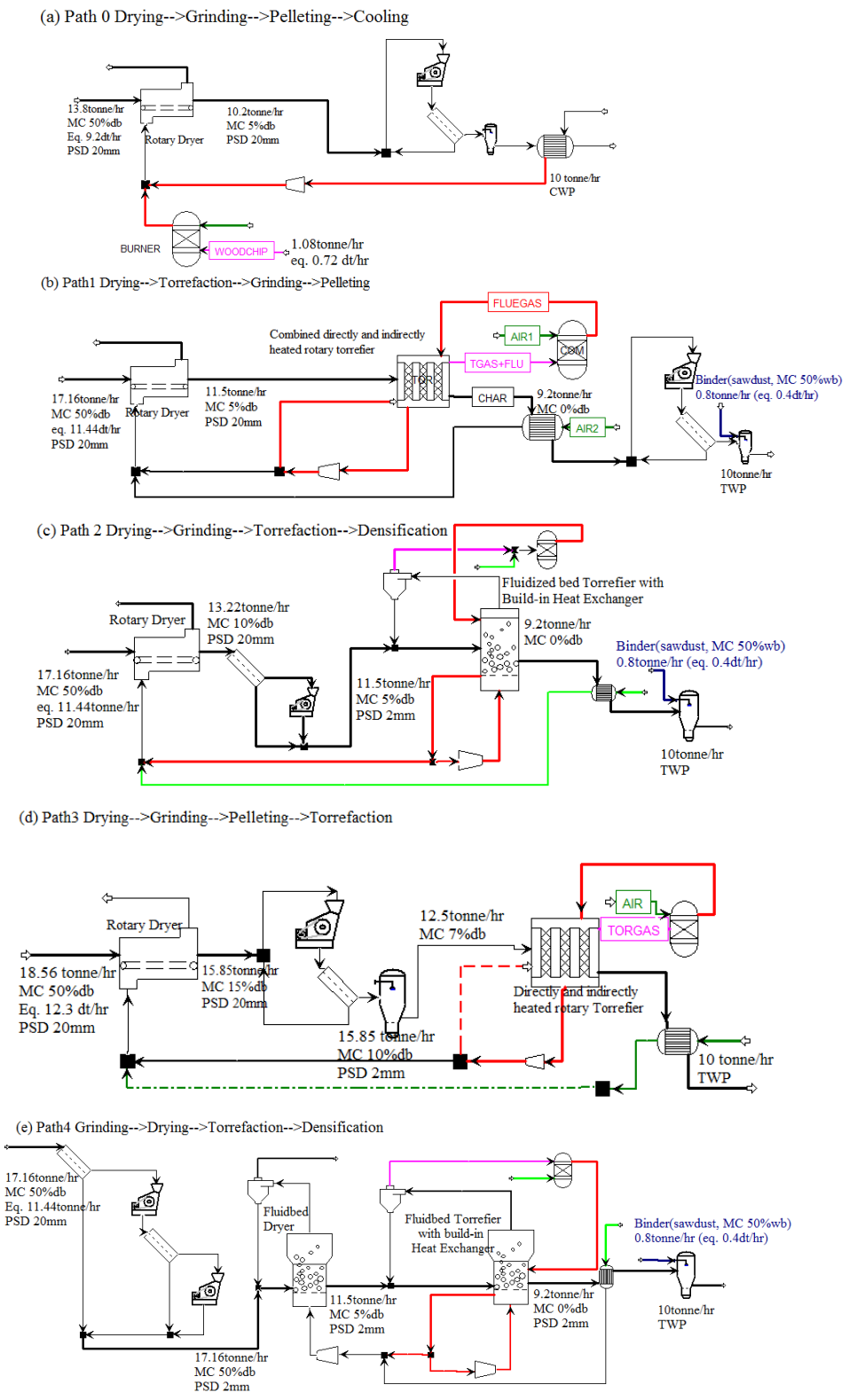

Figure 4.2 Conceptual design of paths 0 to 4 with selected equipment, mass flow, and integrated heat flow

4.2.1 Torrefaction

The torrefier configurations considered in this chapter are illustrated in Figure 1.3 (b) and Figure 3.10, with direct and indirect heating for both fluidized and rotary torrefiers. The design principles of the torrefier and integrated thermal system are:

(1) To avoid the use of N_2 by recycling combustion flue gases. The recycled flue gases must satisfy the following two constraints:
    (a) the temperature of the flue gases that contact with solid biomass should be lower than the biomass ignition temperature (usually 350 ºC [105], [106]);
    (b) O_2 content in the flue gases should be lower than 10% to avoid severe biomass oxidation [107].

(2) The combustion temperature should be as high as possible to maintain volatiles combustion without the need of catalyst. This can be achieved by adjusting the temperature and particle residence time of the torrefaction reactor.

(3) To achieve auto-thermal operation, or, if not achievable, to recover heat as much as possible to reduce additional fuel usage.

The key design parameters of the thermal system are the torrefaction operation conditions, including temperature and biomass weight loss, and the flue gases recycle ratio. As shown in Figure 3.9 (b) and Figure 3.10 (b), for biomass initial moisture content of 50wt%db, there are many sets of torrefaction operation conditions that enable auto-thermal operation, either at low temperature but with high biomass weight loss, i.e. 270 ºC, with 28% weight loss, or at high temperature with low biomass weight loss, i.e. 300 ºC, with 23% biomass weight loss. Since the torrefied biomass (char) is the product, as discussed in connected with Figure 3.5, the solid product energy yield is to be maximized implying low

biomass weight loss. Therefore, torrefaction should be operated at high temperature to minimize biomass weight loss. An initial operating condition is set at 300 ºC. It should be noted that this is the mean temperature of the solid phase in the torrefier. In the fluidized bed, the solid phase is assumed to be perfectly mixed, so that all the particles are at 300 ºC. In the rotary torrefier, the solid phase is in plug flow, so that its temperature may change along the horizontal direction; the mean temperature of inlet and outlet solids is therefore designed to be 300 ºC, and the torgas HHV and torrefied biomass HHV are evaluated for this temperature. According to Figure 3.9 (b), when torrefaction is carried out at 300 ºC, the system can achieve auto-thermal operation with 23% of biomass weight loss without N_2 and flue gases recycling. For the configuration shown in Figure 4.2, the system is expected to achieve auto-thermal operation with less than 23% of biomass weight loss, due to recycling of the hot flue gases.

Following a preliminary scoping simulation, it was found that when torrefaction is carried out at 300°C with 20% weight loss, with part of the flue gases recycled to the torrefier, the system can achieve auto-thermal operation. Also, combustion of torgas can be sustained without catalyst. For details of the flowsheet, flue gases recycle ratio at different configurations, hydrodynamics, and temperature profiles of solid and gas phases, the readers are referred to Appendix D . The torgas is combusted and integrated with torrefaction and drying in paths 1, 2, 3, and 4. For torrefaction of wood chips, rotary torrefiers with direct and indirect heating are used in paths 1 and 3, respectively. Fluidized bed torrefiers with immersed heat exchangers are used for torrefaction of sawdust particles in paths 2 and 4.

4.2.2 Drying

The drying goals are different in different pathways. For the cases when drying is followed by torrefaction, the biomass is required to have all of its moisture removed, thus the drying target is assumed as MC 0wt%db. For the cases that drying is followed by grinding, the drying target is set as MC 15wt%db [108].

Directly heated rotary dryers are used to dry the large wood chips (20 mm) in Paths 0-3. A fluidized bed dryer is applied to dry sawdust particles (1 mm) used as the raw material in Path 4. The drying gas is a mix of flue gases and air. Air flowrate and the biomass mean residence time are the design parameters for the dryers, as shown in Figure 4.3. Since this study focuses on the overall performances of the whole flowsheet, rather than unit operation conditions, only one set of air flowrate and mean residence time are analyzed for the drying processes. Details of the drying processes are provided in Appendix D .

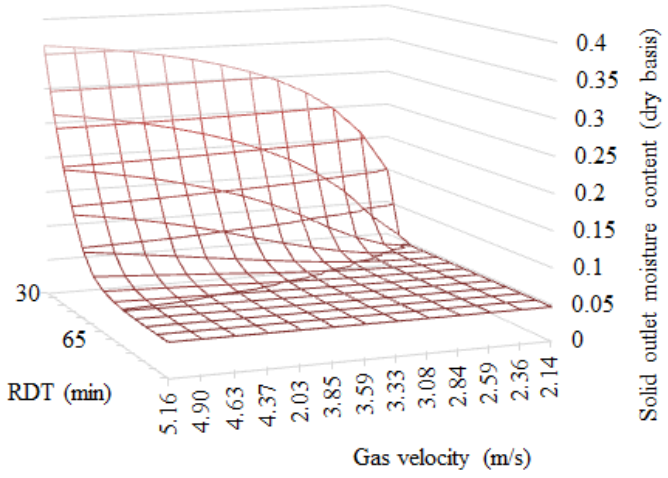

Figure 4.3 Drying process design parameters: biomass mean residence time and drying air gas velocity influence on the drying effect

In Paths 1-4, the drying heat is provided by recycled flue gases. In Path 0, the wet wood chips are burned to provide heat for the drying process, which mass flowrate needs to be quantified. In Path 0, 3.6 t/hr of water is needed to be removed in order to reduce the moisture content of feedstock from MC 50wt%db to MC 15wt%db. Generally, the drying process energy consumption ranges from 3 to 5 MJ/kg water removed. Here, conventional drying technology is applied, it is assumed that the drying heat is 4 MJ/kg water removed. The flow rate of the wood chips needed for the drying operation is calculated as 1.08 t/hr (equal to 0.72 dt/hr) as shown in Eq. (4.1). These wood chips consumptions are grouped to raw material consumptions. Thus, in Path 0, the total raw material consumption is 14.88 t/hr (equal to 9.92 dt/hr).

$$\dot{m}_{wc} = \left(3.6 \frac{\text{t water}}{\text{hr}}\right) \cdot \left(4 \frac{\text{GJ}}{\text{t water removed}}\right) / \left(13.36 \frac{\text{GJ}}{\text{t}}\right) \quad (4.1)$$

4.2.3 Grinding

The grinding process is carried out to reduce the biomass particle size from 20 mm to 1 mm. The commercial-scale hammer mills are applied for biomass samples with different physical properties: MC 15wt%db for Paths 0, 2, 3, torrefied biomass (torrefied at 300°C with 20% biomass weight loss) for Path 1, MC 50wt%db for Path 4. Key parameters of biomass grinding for different pathways are summarized in Table 4.3, with detail discussions of the specific energy consumption presented in section 2.2.4. Hammer mill driven power is selected according to equipment supplier's website [109], [110]. Required number of machines is calculated according to Eq. (2.8). HHVs of the CWP and the TWP are 17 GJ/t and 21 GJ/t according to Mott and Spooner's correlation with a 20% heat loss considered.

The electricity energy used for the biomass grinding to produce 1 GJ of pellet product is calculated as Eq. (4.2).

$$E_{grinding} = \frac{spe_{grinding,MC} \cdot \dot{m}_{grinding}}{HHV_{WP} \cdot \dot{m}_{WP}} \quad (4.2)$$

Table 4.3 Key parameters of the grinding processes for CWP (Path 0) and TWP (Paths 1-4) production pathways

Path	$\dot{m}_{grinding}$ (t/hr)	Biomass properties	$spe_{grinding,MC_i}$ (MJ/t)	HHV_{WPs} (GJ/t)	$\dot{m}_{WPs}$ (t/hr)	Driven power (kw) [109], [110]	Hammer mill number
Path	10.2	MC 15wt%db	427	17	10	400	3
Path	10	Torrefied	38	21	10	120	1
Path	13.22	MC 15wt%db	427	21	10	400	4
Path	15.85	MC 15wt%db	427	21	10	380	5
Path	17.16	MC 50wt%db	854	21	10	400	10

$\dot{m}_{grinding}$: biomass mass flowrate in the grinding machine
MC: biomass moisture content
$spe_{grinding,MC_i}$: specific energy consumption of grinding biomass with different moisture content
HHV_{WPS}: HHV of the conventional and torrefied wood pellet
$\dot{m}_{WPs}$: mass flowrate of the wood pellet product

It should be noted that in the real operation, the energy consumptions of the biomass grinding processes varies with different biomass properties, i.e. moisture content, species, particle sizes, and hammer mill operating conditions, i.e. rotation speed, screen sizes, and capacities of the equipment. Therefore, the value ranges widely as summarized in Table 2.5, Table B.1, and Table B.2. Uncertainty analysis will be carried out to assess their impacts.

4.2.4 Pelleting

The pelleting process needs to densify pinewood particles from 1 mm to uniform sizes with 6 mm in diameter and 40 mm in length [78]. Two groups of biomass particles are pelletized: the biomass with MC 10wt%db from Paths 0 and 3, and the torrefied biomass (300°C and 20% weight loss) from Paths 1, 2, and 4. Sawdust is used as binders in Paths 1, 2,

and 3 at a fraction of 8wt% (eq. 0.8t/hr, or 0.4dt/hr) to increase the strength and inter-particle bonding of torrefied biomass. Specific energy consumption for pelleting different biomass is discussed in section 2.2.5. Pelleting machine's driven power is selected according to equipment supplier's website [109], [110]. The required number of machines is calculated according to Eq. (2.10). Key parameters of pelleting processes are summarized in Table 4.4. The electricity energy used for the biomass pelleting to produce per GJ of pellet product is calculated as Eq. (4.3).

$$E_{pelleting} = \frac{spe_{pelleting,MC} \cdot \dot{m}_{pelleting}}{HHV_{WP} \cdot \dot{m}_{WP}} \quad (4.3)$$

Table 4.4 Key parameters of the pelleting processes for CWP (Path 0) and TWPs (Paths 1-4) production pathways

Path	$\dot{m}_{pelleting}$ (t/hr)	Biomass properties	$spe_{pelleting,MC_i}$ (MJ/t)	HHV_{WPs} (GJ/t)	$\dot{m}_{WPs}$ (t/hr)	Driven power (kw)	Pelleting machine number	Binder (sawdust) dt/hr
Path 0	10	MC	270	17	10	370	2	0
Path 1	10	Torrefied	340	21	10	290	3	0.4
Path 2	10	Torrefied	340	21	10	290	3	0.4
Path 3	10	Torrefied	340	21	10	400	3	0
Path 4	12.5	MC	270	21	10	290	3	0.4

$\dot{m}_{pelleting}$: biomass mass flowrate to the pelleting machine
MC: biomass moisture content
$spe_{pelleting,MC_i}$: specific energy consumption of biomass pelletization with different moisture content
HHV_{WPs}: HHV of the conventional and torrefied wood pellet
$\dot{m}_{WPs}$: mass flowrate of the wood pellet product

Similar to the grinding process, the energy consumptions of the pelleting process varies with different biomass properties and operating conditions, as summarized in Table 2.6 and Table B.3. An uncertainty analysis will also be carried out in later sections.

4.3 Methodology

Process modeling and simulation are carried out based on Aspen Plus and FORTRAN in order to quantify the equipment sizes and operation conditions of each thermal unit in the above five pathways. Detail models of these units are presented in Appendix B . The simulation results of equipment specifications are then put into Aspen Economic Analyzer to quantify the capital and operating costs of the pellet plants. Detail models and assumptions of the techno-economic evaluations are presented in Appendix C .

4.4 Results and discussion

It is important to notice that the following discussions of the "3E" metrics of the TWPs production pathways under base case assumptions are under auto-thermal operation conditions. In another word, if the thermal systems can-not achieve auto-thermal operation, additional fuels will be required, e.g. by burning natural gas or biomass to provide additional heat. In this case, the conclusions may be different from the current study. Parameters which could change the auto-thermal operations include (a) biomass species which influence the biomass torrefaction heat demand and torgas HHVs, (b) biomass initial moisture content which determines the drying heat demand, (c) torrefaction operation conditions which determines the torrefaction heat demand and torgas HHVs, and (d) drying technologies (heat demand). The non-auto-thermal operation cases are not investigated in this study because firstly it should be avoided through appropriate process integration if the systems are able to achieve auto-thermal operation; secondly, the base case represents a typical scenario of the BC CWP and TWPs manufacturing processes; and lastly uncertainty analysis will be carried out to further confirm the confidence of the current analysis.

Simulation results of the conventional and torrefied wood pellet production pathways are provided in Appendix D , which includes the stream information, unit operation conditions, and key parameters of drying and torrefaction units, e.g. sizes, heat and mass transfer coefficient, and residence time.

4.4.1 "3E" metrics

4.4.1.1 Energy consumption

The four TWP production pathways achieved auto-thermal operations. Thus, no extra fuels are needed for the thermal units of these pathways. In path 0 for CWP production, the drying heat is provided by burning woodchips, which are grouped to the raw material flowrates. Therefore, electricity is the only types of energy consumed in these five wood pellet pathways.

It should be noted that under the base case torrefaction operating conditions (300°C, 20% biomass weight loss), there exists waste energy in Path 2 and Path 4, as shown in Table 4.5. After providing heat for torrefaction and drying, the flue gases are treated (cooling and dust control) and discharged. The waste energy is defined as the extra energy carried by the exhaust flue gases but cannot be sold as utilities ($30^{o}C<T<80^{o}C$). Therefore, there is a potential to further improve the process efficiency of Path 2 and Path 4. Possible ways are to decrease torrefaction temperature or reduce biomass weight loss to lower torgas HHV is decreased.

Table 4.5 Energy consumptions of CWP and TWP production pathways

Items	Path 0	Path 1	Path 2	Path 3	Path 4
Raw material consumption (t/hr)	14.88	17.16	17.16	18.65	17.16
Raw material HHV (GJ/t)	13.36[a]	13.36[a]	13.36[a]	13.36[a]	13.36[a]
Electricity consumption (KW)	2612	1814	2781	3768	5470

Items	Path 0	Path 1	Path 2	Path 3	Path 4
Wood pellet product flow rate (t/hr)	10	10	10	10	10
Wood pellet product HHV (GJ/t)	17[a]	21[a,b]	21[a,b]	21[a,b]	21[a,b]
Waste energy of flue gases (GJ/hr)	0	0	-5.76	0	-14.71

a: calculated based on element evolutions and Mott and Spooner correlation
b: torrefaction operation conditions, 300°C , 20% weight loss and 20% heat loss

The total primary energy consumption of each pathway to produce 1 GJ of wood pellet $E_{ene,production}$ is calculated according to Eq. (4.4). The wasted energy credits in Path 2 and Path 4 are not included in the primary energy consumption metrics.

$$E_{ene,production} = \sum_{U} e_U / \xi_{ele} \quad (4.4)$$

Where e indicates the electricity consumption in GJ/GJ wood pellet, U indicates the unit operation of drying, torrefaction, grinding, pelleting, air-compression for drying and torrefaction units. ξ_{ele} is the electricity generation efficiency of mixed fuel. In BC, electricity is sourced 90% from hydro power ($\xi_{hydro} = 100\%$) and about 10% from NG ($\xi_{NG} = 45\%$), thus $\xi_{ele} = 94.5\%$ (Environment and Climate Change Canada 2017, Table A13-12).

Figure 4.4 shows the primary energy consumption of the production process for different pathways, with detail values are given in section D.5 Table D.14. Path 1 uses minimum primary energy (0.041 GJ/GJ pellet), which is 43% lower than the primary energy input in Path 0 (0.073 GJ/GJ). Path 2 (0.063 GJ /GJ pellet) also uses less primary energy than Path 0. Path 3 (0.086 GJ/GJ) and Path 4 (0.125 GJ/GJ) consume higher energy than Path 0. Grinding, pelleting, and air compression used for drying are the major electricity users. Besides, thanks to the auto-thermal heat integration, process primary energy consumption mainly comes from electricity. Electricity consumption in grinding operation varies

significantly for different pathways, which is a dominant category that differentiates these pathways. Especially for Path 1 with grinding following torrefaction consumes much lower electricity. Thus, torrefaction should be carried out, if possible, before grinding to save electricity.

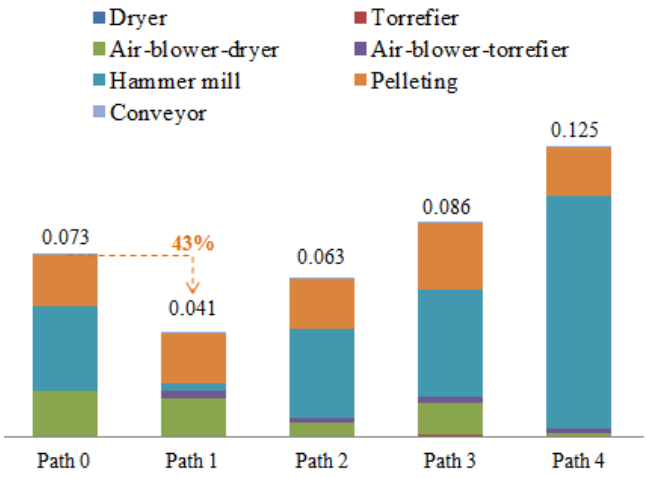

Figure 4.4 Primary energy consumption of the CWP (Path 0) and TWPs (Paths 1-4) production pathways (in GJ primary energy input/GJ pellet produced)

The production process solid product energy yield ratio η_{WPs} is an indicator for energy efficiency in different process configurations, which is defined as the total energy embedded in the product divided by the total primary energy inputs as expressed by Eq. (4.5). The waste energy credits in Path 2 and Path 4 are not included in the solid product energy yield metrics.

$$\eta_{WP} = \frac{HHV_{WP} \cdot \dot{m}_{WP}}{\sum_U e_U/\xi_{ele} + HHV_{raw} \cdot \dot{m}_{raw}} \quad (4.5)$$

Where $HHV_{WPs} \cdot \dot{m}_{WPs}$ and $HHV_{raw} \cdot \dot{m}_{raw}$ are the sum of the total energy embedded in the product and the raw material. These parameters and values are summarized in Table 4.5.

Note that the electricity and fuel used for piping, equipment setting, office lighting, and other fuel consumption is not included in this ratio calculation, thus this energy yield ratio is expected to be higher than the real value.

Figure 4.5 shows that Paths 1, 2 and 4 have higher energy yields in comparison with Path 0. Among these pathways, Path 1 has the highest energy yield, followed by Path2, suggesting these pathways are preferred in energetic efficiency point of view.

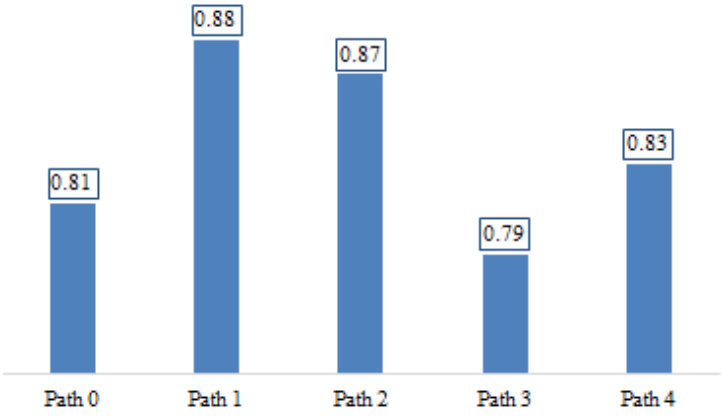

Figure 4.5 Solid product energy yields of conventional (Path 0) and the torrefied (Paths 1-4) production pathways

4.4.1.2 Environmental impacts

GHG emissions of the wood pellet production process are derived from electricity consumption and the materials used for the equipment construction, as expressed by Eq. (4.6).

$$E_{ene,production} = \sum_{U} e_U \cdot EF_{ele} + \sum_{U} \sum_{M} EM_U \cdot EF_M \quad (4.6)$$

Where e_U is the mixed electricity that used to produce per unit (GJ) of the wood pellet. EF_{ele} is the CO_2 equivalent emission factor of the BC electricity, which is 26987 gCO_2eq/GJ-

electricity generated according to BC electricity mix (GHGenius 4.3. 2018 BC), EM_U is the amount of raw material used to construct the equipment U, which is annualized based on 20 years life cycle at 8000 hr/year and 10 t/hr product capacity calculated by Eq. (4.7). EF_M indicates the material emission factor. Two types of raw material are used, carbon steel for all the equipment and rubber that used for belt conveyor. Emission factors are 154833 gCO_2eq/t-carbon steel and 2547000 gCO_2eq/t –rubber, respectively.

$$EM_U\left(\frac{\text{t material}}{\text{GJ pellet}}\right) = \frac{EM'_u(\text{t material})}{((20\ \text{year}) * \left(\frac{80{,}000\text{t}}{\text{year}}\right))/HHV_{WPs}} \quad (4.7)$$

Where EM' is the material that used for each equipment**,** which is evaluated by Aspen Plus Economic Evaluator when the equipment sizes are determined by process modeling and simulation, which value is provided in section D.5 Table D.14.

Figure 4.6 shows the GHG impacts of the five pathways in gCO_2eq/GJ pellet produced. Emissions associated with infrastructure are negligible (less than 10%) in comparison with electricity consumptions, which are proportional to the energy consumptions as shown in Figure 4.5. Path 1 (900 gCO_2eq/GJ) has the lowest amount of GHG emissions which can help reduce 600 gCO_2eq/GJ (40% of reduction) of emissions in comparison with Path 0 (1500 gCO_2eq/GJ). Path 2 (1800 gCO_2eq/GJ) also has less GHG emission than Path 0. Path 3 (1800 gCO_2eq/GJ) and Path 4 (2600 gCO_2eq/GJ have higher GHG emissions in comparison with Path 0 at the pellet plant gate. But due to the densified energy content of TWP, this conclusion may change when the pellet product is delivered to different markets with long distance transportation.

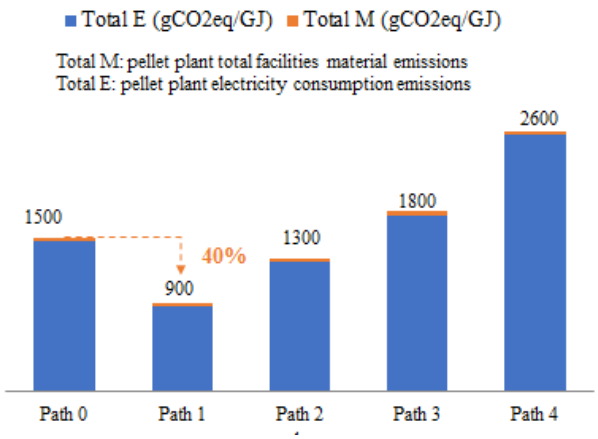

Figure 4.6 GHG emissions of CWP (Path 0) and TWPs (Paths 1-4) production pathways (in gCO2eq/ GJ wood pellet produced)

4.4.1.3 Economic production costs

The economic performance is quantified by using production cost in $/GJ produced, which includes the total capital cost and the operating cost. The total capital cost includes the equipment purchasing cost, installation cost, plant bulk cost (including piping, civil, steel, instrumentation, electrical, insulation, and paint), contract fee, contingencies fee, and others. The total operating cost contains raw material supply cost, total operating labor, and maintenance cost, total utility cost, operating cost and lab supplies, plant overhead, and general and administration (G &A) costs. Detail description of these cost categories are summarized in Table C.3. Detail cost categories of the five pathways are listed in Table 4.6. Details on evaluated equipment sizes and equipment purchasing costs are given in Appendix D , Table D.14.

Figure 4.7 shows the production costs and the cost break-downs of the five pathways based on Table 4.6. Path 1 (3.69 $/GJ) is the most economically beneficial configuration,

which can help reduce 0.42 $/GJ (10%) of cost in comparison with Path 0 (4.11 $/GJ). Path 2 (3.85 $/GJ) is also economically better than Path 0 at the pellet plant gate, which can help reduce 7.5% of the total production cost. Path 3 (4.38 $/GJ) and Path 4 (4.37 $/GJ) require higher production costs in comparison with Path 0. The most distinctive cost difference among the TWP production pathways is the electricity cost. Path 1 and Path 2, which put torrefaction before pelleting are benefiting from lower electricity consumptions during the pelleting stage. Specifically, Path 1 has the lowest grinding electricity consumption, which makes it the most economically feasible pathway among others.

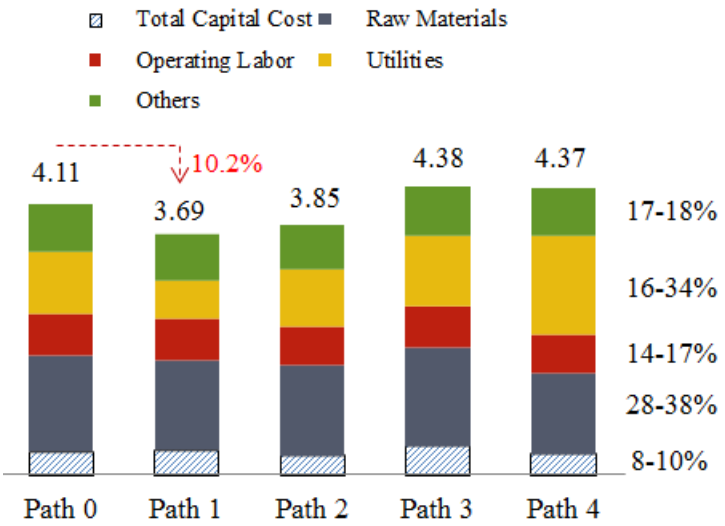

Figure 4.7 Wood pellet production costs (in $/GJ produced) and cost break-downs of the CWP (Path 0) and TWP (Paths 1-4) production pathways

Besides, the cost break-down analysis reveals that the capital investment only accounts for 7.1% to 10.3%, while the operating costs count for the other 89.7% to 92.9%, of the total production cost. Note that the total capital cost is annualized over 20 years. In other words, transforming or upgrading the existing CWP plant to torrefied wood

pellet plant will have long-term benefits. Among the operating costs, the most costive items are the raw materials (accounts for 31.2% to 38.3% of the production costs), the utility (14.8% to 31.2% of the production costs), and the total operating labor and maintenance cost (13.5% to 17.6% of the production cost). This suggests that pellet plant should be located close to biomass resources, with cheap electricity and labor costs.

Table 4.6 Production costs of CWP (Path 0) and TWPs (Path 1-4) production pathways

	Path 0			Path 1			Path 2			Path 3			Path 4		
HHV of the pellet (MJ/kg)	17			20.9			20.9			20.9			20.9		
	$	$/t	$/GJ	$	$/t	$/GJ	$	$/t	$/GJ	$	$/t	$/GJ	$	$/t	$/GJ
Total Capital Cost	9,321,299	5.83	0.34	12,250,590	7.66	0.37	9,648,131	6.03	0.29	14,609,520	9.13	0.43	10,078,068	6.54	0.31
Purchased Equipment	2,778,500	1.74	0.10	4,164,700	2.60	0.12	2,402,600	1.50	0.07	5,229,600	3.27	0.16	2,114,900	1.32	0.06
Equipment Setting	113,198	0.07	0.00	183,169	0.11	0.01	101,602	0.06	0.00	228,606	0.14	0.01	78,683	0.05	0.00
Piping	419,738	0.26	0.02	638,998	0.40	0.02	441,270	0.28	0.01	705,130	0.44	0.02	444,432	0.28	0.01
Civil	200,393	0.13	0.01	313,958	0.20	0.01	208,072	0.13	0.01	399,155	0.25	0.01	187,706	0.12	0.01
Steel	41,937	0.03	0.00	41,937	0.03	0.00	59,081	0.04	0.00	41,937	0.03	0.00	76,226	0.05	0.00
Instrumentation	406,665	0.25	0.01	470,657	0.29	0.01	532,712	0.33	0.02	500,995	0.31	0.01	681,239	0.43	0.02
Electrical	1,062,368	0.66	0.04	1,011,586	0.63	0.03	1,074,186	0.67	0.03	1,230,003	0.77	0.04	1,340,176	0.84	0.04
Insulation	27,550	0.02	0.00	26,840	0.02	0.00	80,794	0.05	0.00	27,303	0.02	0.00	102,532	0.06	0.00
Paint	11,752	0.01	0.00	13,511	0.01	0.00	16,860	0.01	0.00	14,726	0.01	0.00	20,113	0.01	0.00
Other	2,425,200	1.52	0.09	2,985,000	1.87	0.09	2,827,600	1.77	0.08	3,384,500	2.12	0.10	3,047,900	1.90	0.09
Subcontracts	0	0.00	0.00	0	0.00	0.00	0	0.00	0.00	0	0.00	0.00	0	0.00	0.00
G and A Overheads	188,529	0.12	0.01	255,911	0.16	0.01	186,869	0.12	0.01	309,140	0.19	0.01	191,472	0.12	0.01
Contract Fee	320,231	0.20	0.01	402,622	0.25	0.01	344,782	0.22	0.01	461,347	0.29	0.01	359,860	0.22	0.01
Escalation	0	0.00	0.00	0	0.00	0.00	0	0.00	0.00	0	0.00	0.00	0	0.00	0.00
Contingencies	1,439,291	0.90	0.05	1,891,599	1.18	0.06	1,489,757	0.93	0.04	2,255,839	1.41	0.07	1,556,143	0.97	0.05
Total Operating Cost	5,122,951	64.04	3.77	5,563,870	69.30	3.32	5,944,634	74.31	3.56	6,599,735	82.50	3.93	6,818,276	85.23	4.06
Raw Materials	1,984,000	24.80	1.46	2,288,000	28.60	1.37	2,280,000	28.50	1.36	2,476,000	30.95	1.48	2,040,000	25.50	1.22
Operating Labor and Maintenance	842,400	10.53	0.62	1,046,000	13.08	0.63	1,001,000	12.51	0.60	1,076,000	13.45	0.64	994,400	12.43	0.59
Utilities	1,305,874	16.32	0.96	972,139	12.15	0.58	1,418,717	17.73	0.85	1,790,866	22.39	1.07	2,477,544	30.97	1.48
Binder (sawdust)	0	0	0	80,000	1.0	0.05	80,000	1.0	0.05	0	0	0	80,000	1.0	0.05
Operating Charges	190,000	2.38	0.14	230,000	2.88	0.14	230,000	2.88	0.14	230,000	2.88	0.14	230,000	2.88	0.14
Plant Overhead	421,200	5.27	0.31	523,000	6.54	0.31	500,500	6.26	0.30	538,000	6.73	0.32	497,200	6.22	0.30
G and A Cost	379,478	4.74	0.28	404,731	5.06	0.24	434,417	5.43	0.26	488,869	6.11	0.29	499,132	6.24	0.30
Total Production cost	14,444,251	69.86	4.11	17,794,461	76.96	3.69	15,592,766	80.34	3.85	21,209,255	91.63	4.38	16,896,343	91.77	4.37

4.4.2 Uncertainty analysis

It is concluded above that it is beneficial to produce TWP rather than CWP in terms of energy efficiency, environmental impacts, and economic costs. In addition, Path 1 is a preferred choice among the other pathways. These conclusions are obtained based on several assumptions (Table 4.1) and average literature data. In addition, the conclusions of the deterministic analysis are based on auto-thermal operation and avoid the use of N_2 and catalyst of the TWP thermal system, and as aforementioned, non-auto-thermal operation cases are not included in this study. To enhance our conclusions for the auto-thermal operation systems, uncertainties analysis will be performed. The uncertainty analysis will include the following aspects:

- Source of uncertainties
- Range of uncertainties
- Distribution of uncertainty parameters
- Cumulative distribution function of the "3E" metrics

4.4.2.1 Uncertainties in energy consumption

When the whole flowsheet achieves auto-thermal operation, electricity is the major energy consumption. Two parameters contribute significantly to the uncertainties in production processes electricity consumptions: specific energy consumptions of the grinding $spe_{grinding,MC_i}$ and the pelleting $spe_{pelleting,MC_i}$ processes. Uncertainties of these two parameters would arise from (a) biomass properties, i.e. biomass moisture content, biomass species, biomass particle sizes, (b) equipment types, i.e. ring die or flat die mill, (c) operation conditions, i.e. rotation speed and biomass flow rate. These parameters with uncertainties are

summarized in Table B.1, Table B.2, and Table B.3, showing a wide variation in different studies.

Assumptions used in the specific energy consumptions calculations of biomass grinding and pelleting in Paths 0-5 in this study have been discussed in sections 2.2.4 and 2.2.5. We have been chosen the most related cases to the current study and used the average value of different studies. Although with large variations, reasonable scaling factors have been revealed through a comprehensive literature review. For example, the specific energy consumption of grinding biomass with MC 15% $spe_{grinding,MC\ 15wt\%db}$ is about 9-15 times of grinding torrefied biomass $spe_{grinding,torrefied}$, with the mean value (11 times) being used for deterministic analysis. The specific energy consumption of densifying biomass with MC 10wt%db $spe_{pelleting,MC\ 10wt\%db}$ is about 1-1.5 times of the $spe_{pelleting,torrefied}$. Here, therefore, 25% of variations are assumed for grinding and pelleting processes. If is considered the above ranges of electricity consumptions have equal probabilities, thus uniform distribution is thus considered, as shown in Table 4.7.

Table 4.7 Uniform probability distribution function parameters of specific energy consumption of grinding and pelleting processes for different pathways with 25% variation

		Biomass property	Mean	Min	Max
Grinding (kJ/kg biomass)	Path 0	MC 15wt%db wood chips 20mm	427[a]	320	533
	Path 1	Torrefied biomass wood chips 20mm	38[b]	28.5	47.5
	Path 2	MC 15wt%db wood chips 20mm	427[a]	320	533
	Path 3	MC 15wt%db wood chips 20mm	427[a]	320	533
	Path 4	MC 50wt%db wood chips 20mm	854[c]	640	1067
Pelleting (kJ/kg biomass)	Path 0	MC 10wt%db biomass particle 1mm	270[d]	202	338
	Path 1	torrefied biomass particle 1mm	340[e]	255	425
	Path 2	torrefied biomass particle 1mm	340[e]	255	425
	Path 3	MC 10wt%db biomass particle 1mm	270[d]	202	338

	Biomass property	Mean	Min	Max
Path 4	torrefied biomass particle 1mm	340[e]	255	425

a: $spe_{grinding,MC\ 15wt\%db}$[75]; more details of discussions refer to section 2.2.4
b: 1/11 of $spe_{grinding,MC\ 15wt\%db}$; more details of discussions refer to section 2.2.4
c: 2 times of $spe_{grinding,MC\ 15wt\%db}$; more details of discussions refer to section 2.2.4
d: $spe_{pelleting,MC\ 10wt\%db}$ [79]; more details of discussions refer to section 2.2.5
e: 1.25 times of $spe_{pelleting,MC\ 10wt\%db}$; more details of discussions refer to section 2.2.5

Figure 4.8 shows the cumulative distribution function (CDF) of the process energy consumption in GJ electricity/ GJ pellet produced. As can be seen, at the specified uncertainties of the parameters, Path 1 has energy consumption in the range of 0.035 to 0.045 GJ/GJ pellet produced, while the other pathways do not show any overlap within Path 1. Thus, it is confident to conclude that Path 1 is the best pathway among all pathways analyzed. Similarly, with a 25% uncertainty in the two parameters, it is safe to conclude that Path 2 is better than Path 0, while Path 3 and Path 4 are worse than Path 0.

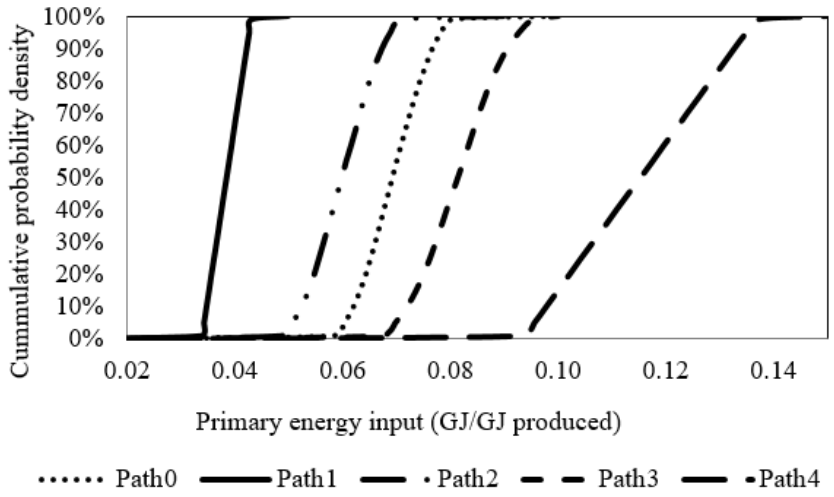

Figure 4.8 Cumulate distribution function of primary energy input/output ratio of different pathways

It should be noticed that since specific energy consumptions of biomass grinding and pelleting processes are very sensitive to biomass properties, i.e. moisture content, species,

particle sizes, operating conditions such as rotation speed, screen sizes, temperature, equipment types, and capacities, thus, the readers should be carefully in using the specific energy consumptions data provided in Table 4.7.

4.4.2.2 Uncertainties in environmental impact

Uncertainties of GHG emissions of the wood pellet production processes could come from two major sources: (1) the primary energy consumption which has been discussed in section 4.4.2.1 and also adopted here, and (2) the electricity emission factors. Two sets of values for BC electricity emission factors are observed: one is 95 tCO_2eq/GWh that calculated based on GHGenius 4.3, which database is from Statistics Canada; the other sets of data are reported by Dowlatabadi et al. [112], who discussed the neglected factors in the BC electricity emission factors reported by BC hydro, which include emissions from business travel, emergency repair trucks, biomass burned to keep waterways clear, as well as the emissions associated with imported electricity to meet domestic demand. Dowlatabadi et al. [112] found that after correction the GHG intensity for BC electricity delivered to BC customers should be close to 140 tCO_2eq/GWh, which is about 1.5 times of the GHGenius 4.3 reported value. We consider these two evaluations have the same probabilities. Thus, a uniform distribution for the BC electricity is assumed. Similarly, we assumed that the emission factors of carbon steel and rubber also follow a uniform distribution, with 1.5 times of variation to those values from SimaPro 8.3, as summarized in Table 4.8.

Table 4.8 Uniform distribution function parameters of the electricity emission factors and material emission factors derived from different sources

Uncertain factors	Min	Max
Carbon steel emission factor (gCO_2eq/t)	399600^{a*}	$4884000^{a\text{-}1*}$
Hydro-electricity emission factor (gCO_2eq/GJ generated)	12782^{b*}	$19173^{b\text{-}1*}$

Uncertain factors	Min	Max
NG to electricity emission factor (gCO_2eq/GJ input)	154833[c*]	232250[c-1*]
Rubber emission factor (gCO_2eq/t)	2547000[d*]	3113000[d-1*]

a*: data source, SimaPro 8.3;
a-1*: data source, assumption which is about 1.5 times of a*;
b*: data source, GHGenius 4.3 based on 2017 BC; 26987
b-1*: data source, Dowlatabadi et al (2011) corrected value, which is about 1.5 times of GHGenius 4.3 value
c*: data source, GHGenius 4.3 based on 2017 BC;
c-1*: data source, Dowlatabadi et al (2011) corrected value, which is about 1.5 times of GHGenius 4.3 value;
d*: data source, SimaPro 8.3;
d-1*: data source, assumption of which is about 1.5 times of d*

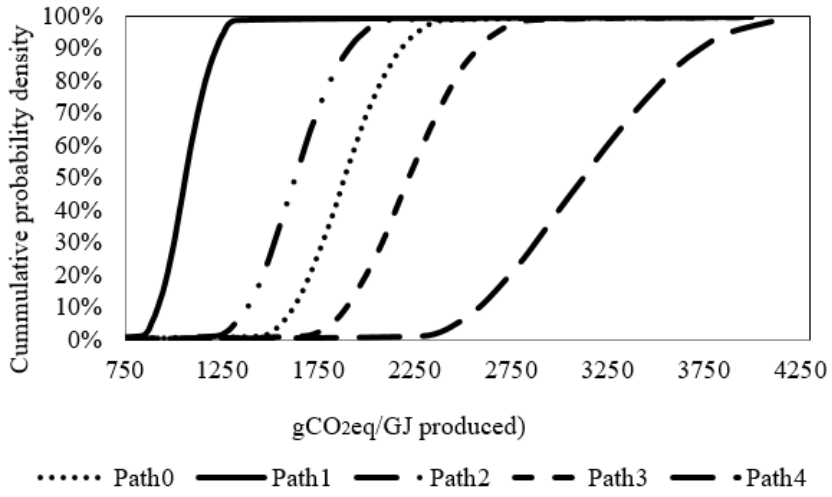

Figure 4.9 Cumulative distribution function of gCO_2eq/GJ pellets for CWP (Path 0) and TWPs (Paths 1-4) production pathways

Figure 4.9 shows the CDF of GHG emissions for the five pathways. Clearly, Path 1 emits less than 1000 gCO_2eq/GJ pellets within the range of specified uncertainties, which is lower than all other pathways, which have 0% possibilities to emit less than 1000 gCO_2eq/GJ of pellets. This reinforces the conclusion that Path 1 is the best pathway in terms of environmental impacts. Path 2 also shows clearly lower GHG emissions than Paths 0, 3 and 4. Again, these conclusions are safe if the torrefaction system achieves auto-thermal

operation, and the energy consumptions of biomass grinding and pelleting processes are in the range of Table 4.7.

4.4.2.3 Uncertainties in production costs

As aforementioned in section 4.4.1.3, the three key parameters contributing to the production costs are raw material, electricity, and the labor costs. To analyze the uncertainties of those three cost parameters, their correlations to the total production costs are investigated by regressing the simulation results, as illustrated in Figure 4.10 for production costs of Path 1 in both $/t (Figure 4.10 a) and $/GJ (Figure 4.10 b).

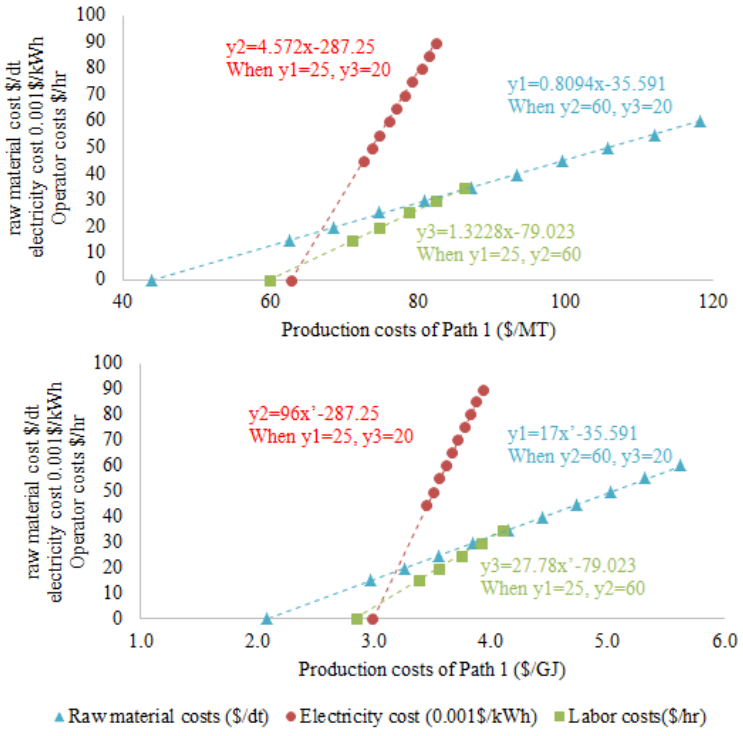

Figure 4.10 Correlations of raw material cost, electricity cost and labor cost to wood pellet production cost in Path 1. (a) production costs in $/t; (b) production cost in $/GJ

Correlations of raw material cost, electricity cost, and the labor cost to the production cost in $/t of different pathways are given in Eq. (4.8) to Eq. (4.12), and in Eq. (4.13) to Eq.

(4.17) for the production cost in $/GJ. These correlations are useful to preliminarily quantify the production costs in different regions with different biomass costs, electricity costs and labor costs.

$$x_{p0} = 0.357y_1 + 0.098y_2 + 0.189y_3 + \vartheta_{p0} \quad (4.8)$$

$$x_{p1} = 0.412y_1 + 0.073y_2 + 0.252y_3 + \vartheta_{p1} \quad (4.9)$$

$$x_{p2} = 0.410y_1 + 0.106y_2 + 0.252y_3 + \vartheta_{p2} \quad (4.10)$$

$$x_{p3} = 0.446y_1 + 0.158y_2 + 0.252y_3 + \vartheta_{p3} \quad (4.11)$$

$$x_{p4} = 0.412y_1 + 0.186y_2 + 0.252y_3 + \vartheta_{p4} \quad (4.12)$$

Where x is the wood pellet production cost in $/t, subscript 0-4 is for pathways 0 to 4. y_1, y_2, and y_3 indicate raw material costs in $/dt, electricity costs in $/MWh, and operator labor costs in $/hr, respectively. ϑ is the uncertainty value in $/t. ϑ_{p0}, ϑ_{p1}, ϑ_{p2}, ϑ_{p3}, ϑ_{p4} are 51.28, 56.24, 59.62, 65.97, and 64.04, respectively, at a raw material cost of 25$/t, electricity cost of 0.06$/kWh, and labor cost of 20$/hr.

$$x'_{p0} = 0.02y_1 + 0.006y_2 + 0.011y_3 + \vartheta'_{p0} \quad (4.13)$$

$$x'_{p1} = 0.02y_1 + 0.003y_2 + 0.012y_3 + \vartheta'_{p1} \quad (4.14)$$

$$x'_{p2} = 0.02y_1 + 0.005y_2 + 0.012y_3 + \vartheta'_{p2} \quad (4.15)$$

$$x'_{p3} = 0.02y_1 + 0.008y_2 + 0.012y_3 + \vartheta'_{p3} \quad (4.16)$$

$$x'_{p4} = 0.02y_1 + 0.009y_2 + 0.012y_3 + \vartheta'_{p4} \quad (4.17)$$

Where x' is the production cost of the torrefied wood pellet in $/GJ, subscript 0 to 4 represent pathway 0 to 4, y_1, y_2, and y_3 indicate raw material cost in $/dt, electricity costs in $/MWh, and operator labor cost in $/hr respectively. ϑ' is the uncertainty constant in $/GJ. ϑ_{p0}', ϑ_{p1}',

ϑ_{p2}', ϑ_{p3}', ϑ_{p4}' are 3.04, 2.68, 2.75, 3.14, and 3.05, respectively, at a raw material cost of 25$/t, electricity cost of 0.06$/kWh, and labor cost of 20$/hr.

Uncertainty in total cost is analyzed based on $/GJ. Uncertainties of these costs could be derived from many ways, e.g. demand and supply, scarcity, and inflation. The normal distribution has been considered for costs because, even though the individual constituent distributions may not be Gaussian, the central limit theorem shows that the combined distribution tends to be approximately Gaussian. In comparison with energy consumption and environmental emission indicators, the economic performance has a higher degree of uncertainty. Here, we studied two cases with a coefficient of variation (CV) at 10% and 30% summarized in Table 4.9.

Table 4.9 Normal distribution function parameters for production costs in $/GJ of CWP (Path 0) and TWPs (Paths 1-4) production pathways

Uncertain factor	Mean **μ**	Case 1		Case 2	
		SD σ	CV	SD σ	CV
y_1	25	2.5	10%	7.5	30%
y_2	60	6	10%	18	30%
y_3	20	2	10%	6	30%
ϑ_{p0}'	3.04	0.304	10%	0.912	30%
ϑ_{p1}'	2.68	0.268	10%	0.804	30%
ϑ_{p2}'	2.75	0.275	10%	0.825	30%
ϑ_{p3}'	3.14	0.314	10%	0.942	30%
ϑ_{p4}'	3.05	0.305	10%	0.915	30%

$\mathrm{CV} = \sigma/\mu$ (coefficient of variation)

Figure 4.11 shows the cumulative probability of the wood pellet production costs under the uncertainties of raw material cost, electricity cost, and the labor cost at (a) 10 % and (b) 30% coefficient of variation. It is clear that, with 10% uncertainty in those parameters,

there is a higher possibility for Path 1 to have a lower total production cost, followed by Path 2. For example, as shown in Figure 4.11 (a), Path 1 has 100% probability to cost less than 4.2 $/GJ, while Path 2 has a 95%, Path 1 has 60%, and Path 3 and 4 have about 35% chances to be cheaper than 4.2 $/GJ. With 30% variation, it is still safe to conclude that Path 1 and Path 2 are better than the others, Path 3 and Path 0 have a similar economic performance, and Path 4 has the highest production cost. Path 1 only shows a slight advantage over Path 2.

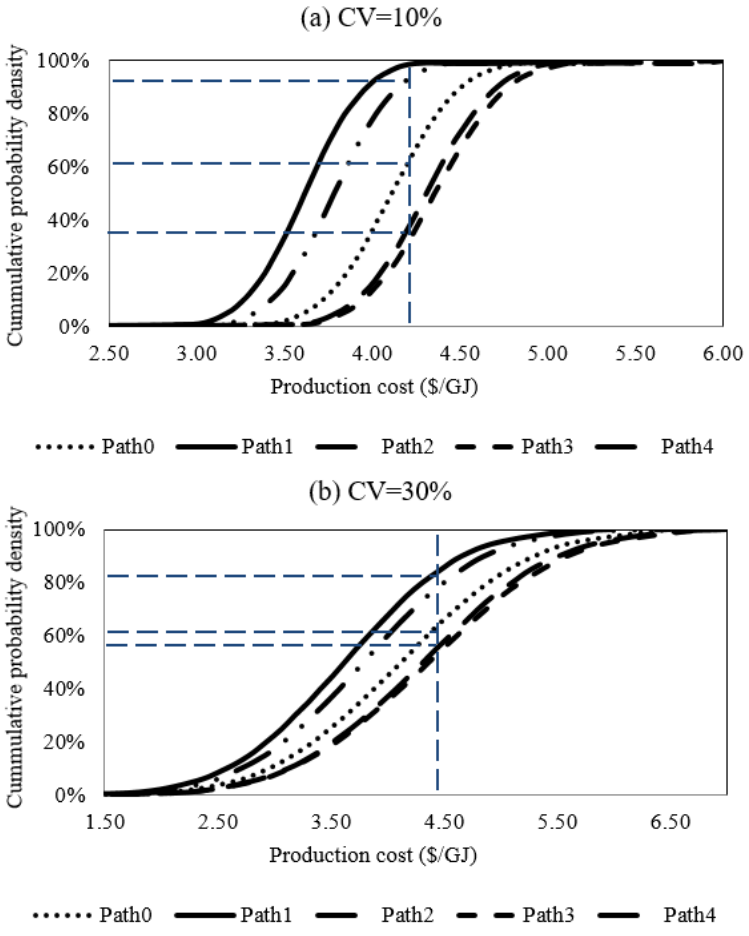

Figure 4.11 Cumulative distribution functions of production costs of different pathways under uncertainties of raw material cost, electricity price, and labor cost (a) with 10% of variation; (b) with 30% of variation

4.4.3 Minimum selling price of BC torrefied wood pellets

Aside from the "3E" impacts, a TWP producer would also care about the minimum selling prices and the investment of return. The BC TWP minimum selling price is evaluated by calculating the net present value (NPV) of the project at the target rate of return (ROR) of 10% and setting the NPV equal to zero at the targeted break-even year, i.e. the target payout period (PO), e.g. within 5 years. The NPV is calculated by Eq. (4.18).

$$\mathrm{NPV} = \sum_{n=0}^{\text{nth year}} \mathrm{DCF_n} = \sum_{n=0}^{\text{nth year}} \frac{\mathrm{CF_n}}{(1+\mathrm{ROR})^n} \tag{4.18}$$

Here $\mathrm{CF_n}$ is the cash flow ($/year) of the project in year n, calculated by

$$\mathrm{CF} = \mathrm{GSR} - \mathrm{TAX} \tag{4.19}$$

and $\mathrm{DCF_n}$ is the discounted cash flow, also known as the present value of the future cash flow; GSR ($/year) is the gross sales revenue calculated by Eq. (4.20) and TAX is the corporate income tax calculated by Eq. (4.21).

$$\mathrm{GSR} = \mathrm{Capacity} \cdot (\mathrm{P_{sale}} - \mathrm{P_{production}}) \tag{4.20}$$

$$\mathrm{TAX} = (\mathrm{GSR} - \mathrm{DC}) \cdot \mathrm{r_{tax}} \tag{4.21}$$

Capacity is the output of pellets in t/year; $\mathrm{P_{sale}}$ is the sale price and $\mathrm{P_{production}}$ the production cost of the wood pellet in $/t; $\mathrm{r_{tax}}$ is the tax rate, 27% in 2018 for Canadian-controlled private corporations (CCPC) [113]. DC is the depreciation cost ($/year). There are four main types of depreciation methods: Straight-line, Double declining balance (DDB), Sum of years digits, and Modified Accelerated Cost Recovery System (MACRS). The DDB and MACRS methods account for higher capital depreciation in the early years, as shown in Figure 4.12. The Government of Canada provides an accelerated Capital Cost Allowance (CCA) rate for

Class 43.1 and 43.2 properties as an incentive to encourage business to invest in specified clean energy generation and energy efficiency equipment [114], For the properties acquired after February 22, 2005 and before 2020, a maximum CCA rate of 50% is allowed for capital deprecation. This is beneficial since faster depreciation allows businesses to deduct greater amounts during the first few years so that investors pay less income tax in the early years; the money saved in comparison with the straight line depreciation can be invested in other businesses. Here, in this work, the straight line and MACRS methods are used and compared. The operating life of all the equipment in the plant is assumed as 20 years.

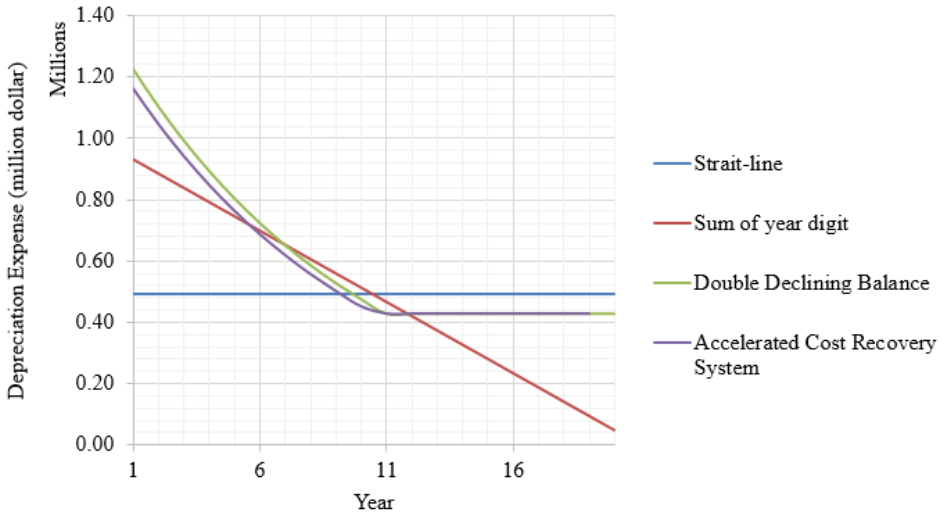

Figure 4.12 Different depreciation methods

Results from the straight line and DDB methods are compared in Figure 4.13 (a). It is seen that using DDB depreciation method reduces the payout period of the project from 4.73 year to 4.64 years, a very small impact. More details of different depreciation methods are provided in Table E.3. The impact of raw material costs on the minimum selling prices is

evaluated using straight line method. Two case studies have been considered, for different raw material costs: 25 $/dt (dry tonne) in case 1 and 15 $/dt in case 2. Figure 4.13 shows the project NPV of Path 1 when the wood pellet is sold at different prices to achieve a 10% ROR. Note that subsidies from the government are not included in this analysis. As can be seen, in order to recover all the investments in 5 years, the TWP has to receive a sales price of least 140 $/t (equivalent to 6.66 $/GJ) when the raw material cost is 25 $/dt, and at least 130 $/t (equivalent to 6.2 $/GJ) if the raw material cost is 15 $/dt. Details of the cash flow based on Path 1 case 1 is provided in Appendix E

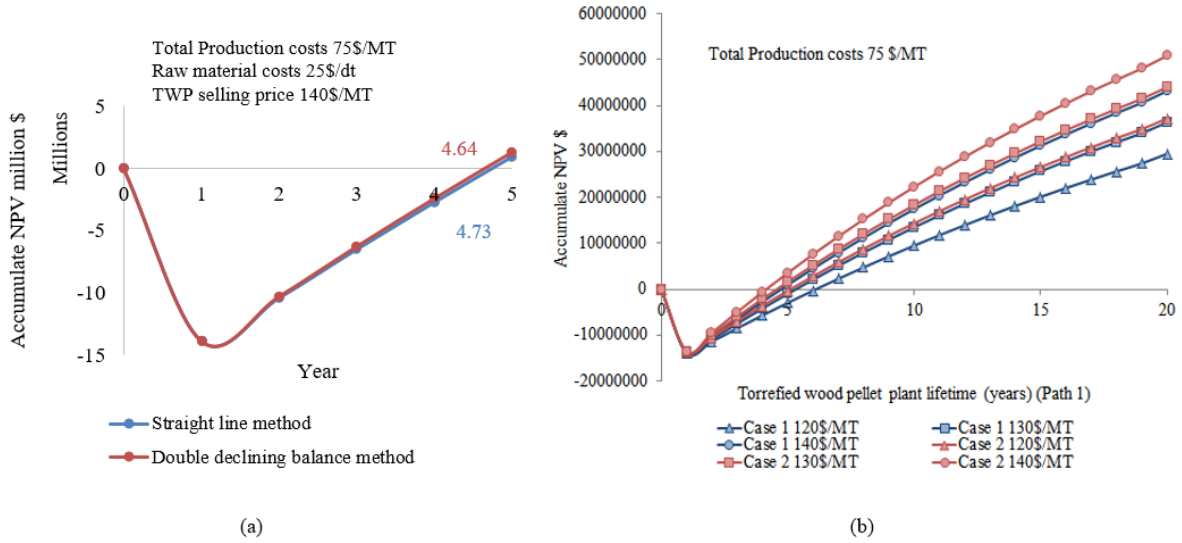

Case 1: raw material cost: 25$/dt; discount rate=10%
Case 2: raw material cost: 15$/dt; discount rate=10%

Figure 4.13 (a) Effect of depreciation method on the cash flow diagram of Path 1; (b) Project cash flow diagram for Path 1 based on straight line depreciation method

When planning an investment project, companies often set a desired rate of return (ROR) to determine the minimum acceptable return percentage in order to be worthwhile: the higher IRR, the better. The project is only acceptable if the internal rate of return (IRR) is

greater than ROR, although firms will not necessarily pursue a project on this basis alone. IRR is the discount rate at which the net present value of an investment becomes 0, as presented by Eq. (4.22); i.e. the IRR of an investment is the discount rate at which the net present value of costs (negative cash flows) equals the net present value of the benefits (positive cash flows) of the investment.

$$\mathrm{NPV(r)} = \sum_{n=0}^{N=10} \frac{\mathrm{CF_n}}{(1+\mathrm{r})^n} = 0 \tag{4.22}$$

The payout period is the time required to recover the investment costs and is calculated according to Eq. (4.23).

$$\mathrm{PO} = \text{ Years with negative NPV} + |\mathrm{NPV}|/\mathrm{PV} \tag{4.23}$$

The profitability index (PI) shows the present value of the benefits relative to the present value of the costs. For each period, this number is calculated by dividing the Present Value (PV) of the Cumulative Cash Inflows (PVI) by the Present Value of the Cumulative Cash Outflows (PVO) at the end the project, e.g. 20th year. A project is acceptable if PI is greater than 1 and rejected if less than 1.

$$\mathrm{PI} = \mathrm{PVI}/\mathrm{PVO} \tag{4.24}$$

The performances of the two cases are presented in terms of these parameters in Table 4.10.

Table 4.10 Investment performances of BC TWP plant with different assumptions (Path 1 as an example)

	Case 1			Case 2		
BC TWP selling price ($/t)	120	130	140	120	130	140
IRR (Internal Rate of Return)	29.11	33.15	37.16	34.41	38.52	42.61
NRR (Net Return Rate)	35.53	42.45	48.98	49.36	56.52	63.23
PO (Payout Period)	6.1	5.31	4.73	5.09	4.56	4.14
PI (Profitability Index)	1.35	1.42	1.48	1.49	1.56	1.63

As can be seen that the pellet plant project is profitable when the BC TWP is sold for 130 $/t or more, and the project can recover its investments in 5 years if the BC TWP is sold for 140$/t or more.

4.4.4 GDP contribution of BC TWPs to provincial economy

Wood pellet manufacturing is a major player of BC's bio-economy. Its contribution to the province gross domestic product (GDP) is not explicitly reported according government report review. Thus, this section aims to quantify the GDP contribution of BC TWP manufacturing with base year assumed as 2017. GDP is a measure of the overall performance of an economy, which can be calculated in two ways, referred to as the production approach and income approach as presented in Table 4.11 [115]. The earning/income approach only includes a firm's value added to avoid duplicated calculation. The value added is the difference between a firm's sales and its purchases of materials and services from other firms. Here, we use the earning approach to predict the potential GDP contribution of BC's wood pellet manufacturing industry, taking Path 1 as an example.

Table 4.11 Overview of the production and earning approaches to quantify GDP contributions

Product Approach	Earnings/Income Approach
GDP= C + I + G + X	GDP= (1) + (2) + (3) + (4) + (5)
C: Consumption -these are personal consumption expenditures	(1) Compensation of labor (wages, salaries, and supplements)
I: Investment -includes gross private investment, generally indicates fixed investment and changes in business inventories.	(2) Revenue
G: Government -government spending	(3) Other property income (rent, interest, proprietors' income)
X: Net Exports	(4) Depreciation
	(5) Net production taxes

The current BC wood pellet capacity is about 2.425 million t/year, accounting for about 66% of national production by the year-end of 2017 [116]. According to the Wood Pellet Association of Canada (WPAC) [117], BC's wood pellet industry employs about 350 workers in facilities for processing and manufacturing, 400 workers in forestry and harvesting operations, and 350 workers in truck-driving and transportation. In this study, the number of labor required is quantified by the Manpower Productivity Expert (MPE) in Aspen ICARUS software. The man hours are quantified according to the plant capacity, process equipment, plant bulks, buildings and other items. In this study, the estimated labors for the wood pellet plant in a capacity of 80,000t/year are 15 as presented in Table 4.12. As can be seen, the BC wood pellet capacity and the industry employees are approximately 30 times of capacity and labors of the wood pellet plant in the current analysis. Therefore, to estimate the annual GDP contribution of BC's wood pellet industry, we simply apply a scale-up factor by assuming that the wood pellet industry GDP components listed in Table 4.11 can be estimated to be 30 times of the Path 1 case in the current study as presented in Table 4.6.

Table 4.12 Wood pellet capacities and labors of BC wood pellet sector and case study in this work (year 2017)

Labor category	Capacity	Labor
BC wood pellet sector	2.425 million t/year	15[a]
Case study	80,000 t/year	350[b]

a: 4 operators per shift, 1 supervision per shift, 8 hours per shift; data evaluated by Aspen Economic Evaluator "Manpower Productivity Expert"
b: workers in facilities for processing and manufacturing, data source, WPAC [117]

(1) Compensation of labor

Labor wages of the case study is 920,000 $/year as shown in Table 4.13. Based on the scale up factor, the compensation of the labor in the BC wood pellet industry is calculated to be about 27.6 million $/year.

Table 4.13 Labor wages of the wood pellet plant in 80,000t/year (year 2017)

Labor category	unit	number
Total operator labor		12
Unit Cost	$/Operator/hr	20
Total Operating Labor Cost	$/year	640,000
Total supervisors labor		3
Unit Cost	$/Supervisor/hr	35
Total Supervision Cost	$/year	280,000
Total wages	**$/year**	**920,000**

(2) Revenue before taxes

Assuming the sale price of the wood pellet is 140 $/t, the wood pellet production cost is evaluated as 75$/t (Table 4.6 for Path 1). Then the revenue before tax for wood pellet plant in this study is calculated by Eq. (4.25) to be 5.2 million/year. The revenue of the BC's wood pellet industry can be predicted by Eq. (4.26) to be 157.625 million/year in 2017.

$$\text{Revenue before tax of Path 1} = (140 - 75)\$/\text{t} * 80{,}000\text{t/year} \quad (4.25)$$

$$\text{Renenue of BC TWPs} = (140 - 75)\$/\text{t} \cdot 2{,}425{,}000\text{t/year} \quad (4.26)$$

(3) Other property income (rent, interest, proprietors' income)

Land rent fees are usually calculated as 1 to 2 % of the inside battery limits (ISBL) [73], which include the costs of purchasing equipment, and the plant bulks, including equipment setting, piping, civil, steel, instrumentation, electrical, insulation, and paint etc. Cost of those categories for Path 1 is presented in Table 4.6. Here, we assume that the land

rental fee is 1.5% of the ISBL, calculated as 0.069 million $/year for Path 1, and 2.07 million $/year for BC wood pellet industry.

Interest costs are paid by the firm to the bank for borrowed money for their capital investments, the wages and other expenses. By assuming that the wood pellet plant will borrow money from the bank to pay for their 40% capital investment and will spend ten years to pay off the fees, then the annualized interests that the bank gets paid are calculated by Eq. (4.27).

$$\text{Interests} = (P \cdot (1 + r)^t - P)/t \quad (4.27)$$

Where P is the principle, assumed as 40% of the capital investments (Table 4.6), equal to 4.9 million dollar; r is the interest rate, assumed at 2.5% annually in 2017; t is the years to pay interests. Bank will receive $3,129,221 in 10 years, annualized to be 0.156 million $/year of interests. The interests of the whole BC wood pellet sector would be 4.68 million $/year.

(4) Depreciation

Depreciation measures the amount of capital that has been used up in a year. In the case of present wood pellet plant study, depreciation is calculated using the simple streamlined depreciation method. In this method, the Salvage Value is subtracted from the Total Project Cost. This result is then divided by the Economic Life of Project, so that the project is depreciated evenly over its economic life. The depreciation of the pellet plant is calculated as 490,023 $/year based on Aspen Economic Evaluator as presented in Table E.1. The whole BC wood pellet industry is simply calculated as 14.7 million $/year.

(5) Net production taxes

Net production taxes are normally introduced as a means of compensating for the pollution that producers emit. This kind of taxes is not charged for wood pellet manufacturing in BC. Thus, this component is considered as 0 for the current cases.

The overall nominal GDP contributions based on 2017 price of the case study Path 1 and the whole BC wood pellet industry are summarized in Table 4.14.

Table 4.14 Nominal GDP contributions of the TWP plant in Path 1 with 80,000t/year of capacity and the BC wood pellet industry with 2,425,000t/year of production capacity in year 2017 and future capacity [8]

Component	This study	BC's capacity in 2017	BC's capacity in future
Capacity (million t/year)	0.08	2,425	3.2 [8]
(1) Compensation of labor (million $/year)	0.92	27.60	36.8
(2) Revenue (million $/year)	5.20	157.625	208
(3) Other property income (rent, interest, proprietors' income) (million $/year)	0.069+0.156	2.07+4.68	2.76+6.42
(4) Depreciation (million $/year)	0.49	14.7	19.6
(5) Net production taxes (million $/year)	0	0	0
GDP contribution (million $/year)	6.83	206.68	273.2

According to [118], BC's real GDP (chained based on 2007 price) in 2017 was 228.2 billion Canadian dollars (178 billion US dollars), within which the manufacturing sector contributes 7.11% [119]. The total BC nominal GDP in 2017 is quantified by

$$\text{Nominal GDP (2017 price)} = \text{Real GDP} \times \text{GDP deflator} \quad (4.28)$$

According to [120], the GDP deflator from 2007 to 2017 is 116.43%. Therefore, at current production capacity of 2.425 million t/year, with minimum selling price of 140 $/t, TWP manufacturing can contribute at least about 1.4% to the BC manufacturing sector, and about 0.1% to the total provincial GDP. If the torrefied wood pellet capacity is expanded to 3.2

million t/year [8], a total of ~273.2 million US dollar will be contributed annually to the provincial economy, which will be equivalent to ~0.15% of the total provincial GDP.

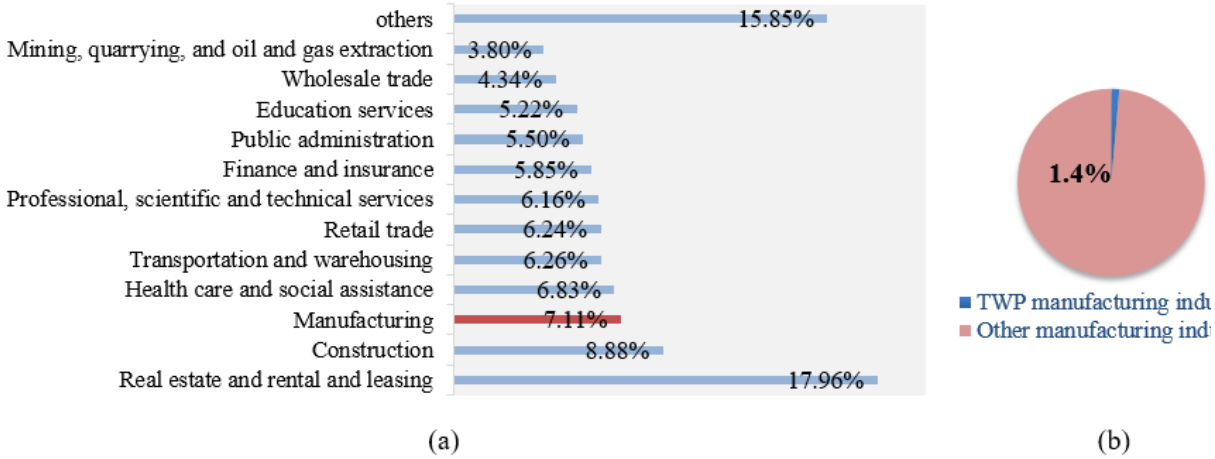

Figure 4.14 (a) 2017 BC GDP share (data source: Statista); (b) quantified 2017 nominal GDP contribution of BC TWP manufacturing to provincial manufacturing sector

4.4.5 Advantages of wood pellet manufacturing in BC

As revealed in this study, electricity mix determines the cleanness of the wood pellet, and electricity price is also a key cost category to the wood pellet production cost. This section thus investigates the influence of electricity mix and electricity prices on the Canadian wood pellet production by province. In the year of 2017, the electricity mix and prices by provinces in Canada are summarized in Table 4.15 [121], [122]. Sensitivities of these two parameters to the wood pellet production costs and environmental impacts are carried out in the simulation platform with capacity in 80,000t/year. For the scenarios to each province, two cases are carried out to compare CWP (Path 0) and TWP (Path 1) as illustrated in Figure 4.15.

As shown in Figure 4.15, provinces located in the left lower corner have both economic and environmental advantages to produce wood pellet because of their clean and low-cost electricity, those provinces include BC, Prince Edward Island (PE), Newfoundland and Labrador (NL), and Quebec (QC). In addition, TWP (Path 1) has clear advantages both economically and environmentally in comparison with the CWP (Path 0). It should be noted that these two factors, the electricity mix and prices will change dynamically with regional power policies and electricity demand in the future.

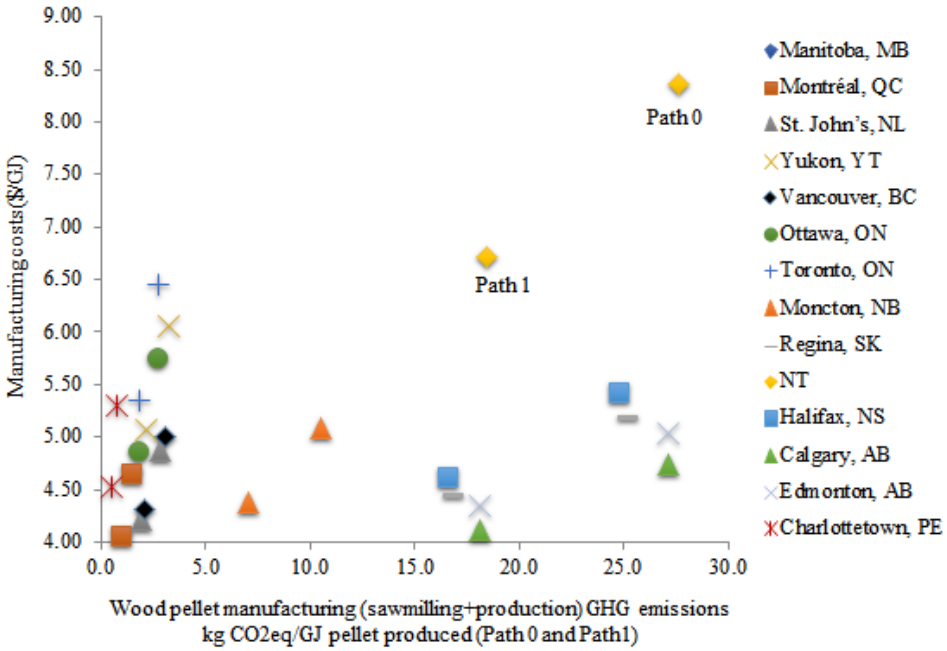

QC: Quebec; NL: Newfoundland and Labrador; BC: British Columbia; ON: Ontario; NB: New Brunswick; SK: Saskatchewan; NS: Nova Scotia; AB: Alberta; PE: Prince Edward Island

Figure 4.15 Canadian wood pellet GHG emissions and production costs by province as a function of electricity generation system and electricity selling prices in 2017

Table 4.15 Electricity generation by region in Canada since 2015 and the electricity price by region in 2017

City/Province	Electricity generation system (%) [a]									Electricity price [b,1] (¢/k W h) (year 2017)
	Hydro	Nuclear	Wind	Biomass	Nature gas	Petroleum	Solar	Coal	Other	
Manitoba, MB	96.6		2.7	0.2	0.2	0.1		0.2		4.68
Montréal, QC	95.5		3.7	0.5	0.1	0.2				4.50
St. John's, NL	95		0.4		0.5	4				5.65[4]
Yukon, YT	94		0.3		0.3	5.4				11.70
Vancouver, BC	90				10					6.33
Ottawa, ON	22.6	58.8	6	1	9.7	0.1	1.8			10.12
Toronto, ON	22.6	58.8	6	1	9.7	0.1	1.8			13.69[2]
Moncton, NB	20.2	33.1	6	3.9	18.1	5.7		12.8		6.75
Regina, SK	14.6		2.7		31.1	0.1		51.5		7.25
NT	10.9		1.3		0.7	84.7	0.1		2.3	23.40
Halifax, NS	9.3		12.9	4.2	12.1	14.8		46.6		8.41
Calgary, AB	2.1		3.8	1.5	38.6	2		51.8	0.3	4.97
Edmonton, AB	2.1		3.8	1.5	38.6	2		51.8	0.3	6.53[3]
Charlottetown, PE			97.4	0.7		1.8	0.1		0.1	7.83[2]
Share of Canada's electricity generation	58.9	15	4	1.4	9.3	1.3	0.5	9.6	0.4	

[a]: data source [121], [123]
[b]: data source [122], data based on large power sector, average prices on April 1, 2017; power demand 5,000kW, consumption 2340000kWh; Voltage 25kV; load factor 65%
1: In US dollar with currency 1Canandian dollar=0.78 US dollar
2: These bills have been estimated by Hydro-Quebec
3: Bills corresponding to consumption levels of 500kW or more have been estimated by Hydro-Quebec based on the applicable general rate
4: Newfoundland and Labrador Hydro rates for customers with a power demand of 30,000kW or more; Newfoundland Power rates for all other customer categories.

The production costs are not only correlated to the electricity prices but also influenced by the raw material and the labor costs. There is no significant difference between the labor costs in different provinces in Canada. But raw material costs could range widely, depending on the scarcity, distances to the pellet plant, and types of raw materials. It is difficult to assign the raw material costs in different provinces, but we can articulate the problem by observing the available forest resources in different regions. Figure 4.16 shows the worldwide third-party certified forest in millions of hectares. BC has a significantly rich biomass resources (53 million hectares), accounting for 33% of Canada's certified biomass forests, with its certified forest being almost equivalent to Russia (59 million hectares) and higher than USA (47 million hectares). Quebec (45.2 million hectares) has the second largest certified forest, followed by Ontario (26.8 million hectares) and Alberta (20.2 million hectares).

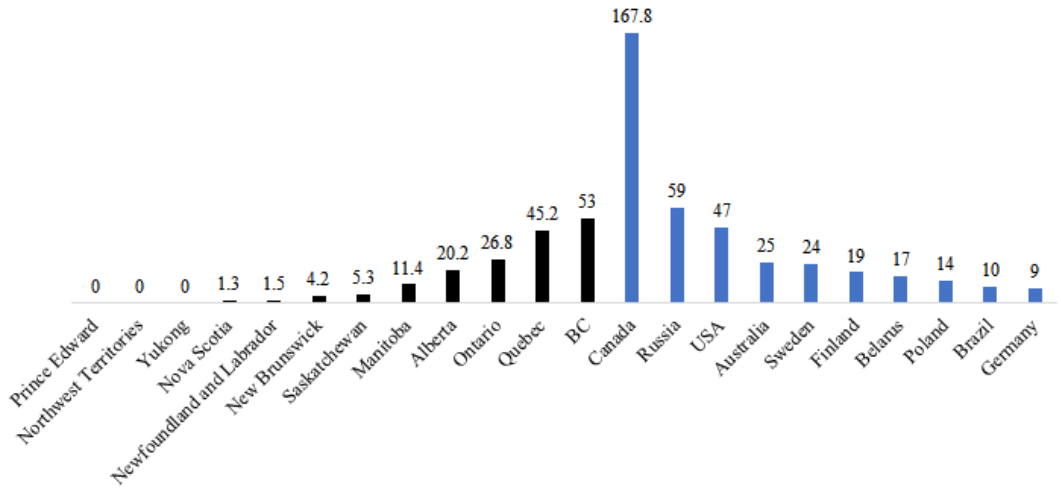

Figure 4.16 Third-party certified forest (2017 year-end) millions of hectares

Figure 4.17 shows the distribution of Canadian wood pellet plants in 2017 [116]. The provinces with both raw material and electricity advantages are BC and QC, located in the western and eastern Canada, who have the regional advantages. Alberta has the raw material advantages, but its coal-based electricity generation system has a high carbon intensity, 17 $kgCO_2eq/GJ$-WP-produced. Ontario has the advantage of abundant raw biomass materials, but due to its high electricity price, the production costs are high (at least 4.3$/GJ). Thus, it is reasonable to state that BC wood pellet industry has regional advantages on both raw material supply and clean electricity system.

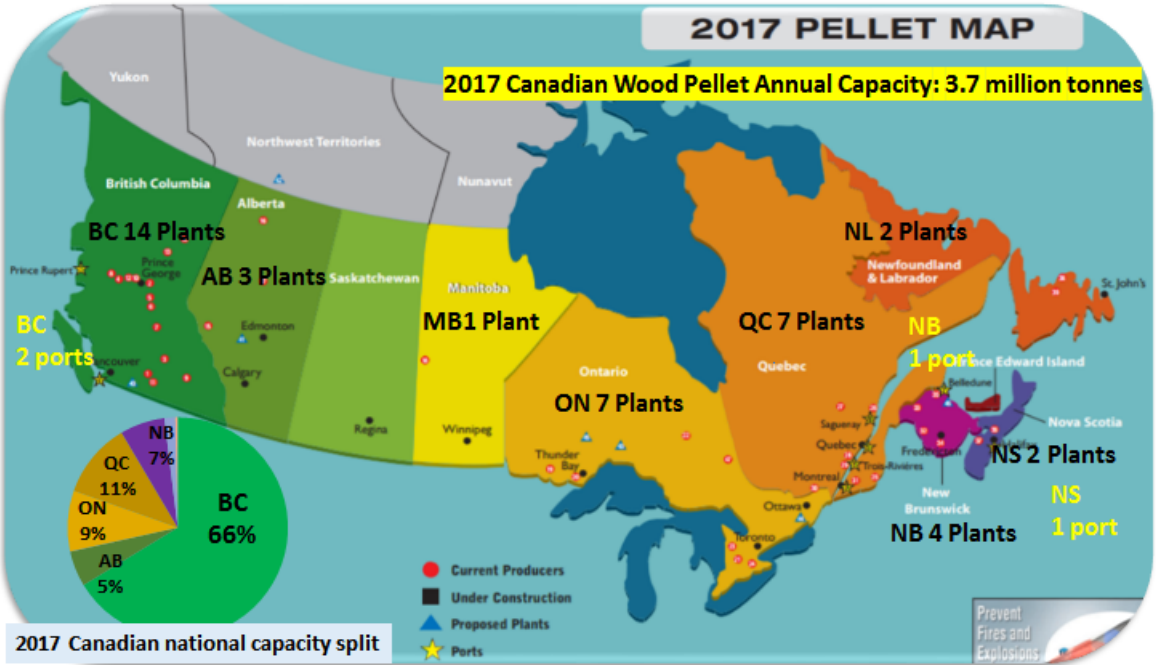

Figure 4.17 2017 Canadian wood pellet map [116]

Overall, BC has the comparative advantages of clean electricity mix, low electricity price, rich biomass resources, well developed wood pellet manufacturing industry, and geographical advantages. Therefore, it is reasonable to predict that BC should continue

developing wood pellet manufacturing.

4.5 Conclusions

An improved TWP production configuration is proposed which avoids using N_2 in torrefaction by recycling flue gases to the torrefier, catalyst is also avoided in combustion, and auto-thermal operation is achieved when torrefaction is operated at 300°C with 20% biomass weight loss. Based on this configuration, detail process simulation is carried out to size the equipment, quantify unit operation conditions and perform heat and mass integrations. The flowsheet configuration is unique, and the modeling is advanced with heat and mass transfer, kinetics, hydrodynamics, and thermodynamics taken into consideration.

The energetic, environment, and economic ("3E") performances of the CWP and TWPs production processes are quantified based on the simulation with uncertainties taken into consideration. It is revealed that producing TWP is beneficial than CWP in terms of the "3E" impacts. Path 1 is the best pathway to produce TWP, which can help reduce about 10% of production cost and 40% of energy consumption and GHG emissions in comparison with the CWP. If possible, torrefaction should always be carried out before grinding, in order to lower the electricity use in grinding. Cost analysis revealed that capital cost only accounts for about 10% of the total production costs, and the other 90% is contributed by the operating cost, within which raw material costs shared 40%, electricity costs shared 20% and the labor costs share 15% of the operating costs. Therefore, wood pellet plant should be located in the region with rich biomass resources, clean electricity mix, and low electricity and labor costs.

However, non-auto-thermal operation systems are not investigated for torrefied wood pellet production processes because it should be avoided through appropriate process

integration to achieve auto-thermal operation. Otherwise, additional fuel and N_2 may be required, which requires further investigations.

The minimum selling price of the BC TWPs would be varies around 6.67 $/GJ, equal to 140 $/t. It is predicted that TWP manufacturing can potentially contributes at least 206.7 million $/year to the provincial economy, sharing 1.4% to the BC manufacturing sector.

BC has comparative advantages in wood pellet manufacturing, with rich biomass resources, clean and low price of electricity, well developed industrial and business relationship, as well as geographical advantages. In addition, with the global expanding demand, BC is expected to continue developing a strong wood pellet manufacturing sector in the future.

Chapter 5: Supply chain analysis of BC wood pellet delivered to different markets

5.1 Introduction

There has been no published research to include different wood pellet production configurations in the supply chain analysis. Also, there is a lack of research to investigate BC wood pellet supply chains in terms of their "3E" impacts. The purposes of this chapter are thus to:

(a) evaluate the "3E" impacts of wood pellets derived from different pathways over the supply chains from BC to different markets including UK, Japan, Ontario, and Alberta.

(b) identify and investigate the hotspots and the sensitive parameters in the supply chains;

(c) quantify the GHG emissions reduction potential of replacing coal with BC WPs;

(d) propose improvement strategies and environmental-economic trade-offs of BC wood pellet in different markets.

5.2 Case study definition and key assumptions

Four destinations are selected as regional examples, namely Drax Power Generation station in UK and Kochi Power Generation station in Japan for overseas markets, and Genesee Power Generation station, which belongs to Capital Power Corporation (CPG) at Alberta and Atikokan Power Generation station, which belongs to Ontario Power Generation (OPG), at Ontario for domestic markets as shown in Figure 5.1. All those power stations are mandated to phase out coal and replaced by wood pellet.

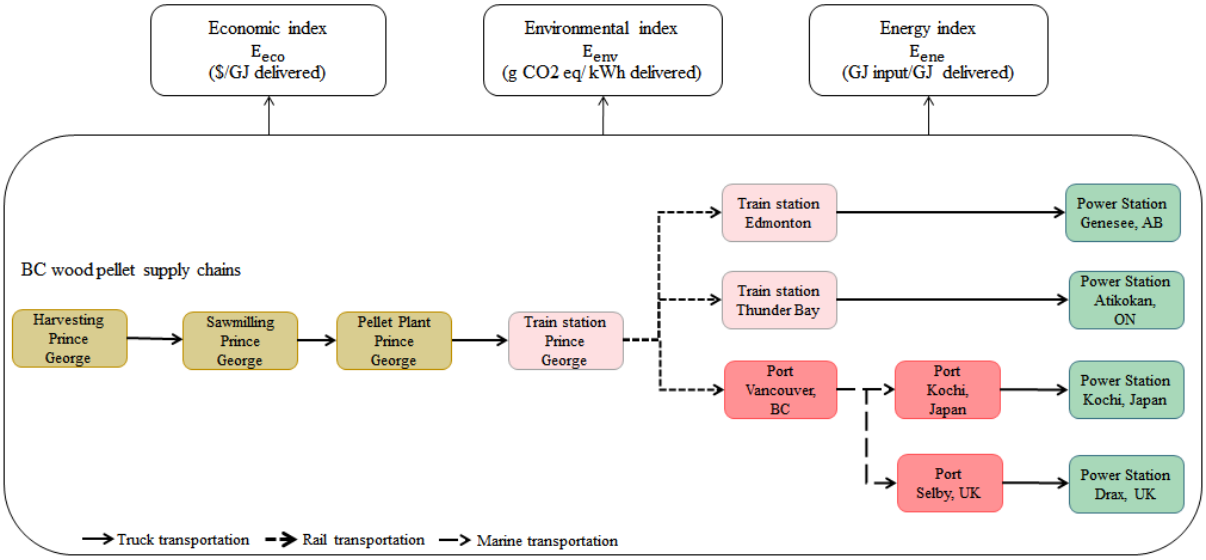

Figure 5.1 System boundary of BC wood pellet supply chains to UK, Japan, Ontario, and Alberta

The system boundaries for the metrics of energy consumption, GHG CO_2 equivalent emissions, and costs in each stage are defined below:

(1) Harvesting stage

Operation tasks involving fossil fuel consumptions and emissions in the phase of planning & layout, road construction, right-of-way logging, logging, camp, and silviculture are included (details refer to section F.1.) Energy consumption and GHG emissions from equipment and vehicle fabrications that involved in the above six phases are not considered in this analysis. Energy consumed and GHG emissions from hauling are not included as part of the harvesting stage but are aggregated into heavy duty truck transportation from harvesting site to sawmilling site.

The costs of biomass harvesting are not individually quantified; nevertheless, they are incorporated in the raw material costs at the wood pellet plant gate.

(2) Sawmilling stage

Electricity consumed for sawmill operation is the only fuel category considered for energy consumption and GHG emissions. According to the report from Canadian Industry Program for Energy Conservation Forest Products Association of Canada (CIEEDAC) [124], in sawmilling plant, electricity is the primary energy consumed with negligible consumption of others, i.e. natural gas, heavy fuel oil, middle distillates, propane, and steam. For details, refer to section F.2.

Costs of sawmilling are not quantified individually but are aggregated into raw material costs at the pellet plant gate.

(3) Production stage

The system boundary for the “3E” metrics is set out in detail in Section 4.1.

(4) Port operation

Energy consumption and GHG emissions associated with fuel and electricity from marine shipping, use of rail, on-road and non-road equipment, and administrative activities associated with port operation are included [125]; details are given in section F.3. Up-and down-stream GHG emissions and energy consumptions associated production or consumption of cargoes, heavy industrial processes on or adjacent to port lands, e.g. chemical or cement manufacturing, are not covered.

Costs of port operation are also neglected in this study.

(5) Storage

Energy consumption in storage facilities is neglected in this study. The energy consumption from construction is negligible when amortized over the long life time (e.g. 20

years). Furthermore, electricity usage for light and ventilation is limited, to avoid waste of energy.

GHG emissions from storage only covers off-gassing emissions from the wood pellets themselves (see section F.4). Emissions from facilities or building construction are not included.

Costs of storage are included in transportation costs.

(6) Transportation

Transportation energy and GHG emissions are associated with (a) vehicle operation, (b) vehicle material & assembly, and (c) the fuel supply chain including fuel dispensing, fuel distribution and storage, fuel production, feedstock transmission, feedstock recovery, feedstock upgrading, land-use changes, cultivation, fertilizer manufacture, gas leaks and flares, CO_2, H_2S removed from NG, emissions displaced categories. Details refer to section F.5.

Costs of transportation include rental or use of vehicles, costs of labour, toll fees, and fuel costs.

(7) End-use

Only GHG emissions from fuel, i.e. CWP/TWPs or coal, are included. Emissions from construction of power plant building and equipment, as well as the utilities used for operation, e.g. electricity for lighting and office heating, are not included.

Differences in cost between firing with coal and firing with biomass are assumed to be small and are therefore not considered.

The base cases for the four supply chains are carried out with the following assumptions:

(a) BC wood pellet supply chains include biomass harvesting, sawmilling, pellet plant manufacturing, port operation (for overseas), storage, transportations, and end-use stages, as shown in Figure 5.1;

(b) The plantation stage is excluded because biomass residues are a waste byproduct from sawmill operations, with lumbers as the main product;

(c) Wood pellet plants are in the capacity of 80,000t/year, and operated auto-thermally with the same conditions as discussed in Chapter 4. Results from Chapter 4 are adopted for the "3E" analysis.

(d) For transportation, fossil fuels are used for all the transportation vehicles and Handymax is used for the marine transportations.

5.3 Methodology and supply chain inventory data

Again, we applied the three metrics to investigate the CWP and TWPs supply chains performances:

(1) delivery costs in $/GJ wood pellets (WPs) delivered to power plants (simplify to $/GJ);

(2) energy consumption in GJ primary energy input/GJ WPs delivered to power plants (simplify to GJ/GJ-WPs);

(3) environmental impacts in gCO_2eq/kWh-WPs-delivered and gCO_2eq/kWh-electricity-generated, depending on different analysis purposes: for WPs supply chain comparisons, the former environmental functional unit is applied, and for coal reduction potential analysis, the later one is used.

Supply chain stages are grouped into two main categories according to their calculation methods: the first category includes harvesting, sawmill operation, production, storage, and port operation stages; the second category includes all transportation segments.

Energy consumption of the supply chains $E_{ene,LC}$ (GJ/GJ) is calculated by Eq. (5.1).

$$E_{ene,LC} = E_{ene,H-P} + E_{ene,trans} \tag{5.1}$$

With $E_{ene,H-P}$ being the total primary energy consumptions of the first category in GJ/GJ, calculated according to Eq. (5.2).

$$\begin{aligned} E_{ene,H-P} &= \sum_{m} \sum_{n} E_{ene,m,n} \\ &= E_{harvesting,n} + E_{storage,n} + E_{port,n} + (e_{saw} \\ &\quad + e_{production})/\xi_e \end{aligned} \tag{5.2}$$

The primary energy consumptions of the individual stages $E_{ene,m}$ (GJ/GJ) are summarized in Table 5.1, where m indicates harvesting, sawmilling, production, storage and port operation, and n indicates different types of primary energy consumptions. e_{saw} and $e_{production}$ are the electricity consumptions of the sawmill and production stages. ξ_e is the electricity generation efficiency.

Table 5.1 Life cycle inventory data of BC wood pellet supply chains

	Energy consumption $\mathbf{E_{ene,m,n}}$			GHG emissions $\mathbf{E_{env}}$ (gCO_2eq/GJ)		Costs ($/GJ) $\mathbf{E_{eco}}$
Stage m	Fuel/ material n	Unit	Amount	$EF_{m,n}$	$\xi_{m,n}$	
Harvesting	Fossil diesel	l/m^3 logs delivered	3.48 [a]	$EF_{m,diesel}$=22352 gCO_2eq/GJ [f]		Group to raw material costs in the production stage
Sawmill	Electricity	GJ/t pellet produced	0.186 [b]	The same as production stage		Group to raw material costs in the production stage
Production	Electricity (90% hydro and10% NG)	GJ electricity/ GJ pellet produced	Path 0=0.069 [c] Path 1=0.039 [c] Path 2=0.060 [c] Path 3=0.081 [c] Path 4=0.110 [c]	$EF_{m,hydro}$ =12,782 gCO_2eq/GJ delivered [f]; $EF_{m,NG}$ = 154,833 gCO_2eq/GJ delivered [f]	$\xi_{m,hydro}$ = 99%; $\xi_{m,NG}$ = 45%	E_{prod}(Path 0) = 4.11 $/GJ [c] E_{prod} (Path 1) = 3.63 $/GJ [c] E_{prod}(Path 2) = 3.80 $/GJ [c] E_{prod}(Path 3) = 4.38 $/GJ [c] E_{prod}(Path 4) = 4.32 $/GJ [c]
	Carbon steel	g/GJ pellet produced	Path 0=6.06 [c] Path 1=6.47 [c] Path 2=5.80 [c] Path 3=8.46 [c] Path 4=6.65 [c]	444,0000 gCO_2eq/ t carbon steel [g]		
	Rubber	g/GJ pellet produced	Path 0=0.038[c] Path 1=0.031[c] Path 2=0.031[c] Path 3=0.031[c] Path 4=0.031[c]	2830,000 gCO_2eq /t rubber [g]		
Storage	0	0	0	E_{env}(CWP)=8600 gCO_2eq/t [d] E_{env}(TWP)=7000 gCO_2eq/t [d]		
Port Operation	0	GJ/t pellet	0.073 [e]	E_{env}=5.246 gCO_2eq/t [e]		

a: detail refers to F.1; data source: [126]
b: detail refers to F.2; data source: [127]
c: data source: simulation results from Chapter 4; electricity average generation efficiency 94.5% (GHGenius 4.3 2018 BC)
d: detail refers to F.4; data source: [128], [129], [130], [131], [132], [133], [134]
e: detail refers to F.3; data source: [125]
f: data source: GHGenius 4.3 2017 Canada
g: data source: SimaPro 8.3

Energy consumption of the transportation stages $E_{ene,trans}$ is calculated by Eq. (5.3).

$$E_{ene,trans} = \sum_{v} \sum_{\boldsymbol{n}} EI_{v,n} \cdot m_{cargo} \cdot d_{v,A-B} / HHV_{pellet} \quad (5.3)$$

Where $EI_{v,n}$ (in kJ/t-km) is the energy intensity of vehicle v using fuel type n, m_{cargo} is the weight of biomass cargo being transported as presented in Table 5.2: for the logs hauling stage (T-T-1) and the raw material collection stage (T-T-2), this value indicates the biomass raw material required to be transported to the pellet plant to produce 1 t of wood pellet; for transportation stages performed after the pellet plant, this value equals 1 t. $d_{v,A-B}$ is the transportation distance from A to B using vehicle v. HHV_{pellet} is the high heating value of the pellet product, which equals 17GJ/t for CWPs, and 21 GJ/t for TWPs, respectively.

Table 5.2 Inventory of the transportation sector

Pathways			Path 0	Path 1	Path 2	Path 3	Path 4
Transportation segment	Sub-segment	Distance (km)	Cargo (t)	Cargo (t)	Cargo (t)	Cargo (t)	Cargo (t)
T-T	T-T-1	150	1.56	1.716	1.716	1.865	1.716
	T-T-2	20	1.56	1.716	1.716	1.865	1.716
	T-T-3	12	1	1	1	1	1
	T-T-AB	80	1	1	1	1	1
	T-T-ON	20	1	1	1	1	1
	T-T-Japan	5	1	1	1	1	1
	T-T-UK	11	1	1	1	1	1
T-R	T-R-Van	770	1	1	1	1	1
	T-R-AB	740	1	1	1	1	1
	T-R-ON	2850	1	1	1	1	1
T-S	T-S-UK	16600	1	1	1	1	1
	T-S-Japan	8300	1	1	1	1	1

T-T-1: heavy-duty truck (HDT) transportation from harvesting site to sawmill site
T-T-2: HDT transportation from sawmill site to pellet plant site
T-T-3: HDT transportation from pellet plant to Prince George railhead
T-T-AB: HDT transportation from Edmonton (AB) railway station to Genesee Power Generation
T-T-ON: HDT transportation from Thunder Bay (ON) railway station to Atikokan Power Generation
T-T-Japan: HDT transportation from port of Kochi to Kochi Power Station

T-T-UK: HDT transportation from port of Selby to Drax Power Station
T-R-Van: railway transportation from Prince George railhead to Vancouver port
T-R-AB: railway transportation from Prince George railhead to Edmonton railway station (Alberta)
T-R-ON: railway transportation from Prince George railhead to Thunder Bay railhead (Ontario)
T-S-UK: marine transportation from Vancouver port to Selby port
T-S-Japan: marine transportation from Vancouver port to Kochi port

Environmental GHG emissions indicator in gCO_2eq/kWh-WPs-delivered is calculated according to Eq. (5.4).

$$E_{env,LC} = E_{env,H-P} + E_{env,trans} \quad (5.4)$$

Where $E_{env,H-P}$ is the total GHG emissions of the first stage in gCO_2eq/kWh-WPs-delivered, which is calculated according to Eq. (5.5).

$$E_{env,H-P} = (E_{ene,harvest} \cdot EF_{fossil} + (e_{Sawmill} + e_{production}) \cdot EF_e + E_{env,storage} + E_{env,port})/(278kWh/GJ) \quad (5.5)$$

Where EF indicates emission factor in gCO_2eq/GJ fuel type n. $E_{ene,harvest}$ is the fossil diesel consumption of harvesting processes to produce per GJ of wood pellets. e_{saw} and $e_{production}$ are the electricity consumptions of the sawmilling and the production stages in GJ electricity/GJ-WPs-delivered. EF_e is the electricity emission factor, which depends on the electricity mix, for example, BC electricity is 90% of hydro and 10% of NG, thus the BC electricity emission factor is also mix of the hydro and NG emission factors proportionally. $E_{env,storage}$is the environmental emission of the wood pellet storage processes. $E_{env,port}$ is the GHG emission of the port operations. Parameters involved in Eq. (5.5) are summarized in Table 5.1, with details referred to Appendix F .

$E_{env,trans}$ is the total environmental emissions of the transportation stages in gCO_2eq/kWh-delivered, which is calculated according to Eq. (5.6).

$$E_{env,trans} = \sum_{v} \sum_{\boldsymbol{n}} (EF_{v,n}/(HHV_{pellet} \cdot (278kWh/GJ))) \cdot m_{cargo} \cdot d_{v,A-B} \quad (5.6)$$

Where $EF_{v,n}$ in gCO_2eq/t_km is the emission factor of the transportation vehicle v using fuel type n, with detail in Table F.4.

Delivery costs of BC CWP and TWPs are calculated based on at quantified minimum selling price (MSP, see section 4.4.3) of 130 $/t (equiv. 6.2 $/GJ) plus the transportation costs $E_{eco,trans}$, as shown in Eq. **(**5.7).

$$E_{eco,LC} = MSP + E_{eco,trans} \quad (5.7)$$

The transportation cost models in different ways $E_{eco,trans}$ are presented in Appendix G , in which Eq. (G.7) is used to calculate the truck transportation cost, Eq. (G.10) is used for calculate railway transportation costs, and Eq. (G.11) is used to calculate the marine transportation costs.

5.4 Results and discussion

5.4.1 3E impacts over the supply chain

Figure 5.2 shows the supply chain "3E" impacts of the BC wood pellet delivered to different power plant destinations in Alberta, Ontario, Japan and the UK. For energetic and environmental metrics, TWPs produced from Paths 1-3 perform better than CWP from Path 0. But due to its high energy density of TWP, there should be a turning distance point for Path 4 to be superior to Path 0. While economically, all the TWPs production pathways performs better than the CWP from Path. Overall, TWP is a better product than CWP, and Path 1 is the best configuration, which can help reduce approximately 22% to 29% of GHG emissions, 25% to 30% of energy consumption and 18% to 22% of costs, in comparison with

the CWP. The impact of the production configuration is significant, which can narrow or even eliminate the "3E" impacts gaps caused by geographical distances. In the later section, an expanded market boundary with different transportation distances will be further discussed.

In addition, the delivery cost to Ontario is higher than the delivery cost to Japan and is similar to UK due to the low marine transportation costs. Life cycle GHG emissions of BC wood pellet delivered to Japan are generally lower than to Ontario.

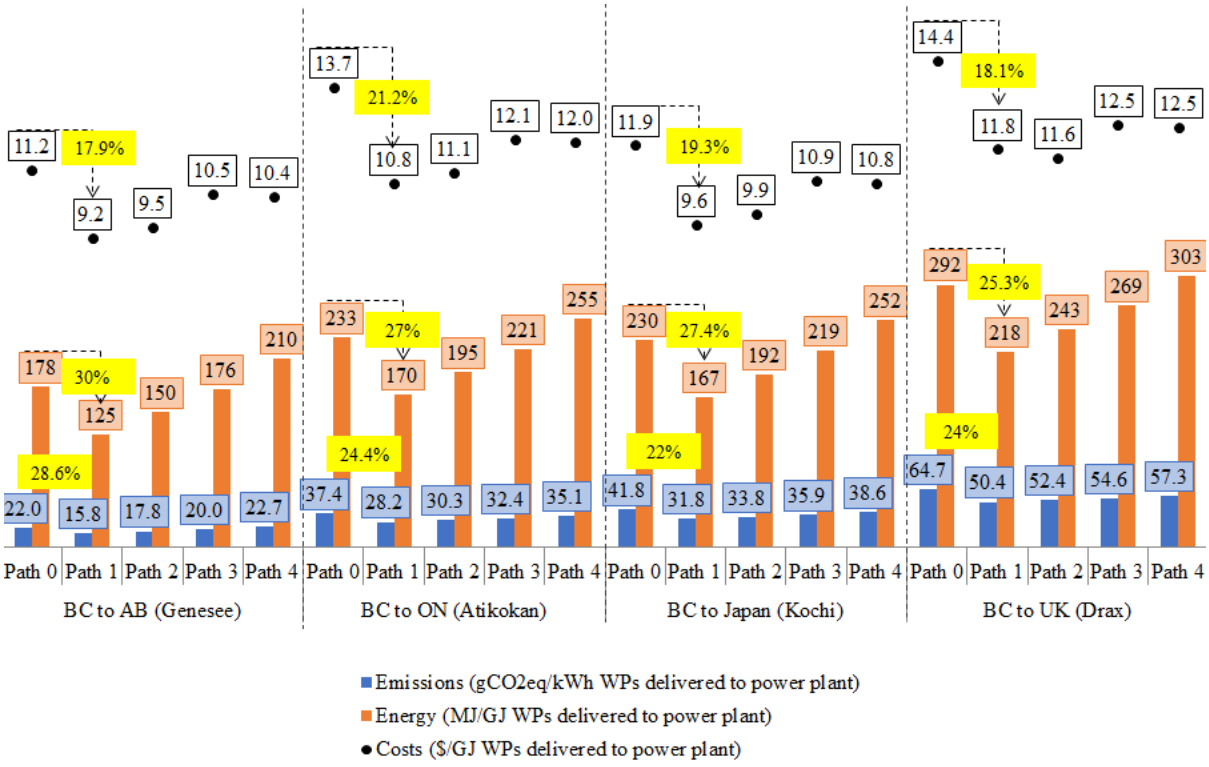

Figure 5.2 "3E" metrics of BC CWP and TWPs delivered to the UK, Japan, Ontario, and Alberta

5.4.2 Supply chain "3E" impacts break-down analysis

In order to identify the hot spots over supply chains, a break-down analysis of the "3E" metrics of different supply chains to different power plants are carried out, as shown in Figure 5.3 (produced in Path 1 as an example).

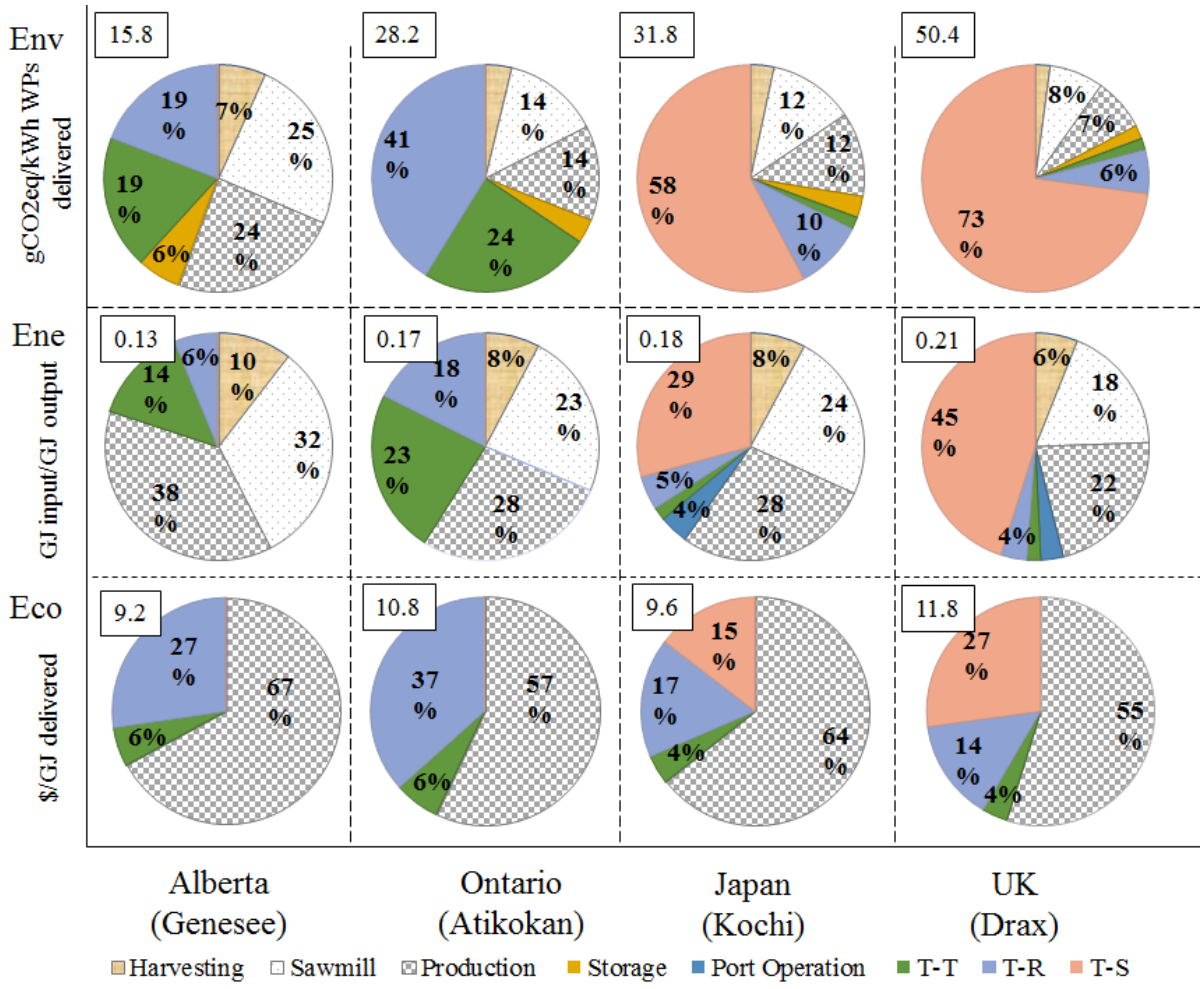

Env in gCO2eq/kWh-WPs delivered to power plants
Ene in GJ-primary-energy-input/GJ-WPs delivered to power plants
Eco in $/GJ-WPs delivered to power plants
Electricity consumption stages: sawmill and production stages

Figure 5.3 Break-down of life cycle "3E" metrics of BC TWPs (Path 1) delivered to the UK, Japan, Ontario, and Alberta power stations

Environmental metrics break-down reveals that transportation sector, including truck, railway, and marine transportation, share over 50% (Alberta) to 85% (the UK) of GHG emissions over supply chains. The electricity consumption stages, including sawmill and pellet production stages, together account for the other 15% (the UK) to 50% (Alberta), respectively. In comparison, emissions from harvesting, port operation, and storage are negligible. Thus, the key solutions to reduce supply chain carbon footprint are (a) to increase efficiencies of the transportation stages, measures e.g. using large vessels, replace fossil fuel with biofuels and improve logistics. Sensitivity analysis of these measures will be carried out in later section; (b) to improve efficiencies of the electricity stages, measures including reduce electricity usage by improve process flowsheet, locate sawmill and pellet plant in the region powered by clean electricity.

Energy consumption break-down shows that transportation segments are still the major energy consumers over the supply chains for most destinations, followed by the electricity usage stages, including sawmilling and production stages. In addition, the individual stage energy consumption contribution ratio is not proportional to the GHG emission shares, i.e. for the case of BC to the UK supply chain, the electricity consumption stages contribute 15% to the GHG emissions, and 40% to energy consumptions, mainly due to BC's clean electricity (90% hydro, 10% NG), which leads to a lower GHG emissions, and makes BC's manufacturing sector environmentally competitive. If the sawmill and pellet plant are located in the fossil electricity intensive region, the total GHG emission is expected to increase significantly in proportion to their energy consumption. BC's clean electricity system and rich biomass resources are a natural endowment for the manufacturing industry, especially the forest-related industry.

Economics metrics break-down suggests that pellet production is the highest cost over the supply chains, sharing about 55% to 67% of the total delivered costs. Therefore, to increase the economic competitiveness of the BC wood pellet, production cost should be reduced. As been revealed in Chapter 4, operating cost categories including raw material, electricity and labor costs are the key cost items. To overseas markets, rail transportation and marine transportation are the other major cost categories, and rail transportation is much more expensive than marine transportation over the same distance.

Overall, it is crucial that wood pellet plant should be located at the region with efficient logistic system, clean and cheap electricity, rich biomass resources and low labor costs. In addition, improving process energy efficiencies is always a useful approach to improve the competitiveness of a product.

5.4.3 Uncertainties

Uncertainty analysis of the BC CWP and TWP supply chains "3E" impacts will include the following aspects:

- Source of uncertainties
- Range of uncertainties
- Distribution of uncertainty parameters
- Cumulative distribution function of the "3E" metrics

5.4.3.1 Energy consumption

Wood pellet supply chain primary energy consumption uncertainties are mainly from (a) the production stage in which the main sources are the grinding and pelleting energy

consumption if the torrefaction systems operate auto-thermally, as discussed in section 4.4.2.1, and (b) harvesting, sawmilling and transportation stages.

In the absence of information on the ranges of the parameters in group (b), the significance of variations in energy consumption have been explored by assuming that the energy consumed in each stage follows a Gaussian distribution with mean being the base case values and a coefficient of variation (CV) of 25%, as summarized in Table 5.3. The normal distribution has been used because, even though the individual constituent distributions may not be Gaussian, the central limit theorem shows that the combined distribution tends to be approximately Gaussian.

Table 5.3 Gaussian distribution parameters of energy consumption in BC wood pellet supply chains

	Uncertain factor	Mean	SD	CV
Harvesting (L/m^3 diesel)		3.48 [a]	0.87	25%
Sawmilling (Primary energy GJ/t pellets)		0.836 [b]	0.209	25%
Production (Primary energy GJ/GJ pellet)	Path0	0.073 [c]	0.01825	25%
	Path1	0.041 [c]	0.01025	25%
	Path2	0.063 [c]	0.01575	25%
	Path3	0.086[c]	0.00215	25%
	Path4	0.125 [c]	0.00312	25%
Transportation (Active Energy Intensity kJ/t_km)	Handymax[f]	124 [d]	31	25%
	Rail	220 [d]	55	25%
	Heavy Duty Truck	1963 [d]	490.75	25%
Port operation (Primary energy GJ/t pellets)		0.073 [e]	0.01825	25%

a: data source [126]
b: data source [127]
c: data source Figure 4.4
d: data source GHGenius 4.3 based on 2017 BC Canada
e: data source [125]
f: Handymax ship vessel size in 450,000DWT/vessel

Figure 5.4 shows the CDF of life cycle primary energy consumption of BC TWP supply chains to different destinations, which confirm that the comparisons explored in this work are robust. As can be seen, allowing for variations in energy consumption, Path1uses consistently less energy than the other pathways. For example, for the BC to UK supply chain, Path 1 has 100% probability to consume less than 0.27 GJ/GJ of primary energy, while Path 2 has about 90% probability, and other pathways have less than 50% of possibility.

In addition, the differences in energy consumption between supplying to Japan and Ontario are within the likely range of variability, so that these two supply chains can be considered as having equal performances. The impact of the process configuration on the supply chain is clearly confirmed; e.g. energy consumption of delivering TWPs derived from Path 4 to Alberta is convincingly higher than TWPs derived from Path 1 and delivered to Japan. In conclusion, with 25% CV, Path 1 remains the best processing sequence to produce TWPs in terms of energy consumption.

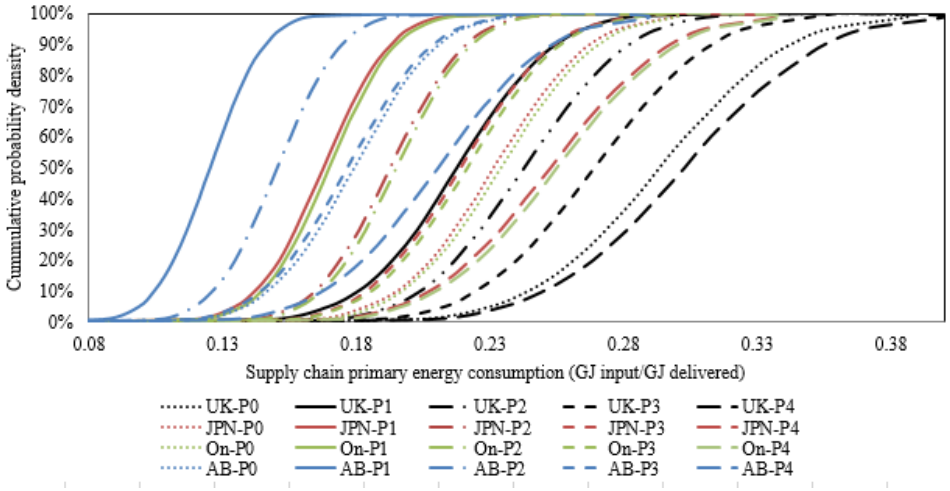

Figure 5.4 Cumulative distribution function of the supply chain primary energy consumptions of BC TWPs (derived from Path1) delivered to the UK, Japan, Ontario, and Alberta (in GJ primary energy input/GJ delivered to power station)

5.4.3.2 Environmental impact

Over the whole supply chain, it is revealed that GHG emissions mainly arise from three stages, namely transportation, production, and sawmill operations, of which the first consumes fuel while the other two are electricity intensive. In comparison, emissions from harvesting, port operation, and storage are negligible. Uncertainties in the supply chain GHG emissions arise from two sources: the primary energy consumption and emission factors. Uncertainties in the primary energy consumption over the supply chains are discussed in section 5.4.3.1, and adopted here. Uncertainties in the BC electricity emission factors have been discussed in section 4.4.2.2; by assuming they follow a uniform distribution functions with two sets of data are observed from Canada Statistics (GHGenius 4.3 BC 2018) and Dowlatabadi et al. Emission factors of the transportation fuel are also calculated by using GHGenius 4.3, following a uniform distribution function as presented in Table 5.4.

Table 5.4 Uniform distribution function parameters of the electricity emission factors and GHG emission factors derived from different resources

Uncertain factor	Min	Max
Carbon steel emission factor (gCO_2eq/t)	399600[a*]	4884000[a-1*]
Hydro to electricity emission factor (gCO_2eq/GJ-electricity-generated)	12782[b*]	19173[b-1*]
NG to electricity emission factor (gCO_2eq/GJ-electricity-generated)	154833[c*]	232250[c-1*]
Rubber emission factor (gCO_2eq/t)	2547000[d*]	3113000[d-1*]
Emission factors of transportation fuel (gCO_2eq/t_km)		
Handymax	12.9 [f]	19.35 [f-1]
Rail	23.8 [f]	37.5 [f-1]
Heavy Duty Truck	189.5 [f]	284.25 [f-1]

a*: data source from SimaPro 8.3;
a-1*: data source assumption which is about 1.5 times of a*;
b*: data source from GHGenius 4.3 based on 2017 BC;
b-1*: data source from Dowlatabadi et al (2011) corrected value, which is about 1.5 times of GHGenius 4.3 value
c*: data source from GHGenius 4.3 based on 2017 BC;
c-1*: data source from Dowlatabadi et al (2011) corrected value, which is about 1.5 times of GHGenius 4.3 value;
d*: data source from SimaPro 8.3;
d-1*: data source assumption which is about 1.5 times of d*
f: data source from GHGenius 4.3 based on 2017 BC

f-1: data assumed as 1.5 times of value f

Figure 5.5 shows the CDF of life cycle GHG emissions of BC TWPs delivered to different destinations. As can be seen, Path 1 has the highest probability to generate less GHG emissions in comparison with other pathways, followed by Path 2, Path 3 and Path 4, and CWPs (Path 0) has the highest probability to have higher GHG emissions. For example, for the BC to AB supply chains in blue, Path 1 has 100% probability to emit less than 17 gCO_2eq/kWh-delivered GHG emissions, while Path 2 has about 70%, and the other pathways have less than 50% chances to emit less than 17 gCO_2eq/kWh-delivered GHG emissions.

Overall, supply to the UK still has the highest GHG emissions. Life cycle GHG emissions for supply to Japan and Ontario depend on the wood pellet production configurations, e.g. Ontario supply chain using Path 0 has higher emissions than supply to Japan using Path 1. The AB supply chains emit least amount of GHG emission.

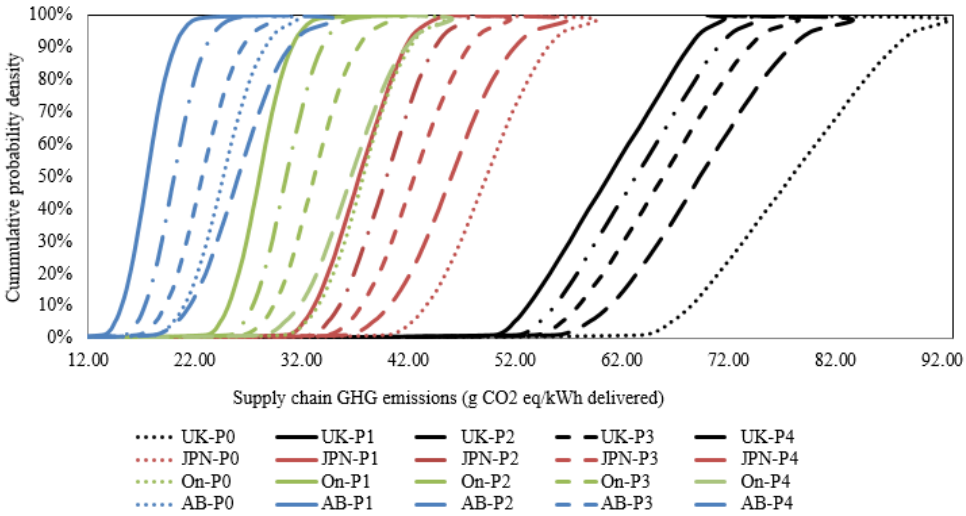

Figure 5.5 Cumulative ditribution function of the supply chain GHG emissions of BC TWPs (derived from Path1) delivered to the UK, Japan, Ontario, and Alberta (in gCO_2eq/kWh-delivered)

5.4.3.3 Economics impacts

Uncertainties in the total costs at different stages over the wood pellet supply chains could arise from the pellet plant stage, as discussed in section 0, and transportation costs, which are assumed to follow a normal distribution. The reason for chosen this distribution is because the combination effects of the complex economic performances may follow normal distribution according to central limit theorems. Mean values are calculated according to the base case assumptions. Two cases with 10% and 30% coefficient of variations are considered as summarized in Table 5.5.

Table 5.5 Gaussian distribution cost parameters over supply chain delivery costs

Uncertain factor		Mean ($/GJ)	Case 1 SD ($/GJ)	CV	Case 2 SD ($/GJ)	CV
T-T-3	CWP	0.25	0.025	10%	0.075	30%
	TWP	0.20	0.020	10%	0.006	30%
T-T-Japan	CWP	0.24	0.024	10%	0.072	30%
	TWP	0.19	0.019	10%	0.057	30%
T-T-UK	CWP	0.25	0.025	10%	0.075	30%
	TWP	0.20	0.020	10%	0.006	30%
Production	CWP	7.05	0.705	10%	2.116	30%
	TWP1	6.16	0.616	10%	1.847	30%
	TWP2	6.48	0.648	10%	1.944	30%
	TWP3	7.46	0.746	10%	2.237	30%
	TWP4	7.40	0.740	10%	2.221	30%
T-R-Vancouver	CWP	2.26	0.226	10%	0.678	30%
	TWP	1.62	0.162	10%	0.486	30%
T-R-AB	CWP	3.52	0.352	10%	1.056	30%
	TWP	2.51	0.251	10%	0.753	30%
T-R-ON	CWP	5.77	0.577	10%	1.731	30%
	TWP	3.96	0.396	10%	1.188	30%
T-S-UK (Handymax)	CWP	4.62	0.462	10%	1.386	30%

Uncertain factor		Mean ($/GJ)	Case 1 SD ($/GJ)	CV	Case 2 SD ($/GJ)	CV
	TWP	3.05	0.305	10%	0.915	30%
T-S-Japan (Handymax)	CWP	2.13	0.213	10%	0.639	30%
	TWP	1.39	0.139	10%	0.417	30%

CV $= \sigma/\mu$ (coefficient of variation)
Mean values are calculated according to the base case assumptions

Figure 5.6 (a) shows the CDF of the BC wood pellet supply chain cost (in $/GJ) with 10% cost variation. TWPs (Paths 1-4) are most likely to cost less than the CWP for all the markets excluding Alberta. For example, the costs of TWPs delivered to UK are definitively lower than 11 $/GJ, while Path 0 only has about 10% probability of being in this range. As for the Alberta market, Path 0 performs equally as Path 4, and both costs are higher than Paths 1, 2, and 3. Overall, Path 1 has a high possibility of being less costly than all the other pathways, followed by Path 2, Path 3 and Path 4. Delivered costs to the UK are the highest, followed by Ontario, Japan, and Alberta. Lastly, Figure 5.6 (a) also shows the importance of the process configuration in lowering the supply chain cost; e.g. delivering one GJ of TWP to Ontario is probably cheaper than delivering one GJ of CWP to Alberta.

Figure 5.6 (b) shows the change of delivery cost when the parameters are distributed with 30% coefficient of variation. Similar trends as case a (10% variation) are observed. However, in this case, the range of likely costs in Path 1 and Path 2 are very close, suggesting that the differences in economic performance between Paths 1 and 2 could be marginal when there is major uncertainty in those economic parameters.In additon, it also shows many overlaps between the CDF of differnet supply chains, suggesting with higher cost variations, the economic performaces of the

overseas markets in EU and Asia Pacific are almost equivalent to the domestic markets in Ontario and Alberta.

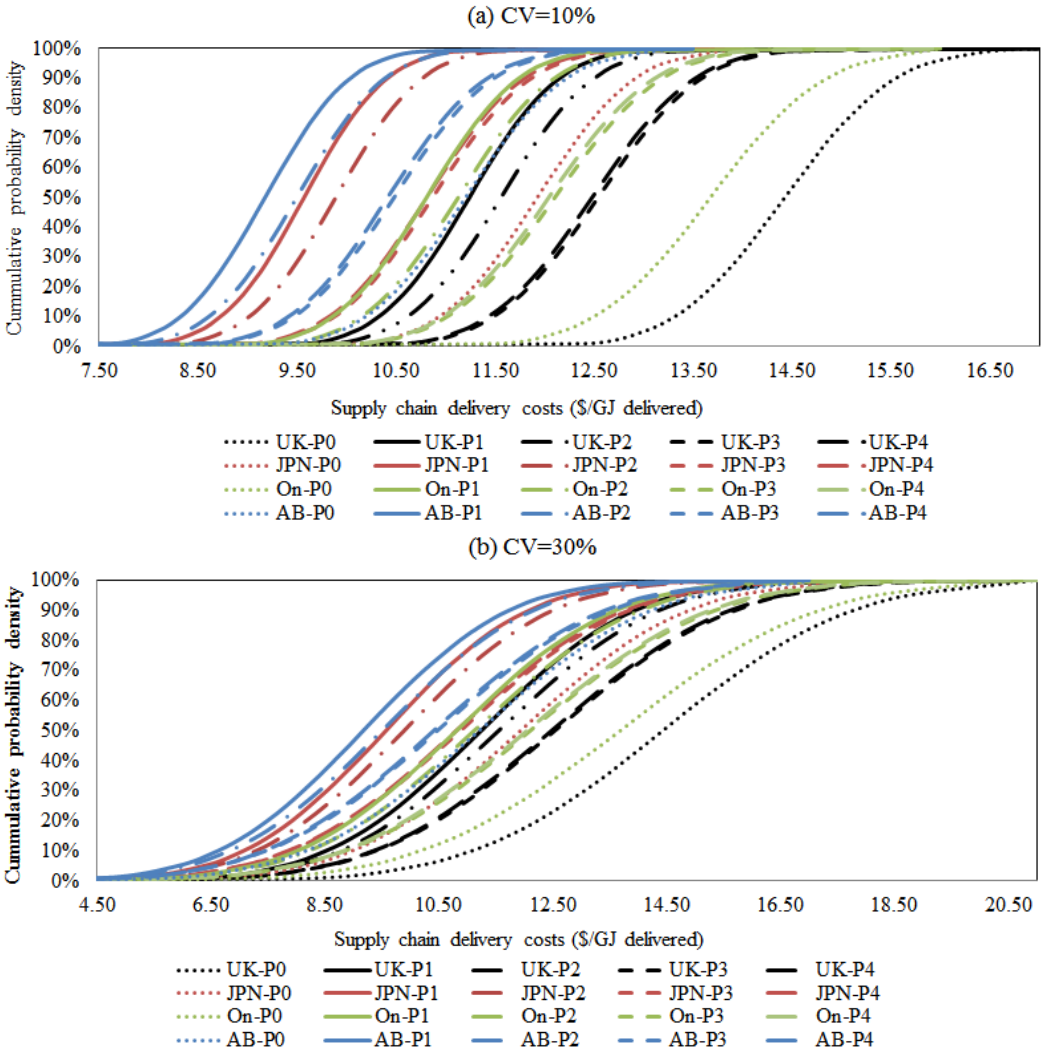

Figure 5.6 Cumulative distribution function of the supply chain delivery costs of BC TWPs (derived from Path1) delivered to the UK, Japan, Ontario, and Alberta (in $/GJ delivered to power stations)

5.4.4 Sensitivity analysis

In practice, at least two measures can be implemented to reduce the GHG emissions: using blended fuel for transportation and switching to a larger size shipping vessel. 65

countries around the world have mandated to promote biofuels [135]. The EU-27 once specified a 10% renewable content by 2020 for cars or trains [136]. Canada has a Renewable Fuel Standard featuring E5 ethanol (the blended fuel contains 5% ethanol and 95% gasoline) and RD2 renewable diesel (blended fuel with 2% biodiesel and 98% fossil diesel). Five provinces have individual provincial mandates, e.g. BC has a E5 and RD4 mandates, and is aiming to achieve E10 and RD10 by 2020; Alberta has E5 and RD2 mandates; Saskatchewan has E7.5 and RD2 mandates; Manitoba has 8.5% ethanol and 2% RD; Ontario is 5% ethanol and RD4 by 2018 [135]. In Asia Pacific, China aims to reach a 10% biofuels mandate by 2020. Main concerns of consumers on biofuels are higher prices and possible damage of biodiesel to some engines. According to Canadian Renewable Fuels Association (CRFA) and US energy department, biofuels prices are almost the same, and sometimes even lower than petroleum-based fuels, and some engines have shown better performances under standard tests than with fossil diesel [135], [137], [138]. Up to now, there is relatively little experience with using biodiesel in train engines. Most engine manufacturers appear to be willing to include B5, but less willing to include the use of higher blends like B10, B15, B20 [139]. In 2007, the Railway Association of Canada partnered with the Federal government to sign a Memorandum of Understanding to reduce locomotive GHG emissions. Several rail companies, such as Southern Railway of BC and Canadian Pacific, are testing the use of biodiesel in their fleets to meet this voluntary reduction [140]. Canadian Pacific has partnered with Natural Resources Canada to test the reliability of a 5% biodiesel blend fuel in cold weather conditions. Results have been promising. In comparison with the car and rail engine applications, marine biodiesel applications are limited due to many technical issues, such as

the cloud point. Through the works of IMO, the current version of ISO08217, 2010 technical fuel standard for marine fuels does not facilitate the introduction of biodiesel[141].

Based on the above information, it is reasonable to explore three cases by performing a sensitivity analysis, as summarized in Table 5.6.

- Case 1 is designed to investigate the influence of marine vessel size on the supply chain delivery costs and GHG emissions of BC CWP and TWP to overseas markets of Japan and the UK power plants. Two types of vessels are compared, Handymax which is usually applied and a larger vessel of Panamax. Influence of torrefaction technology is also compared with the effects of changing vessels.
- Case 2 is used to examine the impact of blended fuel (5% of biodiesel blends) for road transportation on supply chains GHG emissions of BC wood pellets to domestic markets of Alberta and Ontario. Influence of torrefaction technology is also compared with the effects of changing fuel types in truck and trains.
- Case 3 are used to examine the impact of blended fuel (10% of biodiesel blends) for road transportation on supply chain GHG emissions of BC wood pellets to domestic markets of Alberta and Ontario. Influence of torrefaction technology is also compared with the effects of changing fuel types in truck and trains.

Table 5.6 Case study assumptions of switching fuel type and ship vessel for the transportation sector

	Truck transportation		Rail transportation		Maine transportation			
	Fuel type	Emission intensity gCO_2eq/t_km	Fuel type	Emission intensity gCO_2eq/t_km	Fuel type	Vessel	Vessel size (DWT)	Emission intensity gCO_2eq/t_km
Base case	B0	189.5	B0	23.8	B0	Handymax	45,000	12.9
Case 1	B0	189.5	B0	23.8	B0	Panamax	80,000	9.7
Case 2	B5	176.8	B5	22.8	B0	Handymax	45,000	12.9
Case 3	B10	164.4	B10	21.0	B0	Handymax	45,000	9.7

B0: fossil fuel
B5: 95% of fossil fuel blends with 5% of biodiesel
B10: 90% of fossil fuel blends with 10% of biodiesel
DWT: deadweight toonage, refers to the carrying capacity of a vessel

Figure 5.7 (a) shows that switching ship size from Handymax to Panamamax can reduce GHG emissions by about 13% and 18% respectively for delivery from BC to Japan and UK. However, this effect is less significant than the effect of the processing configuration; e.g. Path 1 can reduce GHG emissions by about 25% in comparison with Path 0. As for the costs, using larger marine vessels can reduce about 5% of the supply chain delivery cost, but the effect is less significant than production configurations (18%).

Figure 5.7 (b) shows the effect of road transport fuel types. Again, it can be concluded that production configurations have the most significant effect (25% of GHG emissions reduction to Alberta and Ontario) in reducing supply chain GHG emissions in comparison with the switch of road transportation fuel (only about 2% GHG reduction for B5 and 5% of reduction for B10 blends).

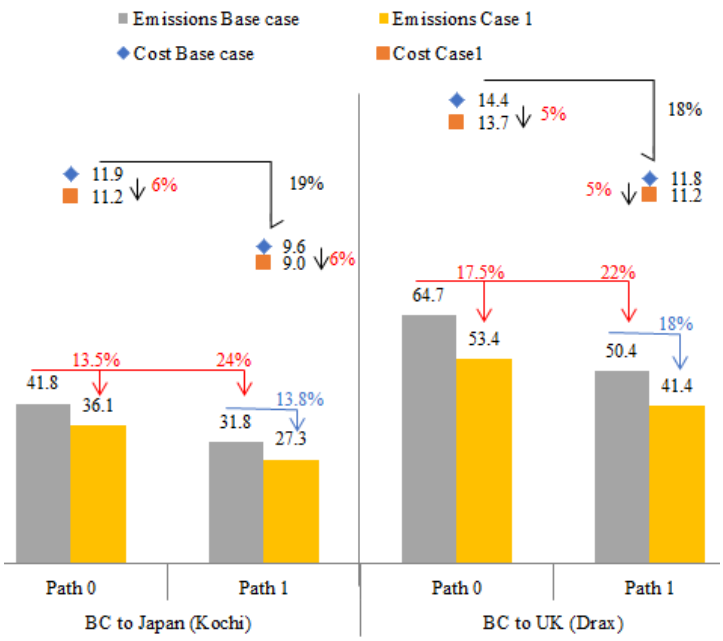

Cost in $/GJ delivered
GHG emissions in g CO2 eq/kwh wood pellet delivered to power plants

(a) Sensiitivity analysis of ship vessel

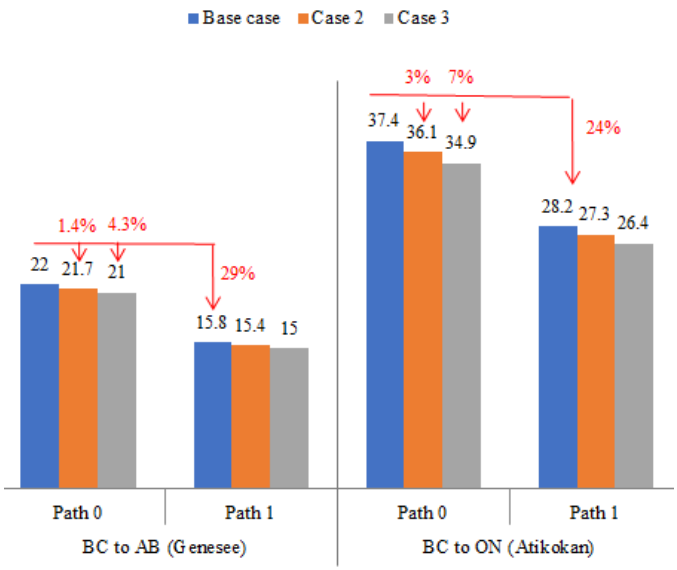

(b) Sensiitivity analysis of road fuel type influence on supply chain GHG emissions in gCO2eq/kWh wood pellet delivered to power plants

Figure 5.7 Sensitivity analysis of transportation: (a) sensitivity of ship vessel sizes on delivered costs and GHG emissions; (b) sensitivity of road fuel blend ratio on GHG emissions

5.4.5 GHG reduction potential for coal replacement

Conversion of a pulverized coal power plant to a pulverized TWP power plant is relatively straightforward in comparison with others, such as to a natural gas power plant which requires major changes of equipment [142]. A sheltered storage is required for strong hydrophilic CWP, while it may not necessary for TWP due to its hydrophobic property [19]. The additional capital investment is negligible since it will be leveraged by long life span of the power plant, which is usually more than 20 years. The cost in fuel fuel (coal or TWP) is thus the key contributor to the GHG emissions.

GHG emissions of electricity generation at the power plant by co-firing TWP with coal at ratio of θ, with indicator $Z_{TWP-coal,\theta}$ in gCO_2eq/kwh-electricity-generated, are calculated by

$$Z_{TWP-coal,\theta} = Z_{coal} \cdot (1-\theta) + Z_{TWP,\theta} \cdot \theta \quad (5.8)$$

The first term $Z_{coal} \cdot (1-\theta)$ is the emission from coal burning, with Z_{coal} as the coal emission intensity in gCO_2eq/kWh-electricity-generated with the value given in Table 5.7, which include several reliable literatures with comprehensive analysis. Here, the mean value 1034 gCO_2eq/kWh-electricity-generated is adopted for coal GHG emission intensity.

Table 5.7 Fuel cycle GHG emissions from coal generation

Reference	Region	Technology	gCO_2eq/kWh electricity generated
GHGenius 4.3 BC 2017	North America		1144.1[a]
Marcela et al [143]	Australia	Black coal	863-941, mean 902
		Brown coal	1175
Fridlerifsson et al. [144]	EU		955
2014 IPCC [145], [146]	EU	Pulverized coal	740- 910, mean 820
2011 IPCC [147]	EU	Various generator types without scrubbing	1001

Reference	Region	Technology	gCO_2eq/kWh electricity generated
Benjamin [148][b]	-	Various generator types with and without scrubbing	960-1050, mean 1005
IEA 2000 [149]	US		1182
Hondo [150]	Japan		975
Whiteker et al. [151][c]	US	Different coal-firing technologies	675-1689, 1182
Mean value			**1034**

a: upstream emissions and combustion efficiencies are included
b: 103 references data
f: 270 references data

The second term of Eq. **(**5.8) $Z_{TWP,\theta} \cdot \theta$ is the emissions from the TWPs combustion. $Z_{TWP,\theta}$ is the wood pellet power generation emission intensity at co-firing ratio of θ, in gCO_2eq/kWh-electricity-generated, which is calculated by Eq. (5.9). It should be noted here that emissions of CO_2 resulting from the combustion of biomass are entirely balanced by the carbon incorporated during regrowth of the forest during the time period considered. Thus, the emissions of wood pellet combustion result only from up-stream stages, including harvesting, sawmilling, production, storage, port operation and transportation.

$$Z_{TWP,\theta} = E_{env,LC}/\xi_{TWP,\theta} \quad (5.9)$$

Where $E_{env,LC}$ is the life cycle GHG emission in gCO_2eq/kWh-WPs delivered to pellet plant, with values shown in Figure 5.2. Here, taking Path 1 as an example, $E_{env,LC}$ is 16 gCO_2eq/kWh-WPs delivered from BC to Genesee (Alberta), 28 gCO_2eq/kWh-WPs delivered from BC to Atikokan (Ontario), 32 gCO_2eq/kWh-WPs delivered from BC to Kochi (Japan), and 50 gCO_2eq/kWh-WPs delivered from BC to Drax (UK), respectively**;** $\xi_{TWP,\theta}$ is the combustion efficiency under different co-firing ratios, with values being reported as 31.4%, and 32.7% for 100% and 20% wood pellet co-firing respectively in Atikokan power

generation station [152]. Here, we assume that 10% wood pellet co-firing efficiency is 32%, as shown in Table 5.8.

Table 5.8 Electricity generation efficiency of wood pellet at different co-firing ratio

	100% coal	100% wood pellet	20% co-firing	10% co-firing
Combustion efficiency	33%[b]	31.4%[a]	32.7%[a]	32%[c]

a: data source [152]
b: data source GHGenius 4.3 2017 BC based
c: data source assumption

CO_2 reduction potentials $RDP_{TWP-coal,\theta}$ in tCO_2eq/year by replacing coal with BC TWPs (Path1) at the power generating stations with different co-firing ratios are calculated by Eq. (5.10).

$$RDP_{TWP-coal,\theta} = ((Z_{coal} - Z_{TWP-coal,\theta}) \cdot 10^{-6}) \cdot (Cap_{power} \cdot 10^{3}) \cdot (333\ \text{days/year}) \cdot (24\ \text{hrs/day}) \quad (5.10)$$

Where $(Z_{coal} - Z_{TWP-coal,\theta})$ in gCO_2eq/kWh is the GHG emissions reduction potential for per unit electricity generated by replacing coal with BC TWPs at a co-firing ratio of θ, $Cap_{power}$is the power plant generation capacity in MW, as summarized in Table 5.9.

Figure 5.8 shows the GHG reduction potentials of using BC TWPs at different generation stations. The Drax generating station in North Eastern England is used as an illustrative example. Drax consists of six 660 MW generating units with a maximum capacity of 3960 MW [153], which accounts for around 20% of the UK's renewable power [154]. In Sep 2018, the Drax group has finished their fourth biomass unit conversion and that they are aiming to phase out coal by 2025 [155]. At present, Drax burns wood pellets from BC and the South Eastern USA. If BC TWPs (derived from Path 1) are used, GHG emissions will be reduced by about 2.75 million tCO_2eq/year with 10% BC TWPs co-firing with coal, 5.53

million tCO_2eq/year with 20% co-firing and 27.44 million tCO_2eq/year with 100% pellet firing, respectively. GHG reduction potentials of other cases in Alberta, Ontario and Japan are also given in Table 5.9.

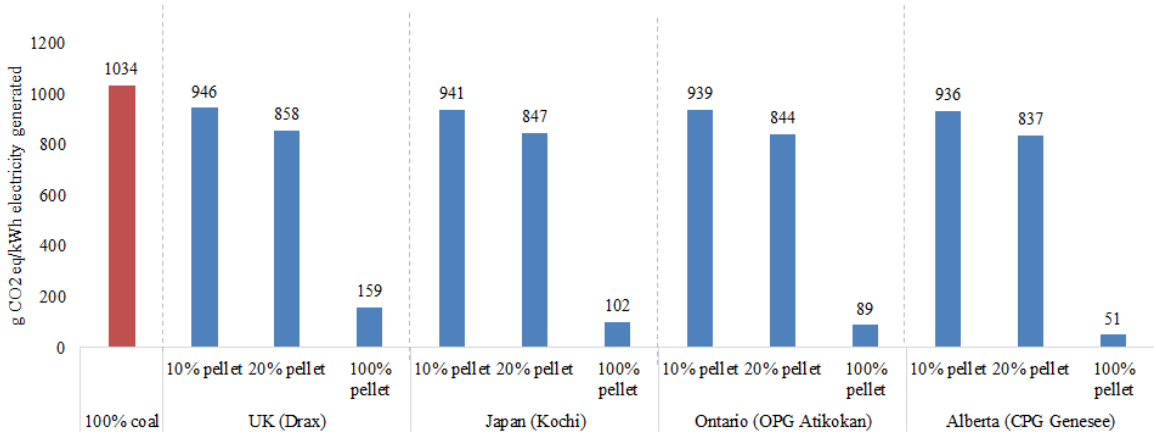

Figure 5.8 GHG emission reduction potential of BC TWPs (derived from Path 1) for power generation by displacing coal at different co-firing ratios (gCO_2eq/kWh electricity generated)

Table 5.9 GHG emission reduction potential (million-t CO_2eq/year) of displacing coal with BC TWPs (derived from Path1) by displacing coal in different power generation stations

Power generation plant	Power generation capacity	GHG reduction potential (million tCO_2eq/year)		
		10% co-firing	20% co-firing	100% co-firing
Drax Power	6×660MW [1]	2.75	5.53	27.44
Kochi Power	660MW [2]	0.49	0.98	4.87
Atikokan Power	205MW [3]	0.15	0.31	1.53
Genesee Power	1266 MW [4]	0.99	1.98	9.86

1: data source [153]
2: data source [156]
3: data source [157]
4: data source [158]

5.4.6 Pareto analysis

This section aims to use an analysis in terms of Pareto optimality to investigate the trade-offs between environmental and economic performances of BC wood pellets for different destinations. Figure 5.9 illustrates the delivery costs (in $/GJ) and the life cycle GHG emissions (in gCO_2eq/kWh electricity generated) of BC wood pellets delivered to different destinations with different co-firing ratios. Those cases located in the left lower corner are the preferred choices with low GHG emissions and low delivery costs. Alberta is the best destination with relatively low GHG emissions and delivery costs, followed by Japan. Ontario and UK have similar delivery costs, but Ontario has lower life cycle GHG emissions. The figure also reveals the significance of the production pathways, e.g. delivery costs to Alberta of CWP from Path 0 could be similar to the delivery costs to Ontario, Japan, and even UK for TWP from Path 1 using large ship vessels.

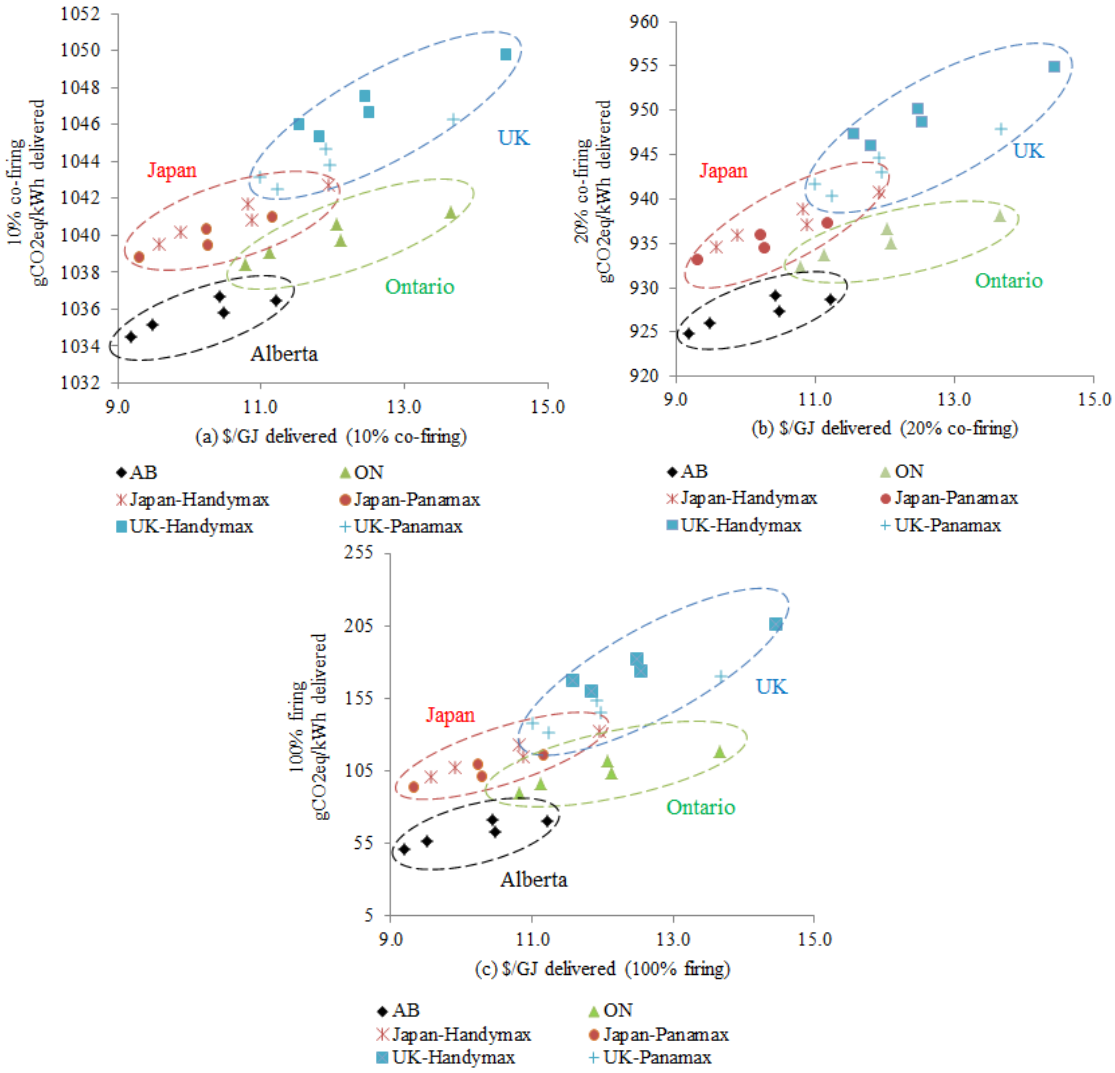

Environmental indicator functional unit in gCO_2eq/kWh-electricity-delivered at power plants
Economic indicator functional unit in $/GJ WPs delivered to power plants

Figure 5.9 Pareto diagram of BC wood pellets delivered to different destinations (a) at 10% of co-firing; (b) at 20% of co-firing; and (c) at 100% of co-firing

5.4.7 Equivalent market analysis

As aforementioned that the economic and environmental performances of the BC wood pellets are distance-dependent, thus, in this section, the environmental and economic equivalent markets of BC TWPs are investigated. Differently from the cases studied above,

in which the TWPs are delivered to specific the power generation plants, here, since it is difficult to locate all the power plants world wild, thus the final destinations are the rail stations in Canada and sea ports for overseas markets. The functional units of the two indicators are: delivery costs in "$/GJ WPs to rail station to domestic/ports to overseas markets" and GHG emissions in "gCO_2eq/kWh-WPs-delivered to rail station to domestic/ports to overseas markets". BC TWPs derived from Path 1 is selected as an example.

The transportation costs are quantified by Eq. (G.7) for truck, Eq. (G.10) for railway, and Eq. (G.11) for marine transportations, respectively. Emissions of the transportations are calculated by Eq. (5.6). Transportation distances of different ways are quoted from google map. Cost and GHG emissions of other stages are calculated through section 5.1, and being presented in Figure 5.2 and Figure 5.3.

Figure 5.11 shows the GHG emissions and the delivery costs of BC TWPs to different destinations. As can be seen, the delivery costs of BC wood pellet to Asia Pacific region are similar to the delivery costs to Alberta, and not much different from Saskatoon; the EU and UK delivery costs are similar to Regina, lower than the delivery costs to Manitoba, Ontario, Quebec, and New Brunswick. Delivery costs to the US Pacific region are similar to BC and Alberta. GHG emissions for delivery to Asia Pacific region are equivalent to from BC to Quebec and New Brunswick; emissions to EU and UK are higher than all other destinations; GHG emissions for pellets delivered to US Pacific coast region are similar to BC, Alberta, Saskatchewan, and Manitoba. Figure 5.11 indicates the advantages of the Asia and US markets, which are both environmentally and economically preferable to the UK and EU markets.

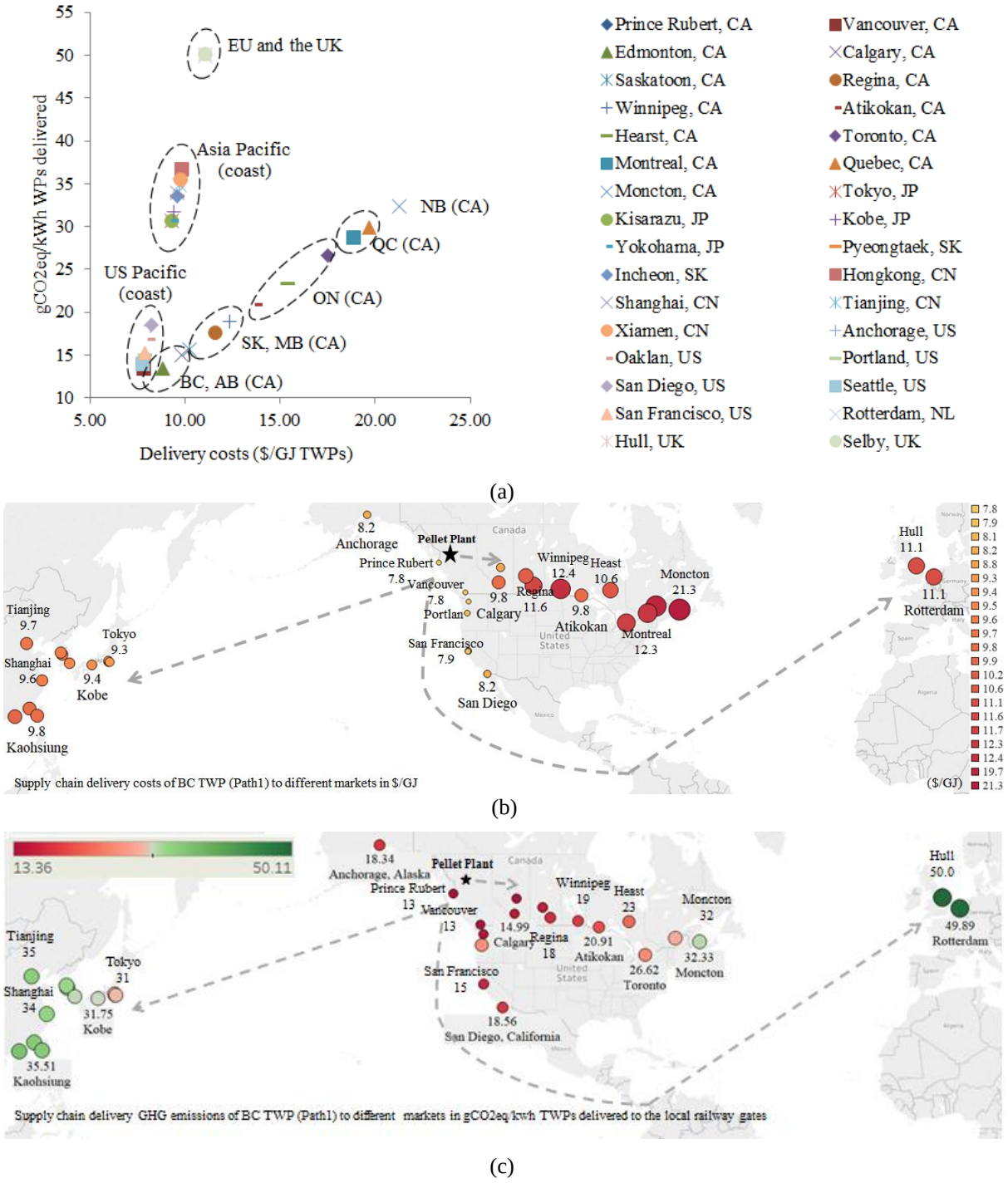

Environmental indicator functional unit in "gCO_2eq/kWh WPs delivered to railway station in domestic markets/port to overseas markets"
Economic delivery cost indicator functional unit in "$/GJ delivered to railway station in domestic markets/port to overseas markets"

Figure 5.10 (a) GHG emissions and delivered costs of BC wood pellets to different destinations: railway stations in Canada and export ports for overseas markets; (b) supply chain delivered costs of BC TWPs to different markets; (c) supply chain GHG emissions of BC TWPs delivered to different markets

5.4.8 Added values of BC and Alberta wood pellets over the supply chains

As discussed in section 4.4.5, BC has advantages in producing wood pellets due to its rich raw material resources and clean electricity. BC's adjacent province Alberta (AB) is also endowed with rich forest resources, with about 20.2 million hectares third-party certified forest, but its wood pellet production capacity only accounts for 3% of Canadian capacity. To understand the major differences between the two adjacent provinces, we compare their wood pellet value chains. Figure 5.11 shows the supply chains of BC and AB wood pellet to different power plants in the UK, Japan, Ontario, and Alberta.

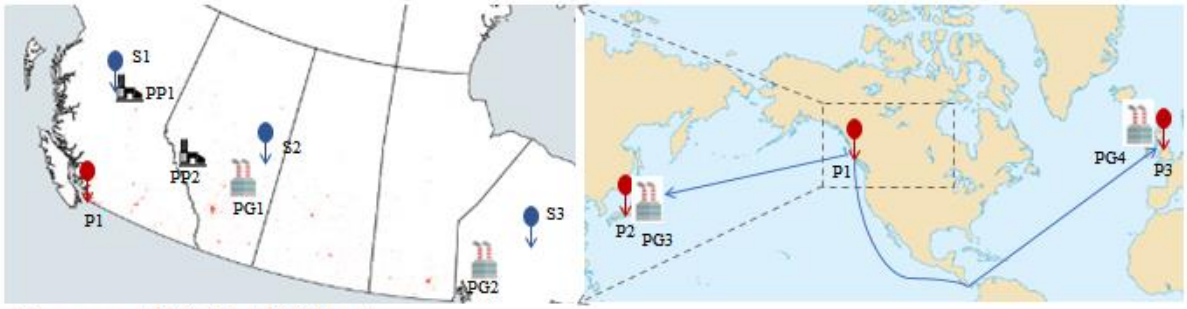

P1: vancouver port; P2: Kochi port; P3: Selby port
PP1: pellet plant (Pacific Bioenergy); PP2: pellet plant (Foothills Forest Products)
PG1: Genesee power station; PG2: Atikokan power station; PG3: Kochi power station; PG4: Drax power station
S1: Prince George rail station; S2: Edmonton rail station; S3: Thunder Bay rail station

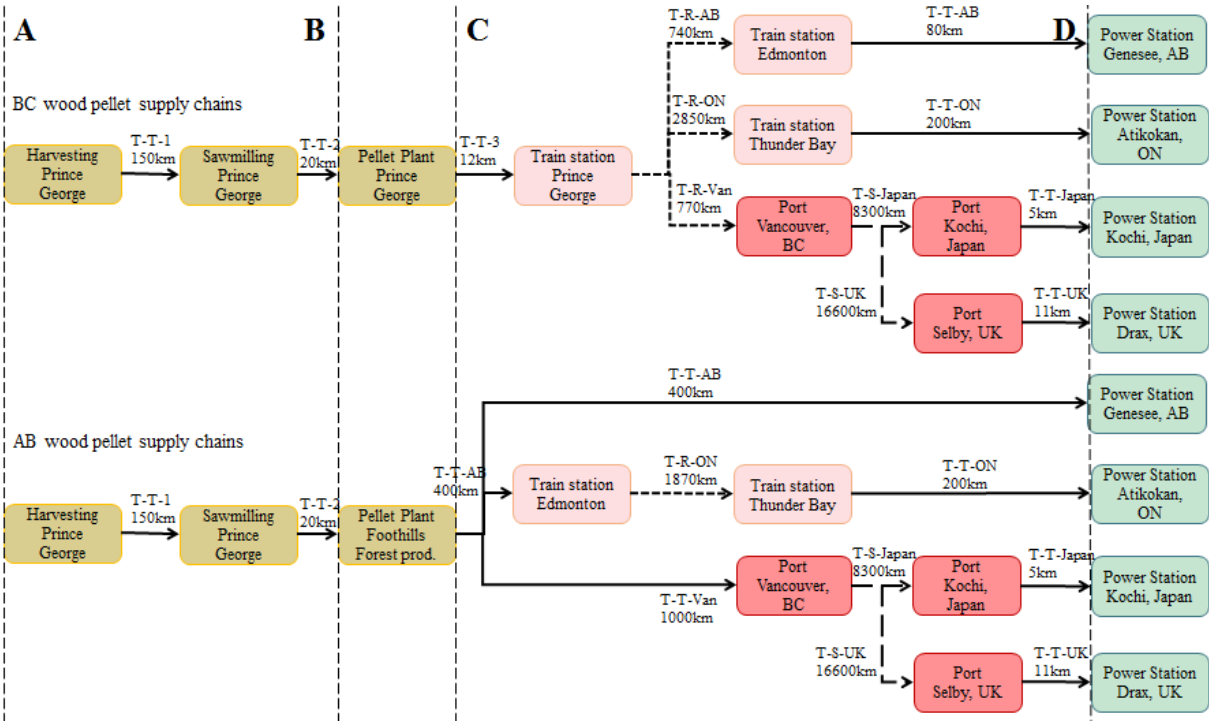

A: place of origin;
B: raw material arrived at pellet plant;
C: wood pellet product at exit of pellet plant gate;
D: wood pellet delivered to power station before combustion;

Figure 5.11 Supply chains of BC and AB wood pellets to different destinations

Two indicators used to compare the BC and AB TWPs supply chains from raw material origin to different power plants are: GHG emissions in "gCO_2eq/kWh TWPs delivered to power plant" and costs in "$/GJ TWPs delivered to power plant". The

cumulative GHG emissions at four typical points A, B, C, and D as shown in Figure 5.11 are calculated as Eq. (5.11) to (5.14).

$$E_{env}(A) = 0 \tag{5.11}$$

$$E_{env}(B) = E_{env}(A) + E_{env}(sawmill) + E_{env}(T - T - 1) + E_{env}(T - T - 2) \tag{5.12}$$

$$E_{env}(C) = E_{env}(B) + E_{env}(production) \tag{5.13}$$

$$E_{env}(D) = E_{env}(C) + E_{env}(Transport_{C-D}) \tag{5.14}$$

The GHG emissions of the sawmilling $E_{env}(sawmilling)$ and production $E_{env}(production)$ stages are calculated by Eq. (5.5), Electricity consumptions of sawmilling and production processes are 0.186 GJ electricity/t TWP (equal to 0.0089 GJ electricity/GJ TWP), and 0.039 GJ electricity/GJ TWP, respectively. Emission factors for BC and Alberta electricity are 26 $kgCO_2eq/GJ$ delivered and 229 $kgCO_2eq/GJ$ delivered, respectively according to Table 4.15. GHG emissions of the transportation stages are calculated by Eq. (5.6). The transportation distances of are shown in Figure 5.11.

Costs at points A and B are calculated according to Eq. (5.15) and Eq. (5.16).

$$E_{eco}(A) = 0 \tag{5.15}$$

$$E_{eco}(B) = E_{eco}(sawdust) = \frac{25\$}{dt} \cdot \frac{1.15 dt}{t\ TWP} \Big/ \frac{21\ GJ\ TWP}{t\ TWP} \tag{5.16}$$

$E_{eco}(B)$ indicates the costs of raw material (sawdust), which already included the sawmilling and transportation (T-T-1 and T-T-2) costs, being 25 $/dt (equal to 1.47 $/GJ when dry biomass HHV is 17GJ/t). According to Table 5.2, the amount of sawdust consumption to produce per t of wood pellet is 1.716 t (equal to 1.15 dt for MC 50wt%db). Therefore, the costs at point B are 1.37 $/GJ for both BC and AB TWPs. Costs at points C are calculated by

$$E_{eco}(C) = E_{eco}(B) + E_{eco}(\text{production}) \cdot (1 + 100\%) \quad (5.17)$$

The second term indicates the wholesale price of the TWPs (Path 1) at the pellet plant gate. As discussed in section 4.4.3, the minimum selling price of TWPs at the pellet plant gate is about 87% of the wood pellet production cost. Here, it is assumed that the selling price of the wood pellet is 200% of the production cost. The production costs of BC and AB TWPs derived from Path 1 are 3.6 $/GJ and 4.2 $/GJ, respectively, which can be quantified by Eq. (4.14) with assumption of raw material costs as 25$/t, labor costs of 20$/hr, and the BC and AB electricity costs at 6.33 and 6.53 ¢/kWh, respectively, according to Table 4.15. Costs at points C are calculated by

$$E_{eco}(D) = E_{eco}(C) + E_{eco}(\text{Transport}_{C-D}) \quad (5.18)$$

The second term $E_{eco}(\text{Transport}_{C-D})$ indicates the total transportation cost from the pellet plant to the power plant, which can be calculated according to Eq. (G.7) for truck transportation cost, Eq. (G.10) for railway transportation cost, and Eq. (G.11) for marine transportation cost, respectively. The transportation distances are as illustrated in Figure 5.11.

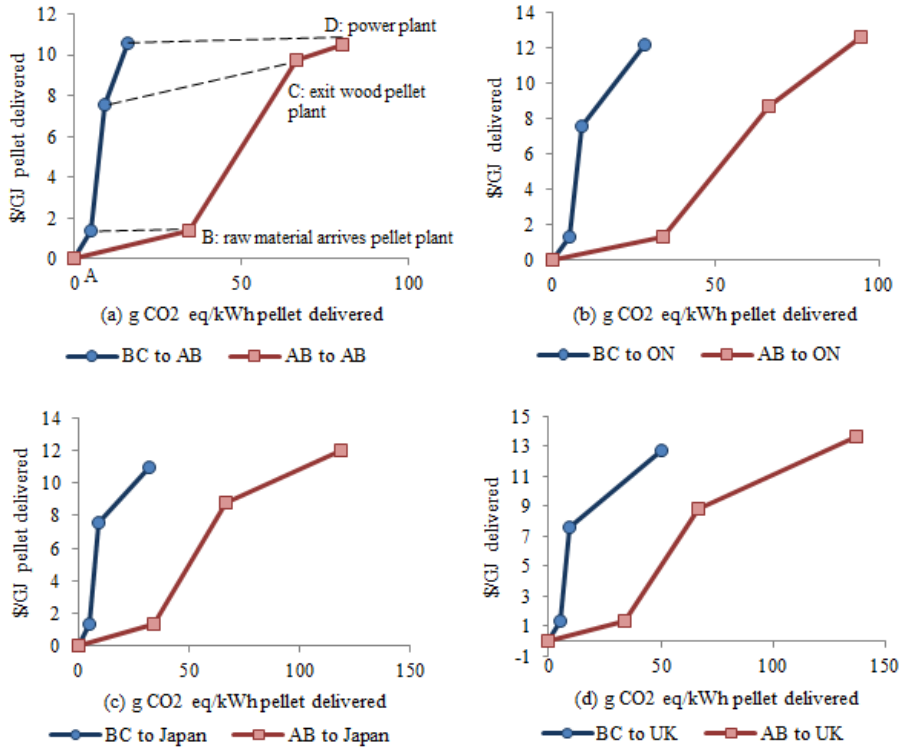

A: place of origin;
B: raw material arrived at pellet plant;
C: wood pellet product at pellet plant gate;
D: wood pellet delivered to power station before combustion;

Figure 5.12 Value-added chains of BC and AB wood pellets to the UK, Japan, Ontario, and Alberta power plants

Figure 5.12 shows the added values for the supply chains from BC and AB to different destinations. As can be seen, BC TWPs are both environmentally and economically advantageous over pellets from AB due to the low electricity price and the clean electricity in BC (Point C). This advantage is magnified when the comparison is based on energy delivered when the pellets are delivered to the power station (point D). Furthermore, the life cycle GHG emissions of AB wood pellet delivered to Ontario are even higher than the BC TWPs delivered to Japan and the UK. Thus, the added-value analysis reinforces the advantage of the BC wood pellet industry.

5.5 Conclusions

"3E" impacts analyses of the BC conventional (CWP) and torrefied wood pellets (TWPs) derived from different pathways delivered to different markets are carried out in this chapter, including Drax Power Generation in UK, Kochi Power Generation in Japan, Atikokan Power Generation in Ontario, and Genesee Power Generation in Alberta. The TWP production processes are operated auto-thermally without the use of N_2 and catalyst through appropriate process design and integration (Chapter 4). It is revealed that:

- TWPs perform better than CWPs over the whole range of likely variation in the key parameters. Therefore, the conclusion that torrefaction should be used is robust. Among all the TWP production pathways, Path 1 is the best choice, which can help reduce about 30% of the "3E" (energetic, environmental, and economic) impacts to all the markets in comparison with the CWP.
- Break-down of the supply chains "3E" metrics revealed that: transportation and electricity consumptions are the major contributors to GHG emissions. The electricity consumptions of the production and the sawmilling processes account for 40 to 70% of the supply chain energy consumptions. However, the GHG emissions of these two stages only account for 15 to 50% of the life cycle GHG emissions, mainly due to BC's clean electricity. Wood pellet production is the highest cost category along the supply chain, accounting for ~50% of the total cost. Thus, reducing production cost is crucially important to increase the competitiveness of BC wood pellets.
- It is more significant to implement torrefaction than switching ship vessel and using blends fuels for road transportation: switching ship vessel from Handymax to Panamax can help reduce about 13% and 18% GHG emissions for delivery from BC

to Japan and UK respectively, while changing CWP to TWP help reduce about 24% and 22% of GHG emissions for Japan and the UK respectively. Economically, the former measure help reduce 5% of costs, while the later measure help reduce 18% of costs to overseas markets. Using B5 and B10 for road vehicles can also help reduce about 2-5% of GHG emissions over the supply chains to Alberta and Ontario. While torrefaction can help reduce 24-29% of GHG emissions to the local markets.

- There is significant GHG emissions reduction potential to replace coal with BC TWPs, even after long transportation distances to EU, Pacific Asia, and domestic markets. The reduction potential is about proportional to the co-firing ratio.
- A Pareto analysis indicates that wood pellets perform better, both environmentally and economically, in Asia Pacific markets than in the domestic and EU markets. Delivery costs to Asia region are equivalent to the delivery costs to Alberta, and delivery costs of BC wood pellet to UK and EU are equivalent to the delivery costs from BC to Ontario. Supply chain GHG emissions of BC wood pellets to Asia region are equivalent to GHG emissions delivered to Alberta. Therefore, for BC producers, the Asia Pacific region should be considered as a future strategically important market.
- Added-value analysis of pellets supplied to UK, Japan, AB, and ON markets confirms the advantages of BC wood pellets over Alberta pellets.

Chapter 6: Conclusions and recommendations to future work

6.1 Conclusions

This thesis aims to investigate several key issues of the BC conventional and torrefied wood pellet (CWP/TWP) supply chains, with a specific focus on modeling of the production stage. The research questions cover multi-scale:

(a) On a **supply chain level**, what are the energetic, environmental, and economic ("3E") impacts of the BC wood pellet supply chains to different markets? What are the key parameters to the "3E" impacts? What is the best way to produce wood pellet, torrefaction or not, and which pathway?

(b) On **the production stage**, can the TWP production process itself achieve auto-thermal operation? What are the auto-thermal operating conditions?

(c) On the **unit level**, what are the sizes and the operating conditions of each unit?

(d) On the **element level**, how do the biomass elements evolve in both solid and gas phases during torrefaction? How does the torrefaction heat change with different operating conditions?

To answer above research questions, we have adopted hybrid methods: the "3E" inventory data of harvesting, sawmilling, port operation, and storage are adopted from literature and government report. Transportation costs models are developed based on quoted prices from website. Specifically, for the production stage, we have developed a simulation platform based on Aspen Plus and FORTRAN programming. The platform contains models for each major unit involved in the five wood pellet production pathways analyzed: including fluidized bed dryer model, rotary dryer model, fluidized bed torrefier model with build-in heat exchanger, and directly and indirectly heated rotary torrefier model. Those models

integrate kinetics, thermodynamics, hydrodynamics, heat and mass transfer, as well as elements evolving. The platform enables carry out reactor sizing, unit operating condition optimization, sensitivity analysis, and heat and mass integration, etc. The outputs of the simulation results are used for the techno-economic evaluations and life cycle analysis.

In Chapter 3, the auto-thermal operation boundaries are identified for the torrefaction system under the logic of "at what torrefaction operation conditions, can the system operate auto-thermally". To quantitatively answer this question, torags HHVs (heat sink), torrefaction heat (heat consumer), and torrefied biomass HHVs (product quality) are quantified at different torrefaction conditions. Key parameters that influence the system auto-thermal operations are investigated, including drying technologies, biomass initial moisture content, flowrate of N_2, and torrefaction operation conditions. The advanced drying technology and avoided use of N_2 can help the system achieve auto-thermal at lower torrefaction temperature and residence time, thus leading to a higher process throughput and solid product yield. An improved configuration is thus proposed to integrate the torrefaction system, which avoids using of N_2 by recycling flue gases to the torrefier, and through carefully design, catalyst is also avoided in combustion. In addition, due to recycle of the hot flue gases, the system auto-thermal operation boundaries are expanded.

Chapter 4 aims to compare CWP with different TWPs production pathways at the pellet plant gate. To quantify the "3E" impacts of different pathways, process modeling and simulation are carried out to size the equipment and determine unit operation conditions. Heat integration is then carried out to achieve auto-thermal operation and avoid use of N_2 and catalyst in the TWPs production processes. It is found that for a typical TWPs production case, with biomass initial moisture content of 50wt%db, the torrefaction system can achieve

auto-thermal operation without use of N_2 and catalyst at 300ºC with 20% of biomass weight loss. It is also revealed that TWPs have lower "3E" impacts than the CWPs. With uncertainties of the key parameters taken into consideration, Path 1 and Path 2 perform better than the other pathways at the pellet plant gate. TWPs can help reduce about 10% of production cost and 40% of energy consumption and GHG emissions in comparison with the CWP. The break-down analysis reveals that: (a) the TWP production process is an electricity intensive process, (b) emissions of TWP production process are thus mainly determined by the local electricity generation, and (c) capital costs only share around 10% of the total costs, while the other 90% comes from the operation, among which raw material costs, labor costs, and the electricity costs are the major categories, and raw material cost is the most sensitive one. With both a clean electricity generation system and rich forest resources, BC has a unique advantage for wood pellet manufacturing. The minimum selling price of BC TWPs is estimated as ~$6.7/GJ (equiv. 140$/t). It is thus predicted that manufacturing of TWP can contribute about 1.4% of GDP to the provincial manufacturing sector, and 0.1% of the provincial total GDP in the year of 2018.

In Chapter 5, CWP and TWPs derived from different pathways are compared on the supply chain level to different markets. By quantifying the "3E" impacts of the BC wood pellets derived from different pathways (Path 0-4) delivered to the power generation stations in UK, Japan, Alberta and Ontario, it is found that, with uncertainties of the major parameters taken into consideration, all the TWPs production pathways (Paths 1-4) perform better than the CWP (Path 0). Thus, it can be concluded that TWP is advantageous over CWP, and Path 1 is the best configuration to produce TWPs, which can help reduce on average about 25% of "3E" impacts compared to CWPs. The break-down analysis revealed that transportation is

the major source of GHG emissions, electricity is the major energy consumption, and production stage incurs the major cost over the life cycle. There is significant GHG reduction potential to replace coal with BC TWPs, even after long transportation distances to the UK, EU countries and Asia Pacific regions. The GHG reduction potential of replacing coal to BC TWPs is about proportional to its co-firing ratio in power plants. A Pareto analysis shows that Asia Pacific markets are both environmentally and economically better than EU and domestic markets. Delivery costs and life cycle emissions for pellets from BC to Asia Pacific are equivalent to Alberta, while costs to EU markets are equivalent to Ontario market. The value-chain analysis revealed the advantages of BC wood pellets over Alberta wood pellets. With those evidences, it is suggested that there is a great market potential for TWP in Canada, especially in BC, with Asia Pacific, UK and EU as the future strategically important markets.

The results revealed in this multi-scale analysis are useful for decision makers from government and business. In addition, the developed simulation platform is useful for engineering analysis and optimization of the production processes.

6.2 Limitations of this work and conclusions

The conclusions of this work rest on a number of key assumptions, each of which has been discussed in detail in the chapter in which it arises. It is necessary to highlight some key parameters that may change the quantitative conclusions of CWP and TWPs production pathways in Chapter 4 and Chapter 5:

1. Non-auto-thermal operation of the TWPs production processes

If the torrefied wood pellet production processes (Paths 1-4) can-not operate auto-thermally, then N_2 and additional fuels, e.g. natural gas or biomass, will be required. In these cases, the conclusions may be different from the current study.

Parameters that may change the energy balances and hence prevent auto-thermal operation of the torrefied wood pellet production processes include biomass species which affects the torrefaction reaction heat demand and calorific value of the torgas, and also biomass initial moisture content which determines the drying heat demand and drying technology. Although the "3E" impacts of the non-auto-thermal operation systems are not investigated in Chapter 4 and 5, the methodology in Chapter 3 and the simulation platform in Chapter 2 can be used to analyze new systems with different configurations or different operating conditions.

2. Specific energy consumptions for grinding and pelleting

Energy consumptions in grinding and pelleting are very sensitive to biomass properties, i.e. biomass species, moisture content, particle size, and hardness and operation conditions, e.g. rotation speed of hammer mill, ring die or flat die, and processing capacities. In this study, the assumed specific energy consumptions of these two units are based on the average value of reported literature data, and the actual values may range widely between different cases. The range of possible values is given in Table 4.7.

6.3 Recommendations for future work

- Further experiments are suggested to be carried out to investigate the element evolution of biomass during torrefaction and the change of the torrefaction heat. Those fundamental researches are essential to improve the elemental level analysis, which is meaningful for process energy balances and integration.

- Pilot scale experiments should be carried out to verify the flowsheet integration so as to identify the bottlenecks for energy efficiency improvements in practices.
- One limitation of the current platform is that it cannot report the risks that exist in the real operation, e.g. recycled flue gases temperature should be lower than the biomass ignition temperature. This leads to the uncertainties in the system analysis. Thus, it is suggested to include the risk report function in the simulator in the future.
- Advantages of BC TWP are worth to be further investigated, especially from a global trade point of view.
- This work has been an example connecting the lower level and the upper level behaviors of a product's supply chains. With the development of data processing technology, the Internet of Things could help increase supply chain efficiencies significantly.

References

[1] BC Ministry of Forests, “British Columbia’s Forests a Geographical Snapshot,” 2003.

[2] pwc, “British Columbia’s Forest Industry and the B.C. Economy in 2016,” 2017.

[3] F. Larock, “The potential of increasing the use of BC forest residues for bioenergy and biofuels,” The University of British Columbia, 2018.

[4] “Certified Forests | naturally:wood | BC Wood, Forestry.” [Online]. Available: https://www.naturallywood.com/sustainable-forests/certified-forests. [Accessed: 06-Jun-2018].

[5] L. J. Corbett, P. Withey, V. A. Lantz, and T. O. Ochuodho, “The economic impact of the mountain pine beetle infestation in British Columbia: Provincial estimates from a CGE analysis,” *Forestry*, vol. 89, no. 1, pp. 100–105, 2016.

[6] A. Walton, “Provincial-Level Projection of the Current Mountain Pine Beetle Outbreak : Update of the infestation projection based on the Provincial Aerial Overview Surveys of Forest Health Conducted from 1999 through 2012 and the BCMPB model (year 10),” 2013.

[7] Industrial Forestry Service Ltd., “Wood Based Biomass Energy Potential of British Columbia Prepared for BC Hydro’s Integrated Resource Planning Process,” 2010.

[8] M. Cocchi, L. Nikolaisen, M. Junginger, C. S. Goh, R. Hess, J. Jacobson, L. P. Ovard, D. Thrän, C. Hennig, M. Deutmeyer, and P. P. Schouwenberg, “Global wood pellet industry market and trade study,” *IEA Bioenergy*, p. 190pp, 2011.

[9] V. Bassett, “Canadian Wood Pellet Opportunities,” in *IEACC-EPPEI Joiint Workshop-Cofiring Biomass with Coal*.

[10] A. Barnes, “2016 Economic State of the B.C. Forest Sector,” *Competitiveness and Innovation Branch*. .

[11] L. Gyekye, “Drax presses ahead with biomass plans | Bioenergy Insight Magazine.” [Online]. Available: https://www.bioenergy-news.com/display_news/12625/drax_presses_ahead_with_biomass_plans/. [Accessed: 01-Jun-2018].

[12] L. Sweetie, P. Borghese, G. Sunrise, R. Cherry, B. Cherry, G. Jubille, and B. Cherry, “Drax Group PLC: Half year results for the six months ended 30 Jun 2017.” Drax Group PLC, 2017.

[13] Gordon Murray, “Drax fires up biomass power,” 2014. [Online]. Available: http://gordonmurray.ca/drax-fires-up-biomass-power. [Accessed: 01-Jun-2018].

[14] D. Thrän, “Global Wood Pellet Industry and Trade Study 2017,” 2017.

[15] W. Strauss, “A short Update on the Japanese Industrial Wood Pellet Markets: Policies, and how they will drive current and future demand,” *Futur. Metrics LLC*, 2017.

[16] “The End of Coal | Ontario.ca.” [Online]. Available: https://www.ontario.ca/page/end-coal. [Accessed: 01-Jun-2018].

[17] “Phasing out coal pollution | Alberta.ca.” [Online]. Available: https://www.alberta.ca/climate-coal-electricity.aspx. [Accessed: 01-Jun-2018].

[18] L. J. R. Nunes, J. C. O. Matias, and J. P. S. Catalão, “A review on torrefied biomass pellets as a sustainable alternative to coal in power generation,” *Renew. Sustain. Energy Rev.*, vol. 40, pp. 153–160, 2014.

[19] S. Proskurina, J. Heinimö, F. Schipfer, and E. Vakkilainen, “Biomass for industrial applications: The role of torrefaction,” *Renew. Energy*, vol. 111, pp. 265–274, 2017.

[20] M. Beets, “A Torrefied Wood Pellet Supply Chain - a detailed cost analysis of the competitiveness of torrefied wood pellets compared to white wood pellets,” Utrecht University, 2017.

[21] J. H. Peng, X. T. Bi, S. Sokhansanj, and C. J. Lim, “Torrefaction and densification of different species of softwood residues,” *Fuel*, vol. 111, pp. 411–421, 2013.

[22] B. Ghiasi, L. Kumar, T. Furubayashi, C. J. Lim, X. Bi, C. S. Kim, and S. Sokhansanj, “Densified biocoal from woodchips: Is it better to do torrefaction before or after densification?,” *Appl. Energy*, vol. 134, pp. 133–142, 2014.

[23] S. Mani, “A Systems analysis of Biomass-PhD thesis,” The University of British Columbia, 2005.

[24] J. Peng, X. T. Bi, C. J. Lim, H. Peng, C. S. Kim, D. Jia, and H. Zuo, “Sawdust as an effective binder for making torrefied pellets,” *Applied Energy*, vol. 157. pp. 491–498, 2015.

[25] W.-H. H. Chen, J. Peng, and X. T. Bi, “A state-of-the-art review of biomass torrefaction, densification and applications,” *Renew. Sustain. Energy Rev.*, vol. 44, pp. 847–866, 2015.

[26] I. Obernberger and G. Thek, *The pellet handbook: The production and thermal utilisation of biomass pellets*, 1st Editio. London: Routledge, 2010.
[27] E. Trømborg, T. Ranta, J. Schweinle, B. Solberg, G. Skjevrak, and D. G. Tiffany, "Economic sustainability for wood pellets production - Acomparative study between Finland, Germany, Norway, Sweden and the US," *Biomass and Bioenergy*, vol. 57, pp. 68–77, 2013.
[28] M. Mobini, J. C. Meyer, F. Trippe, T. Sowlati, M. Fröhling, and F. Schultmann, "Assessing the integration of torrefaction into wood pellet production," *J. Clean. Prod.*, vol. 78, pp. 216–225, 2014.
[29] H. Shahrukh, A. Olajire, A. Kumar, B. Ghiasi, L. Kumar, and S. Sokhansanj, "Biomass and Bioenergy Techno-economic assessment of pellets produced from steam pretreated biomass feedstock," *Biomass and Bioenergy*, vol. 87, pp. 131–143, 2016.
[30] D. Agar, J. Gil, D. Sanchez, I. Echeverria, and M. Wihersaari, "Torrefied versus conventional pellet production - A comparative study on energy and emission balance based on pilot-plant data and EU sustainability criteria," *Appl. Energy*, vol. 138, no. February 2016, pp. 621–630, 2015.
[31] P. C. a. Bergman and H. J. Veringa, "Combined torrefaction and pelletisation," *Analysis*, no. July, p. 29, 2005.
[32] D. A. Agar, "A comparitive economic analysis of torrefied pellet production based on state-of-the-art pellets," *Biomass and Bioenergy*, vol. 97, pp. 155–161, 2017.
[33] M. Mobini, T. Sowlati, and S. Sokhansanj, "A simulation model for the design and analysis of wood pellet supply chains," *Appl. Energy*, vol. 111, pp. 1239–1249, Nov. 2013.
[34] M. Mobini, "On the design and analysis of forest biomass to biofuel and bioenergy supply chains-PhD Thesis," University of British Columbia, 2015.
[35] J. Koppejan, S. Sokhansanj, S. Melin, and S. Madrali, "Status overview of torrefaction technologies," 2012.
[36] R. I. Radics, R. Gonzalez, and S. S. Kelley, "Systematic Review of Torrefied Wood Economics," *Bioresources*, vol. 12, no. 3, pp. 6868–6884, 2017.
[37] "Ochoco Lumber Company." [Online]. Available: http://ochocolumber.com/. [Accessed: 09-Jul-2018].
[38] P. C. a Bergman, a R. Boersma, R. W. R. Zwart, and J. H. a Kiel, "Torrefaction for biomass co-firing in existing coal-fired power stations," 2005.
[39] A. Shah, M. J. Darr, D. Medic, R. P. Anex, S. Khanal, and D. Maski, "Techno-economic analysis of a production-scale torrefaction system for cellulosic biomass upgrading," *Biofuels, Bioprod. Biorefining*, vol. 6, no. 1, pp. 45–57, 2012.
[40] F. S. Syu and P. T. Chiueh, "Process simulation of rice straw torrefaction," *Sustain. Environ. Res.*, vol. 22, no. 3, pp. 177–183, 2012.
[41] R. Clift, "Metrics for supply chain sustainability," in *Technological Choices for Sustainability*, Berlin, Heidelberg: Springer Berlin Heidelberg, 2004, pp. 239–253.
[42] A. Azapagic and S. Perdan, "Indicators of Sustainable Development for Industry: A General Framework," *Process Saf. Environ. Prot.*, vol. 78, no. 4, pp. 243–261, Jul. 2000.
[43] Aspentech V8.2, "Aspen Plus Getting Started Modeling Processes with Solids," 2013.
[44] S. Kieseler, Y. Neubauer, and N. Zobel, "Ultimate and proximate correlations for estimating the higher heating value of hydrothermal solids," *Energy and Fuels*, vol. 27, no. 2, pp. 908–918, 2013.
[45] S. Rönsch and H. Wagner, "Calculation of heating values for the simulation of thermo-chemical conversion plants with Aspen Plus," *Dtsch. Biomasseforschungszentrum*, 2012.
[46] N. Y. Kirov, "Specific Heats and Total Heat Contents of Coals and Related Materials are Elevated Temperatures," *BCURA Mon. Bull.*, pp. 29–33, 1965.
[47] M. Prins, K. Ptasinki, and F. Janssen, "Torrefaction of woodPart 2. Analysis of products," *J. Anal. Appl. Pyrolysis*, vol. 77, no. 1, pp. 35–40, 2006.
[48] J. Deng, G. jun Wang, J. hong Kuang, Y. liang Zhang, and Y. hao Luo, "Pretreatment of agricultural residues for co-gasification via torrefaction," *J. Anal. Appl. Pyrolysis*, vol. 86, no. 2, pp. 331–337, 2009.
[49] Z. Wang, "Biomass torrefaction in slot-rectangular spouted beds-PhD Thesis," The University of British Columbia, 2017.
[50] T. Nocquet, C. Dupont, J. M. Commandre, M. Grateau, S. Thiery, and S. Salvador, "Volatile species release during torrefaction of wood and its macromolecular constituents: Part 1 - Experimental study," *Energy*, vol. 72, pp. 180–187, 2014.
[51] T. Nocquet, C. Dupont, J. Commandré, S. Thiery, S. Salvador, T. Nocquet, C. Dupont, J. Commandré,

M. Grateau, C. Dupont, and J. Commandre, “Volatile species release during torrefaction of biomass and its macromolecular constituents : Part 2-Modeling study,” *Energy*, vol. 72, pp. 188–194, 2014.
[52] R. B. Bates and A. F. Ghoniem, “Biomass torrefaction: Modeling of volatile and solid product evolution kinetics,” *Bioresour. Technol.*, vol. 124, pp. 460–469, 2012.
[53] L. Chen, C. Dupont, S. Salvador, M. Grateau, G. Boissonnet, and D. Schweich, “Experimental study on fast pyrolysis of free-falling millimetric biomass particles between 800 °C and 1000 °C,” *Fuel*, vol. 106, pp. 61–66, 2013.
[54] E. Peduzzi, G. Boissonnet, G. Haarlemmer, C. Dupont, and F. Maréchal, “Torrefaction modelling for lignocellulosic biomass conversion processes,” *Energy*, vol. 70, pp. 58–67, 2014.
[55] M. J. Prins, K. J. Ptasinski, and F. J. J. G. Janssen, “More efficient biomass gasification via torrefaction,” *Energy*, vol. 31, no. 15, pp. 3458–3470, 2006.
[56] H. Rezaei, C. J. Lim, A. Lau, X. Bi, and S. Sokhansanj, “Development of empirical drying correlations for ground wood chip and ground wood pellet particles,” *Dry. Technol.*, vol. 35, no. 12, pp. 1423–1432, 2017.
[57] M. H. Lisboa, D. S. Vitorino, W. B. Delaiba, J. R. D. Finzer, and M. A. S. Barrozo, “A study of particle motion in rotary dryer,” *Brazilian J. Chem. Eng.*, vol. 24, no. 3, pp. 365–374, 2007.
[58] D. Jia, “Heat and Mass Transfer in Pulsed Fluidized Bed of Biomass-PhD Thesis,” The University of British Columbia, 2017.
[59] W.-C. Yang, *HANDBOOK of FLUIDIZfiTION and FLUID-PARTICLE SYSTEMS*, 1st ed. CRC Press, 2003.
[60] O. Kunii, Daizō, Levenspiel, *Fluidization engineering*, 2nd ed. Butterworth-Heinemann, 1991.
[61] J. W. J. Werther, “Expansion Behavior of Gas Fluidized Beds in the Turbulent Regime,” *A.I.Ch.E Symp. Ser*, vol. 90, no. 301, pp. 31–44, 1994.
[62] A. Puettmann, E. U. Hartge, and J. Werther, “Application of the flowsheet simulation concept to fluidized bed reactor modeling. Part I: Development of a fluidized bed reactor simulation module,” *Chem. Eng. Process. Process Intensif.*, vol. 60, pp. 86–95, 2012.
[63] A. Puettmann, E. U. Hartge, and J. Werther, “Application of the flowsheet simulation concept to fluidized bed reactor modeling. Part II-Application to the selective oxidation of n-butane to maleic anhydride in a riser/regenerator system,” *Chem. Eng. Process. Process Intensif.*, vol. 57–58, pp. 86–95, 2012.
[64] J. Werther, “Scale-up modeling for fluidized bed reactors,” *Chem. Eng. Sci.*, vol. 47, no. 9–11, pp. 2457–2462, 1992.
[65] J. Werther and E.-U. Hartge, “Modeling of Industrial Fluidized-Bed Reactors,” *Ind. Eng. Chem. Res.*, vol. 43, no. 18, pp. 5593–5604, 2004.
[66] C. Y. Wen, “Noncatalytic heterogeneous solid-fluid reaction models,” *Ind. Eng. Chem.*, vol. 60, no. 9, pp. 34–54, Sep. 1968.
[67] M. J. C. Van Der Stelt, “Chemistry and reaction kinetics of biowaste torrefaction-PhD Thesis,” Eindhoven University of Technology, 2010.
[68] J. H. Peng, “A study of softwood torrefaction and densification for the production of high quality wood pellets-PhD Tehsis,” University of British Columbia, 2012.
[69] M. M. Bi, Xiaotao, *Multiphase reactors for biomass processing and thermochemical conversions*, 1st ed., vol. Chapter 11. Wiley, 2017.
[70] L. Wang, E. Barta-Rajnai, T. Skreiberg, R. Khalil, Z. Czégény, E. Jakab, Z. Barta, and M. Grønli, “Effect of torrefaction on physiochemical characteristics and grindability of stem wood, stump and bark,” *Appl. Energy*, vol. 227, pp. 137–148, 2017.
[71] Q. Hu, H. Yang, H. Xu, Z. Wu, C. J. Lim, X. T. Bi, and H. Chen, “Thermal behavior and reaction kinetics analysis of pyrolysis and subsequent in-situ gasification of torrefied biomass pellets,” *Energy Convers. Manag.*, vol. 161, pp. 205–214, 2018.
[72] M. J. Prins, K. J. Ptasinski, and F. J. J. G. Janssen, “Torrefaction of wood. Part 1. Weight loss kinetics,” *J. Anal. Appl. Pyrolysis*, vol. 77, no. 1, pp. 28–34, 2006.
[73] R. S. Gavin Towler, *Chemical Engineering Design*, 1st ed. Elsevier, 2008.
[74] “CS Cone Crusher.” [Online]. Available: http://www.innhf.eu/products/cs-cone-crusher.html. [Accessed: 06-Jul-2018].
[75] L. S. Esteban and J. E. Carrasco, “Evaluation of different strategies for pulverization of forest

biomasses," *Powder Technol.*, vol. 166, no. 3, pp. 139–151, 2006.
[76] L. Cadoche and G. D. López, "Assessment of size reduction as a preliminary step in the production of ethanol from lignocellulosic wastes," *Biol. Wastes*, vol. 30, no. 2, pp. 153–157, 1989.
[77] B. Colin, J. L. Dirion, P. Arlabosse, and S. Salvador, "Quantification of the torrefaction effects on the grindability and the hygroscopicity of wood chips," *Fuel*, vol. 197, pp. 232–239, 2017.
[78] Natural Resources Canada, "Natural Resources Canada solid biofuels bulletin series #4 – Graded Wood Pellets," *Natural Resources Canada-SOLID BIOFUELS BULLETIN SERIES*, no. 3. .
[79] R. Jannasch, Y. Quan, and R. Samson, "A process and energy analysis of pelletizing switchgrass: Final Report prepared for Natural Resource Canada, Alternative Energy Division," 2001.
[80] L. Cao, X. Yuan, H. Li, C. Li, Z. Xiao, L. Jiang, B. Huang, Z. Xiao, X. Chen, H. Wang, and G. Zeng, "Complementary effects of torrefaction and co-pelletization: Energy consumption and characteristics of pellets," *Bioresour. Technol.*, vol. 185, pp. 254–262, 2015.
[81] H. Li, X. Liu, R. Legros, X. T. Bi, C. Jim Lim, and S. Sokhansanj, "Pelletization of torrefied sawdust and properties of torrefied pellets," *Appl. Energy*, vol. 93, pp. 680–685, 2012.
[82] B. Linnhoff and S. Ahmad, "Cost optimum heat exchanger networks—1. Minimum energy and capital using simple models for capital cost," *Comput. Chem. Eng.*, vol. 14, no. 7, pp. 729–750, Jul. 1990.
[83] J. Rath, M. G. Wolfinger, G. Steiner, G. Krammer, F. Barontini, and V. Cozzani, "Heat of wood pyrolysis," *Fuel*, vol. 82, no. 1, pp. 81–91, 2003.
[84] J. M. Faleeva, V. A. Sinelshchikov, G. A. Sytchev, and V. M. Zaichenko, "Exothermic effect during torrefaction," *J. Phys. Conf. Ser.*, vol. 946, no. 1, 2018.
[85] L. Khezami, A. Chetouani, B. Taouk, and R. Capart, "Production and characterisation of activated carbon from wood components in powder: Cellulose, lignin, xylan," *Powder Technol.*, vol. 157, no. 1–3, pp. 48–56, 2005.
[86] H. Yang, R. Yan, H. Chen, D. H. Lee, and C. Zheng, "Characteristics of hemicellulose, cellulose and lignin pyrolysis," *Fuel*, vol. 86, no. 12–13, pp. 1781–1788, 2007.
[87] W. S. L. Mok and M. J. Antal, "Effects of pressure on biomass pyrolysis. II. Heats of reaction of cellulose pyrolysis," *Thermochim. Acta*, vol. 68, no. 2–3, pp. 165–186, 1983.
[88] I. Milosavljevic, V. Oja, and E. M. Suuberg, "Thermal effects in cellulose pyrolysis: Relationship to char formation processes," *Ind. Eng. Chem. Res.*, vol. 35, no. 3, pp. 653–662, 1996.
[89] J. Cho, J. M. Davis, and G. W. Huber, "The intrinsic kinetics and heats of reactions for cellulose pyrolysis and char formation," *ChemSusChem*, vol. 3, no. 10, pp. 1162–1165, 2010.
[90] Willliam S.-L. Mok and Michael J. Antal. Jr., "Effects of pressure on biomass pyrolysis. II. Heat of reaction of cellulose pyrolysis," *Thermochim. Acta*, vol. 68, pp. 165–186, 1983.
[91] R. B. Bates and A. F. Ghoniem, "Biomass torrefaction: Modeling of reaction thermochemistry," *Bioresour. Technol.*, vol. 134, pp. 331–340, 2013.
[92] A. Ohliger, M. Förster, and R. Kneer, "Torrefaction of beechwood: A parametric study including heat of reaction and grindability," *Fuel*, vol. 104, pp. 607–613, 2013.
[93] M. J. Prins, K. J. Ptasinski, and F. J. J. G. Janssen, "Torrefaction of wood," *J. Anal. Appl. Pyrolysis*, vol. 77, no. 1, pp. 35–40, Aug. 2006.
[94] A. F. Roberts and G. Clough, "Thermal decomposition of wood in an inert atmosphere," *Symp. Combust.*, vol. 9, no. 1, pp. 158–166, 1963.
[95] H. C. Kung and A. S. Kalelkar, "On the heat of reaction in wood pyrolysis," *Combust. Flame*, vol. 20, no. 1, pp. 91–103, 1973.
[96] C. A. Koufopanos, N. Papayannakos, G. Maschio, and A. Lucchesi, "Modelling of the pyrolysis of biomass particles. Studies on kinetics, thermal and heat transfer effects," *Can. J. Chem. Eng.*, vol. 69, no. 4, pp. 907–915, 1991.
[97] Y. Haseli, "Process Modeling of a Biomass Torrefaction Plant," *Energy & Fuels*, vol. 32, no. 4, pp. 5611–5622, 2018.
[98] V. Strezov, B. Moghtaderi, and J. A. Lucas, "Computational calorimetric investigation of the reactions during thermal conversion of wood biomass," *Biomass and Bioenergy*, vol. 27, no. 5, pp. 459–465, 2004.
[99] C. Fushimi, Y. Kansha, M. Aziz, K. Mochidzuki, S. Kaneko, A. Tsutsumi, K. Matsumoto, K. Yokohama, K. Kosaka, N. Kawamoto, K. Oura, Y. Yamaguchi, and M. Kinoshita, "Novel Drying Process Based on Self-Heat Recuperation Technology," *Dry. Technol.*, vol. 29, no. 1, pp. 105–110,

2010.
[100] A. S. Mujumdar, “Research and Development in Drying: Recent Trends and Future Prospects,” *Dry. Technol.*, vol. 22, no. 1–2, pp. 1–26, 2004.
[101] K. J. Chua, S. K. Chou, and W. M. Yang, “Advances in heat pump systems: A review,” *Appl. Energy*, vol. 87, no. 12, pp. 3611–3624, 2010.
[102] J. G. Brammer and A. V. Bridgwater, “Drying technologies for an integrated gasification bio-energy plant,” *Renew. Sustain. energy Rev.*, vol. 3, no. 4, pp. 243–289, 1999.
[103] Y. Liu, M. Aziz, Y. Kansha, and A. Tsutsumi, “Drying Energy Saving by Applying Self-Heat Recuperation Technology to Biomass Drying System,” *Chem. Eng. T*, vol. 29, no. 2011, pp. 577–582, 2012.
[104] M. S. Rahman, C. O. Perera, and C. Thebaud, “Desorption isotherm and heat pump drying kinetics of peas,” *Food Res. Int.*, vol. 30, no. 7, pp. 485–491, 1997.
[105] J. Li, M. C. Paul, and K. M. Czajka, “Studies of Ignition Behavior of Biomass Particles in a Down-Fire Reactor for Improving Co-firing Performance,” *Energy & Fuels*, vol. 30, no. 7, pp. 5870–5877, Jul. 2016.
[106] J. M. Jones, A. Saddawi, B. Dooley, E. J. S. Mitchell, J. Werner, D. J. Waldron, S. Weatherstone, and A. Williams, “Low temperature ignition of biomass,” *Fuel Process. Technol.*, vol. 134, pp. 372–377, 2015.
[107] Z. Wang, H. Li, C. J. Lim, and J. R. Grace, “Oxidative torrefaction of spruce-pine-fir sawdust in a slot-rectangular spouted bed reactor,” *Energy Convers. Manag.*, vol. 174, pp. 276–287, Oct. 2018.
[108] J. Tumuluru, “Effect of Deep Drying and Torrefaction Temperature on Proximate, Ultimate Composition, and Heating Value of 2-mm Lodgepole Pine (Pinus contorta) Grind,” *Bioengineering*, vol. 3, no. 2, p. 16, 2016.
[109] “Large Ring Die Wood Pellet Machine for Sale.” [Online]. Available: http://www.gemco-energy.com/large-wood-pellet-machine.html. [Accessed: 08-Jul-2018].
[110] “Compact Feed Pellet Line_Liyang Huasheng Machinery Co.,Ltd.” [Online]. Available: http://www.hsbiopellet.com/product/Pellet-Press/217.html. [Accessed: 08-Jul-2018].
[111] Environment and Climate Change Canada, “National Inventory Report 1990-2015: Greenhouse Gas Sources and Sinks in Canada. Canada’s Submission To the UNFCCC. Part 3,” 2017.
[112] Hadi Dowlatabadi, “Lifecycle analysis of GHG intensity in BC’s energy sources,” *Pacific Institute for Climate Solutions*. 2011.
[113] KPMG, “Corporate Tax Rates: Federal and Provincial/Territorial Tax Rates for Income Earned by a CCPC-2018,” 2017.
[114] Natural Resources Canada, “Technical Guide to Class 43.1 and 43.2,” 2013.
[115] P. A. Samuelson and W. D. Nordhaus, *Economics*, 19th ed. Boston: McGraw-Hill/Irwin, 2010.
[116] “Canadian Biomass 2017 Pellet Map,” *Canadian Biomass Magazine*, 2018. [Online]. Available: https://www.canadianbiomassmagazine.ca/images/cbm_pelletmap2017_revisedlr.pdf. [Accessed: 11-Jun-2018].
[117] Wood Pellet Association of Canada, “British Columbia’s Wood Pellet Industry,” 2011.
[118] Statista, “GDP of British Columbia, Canada 2000-2017 | Statistic.” [Online]. Available: https://www.statista.com/statistics/577563/gdp-of-british-columbia-canada/. [Accessed: 28-Jun-2018].
[119] Statista, “British Columbia GDP distribution, by industry Canada 2017| Statistic.” [Online]. Available: https://www.statista.com/statistics/608359/gdp-distribution-of-british-columbia-canada-by-industry/. [Accessed: 28-Jun-2018].
[120] “2007 dollars in 2017 | Canada Inflation Calculator.” [Online]. Available: http://www.in2013dollars.com/2007-CAD-in-2017. [Accessed: 08-Oct-2018].
[121] J. Moorhouse and M. Wolinetz, “Biofuels in Canada: Tracking progress in tackling greenhouse gas emissions from transportation fuels,” *Navius Res. Clean Energy Canada*, no. March, pp. 3–5, 2016.
[122] D. L. E. S. Grandes, “2017 Comparaison of Electricity Prices in Major North American Cities,” 2017.
[123] “Electricity facts | Natural Resources Canada.” [Online]. Available: https://www.nrcan.gc.ca/energy/facts/electricity/20068#L3. [Accessed: 10-Sep-2018].
[124] J. Nyboer, “A Review of Energy Consumption and Related Data in the Canadian Wood Products Industry :1990, 1995 to 2006,” Vancouver, 2008.
[125] Port of Vancouver, “2015 Port Emissions Inventory Report,” 2015.

[126] S. M. Sambo, “Fuel consumption for ground-based harvesting systems in western Canada,” *FERIC*, vol. 3, no. 29, pp. 1–12, 2002.
[127] A. Pa, J. S. Craven, X. T. Bi, S. Melin, and S. Sokhansanj, “Environmental footprints of British Columbia wood pellets from a simplified life cycle analysis,” *Int. J. Life Cycle Assess.*, vol. 17, no. 2, pp. 220–231, 2012.
[128] X. Kuang, T. J. Shankar, S. Sokhansanj, C. J. Lim, X. T. Bi, and S. Melin, “Effects of headspace and oxygen level on off-gas emissions from wood pellets in storage,” *Ann. Occup. Hyg.*, vol. 53, no. 8, pp. 807–813, 2009.
[129] F. Yazdanpanah, S. Sokhansanj, C. J. Lim, A. Lau, X. Bi, and S. Melin, “Stratification of off-gases in stored wood pellets,” *Biomass and Bioenergy*, vol. 71, pp. 1–11, 2014.
[130] W. Guo, “Self-heating and spontaneous combustion of wood pellets during storage-PhD Thesis,” The University of British Columbia, 2013.
[131] X. Kuang, T. J. Shankar, X. T. Bi, S. Sokhansanj, C. Jim Lim, and S. Melin, “Characterization and kinetics study of off-gas emissions from stored wood pellets,” *Ann. Occup. Hyg.*, vol. 52, no. 8, pp. 675–683, 2008.
[132] J. S. Tumuluru, C. Jim Lim, X. T. Bi, X. Kuang, S. Melin, F. Yazdanpanah, and S. Sokhansanj, “Analysis on storage off-gas emissions from woody, herbaceous, and torrefied biomass,” *Energies*, vol. 8, no. 3, pp. 1745–1759, 2015.
[133] T. M. Attard, M. Arshadi, C. Nilsson, V. L. Budarin, E. Valencia-Reyes, J. H. Clark, and A. J. Hunt, “Impact of supercritical extraction on solid fuel wood pellet properties and off-gassing during storage,” *Green Chem.*, vol. 18, no. 9, pp. 2682–2690, 2016.
[134] E. Borén, F. Yazdanpanah, R. Lindahl, C. Schilling, R. P. Chandra, B. Ghiasi, Y. Tang, S. Sokhansanj, M. Broström, and S. H. Larsson, “Off-Gassing of VOCs and Permanent Gases during Storage of Torrefied and Steam Exploded Wood,” *Energy and Fuels*, vol. 31, no. 10, pp. 10954–10965, 2017.
[135] “Biofuels Mandates Around the World 2018 : Biofuels Digest.” [Online]. Available: http://www.biofuelsdigest.com/bdigest/2018/01/01/biofuels-mandates-around-the-world-2018/. [Accessed: 10-Jun-2018].
[136] “Biofuels Mandates Around the World : Biofuels Digest.” [Online]. Available: http://www.biofuelsdigest.com/bdigest/2011/07/21/biofuels-mandates-around-the-world/. [Accessed: 10-Jun-2018].
[137] “Alternative Fuels Data Center: Fuel Prices.” [Online]. Available: https://www.afdc.energy.gov/fuels/prices.html. [Accessed: 10-Jun-2018].
[138] “Alternative Fuels Data Center: Diesel Vehicles Using Biodiesel.” [Online]. Available: https://www.afdc.energy.gov/vehicles/diesel.html. [Accessed: 10-Jun-2018].
[139] “ETIP Bioenergy-SABS.” [Online]. Available: http://www.etipbioenergy.eu/?option=com_content&view=article&id=295. [Accessed: 10-Jun-2018].
[140] Canadian Renewable Fuels Association, “Evolution and growth from biofules to bioeconomy.” Canadian Renewable Fuels Association, 2017.
[141] A. Florentinus, C. Hamelinck, A. van den Bos, R. Winkel, and C. Maarten, “Potential of biofuels for shipping,” 2012.
[142] William Stauss, “The Many Benefits of Replacing Coal With Wood Pellet Fuel | Biomassmagazine.com,” *Biomass Magazine*, Biomass Magazine, 2014.
[143] C. D. Marcela Bilek, Clarence Hardy, Manfred Lenzen, “Lfie-Cycle Energy Balance and Greenhouse Gas Emissions of Nuclear Energy in Australia,” 2006.
[144] I. B. Fridleifsson, R. Bertani, E. Huenges, J. W. Lund, and A. Ragnarsson, “The possible role and contribution of geothermal energy to the mitigation of climate change,” in *IPCC Geothermal 11 February 2008 Meeting*, 2008, pp. 59–80.
[145] V. Krey, O. Masera, G. Blanforde, T. Bruckner, R. Cooke, K. Fish-Vanden, H. Haberl, E. Hertwich, E. Kriegler, D. Müller, S. Paltsev, L. Price, S. Schlömer, D. Uerge-Vorsatz, D. Van Vuuren, and T. Zwickel, “Annex II: Metrics & Methodology.,” *Clim. Chang. 2014 Mitig. Clim. Chang. Contrib. Work. Gr. III to Fifth Assess. Rep. Intergov. Panel Clim. Chang.*, pp. 1281–1328, 2014.
[146] S. Schlömer, T. Bruckner, L. Fulton, E. Hertwich Austria, A. U. McKinnon, D. Perczyk, J. Roy, R. Schaeffer, G. Hänsel, D. de Jager, T. Bruckner, L. Fulton, E. Hertwich, A. McKinnon, D. Perczyk, J. Roy, R. Schaeffer, R. Sims, P. Smith, R. Wiser, R. Pichs-Madruga, Y. Sokona, E. Farahani, S. Kadner,

K. Seyboth, A. Adler, I. Baum, S. Brunner, P. Eickemeier, B. Kriemann, J. Savolainen, S. Schlömer, C. von Stechow, T. Zwickel, and J. Minx, “ANNEX III Technology-specific Cost and Performance Parameters,” 2014.
[147] R. Pichs-Madruga, K. Seyboth, P. Eickemeier, P. Matschoss, G. Hansen, S. Kadner, S. Schlömer, T. Zwickel, and C. Von Stechow, “2011： Annex II: Methodology. In IPCC Special Report on Renewable Energy Sources and Climate Change Mitigation,” 2011.
[148] B. K. Sovacool, “Valuing the greenhouse gas emissions from nuclear power: A critical survey,” *Energy Policy*, vol. 36, pp. 2940–2953, 2008.
[149] OECD Nuclear Energy Agency., “Externalities and energy policy : the Life cycle analysis approach ; Workshop Proceedings, Paris, France, 15-16 November 2001,” Nuclear Energy Agency, Organisation for Economic Co-operation and Development, 2002.
[150] H. Hondo, “Life cycle GHG emission analysis of power generation systems: Japanese case,” *Energy*, vol. 30, pp. 2042–2056, 2005.
[151] M. Whitaker, G. A. Heath, P. O’donoughue, and M. Vorum, “Life Cycle Greenhouse Gas Emissions of Coal-Fired Electricity Generation Systematic Review and Harmonization,” 2012.
[152] Y. Zhang, J. Mckechnie, D. Cormier, R. Lyng, W. Mabee, A. Ogino, and H. L. Maclean, “Life cycle emissions and cost of producing electricity from coal, natural gas, and wood pellets in Ontario, Canada,” *Environ. Sci. Technol.*, vol. 44, no. 1, pp. 538–544, 2010.
[153] “Drax power station - SourceWatch.” [Online]. Available: https://www.sourcewatch.org/index.php/Drax_power_station. [Accessed: 18-Jun-2018].
[154] “Our history - Drax.” [Online]. Available: https://www.drax.com/about-us/our-history/. [Accessed: 18-Jun-2018].
[155] “Drax closer to coal-free future with fourth biomass unit conversion - Drax,” *Drax website*. [Online]. Available: https://www.drax.com/press_release/drax-closer-coal-free-future-fourth-biomass-unit-conversion/. [Accessed: 08-Sep-2018].
[156] “Coal-Fired Plants in Japan,” *Gallery*, 08-Feb-2014. [Online]. Available: http://www.industcards.com/st-coal-japan.htm. [Accessed: 18-Jun-2018].
[157] “Atikokan Generating Station - Wikipedia.” [Online]. Available: https://en.wikipedia.org/wiki/Atikokan_Generating_Station. [Accessed: 18-Jun-2018].
[158] Capital Power, “Genesee Generating Station Units 4 & 5 A New Power Generation Opportunity for Alberta,” Genesee Cooling Pond, 2013.
[159] “Aspen Plus ® 8.4.” .
[160] J. HAYDARY, *CHEMICAL PROCESS DESIGN AND SIMULATION : aspen plus and aspen hysys applications.*, 1st ed. JOHN WILEY, 2018.
[161] Aspen Technology Inc., “Aspen Physical Property System - Physical Property Methods. Version Number: V7.2.” Aspen Plus 8.4, 2010.
[162] I. . Institute of Gas Technology (Chicago, *Coal conversion systems : technical data book / prepared for U.S. Department of Energy, Assistant Secretary for Energy Technology, Division of Coal Conversion*. Washington: Washington : U.S. Govt. Print. Off., 1978, 1978.
[163] D. A. van Meel, “Adiabatic convection batch drying with recirculation of air,” *Chem. Eng. Sci.*, vol. 9, no. 1, pp. 36–44, 1958.
[164] H. Rezaei, “Physical and thermal characterization of ground chip and ground pellet particles-PhD Thesis,” University of British Columbia, 2017.
[165] D. R. Nhuchhen, P. Basu, and B. Acharya, “Investigation into overall heat transfer coefficient in indirectly heated rotary torrefier,” *Int. J. Heat Mass Transf.*, vol. 102, pp. 64–76, 2016.
[166] G. W. J. Wes, A. a. H. Drinkenburg, and S. Stemerding, “Heat transfer in a horizontal rotary drum reactor,” *Powder Technol.*, vol. 13, no. 2, pp. 185–192, 1976.
[167] P. E. Mason, L. I. Darvell, J. M. Jones, and A. Williams, “Comparative Study of the Thermal Conductivity of Solid Biomass Fuels,” *Energy & Fuels*, vol. 30, no. 3, pp. 2158–2163, 2016.
[168] S.-Q. Li, L.-B. Ma, W. Wan, and Q. Yao, “A Mathematical Model of Heat Transfer in a Rotary Kiln Thermo-Reactor,” *Chem. Eng. Technol.*, vol. 28, no. 12, pp. 1480–1489, 2005.
[169] J. Kelly, “Flight design in rotary dryers,” *Dry. Technol.*, vol. 10, no. 4, pp. 979–993, 1992.
[170] F. P. Incropera, D. P. DeWitt, T. L. Bergman, and A. S. Lavine, “Fundamental of Heat and Mass Transfer,” *John-Wiley & Sons Inc*. p. 997, 2006.

[171] A. A. Boateng and P. V. Barr, “A thermal model for the rotary kiln including heat transfer within the bed,” *Int. J. Heat Mass Transf.*, vol. 39, no. 10, pp. 2131–2147, 1996.
[172] D. J. Schell and C. Harwood, “Milling of lignocellulosic biomass - Results of pilot-scale testing,” *Appl. Biochem. Biotechnol.*, vol. 45–46, no. 1, pp. 159–168, 1994.
[173] V. S. P. Bitra, A. R. Womac, N. Chevanan, P. I. Miu, C. Igathinathane, S. Sokhansanj, and D. R. Smith, “Direct mechanical energy measures of hammer mill comminution of switchgrass, wheat straw, and corn stover and analysis of their particle size distributions,” *Powder Technol.*, vol. 193, no. 1, pp. 32–45, 2009.
[174] S. Mani, L. G. Tabil, and S. Sokhansanj, “Grinding performance and physical properties of wheat and barley straws, corn stover and switchgrass,” *Biomass and Bioenergy*, vol. 27, no. 4, pp. 339–352, 2004.
[175] A. N. Rollinson and O. Williams, “Experiments on torrefied wood pellet: study by gasification and characterization for waste biomass to energy applications,” *R. Soc. Open Sci.*, vol. 3, no. 5, p. 150578, 2016.
[176] K. L. Iroba, O. D. Baik, and L. G. Tabil, “Torrefaction of biomass from municipal solid waste fractions II: Grindability characteristics, higher heating value, pelletability and moisture adsorption,” *Biomass and Bioenergy*, vol. 106, pp. 8–20, 2017.
[177] H. Tolvanen, T. Keipi, and R. Raiko, “A study on raw, torrefied, and steam-exploded wood: Fine grinding, drop-tube reactor combustion tests in N2/O2and CO2/O2atmospheres, particle geometry analysis, and numerical kinetics modeling,” *Fuel*, vol. 176, pp. 153–164, 2016.
[178] S. Sokhansanj, “Cost of producing wood pellets,” 2015.
[179] S. E. R. Institute, T. B. Reed, and U. S. D. of Energy, “A Survey of Biomass Gasification,” vol. II, no. 2. c., 1979.
[180] S. Risovic, I. Dukic, and K. Vuckovic, “Energy Analysis of Pellets Made of Wood Residues,” *Croat. J. For. Eng.*, vol. i, no. 29, pp. 95–108, 2008.
[181] J. S. Tumuluru, “Specific energy consumption and quality of wood pellets produced using high-moisture lodgepole pine grind in a flat die pellet mill,” *Chem. Eng. Res. Des.*, vol. 110, pp. 82–97, 2016.
[182] J. Jackson, A. Turner, T. Mark, and M. Montross, “Densification of biomass using a pilot scale flat ring roller pellet mill,” *Fuel Process. Technol.*, vol. 148, pp. 43–49, 2016.
[183] and U. B. H. Wolfgang Stelte, Anand R. Sanadi, Lei Shang, Jens K. Holm, Jesper Ahrenfeldt, “Recent developments in biomass pelletization – a review,” *BioResources*, vol. 7, no. Neville 2011, pp. 4451–4490, 2012.
[184] M. S. Peters, K. D. Timmerhaus, and R. E. West, *Plant Design and Economics for Chemical Engineers*, 5th editio. New York, United States: McGraw-Hill Education, 2002.
[185] G. D. Ulrich and P. T. Vasudevan, *Chemical engineering process design and economics : a practical guide.*, 2nd editio. Durham, N.H. : Process Publishing Company, 2004.
[186] R. (Chemical engineer) Smith, *Chemical process design and integration*, 2nd editio. John Wiley & Sons, Ltd, 2005.
[187] R. Turton, *Analysis, synthesis, and design of chemical processes*, 4th editio. Prentice Hall, 2012.
[188] “工业转筒烘干机_厂家直销 - 阿里巴巴.” [Online]. Available: https://detail.1688.com/offer/560518344909.html?spm=a261b.2187593.1998088710.42.416e0114M75ccb. [Accessed: 08-Jul-2018].
[189] “Dryer_Liyang Huasheng Machinery Co.,Ltd.” [Online]. Available: http://www.hsbiopellet.com/product/Dryer/index.html. [Accessed: 08-Jul-2018].
[190] “Industry Activated Carbon Or Limestone Rotary Kiln.” [Online]. Available: https://chaozhongchina.en.alibaba.com/product/60671507596-805311623/For_Cement_Or_Lime_Professional_Supply_Rotary_Kiln.html?spm=a2700.details.pronpeci14.1.2e284866vmQBLq. [Accessed: 27-Aug-2018].
[191] “Industrial Vibration Fluidized Bed Dryer.” [Online]. Available: https://www.alibaba.com/product-detail/Industrial-vibration-fluidized-bed-dryer-for_60383940129.html?spm=a2700.7724838.2017115.172.64d65ad9XeiO07. [Accessed: 27-Aug-2018].
[192] “Rotary Dryer Price.” [Online]. Available: https://www.alibaba.com/product-detail/Rotary-Dryer-Price-Coal-Silica-Sand_60654608392.html?spm=a2700.galleryofferlist.normalList.144.3c054ed8CjL1R0. [Accessed: 27-Aug-2018].

[193] “Rotary Drying Machine for Sale.” [Online]. Available: http://strommashina.com/category/rotary-dryers/. [Accessed: 27-Aug-2018].
[194] “Mobile Harmless System Treating Petroleum Field’s Sludge.” [Online]. Available: https://chaozhongchina.en.alibaba.com/product/60791997588-804930356/Environmental_Protection_Plant_Mobile_Harmless_System_Treating_Petroleum_Field_s_Sludge.html?spm=a2700.icbuShop.prewdfa4cf.4.6b5b5d89GOe1eI. [Accessed: 27-Aug-2018].
[195] “Transport Equipment Enclosed FU Type Scraper Chain Conveyor.” [Online]. Available: https://chaozhongchina.en.alibaba.com/product/60699114476-805015065/Transport_Equipment_Enclosed_FU_Type_Scraper_Chain_Conveyor.html?spm=a2700.icbuShop.prewdfa4cf.7.7b424015gYuIa9. [Accessed: 27-Aug-2018].
[196] “工业锅炉用引风机.” [Online]. Available: https://detail.1688.com/offer/527931684012.html?spm=a261b.2187593.0.0.eb2f460VPTRle. [Accessed: 27-Aug-2018].
[197] “Fine Power Grinding Machine Wholesale Price.” [Online]. Available: https://chaozhongchina.en.alibaba.com/product/60666002543-805138452/Energy_Saving_Fine_Power_Grinding_Machine_Wholesale_Price_Vertical_Limestone_Grinding_Raymond_Mill_Machine.html?spm=a2700.icbuShop.prewdfa4cf.1.491e1b17UPbxsG. [Accessed: 27-Aug-2018].
[198] “Husk Wood Sawdust Cow Dung Pellet Machine.” [Online]. Available: https://www.alibaba.com/product-detail/ROTEXMASTER-Machinery-plant-good-price-rice_60681646986.html?spm=a2700.7724838.2017115.156.2d677011Rt2Td1. [Accessed: 27-Aug-2018].
[199] “Belt Conveyors | eBay.” [Online]. Available: https://www.ebay.com/b/Belt-Conveyors/131199/bn_78213395. [Accessed: 08-Jul-2018].
[200] “Belt Conveyors For Sale in Canada & USA | AgDealer.” [Online]. Available: https://www.agdealer.com/listings/belt-conveyor. [Accessed: 08-Jul-2018].
[201] A. Pa, “Development of British Columbia Wood Pellet Life Cycle Inventory and its Utilization in the Evaluation of Domestic Pellet Applications-Master’s Thesis,” University of British Columbia, 2010.
[202] M. R. Milota, C. D. West, and I. D. Hartley, “Gate-To-Gate Life-Cycle Inventory of Softwood Lumber Production,” *Wood Fiber Sci.*, vol. 37, pp. 47–57, 2006.
[203] “Pellet Hub | Wood Pellet Association of Canada.” [Online]. Available: https://www.pellet.org/wpac-news/pellet-hub. [Accessed: 10-Jun-2018].
[204] S. Sénéchal and G. Grassi, “Logistic Management of Wood Pellets; Data Collection on Transportation, Storage & Delivery Management,” *Brussels, EUBIA-European Biomass Industry Association*. pellets @ las, 2009.
[205] V. Fraser and P. Authority, “Port of Vancouver Statistics Overview 2016.” 2016.
[206] “Truck Leasing and Rental in British Columbia.” [Online]. Available: https://www.inland-group.com/en-ca/lease-rental/. [Accessed: 11-Jul-2018].
[207] “Prices, Tariffs and Transit Times | Customer Centre | cn.ca.” [Online]. Available: https://www.cn.ca/en/customer-centre/prices-tariffs-transit-times/. [Accessed: 11-Jul-2018].
[208] “International container shipping | Freight broker and forwarder.” [Online]. Available: https://www.searates.com/. [Accessed: 11-Jul-2018].
[209] A. K. Erin Searcy, Peter Flynn, Emad Ghafoori, “The Relative Cost of Biomass Energy Transport E RIN S EARCY , P ETER F LYNN ,* E MAD G HAFOORI ,” *Appl. Biochem. Biotechnol.*, vol. 136–140, pp. 639–652, 2007.
[210] A. Pirraglia, R. Gonzalez, and D. Saloni, “Techno-economical analysis of wood pellets production for U.S. manufacturers,” *BioResources*, vol. 5, no. 4, pp. 2374–2390, 2010.
[211] A. Kumar, J. B. Cameron, and P. C. Flynn, “Pipeline transport and simultaneous saccharification of corn stover,” *Bioresour. Technol.*, vol. 96, no. 7, pp. 819–829, 2005.
[212] C. N. Hamelinck, R. A. A. Suurs, and A. P. C. Faaij, “International bioenergy transport costs and energy balance,” *Biomass and Bioenergy*, vol. 29, no. 2, pp. 114–134, 2005.
[213] X. Lu, M. R. Withers, N. Seifkar, R. P. Field, S. R. H. Barrett, and H. J. Herzog, “Biomass logistics analysis for large scale biofuel production: Case study of loblolly pine and switchgrass,” vol. 183, pp. 1–9, 2015.

[214] Y. Nie and X. Bi, “Life-cycle assessment of transportation biofuels from hydrothermal liquefaction of forest residues in British Columbia,” *Biotechnol. Biofuels*, vol. 11, no. 1, pp. 464–475, 2018.
[215] H. Mahmudi and P. C. Flynn, “Rail vs truck transport of biomass,” *Appl. Biochem. Biotechnol.*, vol. 129, no. 1–3, pp. 88–103, 2006.
[216] D. Mcpherrin, “Development of a Feedstock-to-Product Chain Model for Densified Biomass Pellets - Master’s Thesis,” Queen’s University, 2017.

Appendices

Appendix A Biomass thermal properties calculation methods

A.1 Heat of formation

The correlation of the formation heat of biomass is shown in Eq. (A.1) (in Btu/lb), which is based on the assumption that combustion results in complete oxidation of all elements except sulfatic sulfur and ash, which are considered inert. Further description of this model refers to *Aspen Help* [159] [160].

$$\Delta_f h^d = \Delta_c h^d - \left(1.418 \times 10^4 w_H^d + 3.278 \times 10^3 w_C^d + 9.264 \times 10^2 w_s^d - 2.418 \times 10^2 w_N^d - 1.426 \times 10^2 w_{cl}^d\right) \quad (A.1)$$

Where $\Delta_c h^d$ is the HHV of the biomass and can be calculated based on the dry and mineral matter free elemental fuel composition, which will be discussed in section A.2. Parameters in Eq. (A.1) are summarized in Table A.1.

Table A.1 Correlations to calculate biomass heat of formation

	Correlations	Heat of formation (btu/lbmole) $\Delta H_{formation}^{idealgas}$		MW	
w_H^d	$w_H^d = \frac{\Delta H_{formation}^{idealgas}(H_2O) - \Delta H_{vaporation}^{298.15}(H_2O)}{MW(H_2)}$	$\Delta H_{formation}^{idealgas}(H_2O)$	-103963	$MW(H_2)$	2
		$\Delta H_{vaporation}^{298.15}(H_2O)$	970		
w_C^d	$w_C^d = \frac{\Delta H_{formation}^{idealgas}(CO_2)}{MW(C)}$	$\Delta H_{formation}^{idealgas}(CO_2)$	-169178	MW(C)	12
w_s^d	$w_s^d = \frac{\Delta H_{formation}^{idealgas}(SO_2)}{MW(S)}$	$\Delta H_{formation}^{idealgas}(SO_2)$	-127618	MW(S)	32
w_N^d	$w_N^d = \frac{\Delta H_{formation}^{idealgas}(NO_2)}{MW(N)}$	$\Delta H_{formation}^{idealgas}(NO_2)$	14264	MW(N)	14
w_{cl}^d	$w_{cl}^d = \frac{2\Delta H_{formation}^{idealgas}(HCl) - \Delta H_{formation}^{liquid}(H_2O)}{MW(Cl_2)}$	$\Delta H_{formation}^{idealgas}(HCl)$	-39686	$MW(Cl_2)$	70.9

Superscripts: d=dry basis, m=mineral-matter-free basis
Subscripts: A=ash, C=carbon, Cl=chlorine, FC=fixed carbon, H=hydrogen, H_2O=moisture, MM=mineral matter, N=nitrogen, O=oxygen, So=organic sulfur, Sp=pyritic sulfur, St=total sulfur, S=other sulfur, VM=volatile matter

A.2 Heat of combustion

Correlations to quantify the biomass HHV ($\Delta_c h^d$) are summarized in Table A.2. Parameters in the correlations are summarized in Table A.3. Details can be refer to *Aspen Help* and [45].

Table A.2 Correlations to calculate biomass heat of combustion

Method	Correlations
Bio	$\mathrm{HHV}_s^{\mathrm{Bioe}} = 100 \cdot \left(a_1 x_C^{dm} + a_2 x_H^{dm} + a_3 x_S^{dm} + a_4 x_O^{dm} + a_5 x_N^{dm}\right) + a_6$
Dulong	$\mathrm{HHV}_s^{\mathrm{Dulong}} = 100 \cdot \left(a_1 x_C^{dm} + a_2 x_H^{dm} + a_3 x_S^{dm} + a_4 x_O^{dm} + a_5 x_N^{dm}\right) + a_5$
Grummel and Davis	$\mathrm{HHV}_s^{\mathrm{GD}} = 100 \cdot \left(\frac{a_2 x_H^{dm}}{1 - x_A^{dm}} + a_5\right) \cdot \left(a_1 x_C^{dm} + x_H^{dm} + a_3 x_S^{dm} + a_4 x_O^{dm}\right)$
Mott and Spooner 1	$\mathrm{HHV}_s^{\mathrm{MS1}} = 100 \cdot \left(a_1 x_C^{dm} + a_2 x_H^{dm} + a_3 x_S^{dm} - a_4 x_O^{dm}\right) + a_7$
Mott and Spooner 2	$\mathrm{HHV}_s^{\mathrm{MS2}} = 100 \cdot \left(a_1 x_C^{dm} + a_2 x_H^{dm} + a_3 x_S^{dm} - \left(\frac{a_6 - a_5 x_O^{dm}}{1 - x_A^{d}}\right) x_O^{dm}\right) + a_7$
IGT	$\mathrm{HHV}_s^{\mathrm{IGT}} = 100 \cdot \left(a_1 x_C^{d} + a_2 x_H^{d-} + a_3 x_S^{d} - a_4 x_A^{d}\right) + a_5$

x_C^{dm}: mass fraction of carbon on dry and matter free basis
x_C^{d}: mass fraction of carbon on dry basis
Subscripts: A=ash, C=carbon, Cl=chlorine, FC=fixed carbon, H=hydrogen, H_2O=moisture, MM=mineral matter, N=nitrogen, O=oxygen, So=organic sulfur, Sp=pyritic sulfur, St=total sulfuer, S=other sulfuer, VM=volatile matter

Table A.3 Parameters in biomass HHV correlations

	Unit	$\mathbf{a_1}$	$\mathbf{a_2}$	$\boldsymbol{a_3}$	$\boldsymbol{a_4}$	$\mathbf{a_5}$	$\boldsymbol{a_6}$	$\boldsymbol{a_7}$
Bioe	Btu/bl	151.2	499.8	45.1	-47.7	27.0	27.0	-189.0
Dulong	Btu/bl	145.4	620.3	40.5	-77.5	-16.0	-	-
Grummer and Davis	Btu/bl	0.33	654.3	0.125	0.16	424.6	-2.0	-
Mott and Spooner 1	Btu/bl	144.5	610.2	40.3	62.5	30.9	66.0	-47.0
Mott and Spooner 2	Btu/bl	144.5	610.2	40.3		-	31.0	-
IGT	Btu/bl	178.1	620.3	80.9	44.9	-5153.0	-	-

A.3 Specific heat capacity

The Kirov correlation (1965) [46] considered biomass to be a mixture of moisture, ash, fixed carbon, and primary and secondary volatile matter. The secondary volatile matter is any volatile matter up to 10% on a dry, ash-free basis; the remaining volatile matter is primary. The correlation developed by Kirov treats the heat capacity as a weighted sum of the heat capacities of the constituents:

$$C_{p,i}^{d} = \sum_{j=1}^{ncn} x_j C_{p,ij} \tag{A.2}$$

$$C_{p,ij} = a_{i,j1} + a_{i,j2}T + a_{i,j3}T^2 + a_{i,j4}T^3 \tag{A.3}$$

Where i indicates component index, j is the constituent index j=1, 2 , ... , ncn, where 1 indicates moisture, 2 is fixed carbon, 3 is primary volatile matter, 4 is secondary volatile matter, and 5 is ash. x_j is the mass fraction of jth constituent on dry basis.

Table A.4 Parameters in biomass specific heat capacity

Symbol	$a_{i,11}$	$a_{i,12}$	$a_{i,13}$	$a_{i,14}$	$a_{i,21}$	$a_{i,22}$	$a_{i,23}$	$a_{i,24}$	$a_{i,31}$	$a_{i,32}$
Value	1.0	0	0	0	0.165	6.8×10^{-4}	-4.2×10^{-7}	0	0.395	8.1×10^{-4}
Symbol	$a_{i,33}$	$a_{i,34}$	$a_{i,41}$	$a_{i,42}$	$a_{i,43}$	$a_{i,44}$	$a_{i,51}$	$a_{i,52}$	$a_{i,53}$	$a_{i,54}$
Value	0	0	0.71	6.1×10^{-4}	0	0	0.18	1.4×10^{-4}	0	0

A.4 Biomass density

Biomass (dry, wet, and torrefied biomass) density $\rho_{biomass}$, is calculated based on DCOALIGT model from Institute of Gas Technology (ITG) in Aspen Plus 8.4, the model uses biomass ultimate and sulfur analysis. Details refer to [161], [162].

$$\rho_i = \frac{\rho_i^{dm}}{\rho_i^{dm}\left(0.42w_{A,i}^{d} - 0.15w_{Sp,i}^{d}\right) + 1 - 1.13w_{A,i}^{d} - 0.5475w_{Sp,i}^{d}} \tag{A.4}$$

Where

$$\rho_i^{dm} = \left(a_{1i} + a_{2i}W_{H,i}^{dm} + a_{3i}\left(wW_{H,i}^{dm}\right) + a_{4i}\left(W_{H,i}^{dm}\right)^3\right)^{-1} \quad (A.5)$$

$$W_{H,i}^{dm} = \frac{10^2(w_{H,i}^{d} - 0.013w_{A,i}^{d} + 0.02w_{Sp,i}^{d})}{1 - 1.13w_{A,i}^{d} - 0.475w_{sp,i}^{d}} \quad (A.6)$$

Where the superscript d indicates dry basis, dm indicates moisture and minor contents free basis, with $a_{1i} = 0.4397$, $a_{2i} = 0.1223$, $a_{3i} = -0.01715$, $a_{4i} = 0.001077$.

$$w^{d} = \frac{w}{1 - w_{H_2O}} \quad (A.7)$$

Where w indicates the value determined for weight fraction, w^d indicates the value on a dry basis, w_{H_2O} indicates the moisture weight fraction. For hydrogen, the formula includes a correction for free-moisture hydrogen:

$$w_H^d = \frac{w_H - 0.119w_{H_2O}}{1 - w_{H_2O}} \quad (A.8)$$

The mineral matter content is calculated using the modified Parr formula:

$$w_{MM} = 1.13w_A + 0.47w_{sp} + w_{cl} \quad (A.9)$$

Correct analysis from a dry and mineral-matter-free basis is calculated as

$$w^{dm} = \frac{w^d - \Delta w^d}{1 - w_{MM}} \quad (A.10)$$

Table A.5 Parameters in biomass mass density

symbol	Description
Δw^{d}	Correction factor for other losses, such as the loss of carbon in carbonates and the loss of hydrogen present in the water constitution of clays
Δw_C^d	$0.014W_A^d+0.005W_{sp}^d$
Δw_H^d	$0.013W_A^d-0.02W_{sp}^d$
W_O^{dm}	$1-W_C^{dm}-W_H^{dm}-W_{sp}^{dm}-W_N^{dm}$
W_S^{dm}	$w_{sr}^{dm} - w_{sp}^{dm} - w_{so}^{dm}$

Subscriots: A=ash, C=carbon, Cl=chlorine, FC=fixed carbon, H=hydrogen, H2O=moisture, MM=mineral matter, N=nitrogen, O=oxygen, So=organic sulfur, Sp=pyritic sulfur, St=total sulfur, s=other sulfur, VM=volatile matter; superscripts d=dry basis, m=mineral-matter-free basis

Appendix B Unit models for thermal system

Unit models of rotary dryer, fluidized bed dryer, directly and indirectly heated rotary torrefier, and fluidized bed torrefier are developed based on Aspen Plus and FORTRAN programming. The following three aspects have to be covered for each unit:

(1) The chemical and physical processes occurring in the unit;

(2) The equations representing those processes;

(3) The computer code that uses the equations;

The first aspect has been presented in Chapter 2. Here, (2) and (3) will be presented.

B.1 Drying

Two groups of biomass particles are to be dried in the current study, 20 mm pine wood chips to be dried in the rotary dryers in Paths 0-3 and 1 mm particles to be dried in fluidized bed dryer in Path 4.

B. 1. 1 Single particle evaporation model

The single particle evaporation model $\dot{M}$ is applied to capture the drying kinetics, as expressed by Eq. (B.1) [163].

$$\dot{M} = \dot{v}(\eta) \cdot \rho_G \cdot k^* \cdot A_p \cdot [Y^*(T_{GS} - Y)] \quad (B.1)$$

Here $A_p = \pi \cdot d_p^2$ is the surface area of one particle with the mean particle diameter d_p, ρ_G is the gas density, $(Y^* (T_{GS}) - Y)$ is the driving potential, which indicates the difference between the moisture content that the gas would have at adiabatic saturation and the moisture content that it actually has at the considered position in the dryer; k^* is the mass transfer coefficient, which is different for rotary dryer and the fluidized bed dryer, which will be discussed in later section. $\dot{v}(\eta)$ is a dimensionless function which takes into account the

physical properties of the material to be dried, as is defined by Eq. (B.2) according to Van Meel [163].

$$\dot{v}(\eta) = \dot{v}(\frac{M - M_{eq}}{M_0 - M_{eq}}) \tag{B.2}$$

Here, the initial moisture content M_0 equals 50wt%db, and M_e equals 0wt%db in this study. The instantaneous moisture content M is calculated according to Rezaei's model [56] based on thin layer drying experiments as shown by Eq. (B.3) [164], in which the biomass moisture content decays exponentially with time.

$$\eta = \frac{M - M_{eq}}{M_0 - M_{eq}} = \exp(-k_{wood} \cdot \tau) \tag{B.3}$$

Where k_{wood} is the drying kinetics constant, correlated to the drying temperature, the biomass initial moisture content, as well as the biomass particle size, as shown in Eq. (B.4) [56]. τ is the mean residence time of the particles in the dryer.

$$k_{wood} = \exp[(0.013T) - (2.372M_0) - (0.035d_p) - 2.095] \tag{B.4}$$

Where T is drying temperature in °C, $M_0$is the constant moisture content, d is the mean particle size in mm.

The instantaneous moisture content M is thus expressed as Eq. (B.5).

$$M = \eta \cdot M_0 = \exp(-k_{wood} \cdot \tau) \cdot M_0 \tag{B.5}$$

This single particle evaporation model is used in modeling both the rotary and the fluidized bed dryer.

B. 1. 2 Rotary dryer model

The governing equations for the mass balances of moisture for the solid phase and gas phase are expressed as Eq. (B.6) and Eq. (B.7). The heat balances for the solid and the gas phases are expressed as Eq. (B.8) and Eq. (B.9).

$$\text{Solid phase:} \dot{m}_s dX = -\dot{M} \cdot N_p \cdot \frac{dz}{L} \tag{B.6}$$

$$\text{Gas phase: } \dot{m}_G dY = \dot{M} \cdot N_P \frac{dz}{L} \tag{B.7}$$

$$\text{Gas phase: } \dot{m}_G \cdot c_{p,G} \cdot dT_G = -h_p \cdot A_p \cdot (T_G - T_S) \cdot N_p \cdot \frac{dz}{L} \tag{B.8}$$

$$\text{Solid phase: } \dot{m}_s \cdot \left(c_{p,G} + X \cdot c_{p,M}\right) dT_S = \left[h_p \cdot A_p \cdot (T_G - T_S) \cdot N_p - \dot{M} \cdot N_p \cdot \Delta h^V\right] \cdot \frac{dz}{L} \tag{B.9}$$

Here $\dot{M}_s$ and $\dot{M}_G$, T_s, and T_G, X and Y are the mass flowrates, temperatures, and the dry-based moisture content of the biomass and the drying gas, respectively; $c_{p,G}$ and $c_{p,M}$ are the specific heat capacity of the drying gas and the liquid moisture; Δh^V is the enthalpy of evaporation. $N_p = \frac{\dot{M}_s \cdot \tau}{\rho_s \cdot \frac{\pi}{6} \cdot d_p^3}$ is the total number of particles, with τ being the mean residence time of particles in the drum.

Mass transfer coefficient $k^* = k_p$

In a co- currently flow rotary dryer, both solid and gas phase travels in plug flows. The mechanism of mass transfer in the rotary dryer has been discussed in section 2.2.2.1.1, which can be represented by a mass transfer coefficient between a single particle and the surrounding gas, k_p. The mass transfer coefficient k^* in Eq. (B.1) is thus calculated by Eq. (B.10) from Ranz and Marshall [60].

$$k^* = k_p = \frac{Sh_p \cdot \delta_G}{d_p} \tag{B.10}$$

$$\mathrm{Sh_p} = 2 + 0.6\mathrm{Re_{sph}^{1/2}}Sc^{1/3} \tag{B.11}$$

$$\mathrm{Re_{sph}} = \frac{u_0 \cdot d_p \cdot \rho_G}{\mu_G},\ \mathrm{Sc_G} = \frac{\mu_G}{\delta_G \cdot \rho_G} \tag{B.12}$$

Here δ_G denotes the diffusion coefficient of gas, $u_0 = |u_s - u_g| \cong u_g$ is the relative velocity, ρ_G is the gas density, μ_G is the dynamic viscosity of gas, $c_{p,G}$ is the specific heat capacity of gas, and λ_G is the thermal conductivity of drying gas.

Heat transfer coefficient h_{gp}

Similar to the mass transfer coefficient, heat transfer coefficient h_{gp} between a single solid particle and surrounding gas phase is applied here, which can be calculated by Eq. (B.13) to Eq.(B.15).

$$h_{gp} = \frac{Nu_p \cdot \lambda_G}{d_p} \tag{B.13}$$

$$Nu_p = 2 + 0.6Re_p^{0.5}{Pr_G}^{0.33} \tag{B.14}$$

$$Pr_G = \frac{\mu_G \cdot c_{p,G}}{\lambda_G} \tag{B.15}$$

Both the heat and mass transfer coefficient models are written in FORTRAN programming and integrated in the convective dryer module in Aspen Plus.

B. 1. 3 Fluidized bed dryer model

Two modules are used to simulate the fluidized bed dryer: a cross flow convective dryer module available in Aspen Plus is used to calculate the required solids residence time based on single particle evaporation kinetics as discussed in section B. 1. 1; a fluidized bed module is used to quantify the minimum fluidization velocity, behaviors of the bubbles and also to size the diameter and height of the drum based on the particle mechanics models.

The governing equations for the heat and mass balances of the solid flow and the vapor flow are shown in Eq. (B.16) to Eq. (B.19).

$$Y_{out} = Y_{in} + (Y^*(T_{GS}) - Y) \cdot (1 - \frac{1}{\exp(\dot{v}(\eta) \cdot NTU_m)}) \quad (B.16)$$

$$X_{out} = X_{in} - \frac{\dot{m}_G \cdot (Y_{out} - Y_{in})}{\dot{M}_S} \quad (B.17)$$

$$T_{G,out} = T_{G,in} + (T_{S,out} - T_{G,in}) \cdot (1 - \frac{1}{\exp(NTU_h)}) \quad (B.18)$$

$$T_{S,out} = T_{S,in} + \frac{\dot{Q} - \dot{m}_G \cdot (Y^* - Y_{out}) \cdot \Delta h^V}{M_p \cdot c_{p,S}} \quad (B.19)$$

Where X_{in}, X_{out}, and Y_{in}, Y_{out} denote inlet and outlet moisture contents in the solid and gas phase, respectively. $T_{G,in}$, $T_{G,out}$, and $T_{S,in}$, $T_{S,out}$ denote inlet and outlet temperature for the solid and gas phase, respectively; M_p is the mass of one dry particle; $NTU_m = \frac{\rho_G \cdot k^* \cdot A_p \cdot N_p}{\dot{M}_G}$ and $NTU_h = \frac{h^* \cdot A_p \cdot N_p}{\dot{M}_G \cdot c_{p,G}}$ denote the number of mass and heat transfer units, in which the mass transfer coefficient k^* and heat transfer coefficient h^* are embodied. $\dot{Q} = h^* \cdot A_p \cdot (T_G - T_S)$ is the heat flow rate from gas to solid phases.

Mass transfer coefficient $k^* = k_{bed}$

As aforementioned in Chapter 2, homogeneous approach is used for calculating fluidized bed dryer mass transfer coefficient. The average mass transfer coefficient of the bed k_{bed}, reported by Resnick and White (1949) [59] for small size fluidized particles, is used here. Thus, $k^*(= k_{bed})$ is calculated by

$$k_{bed} = Sh_{bed} \cdot \delta_G / d_p \quad (B.20)$$

Here the Sherwood number for particle size in 1mm is adopted from Resnick and White (1949) ([59]).

$$\mathrm{Sh_{bed}} = 0.2\mathrm{Re_p^{0.937}} \text{ for } 30 < \mathrm{Re} < 90 \tag{B.21}$$

It should be noticed that $\mathrm{Re_p} = \frac{u_{mf} \cdot d_p \cdot \rho_G}{\mu_G}$.

Heat transfer coefficient $\mathbf{h_{bed}}$

Heat transfer from the wall surface to the solid and gas phases in the fluidized bed dryer is neglected in this study. Similar to the mass transfer coefficient, here, an overall bed heat transfer coefficient $h^* = h_{bed}$ is applied to estimate the overall heat transfer performances of the fluidized bed, which is calculated according to Eq. (B.22).

$$h^* = h_{bed} = \frac{\mathrm{Nu_{bed}} \cdot \lambda_G}{d_p} \tag{B.22}$$

Kunii and Levenspiel [60] collected data from 22 studies on heat transfer in gas fluidized beds and found that when the particle Reynolds number $\mathrm{Re_p}$ is higher than 100, the gas fluidized bed overall Nusselt number falls between the values of single particles and fixed beds; when $\mathrm{Re_p}$ is lower than 100, Nusselt number falls dramatically with the values lower than 2, and the bed Nusselt number $\mathrm{Nu_{bed}}$ can be calculated by Eq. (B.23) and Eq. (B.24) .

$$\mathrm{Nu_p}\left(2 + 0.6\mathrm{Re_p^{0.5}Pr_G}^{0.33}\right) < \mathrm{Nu_{bed}} < \mathrm{Nu_{fixed}}(2 + 1.8\mathrm{Re_p^{0.5}Pr_G}^{0.33}), \quad (\mathrm{Re_p} > 100) \tag{B.23}$$

$$\mathrm{Nu_{bed}} = 0.03\mathrm{Re_p^{1.3}}\text{ , } (\mathrm{Re_p} < 100) \tag{B.24}$$

Here, $\mathrm{Re_p} = \frac{u_{mf} \cdot d_p \cdot \rho_G}{\mu_G}$.

Both heat and mass transfer coefficient models are written in FORTRAN programming, and integrated to the cross flow convective dryer module in Aspen Plus.

Mechanics

Mechanics of the fluidized bed dryer is calculated by using a fluidized bed module available in Aspen Plus. This module is responsible to quantify the minimum fluidization velocity, superficial velocity, behaviors of bubbles, cross sectional area, and the height of the fluidized bed so as to determine the drying gas flowrate and heat and mass transfer rates in the cross-flow convective dryer module (with solids fed from one end and discharged from the other end, moving horizontally), which is responsible to capture the falling rate drying period kinetics and solid mean residence time. Detail mechanic models of the fluidized bed are available in Aspen HELP, and additional introduction materials of the model can be found in Werther et al. [65], [62], [64].

B.2 Torrefaction

B. 2. 1 Rotary torrefier

Assumptions of the model

In a directly and indirectly heated rotary torrefier, the flue gases travel in the shell of the drum to provide heat to the solid indirectly, and then go to the tube side of the drum to contact with solid directly. Following assumptions are made for the model:

(a) The drum is considered to have a uniform solid filling fraction ($F_{ff} = 0.1$) along the reactor length;

(b) Reactors are installed with three axial rectangular flights, these flights help to lift up the solid and maintain the cascaded motion of particles. The heat transfer from the flights to the bed is neglected;

(c) There is limited flow of gas (mixture of recycled flue gases and torgas) to reduce its influence on torrefaction reaction. Therefore, heat transfer from gas to solid particles is neglected; major heat is transferred to the particles through the contact with the wall;

(d) The temperature within the bulk solids is uniform at a given axial location of the drum;

Two fluid temperature profiles are significantly important: (1) temperature profile of flue gases at the shell side, because the temperature at the exit of shell side $T_{G,out_{sh}}$determines whether the flue gases can be injected into the tube side. $T_{G,out_{sh}}$ should be lower than the biomass ignition temperature (350°C [105], [106]); (2) the temperature profile of the solid biomass in the tube side, which determines the torrefaction heat and HHVs of torgas and torrefied biomass. Therefore, an overall heat transfer coefficient between these two fluids is developed. The governing enthaly balance equations of the shell side gas and the tube side solids are given in Eq. (B.25) to Eq. (B.27).

$$\sum \dot{m}_{G,sh} c_{p,G,sh} \frac{dT_{G,sh}}{dz} = h_o A_{wall} \Delta T_m \tag{B.25}$$

$$\sum \dot{m}_{s_{tu}} c_{p,S,tu} \frac{dT_{s,tu}}{dz} = h_o \, A_{wall_{tu}} \Delta T_m + \Delta H_{tor}(T) \tag{B.26}$$

$$\Delta T_m = \frac{\left(T_{G,sh_{in}} - T_{s,tu_{out}}\right) - (T_{G,sh_{out}} - T_{s,tu_{in}})}{\ln(\frac{T_{G,sh_{in}} - T_{s,tu_{out}}}{T_{G,sh_{out}} - T_{s,tu_{in}}})} \tag{B.27}$$

Where $\dot{m}_{G_{sh}}$, $c_{pG,sh}$, $T_{G,sh}$, $T_{G,in_{sh}}$ and $T_{G,out_{sh}}$ are the shell side flue gases mass flow rate, specific heat capacity, temperature, and temperature of the flue gases coming and exiting from the shell respectively; $\dot{m}_{s_{tu}}$, $c_{ps_{tu}}$, $T_{s_{tu}}$, $T_{s,in_{tu}}$ and $T_{s,out_{tu}}$ are the wood chips mass flow, specific heat capacity, temperature , solid temperatures in and out the of rotary kiln tube, respectively; ΔT_m is the log-mean temperature difference, z is the horizontal length location of the rotary kiln, $\Delta H_{tor}(T)$ is the torrefaction reaction heat, $A_{wall_{tu}}$ is the overall area of the tube wall, and h_o is the overall surface heat transfer coefficient between the shell side gas and the tube side wood chips.

Mathematical models of overall heat transfer coefficient

An overall heat transfer coefficient model is developed and expressed as Eq. (B.28). The rate of heat transfer from the shell side hot gas to the tube side solids is governed by three thermal resistances,

(1) the overall heat transfer resistance in the tube side h_{tu},

(2) thermal resistance of the tube wall,

(3) the overall heat transfer resistance in shell side h_{sh}.

$$h_o = \frac{1}{\frac{1}{h_{tu}} + \frac{\epsilon_{wall_{tu}}}{\lambda_{wall_{tu}}} + \frac{1}{h_{sh}}} \tag{B.28}$$

The tube wall thickness is in the order of 3 mm, and the thermal conductivity is 220 W/m-K, thus the thermal resistance of the tube wall is neglected in this study. Then Eq. (B.28) is reduced to Eq. (B.29).

$$h_o = \frac{1}{\frac{1}{h_{tu}} + \frac{1}{h_{sh}}} \tag{B.29}$$

h_{tu}--The overall tube side heat transfer coefficient consists of (a) heat transfer from covered tube wall to the covered solid particles h_{cw-cb} and (b) heat transfer from the wall to the gas through convection h_{ew-eg}. Therefore, the overall tube side heat transfer coefficient h_{tu} can be expressed as Eq. (B.30).

$$h_{tu} = \vartheta_d \underbrace{h_{cw-cb}}_{\text{wall to bulk solids}} + (1-\vartheta_d) \underbrace{h_{ew-eg}}_{\text{wall to gas}} \quad \text{(B.30)}$$

Where ϑ_d is the average of the wall area covered by the solids, usually assumed as 0.2 [165].

h_{cw-cb}--The tube wall to the particles heat transfer resistance contains two parts:

(a) $1/ h_{sb}$, the average thermal resistance across the solid pack being lifted, which is similar to that of particle packets in a fluidized bed [166], [165], thus can be expressed by Eq. (B.31) [165];

(b) $1/h_{ws}$, the thermal resistance due to the thin gas film between the wall and the first layer of particles, which can be expressed by Eq. (B.33).

$$\underbrace{\frac{1}{h_{sb}}}_{\text{thermal resistance of solid packs}} = \left(\frac{\pi t_c}{4k_{bs_{tu}} C_{p,bs_{tu}} \rho_{bs_{tu}}}\right)^{0.5} \quad \text{(B.31)}$$

Where $C_{p,bs}$ is the specific heat capacity of bulk solids, $\rho_{bs} = 350 kg/m^3$ [167] is the density of the bulk solids, and t_c is the average solid contact time with hot surface per cascaded cycle, which can be calculated according to Eq. (B.32) [168], [165].

$$t_c = \frac{\phi_s}{180\omega} = \frac{108.46F_{ff}^{0.357}}{180 * (0.1047 rpm)} \quad \text{(B.32)}$$

Where $\phi_s = 108.46F_{ff}^{0.357}$ is the half filling angle of the solid inside the reactor, $\omega = 0.1047$ rpm (5rpm) is the angular speed of the rotating drum, F_{ff} is the solid filling fraction,

Kelly [169] recommended that the maximum allowable solid filling fraction would be only up to 0.1.

$$\underbrace{\frac{1}{h_{ws}}}_{\text{wall and first layer of particles}} = \frac{\psi d_p}{\lambda_{g_{tu}}} \tag{B.33}$$

Where $\lambda_{g_{tu}}$ is the thermal conductivity of gas inside the tube, ψ is the thickness of the gas film as the fraction of particle diameter ψ =0.085, d_p is the effective particle diameter, and λ_{bs} is the thermal conductivity of bulk solids [167].

h_{cw-cb} is calculated by Eq. (B.34),

$$h_{cw-cb} = \frac{1}{\frac{\psi d_p}{\lambda_{g_{tu}}} + \left(\frac{\pi t_c}{4k_{bs_{tu}} C_{p,bs_{tu}} \rho_{bs_{tu}}}\right)^{0.5}} \tag{B.34}$$

h_{ew-eg}--<u>The tube wall to gas heat transfer</u> is mainly from natural convection inside a horizontal pipe, thus its average value can be calculated by the Churchill and Chu equation [170], as express by Eq. (B.35).

$$h_{ew-eg} = \frac{\lambda_{G_{tu}}}{D_{tu}} \left[0.6 + \frac{0.387 Ra_{tu}^{\frac{1}{6}}}{\left\{1 + \left(\frac{0.559}{Pr_{tu,G}}\right)^{\frac{9}{16}}\right\}^{\frac{8}{27}}} \right]^2 \tag{B.35}$$

$$Ra_{tu} = g\xi_v \left(T_{wall_{tu}} - T_{G_{tu}}\right) D_{tu}{}^3 / \mu_{G_{tu}} \delta_{G_{tu}} \ (10^{-5} < Ra_{tu} < 10^{12}) \tag{B.36}$$

$$Pr_{tu,G} = c_{pG_{tu}} \mu_{G_{tu}} / \lambda_{G_{tu}} \tag{B.37}$$

Where $\xi_v$is the volumetric expansion coefficient of gas, $\mu_{G_{tu}}$is the dynamic viscosity of gas in the tube, $\delta_{G_{tu}}$is the thermal diffusivity of gas inside the tube, D_{tu} is the tube diameter, and

$T_{G_{tu}}$ is the mean temperature of the gas in the tube side. Here, we assume a temperature difference of 10 K between the tube side gas and the wall, $T_{w_{tu}} - T_{G_{tu}} = 10K$.

h_{sh}--The tube wall absorbs heat from the shell side gas through forced convection h_{sh}^{c} and radiation h_{g-w}^{r} as shown in Eq. (B.38),

$$h_{sh} = h_{sh}^{c} + h_{g-w}^{r} \tag{B.38}$$

In the shell side with the gas flow over the tube wall, heat transfer can be considered as <u>forced convection between fluids over horizontal plates</u> h_{sh}^{c}. The classic equation for turbulent convection is applied as shown Eq. (B.39) [171].

$$h_{sh}^{c} = \frac{Nu_{sh}\lambda_{G_{sh}}}{D_{e_{sh}}} \tag{B.39}$$

$$Nu_{sh} = 0.023 Re_{sh}^{0.8} Pr_{sh}^{0.4} \tag{B.40}$$

$$Re_{sh} = D_{e_{sh}}\rho_{G_{sh}}u_{G_{sh}}/\mu_{Gsh} \tag{B.41}$$

$$Pr_{sh} = c_{pg_{sh}}\mu_{G_{sh}}/\lambda_{G_{sh}} \tag{B.42}$$

Where $\lambda_{G_{sh}}$ is the thermal conductivity of gas, $D_{e_{sh}} = D_{sh} - D_{tu}$ is the effective diameter of the shell, $\rho_{G_{sh}}$ is the density of gas, $u_{G_{sh}}$ is the velocity of gas, $\mu_{G_{sh}}$ dynamic viscosity of gas, $c_{pG_{sh}}$ is the specific heat of gas in the shell side.

<u>Radiative heat transfer coefficient h_{g-w}^{r}</u> is calculated according to Eq. (B.43) according to Vaillant (1965) [168].

$$h_{g-w}^{r} = C'e'\sigma T_{g_{sh}}^{3} \tag{B.43}$$

$$C' = \{1 + \frac{T_a}{T_{G_{sh}}} + \left(\frac{T_a}{T_{G_{sh}}}\right)^2 + \left(\frac{T_a}{T_{G_{sh}}}\right)^3\} \tag{B.44}$$

Where T_a is the ambient temperature, e' is the emissivity=1, $\sigma = 5.670310^{-8}W/m^2K^4$ is the Stefan-Boltzmann constant.

The overall heat transfer coefficient between the shell side gas and the tube side solid is expressed as Eq. (B.45).

$$h_o = \frac{1}{\frac{1}{\delta_d \frac{1}{\frac{\psi d_p}{k_g} + \left(\frac{\pi t_c}{4 k_{bs} C_{pbs} \rho_{bs}}\right)^{0.5}} + (1-\delta_d)\frac{k_{g_{tu}}}{D}\left[0.6 + \frac{0.387 Ra_{tu}^{\frac{1}{6}}}{\left\{1+\left(\frac{0.559}{Pr_{tu}}\right)^{\frac{9}{16}}\right\}^{\frac{8}{27}}}\right]^2} + \frac{1}{\frac{Nu_{sh} k_{g_{sh}}}{D_{e_{sh}}} + C' e \sigma T_{sh}^3}} \quad \textbf{(B.45)}$$

The heat transfer model $\boldsymbol{h_0}$ is written in FORTRAN programming, and linked to the RPLUG reactor module to simulate the directly and indirectly heated rotary torrefier.

B. 2. 2 Fluidized bed torrefier

Fluidized bed torrefier is simulated by using the fluidized bed module with build-in heat exchanger available in Aspen Plus. Detail mathematic models can be found in Aspen Help and Werther et al [65], [62], [64].

B.3 Grinding

Literature review of specific energy consumptions for biomass grinding using different commercial hammer mills are summarized in Table B.1. Specific energy consumptions of lab scale biomass grinding are summarized in Table B.2.

Table B.1 Specific energy consumption of biomass grinding using commercial hammer mills

Reference	Biomass	Machine	Speed (rpm)	Screen	Specific energy (kJ/kg)
[172]	hardwood	hammer mill	2500	20mm to 3mm	288
[79]	switchgrass	hammer mill	2000	5.6mm	162
	switchgrass (MC	hammer mill		5.6mm	201
[75]	poplar chips	hammer mill	3000	15mm to1.5mm	307
	pine chips (MC15%wb)				427

Reference	Biomass	Machine	Speed (rpm)	Screen	Specific energy (kJ/kg)
	pine bark				71
[76]	hardwood chips	hammer mill	3000	1.6mm	468
				3.2mm	414
[173]	switchgrass	hammer mill	2000 to	25mm to 3.2mm	114 to 156
	wheat straw		2000 to		125 to 162
	corn stover (MC10%wb)		2000 to		103 to 150
[174]	wheat straw	hammer mill	3600	7mm to 1.6mm	158
	barley straw			20mm to 1.6mm	97
	core stover (MC			12mm to 1.6mm	72
	switchgrass			7mm to 1.6mm	212

Table B.2 Specific energy consumption of grinding biomass of different properties

Reference	Biomass properties	Specific energy (kJ/kg)
[77]	wood chips 5-15mm (MC 50wt%wb)	900
	wood chips 5-15mm (MC 20wt%wb)	600
	wood chips 5-15mm (MC 15wt%wb)	450
	wood chips 5-15mm (MC 0wt%wb)	200
	Torrefied wood chips 5-15mm with 10% wl	100
	Torrefied wood chips 5-15mm with 20% wl	50
	Torrefied wood particles 1mm with 15% wl	30
[175]	torrefied biomass	90
	dry wood	1486
[22]	torrefied biomass	39
	conventional biomass	292
[76]	raw beech chips	990
	raw spruce	880
	dry spruce MC 0wt%db	504
	torrefied spruce at 300°C	90
	torrefied beech at 260°C	144
	torrefied spruce at 260°C	216
	torrefied beech at 280°C	90
	torrefied spruce at 280°C	162

Reference	Biomass properties	Specific energy (kJ/kg)
[70]	raw stem wood	792
	raw stump	576
	raw bark	144
	torrefied stem wood at 300°C 30min	52
	torrefied stump at 300°C 30min	53
	torrefied bark at 300°C 30min	45
	torrefied stem wood at 275°C 30min	200
	torrefied stump at 275°C 30min	120
	torrefied bark at 275°C 30min	60
[176]	raw woody construction demolition waste 50wt%wb	2160
	torrefied CDW (30min)	720
[177]	torrefied wood pellet	40
	raw wood pellet	100
[178]		

wl: weight loss

B.4 Pelletization

Literature review of biomass pelletization in lab and commercial scales are summarized in Table B.3.

Table B.3 Reported specific energy consumption of the biomass pelletization process

Reference	Capacity	Biomass properties	Specific energy (kJ/kg)
[179]	Lab	CWP from sawdust	132.48
		MSW	59.04
[79]	2t/hr	CWP from switchgrass	268.2
[180]		CWP from softwood	216
[174]		CWP from Alfalfa	108
[174]	Lab	CWP from wheat straw	
		CWP from barley straw	
		CWP from corn stover (MC 15wt%wb)	31
		CWP from switchgrass	
[22]	Lab	TWP from torrefied Douglas fir (without binder)	1164

Reference	Capacity	Biomass properties	Specific energy (kJ/kg)
		TWP from torrefied Douglas fir (with 7wt% wheat flour as binder)	461
		CWP from non-treated Douglas fir (15wt%wb)	757
[68]	Lab	CWP from spruce	29
		CWP from pine	27.5
		CWP from fir	31.4
		CWP from SPF	31.23
		CWP from pine bark	18.72
		TWP from spruce	30.7
		TWP from pine	31.56
		TWP from fir	34.05
		TWP from SPF	35.64
		TWP from pine bark	28.26
[24]	Lab	CWP from pine sawdust	39.1
		TWP from pine sawdust (without binder)	52.8
		TWP from pine sawdust (with 10wt% sawdust as binder)	50.7
		TWP from pine sawdust (with 20wt% sawdust as binder)	46.2
		TWP from pine sawdust (with 30wt% sawdust as binder)	42.9
[181]	Lab	CWP from lodgepole pine MC 33wt%wb	658.8
[80]	Lab	CWP from raw cedarwood sawdust 1mm	32
		TWP from cedarwood sawdust 1mm torrefied at 300°C	34
		TWP from cedarwood sawdust 1mm torrefied at 270°C	34
		TWP from cedarwood sawdust 1mm torrefied at 240°C	36
		CWP from raw camphorwood sawdust 1mm	27
		TWP from camphorwood 1mm torrefied at 300°C	41
		TWP from camphorwood 1mm torrefied at 270°C	35
		TWP from camphorrwood 1mm torrefied at 240°C	31
[182]	Pilot scale (9 kg/hr)	CWP from cornstover MC 15wt%db	360
		CWP from cornstover MC 20wt%db	684
		CWP from cornstover MC 25wt%db	1008
		CWP from miscanthus MC 15wt%db	1160
		CWP from miscanthus MC 20wt%db	900
		CWP from miscanthus MC 25wt%db	650

Reference	Capacity	Biomass properties	Specific energy (kJ/kg)
		CWP from swtichgrass MC 20wt%db	540
		CWP from miscanthus MC 25wt%db	540
		CWP from wheat straw MC 20wt%db	600
[183]	General	CWP from biomass	57-176
[81]	Lab	CWP from	28
		TWP (300°C 28%weight loss)	42
		TWP (290°C 30% weight loss)	48
		TWP (280°C 30% weight loss)	38

Appendix C Techno-economic evaluation models and assumptions

Techno-economic evaluation and investment analysis are carried out based on Aspen Economic Evaluator ICARUS. This section presents the economic evaluation assumptions and details. The total production costs consist of capital cost (CAPEX) and operating costs (OPEX).

C.1 Review of production cost categories

Process economics methods are available, including those of Peters et al. [184], Ulrich et al. [185] Smith et al. [186], and Turton et al. [187]. A general review of the total project costs is presented in Table C.1.

Table C.1 Components of chemical plant project costs

	Sub-items	Brief description	Sub-items	Sub-times	Estimation
Capital investment	Fixed capital investment	Total cost of designing, constructing, and installing a plant and the associated modifications needed to prepare the plant site	Inside battery limits (ISBL)	Direct field costs	All the major process equipment
					Bulk items, e.g. piping, valves, wiring, instruments, structures, insulation, paint, lube oil, solvents, catalysts, etc.
					Civil works such as road, foundations, piling, buildings, sewers, ditches, embankments, etc.
					Installation labor and supervision
				Indirect field costs	Construction costs
					Field expenses and services
					Construction insurance
					Labor benefits and burdens
					Miscellaneous overhead items e.g. agents' fees, legal costs, import duties etc.
			Offsite costs (OSBL)		20% to 50% of ISBL
			Engineering and construction costs		small project (30% of ISBL plus OSBL); large project (10% of ISBL plus OSBL)
			Contingency charges		10% of ISBL plus OSBL
	Working capital	Typically, 15% of fixed capital. Additional money needed, above what it cost to build the plant, to start the plant up and run it until it starts earning income	Value of raw material inventory		2 weeks' delivered cost of raw materials
			Value of product and by product inventory		2 weeks' cost of production
			Cash on hand		1 week’s cost of production
			Accounts receivable		1 month's cost of production
			Credit for accounts payable		1 month's delivered cost
			Spare parts inventory		1% to 2% of ISBL plus OSBL investment cost
Operating cost	Variable costs of production	can be reduced by more efficient design or operation of the plant	Raw material cost		
			Utilities		electricity, fuel, cooling water, steam etc.

	Sub-items	Brief description	Sub-items	Sub-times	Estimation
			Consumables		solvents, acids, bases, inert materials, corrosion inhibitors etc.
			Effluent disposal		solid, liquid, gas wastes treatment
			Packaging and shipping		drums, bags, tankers, freight charges etc.
	Fixed costs of production	Not easily influenced by better design or operation of the plant. Incurred regardless of the plant operation rate or output, if the plant cuts back its production, these costs are not reduced.	Operating labor		operating workers
			Supervision		25% of operating labor
			Direct salary overhead		40 to 60% of operating labor plus supervision
			Maintenance		3 to 5% of ISBL
			Property taxes and insurance		1 to 2% of ISBL
			Rent of land		1 to 2% of ISBL
			General plant overhead		65% of total labor plus maintenance
			Allocated environmental charges to cover superfund payments		1% of ISBL plus OSBL
			Running license fees and royalty payments		those not capitalized at the start of the project
			Capital charges		include interest payments due on any debt or loans used to finance the project
			Sales and marketing costs		some cases considered as part of general plant overhead

C.2 Capital investment costs (CAPEX)

Capital costs are one-time expenses, typically incurred at the beginning of a project. Total capital is the sum of fixed capital and working capital. Usually, to estimate total capital, one begins by determining the major equipment costs based on the capacity parameters from the equipment size. Table C.2 summarizes the methods to estimate capital costs.

Table C.2 Method to estimate capital costs

Methods	Description	
Rapid cost	Historic cost data	$C_2 = C_1\left(\frac{S_2}{S_1}\right)^n$ or $C_2 = \frac{C_1}{S_1^n} \times S_2^n = aS_2^n$
	Step count method (Bridgewater's method)	$Q \geq 60{,}000: C = 3200 \cdot N \cdot \left(\frac{Q}{s}\right)^{0.675}$ $Q < 60{,}000: C = 280{,}000 \cdot N \cdot \left(\frac{Q}{s}\right)^{0.3}$
	Manufactured products	TCOP=2*material cost
Factorial method	Long factors (1948)	$C = F(\sum C_e)$ F=3.1 for solids processing plant; F=4.74 for fluid processing plant; F=3.63 for mixed fluids-solids processing plant.
	Hand factors (1985)	$C = F(\sum C_e)$ F=2.5 for compressors; F=4 for distillation columns; F=2 for fired heaters; F=3.5 for heat exchangers; F=4 for instruments; F=2.5 for miscellaneous equipment; F=4 for pressure vessels; F=4 for pumps.
	Detailed Factorial estimates (Guthrie 1969)	$C = \sum_{i=1}^{i=M} C_{e,i,CS}[(1+f_p)f_m + (f_{er}+f_{el}+f_i+f_c+f_s+f_l)]$ or$C = \sum_{i=1}^{i=M} C_{e,i,A}[(1+f_p) + (f_{er}+f_{el}+f_i+f_c+f_s+f_l)/f_m]$
Estimating purchased equipment costs		$C_e = a + bS^n$

C_2: ISBL capital cost of the plant with capacity S_2, in $, US Gulf Coase, 2000 basis
C_1: ISBL capital cost of the plant with capacity S_1
N: typically 0.8 to 0.9 for processes that use a lot of mechanical work or gas compression; for typical petrochemical processes, n is 0.7; for small scale, high instrumented processes n is in the range of 0.4 to 0.5; average across the whole chemical industry, n=0.6
Q=plant capacity in metric tons per year;
S=reactor conversion;
N=number of functional units
$\sum C_e$=total delivered cost of all the major equipment items: reactors, tanks, columns, heat exchangers, furnaces, etc.
F= an installation factor, later widely known as a Lang factor

$C_{e,i,CS}$=purchased equipment cost of equipment I in carbon steel;
$C_{e,i,A}$=purchased equipment cost of equipment I in alloy;
M=total number of pieces of equipment;
f_p= installation factor for piping;
f_{er}=installation factor for equipment erection;
f_{el}=installation factor for electrical work;
f_i=installation factor for instrumentation and process control;
f_c=installation factor for civil engineering work;
f_s=installation factor for structures and buildings;
f_l=installation factor for lagging, insulation, or paint.
C_e= purchased equipment cost on a US gulf Coast basis, January 2006 (CE index=478.6, NF refinery inflation index=1961.6);
a, b= cost constraints
S=size parameter
N=exponent for that type of equipment

Because baseline cost data and cost-to-capacity correlations typically only apply to a specific year, one needs to adjust the resulting cost estimates to match current market conditions. A yearly cost index can be used, such as the Chemical Engineering Plant Cost Index (CEPCI) or the Marshall and Swift Equipment Cost Index, and the Eq. (C.1).

$$C_2 = C_1 \times (I_2/I_1) \quad \text{(C.1)}$$

Where C is the cost in year 1 or 2 and i is the cost index in year 1 and 2.

The ICARUS software uses a combination of mathematical models and expert systems to develop cost estimates. Costs are based on the materials and labor required rather than installation factors. Aspen In-Plant Cost Estimator includes a comprehensive bank of more than 400 models for process equipment, plant bulks, site development, buildings and other items. The design and cost models are based on international industry standard design methods and procedures (that is, ASME, API, TEMA, NEMA, JIS, BS5500). In-Plant Cost Estimator generates a mechanical design for each project component. Then the system automatically uses the design installation material quantities to calculate the capital costs. Additionally, the Manpower Productivity Expert (MPE) application, which is integrated into Aspen In-Plant Cost Estimator, uses expert knowledge to determine field manpower productivity for a construction site.

Table C.3 Capital cost categories evaluated by Aspen Economic Evaluator ICARUS expert system

Cost category	Description
Purchased Equipment	The total material cost of process equipment.
Equipment setting	The total construction labor cost for setting equipment in place.
Plant bulks	Plant bulks include piping, civil, steel, instrumentation, electrical, insulation, and paint costs categories. The cost reported for each of these items indicates the total material and construction labor cost calculated for the category.
Other	This item is the total of the following costs: design, engineering, and procurement costs; material charges (freight and taxes); and construction field indirect costs (fringe benefits, burdens, consumables/small tools, insurance, equipment rental, field services, field office construction supervision, and plant start-up).
Subcontracts	The total cost of subcontracted work.
G and A Overheads	General and administrative costs associated with engineering, materials, and construction work.
Contract Fee	The total cost of contract fees for engineering, material, construction, any subcontracted work.
Escalation	The total capital costs escalation amount.
Contingencies	The additional costs required to bring this project to completion.

C.3 Operating expenditures (OPEX)

Operating cost categories are also evaluated by Aspen Economic Evaluator expert, with assumptions as presented in Table C.4.

Table C.4 Assumptions for operating costs estimation in current study

	Cost category		Description
①	**Total Operating Cost**	$C_{\text{Total operating}}$	①=②+③+⑥+⑦+⑧+⑨
②	Raw Materials	$C_{\text{raw material}}$	$C_{\text{raw material}} = P_{\text{raw}} \cdot f_{\text{feedstock}} \cdot c_{\text{annual}}$
③	Operating Labor and Maintenance	$C_{\text{labor and maintenance}}$	$C_{\text{labor and maintenance}}$
④	Operating labor cost	C_{labor}	$C_{\text{labor}} = \sum_{i} P_{\text{labor,i}} \cdot n_{\text{labor,i}} \cdot 1.11$
⑤	Maintenance cost	$C_{\text{maintenance}}$	$C_{\text{maintenance}} = C_{\text{fixed}} \cdot (3\%\sim6\%)$
⑥	Utilities	$C_{\text{utilities}}$	$C_{\text{utilities}} = P_{\text{utility}} \cdot u_{\text{unit}} \cdot c_{\text{annual}}$
⑦	Operating Charges	$C_{\text{operating charges}}$	⑦=④*0.25
⑧	Plant Overhead	$C_{\text{plant overhead}}$	⑧=③*0.5
⑨	G and A Cost	$C_{\text{G and A}}$	⑨=⑩*0.08
⑩	**Subtotal operating cost**	$C_{\text{subtotal operating}}$	⑩=②+③+⑥+⑦+⑧

Appendix D Results of process modeling and simulation of four pathways

This file summarizes the modeling and the simulation results of the four torrefied wood pellet production pathways, those include:

(1) Flowsheet layout and components in the streams of the processes;

(2) Key parameter values of the drying, torrefaction, and the combustion processes;

(3) Performances of the simulated dryers and the torrefiers.

D.1 Modeling and simulation results of Path1

Figure D.1 shows the simplified configuration of Path 1, Table D.1 is the stream information of Path 1.

Flowsheet information

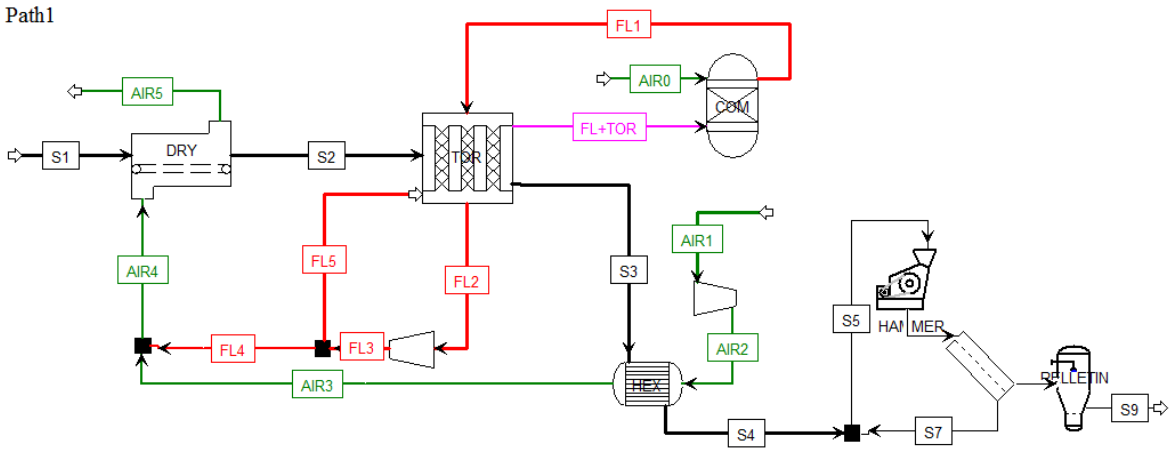

Figure D.1 Flowsheet layout of Path1

Table D.1 Stream information of Path 1

	S1	S2	S3	S4	FL1	FL2	FL3	FL4	FL5	INCOM	AIR0	AIR1	AIR2	AIR3	AIR4	AIR5
Temperature K	295	306	698.7	313.1	1272.3	817	830.2	830.2	830.2	607.4	298.1	298.1	303.9	323.2	334.1	304.9
Pressure atm	1	1	1	1	1	1	1.05	1.05	1.05	1	1	1	1.05	1.05	1	1
Mass VFrac	0	0	0	0	1	1	1	1	1	1	1	1	1	1	1	1
Mass SFrac	0.67	0.941	1	1	0	0	0	0	0	0	0	0	0	0	0	0
Mass Flow kg/hr	17160	12222	9201	9201	32465	32465	32465	21794	10671	32465	8630	406885	406885	406885	417556	422494
Volume Flow l/min	143	60	120	120	2073650	1331480	1288640	865070	423566	979190	122325	5708500	5542340	5894000	6575430	6116270
Density lb/cuft	125.05	210.7	80.05	80.05	0.016	0.025	0.026	0.026	0.026	0.034	0.073	0.074	0.076	0.072	0.066	0.072
Mass Flow kg/hr																
H_2O	5663	724			4785	4785	4785	3212	1573	4124					1573	6511
CO					0.006	0.006	0.006	0.004	0.002	84					0.002	0.002
$C_2H_4O_2$										352						
$C_5H_4O_2$										304						
CH_4O					trace	trace	trace	trace	trace	252					trace	trace
CH_2O_2					trace	trace	trace	trace	trace	136					trace	trace
CO_2					4252	4252	4252	2854	1397	2433					1397	1397
O2					1536	1536	1536	1031	505	2889	1812	117997	117997	117997	118501	118501
V0					trace	trace	trace	trace	trace						trace	trace
CH_4					21892	21892	21892	14696	7196	21892	6818	288888	288888	288888	296084	296084
Biomass dry bone	11497	11497														
CHAR			9201	9201												

Convective dryer results of Path1

Table D.2 Modeling results of convective dryer of Path 1

Variable	Meaning	Units	Value
ρ_G	Mass density of the drying gas	kg/cum	1.06
d_p	Biomass particle size	meter	0.02
μ_G	Dynamic viscosity of drying gas	kg/m-sec	4.15E-5
λ_G	Thermal conductivity of drying gas	kW/m-K	2.827E-5
$c_{p,G}$	Specific heat capacity of dry gas	kJ/kg-K	1.01
u_0	Velocity of drying gas	m/s	3.87
δ_G	diffusion coefficient of vapor in the gas	m^2/sec	2.64E-5
Dimensionless number			
Re	Reynolds number of particle	UNITLES	1977
Sc	Schimit number	UNITLES	1.39
Sh	Sherwood number	UNITLES	31.78
Pr	Prandtl number	UNITLES	1.48
Nu	Nusselt number	UNITLES	32.38
Heat and mass transfer coefficients			
k_p	Mass transfer coefficient of a single particle and surrounding gas	m/s	0.044
h_p	Heat transfer coefficient between a single particle and the gas	kJ/sec-sqm-K	0.052
Dryer specifications			
D	Diameter of the dryer	meter	6
L	Length of the dyer	meter	40
RDT[a]	Biomass mean residence time	min	120

a: RDT is a design parameter in the modeling to achieve the drying goal of the biomass; its value can be tested by $RDT = V_{drum} \cdot F_{ff}/\dot{m}_S$

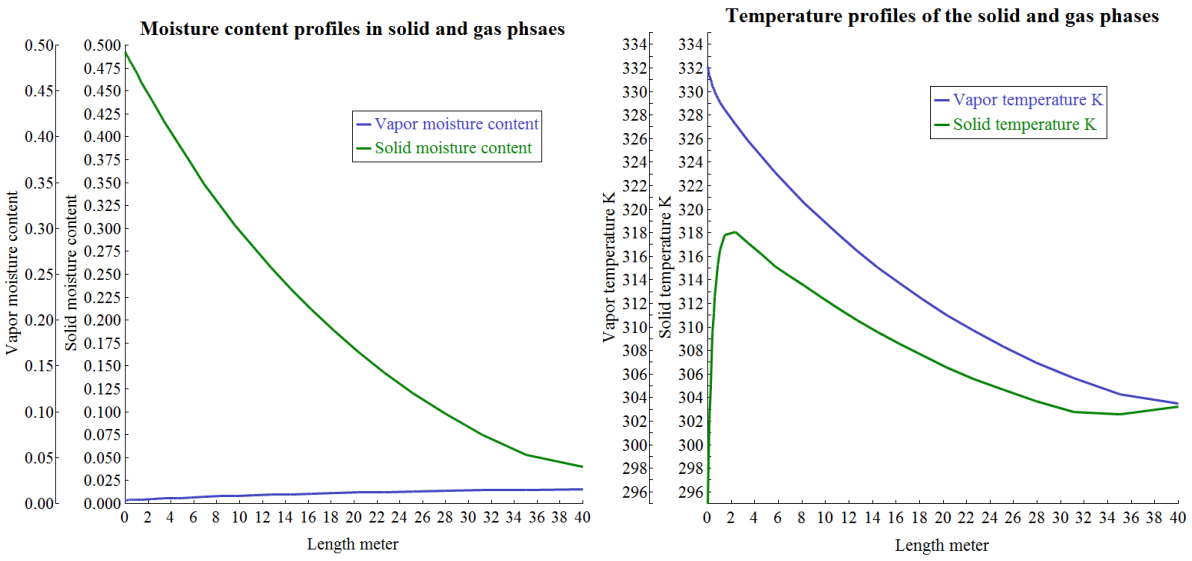

Figure D.2 (a) moisture content profiles of the biomass and the drying gas along the convective dryer; (b) temperature profiles of the biomass and the drying gas along the convective dryer

Rotary torrefier results of Path1

Table D.3 Rotary torrefier parameters of Path1

Variable	Meaning	Units	Value
h_{ex}	Overall heat transfer coefficient between the shell side gas and the tube side solid	kW/sqm-K	0.0405
h_{tu}	Overall heat transfer coefficient of the tube side of the rotary torrefier	kW/sqm-K	0.0405
h_{sh}	Overall heat transfer coefficient of the shell side of the rotary torrefier	kW/sqm-K	152.06
h_{ewb}	Average effective heat transfer coefficient from the tube wall to the bulk solid	kW/sqm-K	0.197
h_{wg}	Average heat transfer coefficient from the tube wall to the tube side gas	kW/sqm-K	0.0014
h_{ws}	Heat transfer coefficient between the wall and the first layer of the gas	kW/sqm-K	0.260
h_{sb}	Heat transfer coefficient from the bed surface to the bulk bed	kW/sqm-K	0.813
h_{sh}^{c}	Forced convection heat transfer coefficient in shell side	kW/sqm-K	0.0029
h_{g-w}^{r}	Radiation heat transfer coefficient in the shell side	kW/sqm-K	152.06
Dimensionless number			
Ra_{tu}	Rayleigh number of gas in tube side	UNITLES	1.56E+8
Pr_{tu}	Prandtl number of gas in tube side	UNITLES	0.819
Ra_{sh}	Rayleigh number in shell	UNITLES	2.2E+11
Nu_{sh}	Nusselt number in shell side	UNITLES	79.37

Variable	Meaning	Units	Value
Re_{sh}	Reynolds number of gas in shell	UNITLES	29863
Pr_{sh}	Prandtl number of gas in shell side	UNITLES	0.784
Thermal properties of biomass			
$\mu_{g_{tu}}$	dynamic/kinematic viscosity of gas in tube	m^2/s	3.27E-05
$\delta_{g_{tu}}$	thermal diffusivity of gas in tube	m^2/s	0.00025
$c_{pg_{tu}}$	Specific heat of gas in the tube	kJ/kg-K	1.30
ξ_v	volumetric expansion coefficient of gas in tube	1/K	0.002
$\rho_{g_{tu}}$	Density of gas in tube of the torrefier	kg/cum	0.436
$\lambda_{g_{tu}}$	Thermal conductivity of gas inside the tube	kW/m-K	5.2E-05
$\lambda_{g_{sh}}$	Thermal conductivity of gas in shell side	kW/m-K	9.2E-05
$\rho_{g_{sh}}$	Density of gas in shell	kg/cum	0.261
$\mu_{g_{sh}}$	Dynamic viscosity of gas in the shell	m^2/s	5.1E-05
$c_{pg_{tu}}$	Specific heat of gas in the tube	kJ/kg-K	1.407
$\lambda_{bs_{tu}}$	Thermal conductivity of bulk solids	kW/m-K	0.00035
$c_{pbs_{tu}}$	Specific heat capacity of the bulk solid in the tube	kJ/kg-K	1.5
$\rho_{bs_{tu}}$	Density of the bulk solids	kg/cum	500
d_p	Effective diameter of the particle	meter	0.02
Drum specifications			
D_{tu}	diameter of tube	meter	2.5
D_{sh}	diameter of shell	meter	5
L	length of drum	meter	47
RDT	Biomass mean residence time	min	40
$u_{g_{sh}}$	gas velocity in the shell side	m/sec	2.35
$u_{g_{tu}}$	gas velocity in the tube side	m/sec	2.80
$\dot{m_{g_{tu}}}$	Flue gases flowrate in the tube side	kg/sec	5.98
$m_{g_{sh}}$	Flue gases flowrate in the shell side	kg/sec	9.02
t_c	average solid contact time with hot surface per cascaded cycle	sec	0.51
T2	Temperature difference of the gas in the shell side and the tube wall	K	10
T1	Temperature difference of tube side gas and wall	K	10
$T_{g_{tu}}$	temperature of gas in the tube	K	1272
F_{ff}	filling fraction		0.1
Rotation speed	rpm		5
$\epsilon_{wall_{tu}}$	Thickness of wall	mm	3

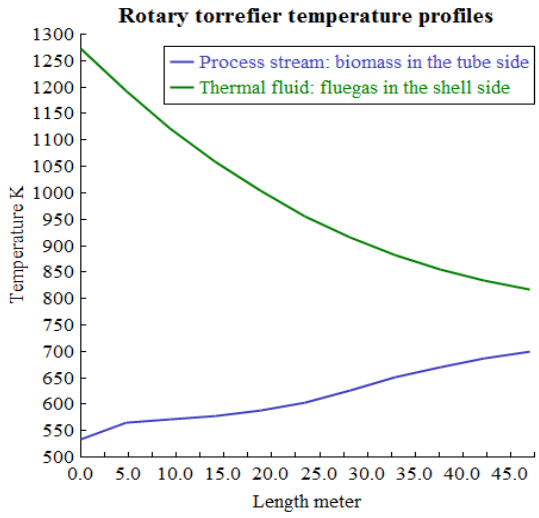

Figure D.3 Temperature profiles of biomass at the tube and flue gases at the shell side of the combined directly and indirectly heated rotary torrefier

D.2 Modeling and simulation results of Path 2

Flowsheet information of Path2

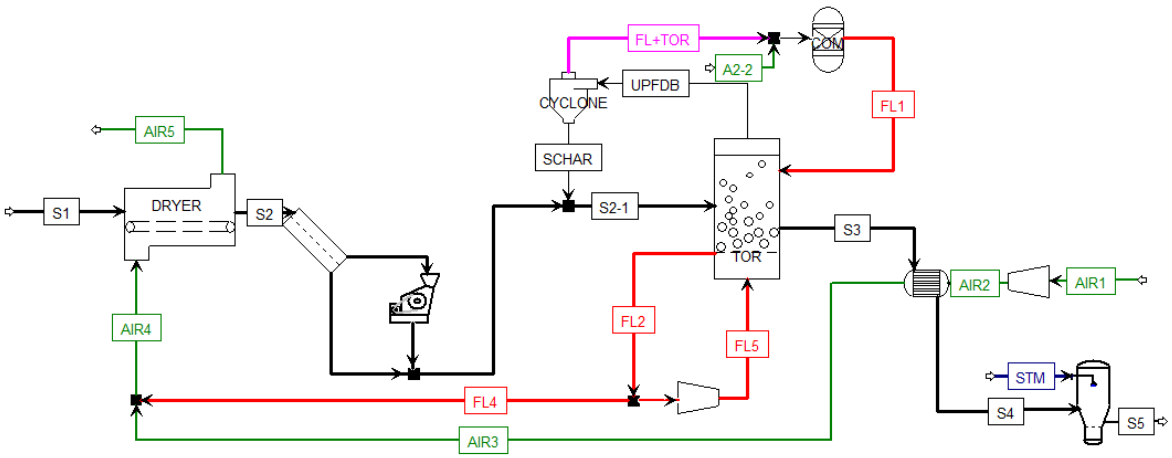

Figure D.4 Flowsheet layout of Path2

Table D.4 Stream information of Path 2

	S1	S2	S3	S4	FL1	FL2	FL4	FL5	IN-COM	AIR0	AIR1	AIR2	AIR3	AIR4	AIR5
Temperature K	295	367.4	800.3	313.1	1282.1	911.7	911.7	991.7	682	298.1	298.1	303.4	363.7	911.7	368.4
Pressure atm	1	1	1.018	1.018	1	1	1	1.3	0.923	1	1	1.05	1.05	1	1
Mass VFrac	0	0	0	0	1	1	1	1	1	1	1	1	1	1	1
Mass SFrac	0.67	0.822	1	1	0	0	0	0	0	0	0	0	0	0	0
Mass Flow kg/hr	17000	13855.26	9184	9184	41885	28078	13806	28078	41885	11506	174379	174379	174379	13806	16951
Volume Flow l/min	141.448	92.115	116.658	116.658	2615530	1246800	613052	1043260	1494320	163100	2446500	2370760	2842290	613052	335690
Density lb/cuft	125.049	156.499	81.907	81.907	0.017	0.023	0.023	0.028	0.029	0.073	0.074	0.077	0.064	0.023	0.053
Mass Flow kg/hr															
H_2O	5610	2465.258			4717.156	3162.268	1554.887	3162.268	4055.714					1554.887	4699
CO					0.002	0.001	0.001	0.001	83.964					0.001	0.001
$C_2H_4O_2$									351.859						
$C_5H_4O_2$									303.565						
CH_4O					trace	trace	trace	trace	251.821					trace	trace
CH_2O_2					trace	trace	trace	trace	136.259					trace	trace
CO_2					6365	4267	2098	4267	4546					2098	2098
O2					3226	2162	1063	2162	4579	2416	50569	50570	50570	1063	1063
V0															
CH_4					trace	trace	trace	trace						trace	trace
N_2					27577	18487	9090	18486	27577	9090	123809	123809	123809	9090	9090
Biomass drybone	11390	11390													
CHAR			9184	9184											

Convective dryer results of Path2

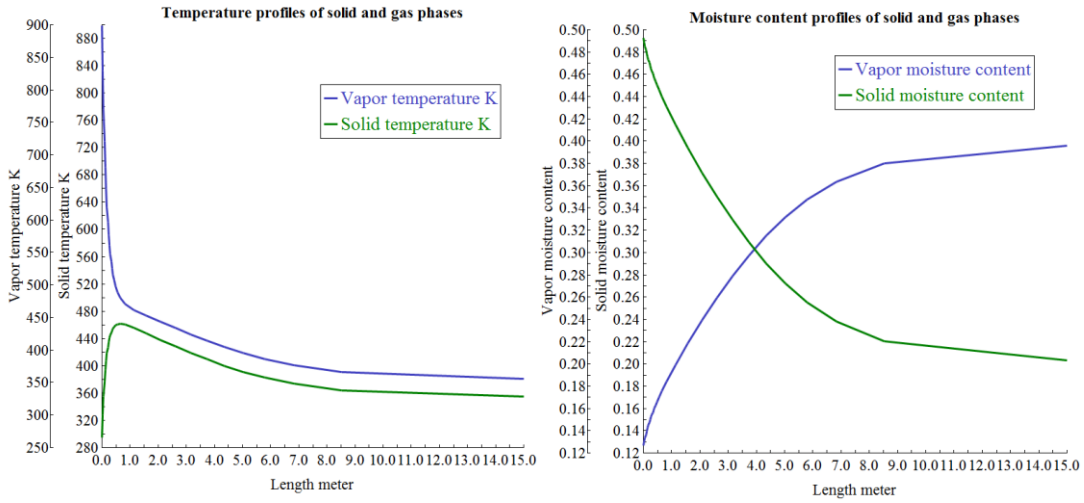

Figure D.5 (a) Biomass temperature profile and drying gas temperature profile along the length of the dryer; (b) solid biomass moisture content and the drying gas moisture content along the length of the dryer in Path 2

Table D.5 Modeling and simulation results of the dryer parameters of Path 2

Variable	Meaning	Units	Value written
ρ_G	Mass density of the drying gas	kg/cum	0.38
d_p	Biomass particle size	meter	0.02
μ_G	Dynamic viscosity of drying gas	kg/m-sec	4.15E-5
λ_G	Thermal conductivity of drying gas	kW/m-K	6.6E-5
$c_{p,G}$	Specific heat capacity of dry gas	kJ/kg-K	1.27
u_0	Velocity of drying gas	m/s	1.42
δ_G	diffusion coefficient of vapor in the gas	m^2/sec	2.82E-5
Dimensionless number			
Re	Reynolds number	UNITLES	261
Sc	Schimit number	UNITLES	3.86
Sh	Sherwood number	UNITLES	17.23
Pr	Prandtl number	UNITLES	0.80
Nu	Nusselt number	kJ/sec-sqm-K	11.00
Heat and Mass transfer coefficients			
k_p	Mass transfer coefficient of a single particle and surrounding gas	m/s	0.024

Variable	Meaning	Units	Value written
h_p	Heat transfer coefficient between surface of the particle and the gas	kJ/sec-sqm-K	0.036
D	Diameter of the dryer	meter	4
L	Length of the dyer	meter	15
RDT	Biomass residence time	min	25

Fluidized bed torrefier results of Path2

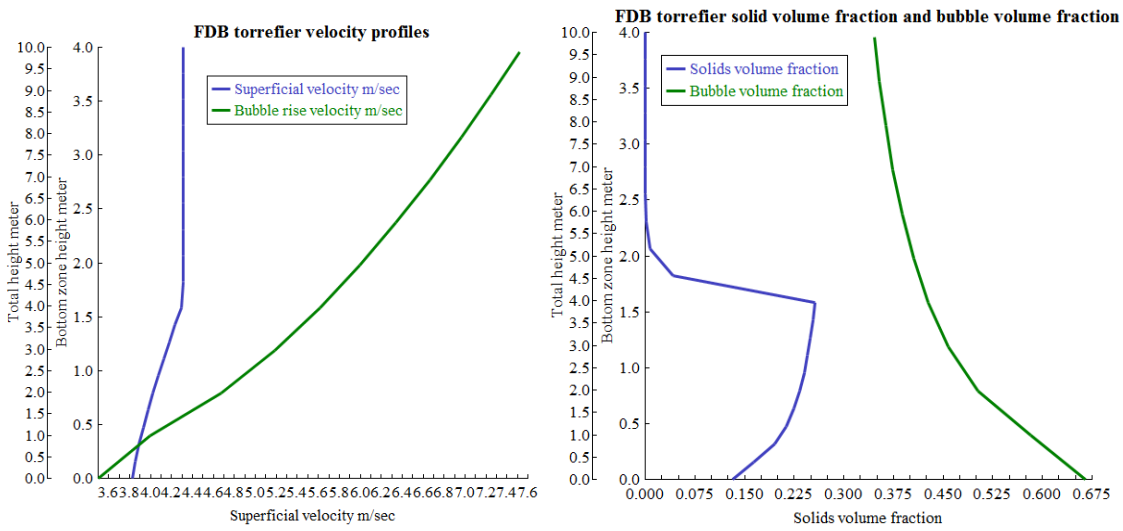

Figure D.6 (a) fluidized bed torrefier velocity profiles; (b) solid volume fraction and bubble volume fraction profiles in the fluidized bed torrefier of Path2

Table D.6 Simulation results of the fluidzied bed torrefier parameters of Path 2

Parameter	Unit	Value
Height of bottom zone	meter	3.96
Height of freeboard	meter	6.04
TDH based on solids volume fraction profile	meter	3.62
Solids holdup	kg	6000
RDT	min	35
Number of particles in bed		1.18E+09
Surface area	sqm	14071

Parameter	Unit	Value
Distributor pressure drop	atm	0.2563
Bottom zone pressure drop	atm	0.1146
Freeboard pressure drop	atm	0.00406
Fluidized bed pressure drop	atm	0.1187
Overall pressure drop	atm	0.375
Minimum fluidziation velocity	m/sec	0.3506

D.3 Modeling and simulation results of Path 3

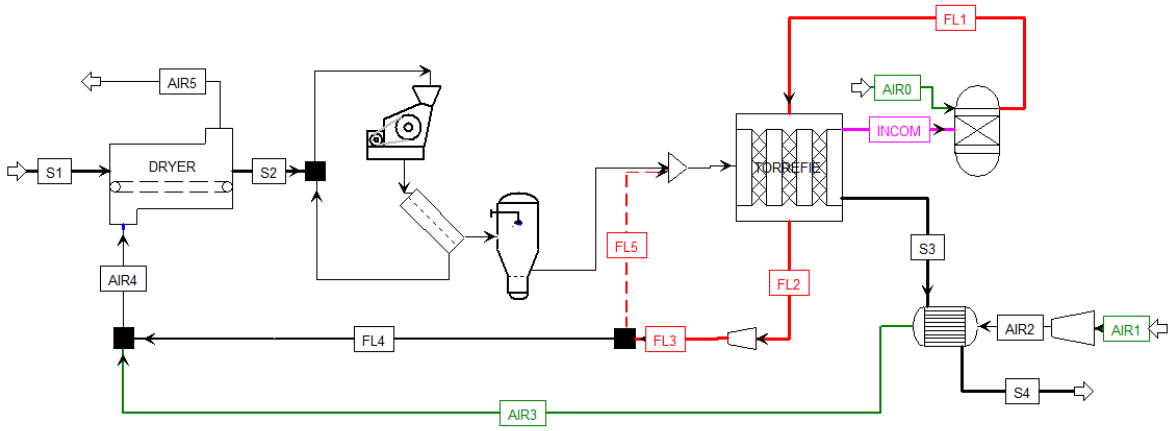

Figure D.7 Flowsheet layout and streams of Path 3

Table D.7 Stream information of Path 3

	S1	S2	S3	S4	FL1	FL2	FL3	FL4	FL5	INCOM	AIR0	AIR1	AIR2	AIR3	AIR4	AIR5
Temperature K	295	324.8	598.1	313.1	1224.5	915.8	930.3	930.3	930.3	595.4	298.1	298.1	303.9	321	336.9	300.8
Pressure atm	1	1	1	1	1	1	1.05	1.05	1.05	1	1	1	1.05	1.05	1	1
Mass VFrac	0	0	0	0	1	1	1	1	1	1	1	1	1	1	1	1
Mass SFrac	0.67	0.932	1	1	0	0	0	0	0	0	0	0	0	0	0	0
Mass Flow kg/hr	18650	13414	10034	10034	35323	35323	35323	10837	24486	26693	8630	348758	348758	348758	359595	364832
Volume Flow l/min	155	68	130	130	2174220	1626090	1573140	482638	1090500	801565	122325	4893000	4750580	5016560	5713040	5220560
Density lb/cuft	125.049	204.923	80.018	80.018	0.017	0.023	0.023	0.023	0.023	0.035	0.073	0.074	0.076	0.072	0.065	0.073
Mass Flow kg/hr																
H_2O	6155	918			5301	5301	5301	1626	3675	4592					1626	6863
CO					0.002	0.002	0.002	0.001	0.001	90					0.001	0.001
$C_2H_4O_2$										377						
$C_5H_4O_2$										326						
CH_4O					trace	trace	trace	trace	trace	270					trace	trace
CH_2O_2					trace	trace	trace	trace	trace	146					trace	trace
CO_2					4672	4672	4672	1433	3239	2722					1433	1433
O2					1573	1573	1573	483	1090	1211	1812	101140	101140	101140	101622	101622
V0																
CH_4																
N_2					23776	23776	23776	7295	16482	16959	6818	247618	247618	247618	254913	254913
Biomass drybone	12496	12496														
DRYBIOMA			168	168												
CHAR			9865	9865												

Convective dryer of Path3

Table D.8 Modeling results of convective dryer of Path 3

Variable	Meaning	Units	Value
ρ_G	Mass density of the drying gas	kg/cum	1.034
d_p	Biomass particle size	meter	0.02
μ_G	Dynamic viscosity of drying gas	kg/m-sec	4.15E-5
λ_G	Thermal conductivity of drying gas	kW/m-K	2.87E-5
$c_{p,G}$	Specific heat capacity of dry gas	kJ/kg-K	1.01
u_0	Velocity of drying gas	m/s	6.4
δ_G	diffusion coefficient of vapor in the gas	m^2/sec	2.74E-5
Dimensionless number			
Re	Reynolds number	UNITLES	3200
Sc	Schimit number	UNITLES	1.46
Sh	Sherwood number	UNITLES	40.5
Pr	Prandtl number	UNITLES	0.72
Nu	Nusselt number	UNITLES	32.5
Heat and mass transfer coefficients			
k_p	Mass transfer coefficient of a single particle and surrounding gas	m/s	0.055
h_p	Heat transfer coefficient between surface of the particle and the gas	kJ/sec-sqm-K	0.047
Dryer specifications			
D	Diameter of the dryer	meter	4
L	Length of the dyer	meter	60
RDT	Biomass residence time	min	85

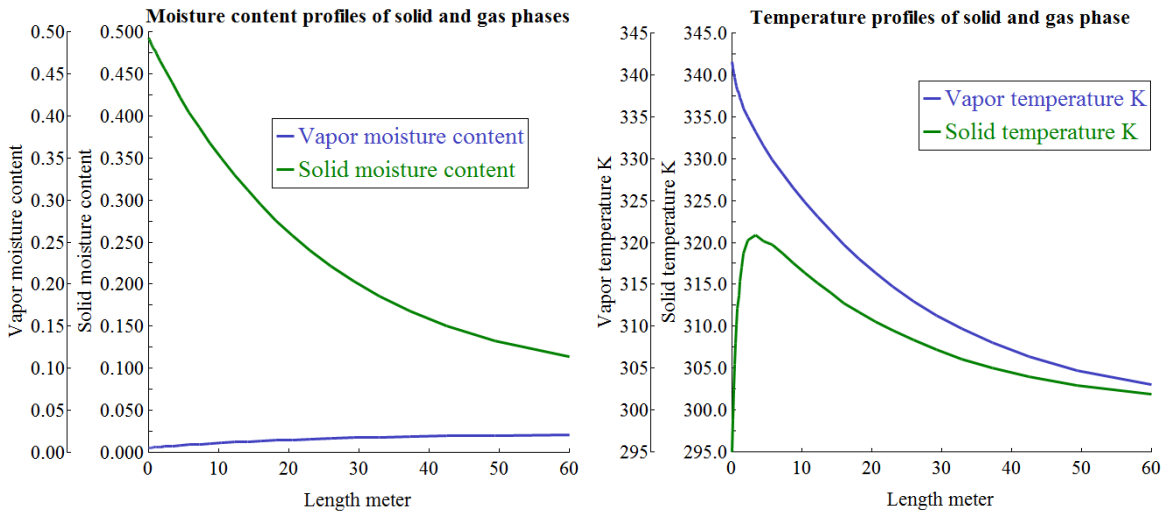

Figure D.8 (a) moisture content profiles of the biomass and the drying gas along the convective dryer; (b) temperature profiles of the biomass fluid and the drying gas fluid along the convective dryer

Rotary torrefier of Path3

Table D.9 Simulation results of the combined directly and indirectly heated rotary torrefier of Path 3

Variable	Meaning	Units	Value
h_0	Overall heat transfer coefficient between the shell side gas and the tube side solid	kW/sqm-K	0.0196
h_{tu}	Overall heat transfer coefficient of the tube side of the rotary torrefier	kW/sqm-K	0.0196
h_{sh}	Overall heat transfer coefficient of the shell side of the rotary torrefier	kW/sqm-K	124.43
h_{ewb}	Average effective heat transfer coefficient from the tube wall to the bulk solid	kW/sqm-K	0.093
h_{wg}	Average heat transfer coefficient from the tube wall to the tube side gas	kW/sqm-K	1.34E-3
h_{ws}	Heat transfer coefficient between the wall and the first layer of the gas	kW/sqm-K	0.107
h_{sb}	Heat transfer coefficient from the bed surface to the bulk bed	kW/sqm-K	0.680
h_{sh}^{c}	Forced convection heat transfer coefficient in shell side	kW/sqm-K	3.1E-3
h_{g-w}^{r}	Radiation heat transfer coefficient in the shell side	kW/sqm-K	124
Dimensionless number			
Ra_{tu}	Rayleigh number of gas in tube side	UNITLES	2.56E+8
Pr_{tu}	Prandtl number of gas in tube side	UNITLES	0.82
Ra_{sh}	Rayleigh number in shell	UNITLES	3.60E+11
Nu_{sh}	Nusselt number in shell side	UNITLES	88

Variable	Meaning	Units	Value
Re_{sh}	Reynolds number of gas in shell	UNITLES	34100
Pr_{sh}	Prandtl number of gas in shell side	UNITLES	0.784
Thermal properties of biomass			
$\mu_{g_{tu}}$	dynamic/kinematic viscosity of gas in tube	m^2/s	2.89E-05
$\delta_{g_{tu}}$	thermal diffusivity of gas in tube	m^2/s	2.89E-05
$c_{pg_{tu}}$	Specific heat of gas in the tube	kJ/kg-K	1.262
ξ_v	volumetric expansion coefficient of gas in tube	1/K	0.002
$\rho_{g_{tu}}$	Density of gas in tube of the torrefier	kg/cum	0.4356
$\lambda_{g_{tu}}$	Thermal conductivity of gas inside the tube	kW/m-K	4.45E-05
$\lambda_{g_{sh}}$	Thermal conductivity of gas in shell side	kW/m-K	8.91E-05
$\rho_{g_{sh}}$	Density of gas in shell	kg/cum	0.280
$\mu_{g_{sh}}$	Dynamic viscosity of gas in the shell	m^2/s	4.86E-05
$c_{pg_{tu}}$	Specific heat of gas in the tube	kJ/kg-K	1.387
c_{pbs}	Specific heat capacity of bulk solids		1.5
$\lambda_{bs_{tu}}$	Thermal conductivity of bulk solids	kW/m-K	3.5E-4
$\rho_{bs_{tu}}$	Density of the bulk solids	kg/cum	350
d_p	Effective diameter of the wood pellet	meter	0.04
Drum specifications			
D_{tu}	diameter of tube	meter	2.5
D_{sh}	diameter of shell	meter	5
L	length of drum	meter	52
RDT	Biomass mean residence time	min	44
$u_{g_{sh}}$	gas velocity in the shell side	m/sec	2.365
$u_{g_{tu}}$	gas velocity in the tube side	m/sec	3.15
$\dot{m_{g_{tu}}}$	Flue gases flowrate in the tube side	kg/sec	9.81
$m_{g_{sh}}$	Flue gases flowrate in the shell side	kg/sec	6.73
t_c	average solid contact time with hot surface per cascaded cycle	sec	0.506
T2	Temperature difference of the gas in the shell side and the tube wall	K	10
T1	Temperature difference of tube side gas and wall	K	10
$T_{g_{tu}}$	temperature of gas in the tube	K	
F_{ff}	filling fraction		0.1
rpm	Rotation speed		5
$\epsilon_{wall_{tu}}$	Thickness of wall	mm	3

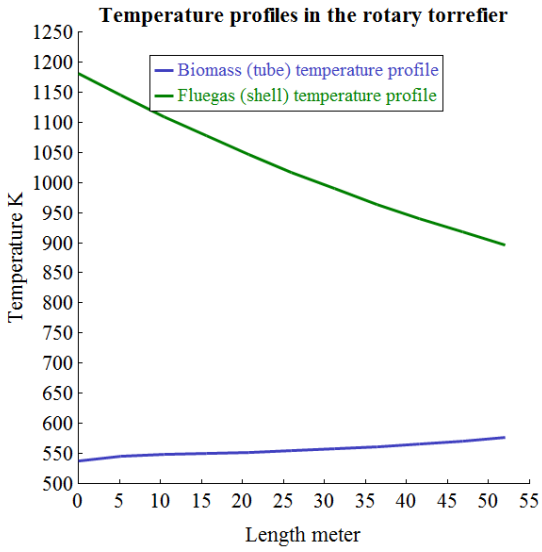

Figure D.9 Temperature profiles of the solid biomass in the rotary torrefier of Path3

D.4 Modeling and simulation results of Path 4

Flowsheet information of Path4

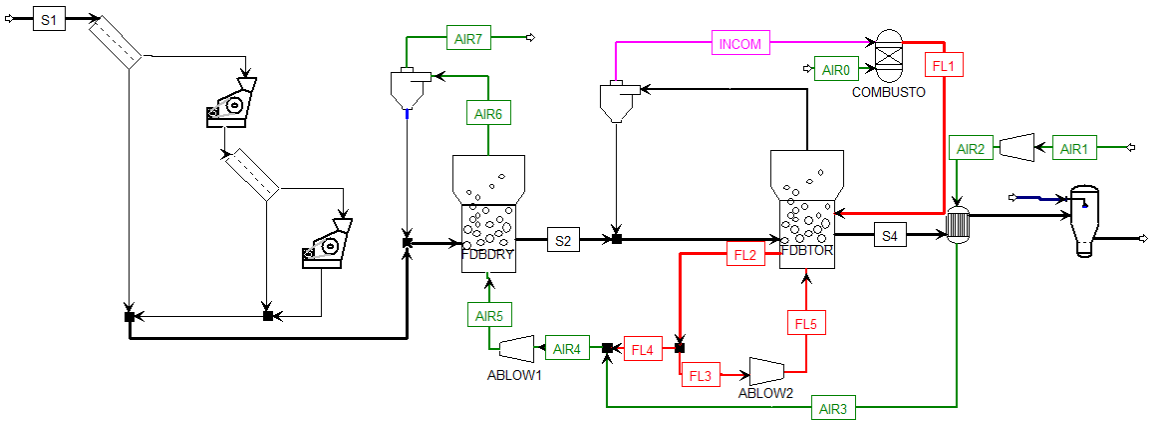

Figure D.10 Flowsheet layout of Path 4

Table D.10 Stream information of Path 4

	S1	S2	S3	S4	IN-COM	FL1	FL2	FL3	FL4	FL5	AIR1	A2-2	AIR4	AIR6
Temperature K	295	339	585	308	574	1208	942	942	942	593	298	518	518	683
Pressure atm	1	1	0.885	0.885	0.884	1	1	1	1	1.1	1	1	1	1
Mass VFrac	0	0	0	0	1	1	1	1	1	1	1	1	1	1
Mass Sfrac	0.67	0.804	1	1	0	0	0	0	0	0	0	0	0	0
Mass Flow kg/hr	18500	15409	8000	8000	34731	34731	34731	27139	7592	26919	20344	5813	14531	22123
Volume Flow l/min	154	105	102	102	1126450	2114910	1649120	1288640	360482	737019	285425	141651	354129	728475
Density lb/cuft	125	153	82	82	0.032	0.017	0.022	0.022	0.022	0.038	0.074	0.043	0.043	0.032
Mass Flow kg/hr														
H_2O	6105	1100			4814.702	5389.868	5389.868	4211.693	1178.175	4037.792				1178.17
CO					73.011	< 0.001	< 0.001	< 0.001	< 0.001					< 0.001
$C_2H_4O_2$					305.964									
$C_5H_4O_2$					263.969									
CH_4O					218.974	trace	trace	trace	trace					trace
CH_2O_2					118.486	trace	trace	trace	trace					trace
CO_2					2934.533	4516.286	4516.286	3529.067	987.218	2691.861				987
O2					3031.596	1855.082	1855.082	1449.579	405.504	1345.931	5899	1686	4214	4620
V0														
CH_4						trace	trace	trace	trace					trace
N_2					22970	22970	22970	17949	5021	18843	14444	4127	10317	15338
Biomass drybone CHAR	12395	12395	9200	9200										

Fluidized bed dryer results of Path4

Table D.11 Simulation results of the fluidized bed dryer parameters of Path 4

Variable	Meaning	Units	Value
D_{AB}	Diffusivity of moisture	m^2/s	5.36E-5
ρ_G	Mass density of the drying gas	kg/cum	0.693
d_p	Biomass particle size	meter	0.001
μ_G	Dynamic viscosity of drying gas	kg/m-sec	2.70E-5
λ_G	Thermal conductivity of drying gas	kW/m-K	3.92E-5
$c_{p,G}$	Specific heat capacity of dry gas	kJ/kg-K	1.06
δ_G	diffusion coefficient of gas	m^2/sec	5.36E-5
u_g	Average gas velocity	m/s	2.72
Dimensionless number			
Re_p	Reynolds number of particle	UNITLES	69.8
Sh	Sherwood number	UNITLES	10.7
Pr	Prandtl number	UNITLES	0.2
Nu	Nusselt number	UNITLES	7.5
Bed heat and mass transfer coefficients			
k_{bed}	Average bed mass transfer coefficient of fluidized bed dryer	m/s	0.573
h_{bed}	Average heat transfer coefficient of fluidized bed dryer	kJ/sec-m2-k	0.296
RDT	Particle mean residence time	min	30

Table D.12 Simulation results of the fluidized bed dryer parameters of Path 4

Parameter	Unit	Value
Height of bottom zone	meter	1.55
Height of freeboard	meter	11.8
Distributor pressure drop	atm	0.807
Bottom zone pressure drop	atm	0.04
Freeboard pressure drop	atm	0.001
Fluidized bed pressure drop	atm	0.04
Overall pressure drop	atm	0.80
Minimum fluidization velocity	m/sec	0.457

Fluidized bed torrefier results of Path4

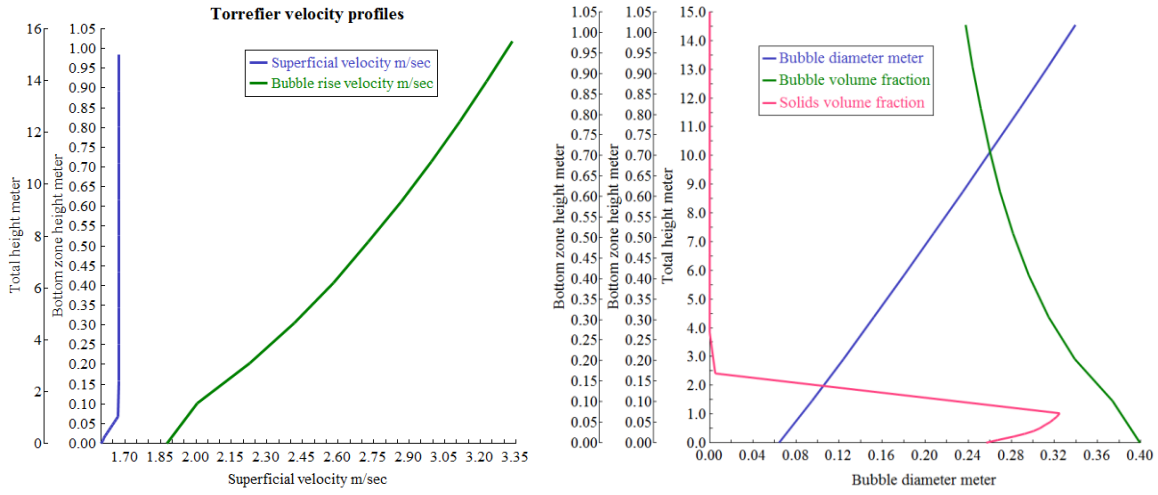

Figure D.11 (a) superficial velocity and bubble rise velocity profiles of the fluidized bed torrefier; (b) biomass solid volume fraction and bubble volume fraction profiles of the fluidized bed torrefier

Table D.13 Simulation results of the fluidized bed torrefier parameters of Path 4

Parameters	Unit	Value
Height of bottom zone	meter	1.02
Height of freeboard	meter	13.98
TDH based on solids volume fraction profile	meter	4.2
Solid holdup	kg	6000
RDT	min	30
Number of particles in bed		7.85E+08
Surface area	sqm	9380
Distributor pressure drop	atm	0.175
Bottom zone pressure drop	atm	0.04
Freeboard pressure drop	atm	0.0016
Fluidized bed pressure drop	atm	0.041
Overall pressure drop	atm	0.216
Minimum fluidization velocity	m/sec	0.48

D.5 Summary of equipment sizes and purchasing costs

Table D.14 summarizes the simulated equipment sizes and the associated heat and power consumption from Aspen Plus, as well as the modules in Aspen Process Economic Analyzer ICARUS 8.4. Major differences exist among different dryers and different torrefiers. The fluidized bed dryer and torrefier are significantly smaller in size than the rotary drum dryer and torrefier, as a result of higher heat and mass transfer efficiency in fluidized beds. Equipment selection (with power specification) for the power consuming units is performed, e.g. the air blower is selected based on the amount of air needed, which is correlated to the drying performance (heat/mass transfer coefficients), the drying goal, and the cross area of the drum; the number of the hammer mills and the pelleting machines are selected based on the electricity demand as discussed in section 3.1.3 and 3.1.4.

Table D.14 Estimated equipment sizes and energy/power consumptions for major equipment

Equipment	Equipment Capacity	Aspen ICARUS module	Specifications	Path 0	Path 1	Path 2	Path 3	Path 4
Dryer	15-18t/hr	Rotary Dryers - Direct Contact Rotary Dryer; Fluidized bed drum - Single Diameter Towers	Size (D×L) (m)	4×30	6×40	4×15	4×60	2.5×10
			Driven Power (KW)	10 [188], [189]	10 [188], [189]	10 [188], [189]	20 [188], [189]	0
			Estimated Cost ($/Equipment set)	1,298,000	1,298,000	916,800	1,709,100	85,100
			Industrial Cost ($/Equipment set)	Rotary 2.5m×40m (max) 80,882-1,485,290 $/set [190] FDB 18,000$/set (0.4t/hr) [191]				
			Estimated Weight (t/Equipment)	100	100	90	150	50
			Industrial Reference Weight (t/Equipment)	50-200 [190], [192], [193]				
			Material	Carbon steel				
Torrefier	10-12t/hr	Rotary Torrefier - Indirect Contact Rotary Drum. Fluidized bed drum- Single Diameter Towers	(Rotary Dsh×Dtu×L) / (FDB D×L) (m)	Na	5×2.5×47	2.5×10	5×2.5×52	2.5×10
			Driven Power (KW)	Na	15 [188], [189]	Na	20 [188], [189]	0
			Estimated Cost ($/Equipment set)	Na	1,449,400	86,000	1,671,000	86,000
			Industrial Cost ($/Equipment)	10,000-1,000,000 $/set [192], 2.5m×40m (max) 80,882-1,485,290 $/set [190]				
			Estimated Weight (t/Equipment)	Na	120	50	120	50
			Industrial Reference Weight (t/Equipment)	50-200 [190], [192], [193]				
			Material	Carbon steel				
Combustor/Burner	3-6MW	Furnaces, Process Heaters - Box	(MW)	3.5	3.705	3.704	3.972	3.704
			Estimated Cost ($/Equipment set)	571,300	543,700	403,300	561,800	403,300
			Industrial Cost ($/Equipment)	30,000-632,000 $/set [192], [194]				
			Estimated Weight (t/Equipment)	5.91	5.91	5.91	6.2	5.91
			Industrial Reference Weight (t/Equipment)	1-6t [194]				
			Material	A 214 Welded carbon steel				
Heat Exchanger	30-50sqm	Conveyors - Closed Belt	Size (sqm)	30	30	30	30	30
			Material	A53	A53	A53	A53	A53
			Estimated Cost ($/Equipment set)	73,800	73,800	73,800	73,800	73,800
			Industrial Cost ($/Equipment)	Enclosed scraper chain conveyer 3,676-24,705 $/set [195]				
Air Blower-Dryer	20-30 cum/sec	Fans, Blowers - Centrifugal fan	Air volume (cum/hr)	342000	342000	146790	293580	77861
			Driven Power (KW)	320	320	250	280	75

Equipment	Equipment Capacity	Aspen ICARUS module	Specifications	Path 0	Path 1	Path 2	Path 3	Path 4
			Number	2	2	1	2	4
			Estimated Cost ($/Equipment set)	269,000	215,600	73,900	188,200	26,300
			Industrial Cost ($/Equipment set)	3600$/set [196]				
			Estimated Weight ($/Equipment set)	2.4	2.4	2.4	2.2	1.0
			Industrial Reference Weight (t/set)	1 [196]				
			Material	Carbon steel				
Air Blower-Torrefier	20-30 cum/sec	Fans, Blowers-Centrifugal fan	Air volume (cum/hr)	0	79200	68089	97565	79200
			Driven Power (KW)	300	150	75	100	75
			Number	0	1.0	1.0	1.0	1.0
			Estimated Cost ($/Equipment set)	NA	39,000	23,900	33,200	25,200
			Industrial Cost ($/Equipment set)	3600$/set [196]				
			Estimated Weight (t/set)	NA	1.2	1.2	1.2	1.2
			Industrial Reference Weight (t/set)	1 [196]				
			Material	Carbon steel				
Hammer mill	10-15t/hr	Crushers - Hammer Med -Non-reversible hammer mill	Electricity consumption (KW)	1210	121	1568	1880	4071
			Driven Power (KW)	400 [110], [109]	120 [110], [109]	400 [110], [109]	380 [110], [109]	400[110], [109]
			Number	3	1	4	5	10
			Estimated Cost ($/Equipment set)	285,900	381,200	381,200	491,500	983,000
			Industrial Cost ($/Equipment set)	10,000-66,441$/sets [197]				
			Estimated Weight (t/set)	2.2	2.2	2.2	2.2	2.2
			Industrial Reference Weight (t/set)	4.2 t[197]				
			Material	Carbon steel				
Pelleting	10t/hr	Customer put-in cost value (cost reference)	Electricity consumption (KW)	745	870	870	1180.825	870
			Driven Power (KW)	370 [110], [109]	290[110], [109]	290[110], [109]	400 [110], [109]	290 [110], [109]
			Number	2.0	3.0	3.0	3.0	3.0
			Estimated Cost ($/Equipment set)	200,000	300,000	300,000	300,000	300,000
			Industrial Cost ($/Equipment set)	20,000-28,000$/set (1-2t/hr) [198]				
			Estimated Weight (t/set)	3.1	3.1	3.1	3.1	3.1

Equipment	Equipment Capacity	Aspen ICARUS module	Specifications	Path 0	Path 1	Path 2	Path 3	Path 4
			Industrial Reference Weight (t/set)	3-3.7 t [5], 5.5 t [198]				
Conveyer		Conveyors - Open Belt	Size (L×W) (m)	20×3	20×3	20×3	20×3	20×3
			Driven Power (KW)	7.5 [199], [200]	7.5 [199], [200]	7.5 [199], [200]	7.5 [199], [200]	7.5 [199], [200]
			Estimated Cost ($/Equipment set)	61,700	61,700	61,700	61,700	61,700
			Industrial Cost ($/Equipment set)	Depend on size				
			Estimated Weight (t/set)	3.0	3.0	3.0	3.0	3.0
			Industrial Reference Weight (t/set)	Depend on size				
			Material	Rubber				

As shown in Figure D.12 (a), Path 2 and Path 4 have relatively lower equipment purchasing costs because of the use of fluidized bed reactors of smaller sizes than rotary drum reactors, but Path 4 has the highest costs for hammer mills. For Path 1 and Path 3, the biggest cost items are the rotary torrefier and the rotary torrefier. According to Table 4.6, total equipment purchasing costs only account for 1.4% to 3.6% of the total production costs as shown in Figure D.12 (b).

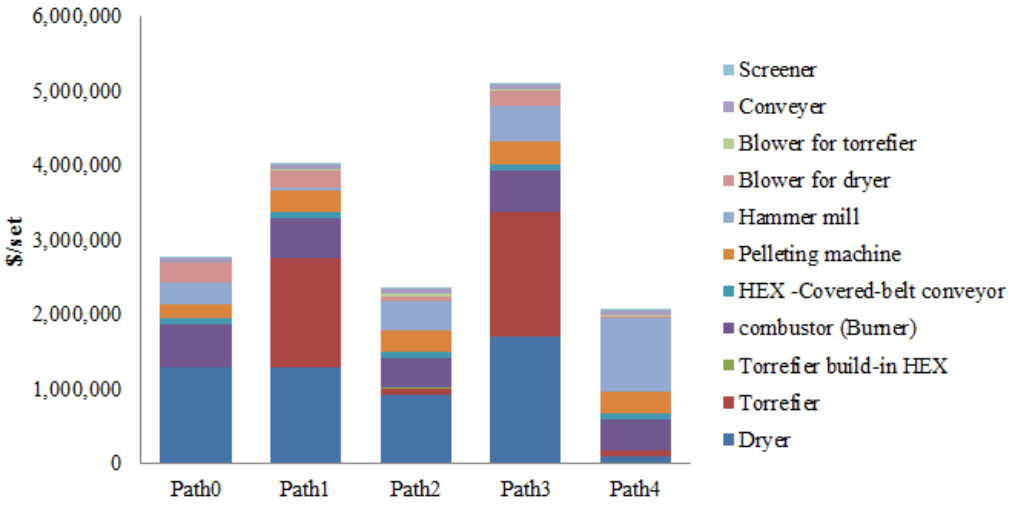

(a)

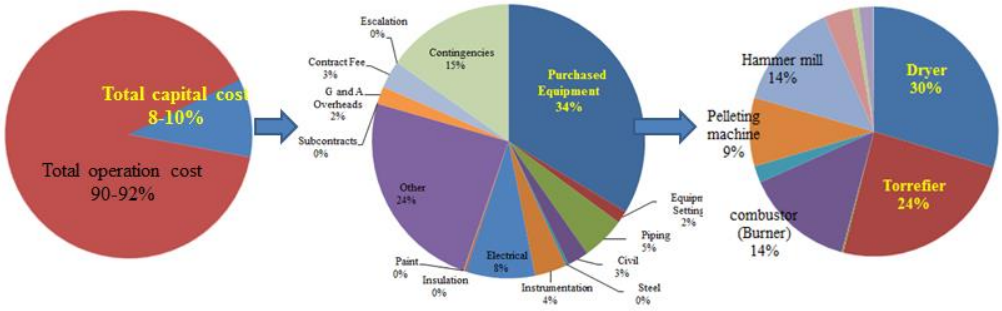

(b)

Figure D.12 (a) Equipment purchasing costs of five wood pellet production pathways; (b) share of equipment costs to total production costs

Appendix E Investment analysis

This file contains the figures of the project investment analysis, taking Path 1 as an example. Table E.1 shows the assumptions and calculated investment parameters of Path 1.Table E.2 is the cash flow information of the investment based on Path 1 (case 1: raw material cost 25$/t; product sale price 140 $/t).

Table E.1 Assumptions of a TWP plant project cash flow analysis (Path 1 as an example)

ITEM	UNITS	
Number of Weeks per Period	Weeks/period	52
Number of Periods for Analysis	Period	20
Duration of EPC Phase	Period	0.69
Duration of EPC Phase and Startup	Period	1.08
Working Capital Percentage	Percent/period	5
Operating Charges (OPCHG)	Percent/period	25
Plant Overhead (PLANTOVH)	Percent/period	50
Raw material cost	$/t	25
Torrefied wood pellet sale price	$/t	140
Total Project Cost (CAPT)	Cost	12,250,590.41
Total Raw Material Cost (RAWT)	Cost/period	2,288,000.00
Total Product Sales (PRODT)	Cost/period	10,400,000.00
Total Operating Labor and Maintenance Cost (OPMT)	Cost/period	1,046,000.00
Total Utilities Cost (UTILT)	Cost/period	972,139.20
Desired Rate of Return/Interest Rate (ROR)	Percent/period	10
ROR Annuity Factor (AF)		10
Tax Rate (TAXR)	Percent/period	27
ROR Interest Factor (IF)		1.1
Economic Life of Project	Period	20
Salvage Value (Percent of Initial Capital Cost)	Percent	20
Depreciation Method		Straight Line
Project Capital Escalation	Percent/period	5
Products Escalation	Percent/period	5
Raw Material Escalation	Percent/period	3.5

ITEM	UNITS	
Operating and Maintenance Labor Escalation	Percent/period	3
Utilities Escalation	Percent/period	3
Start Period for Plant Startup	Period	1
Desired Return on Project for Sales Forecasting	Percent/Period	10.5
End Period for Economic Life of Project	Period	20
G and A Expenses	Percent/Period	8
Duration of EP Phase before Start of Construction	Period	0.46

Influences of capital depreciation method to the project profitability index are shown in Figure E.1. As can be seen, that depreciation method has minor influence to the project profitability.

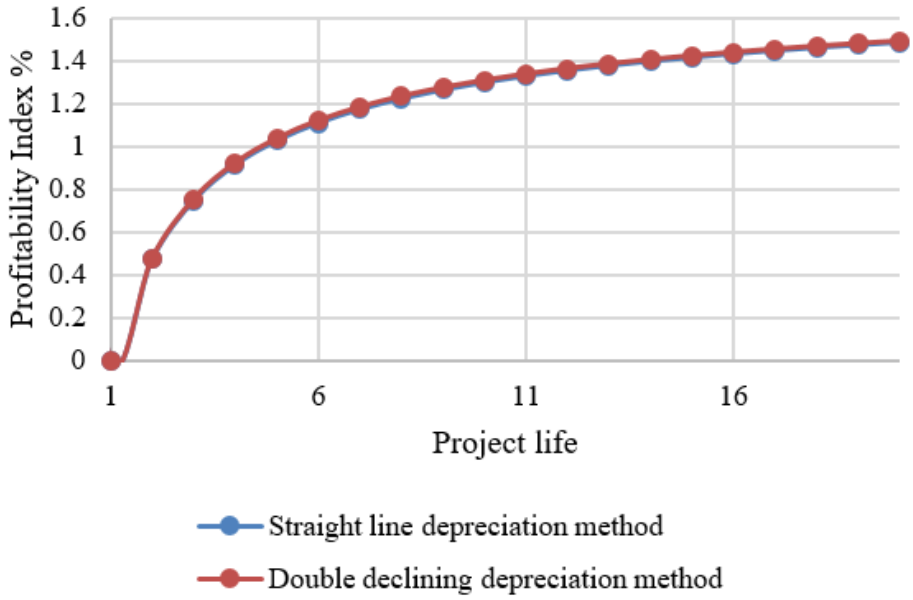

Figure E.1 Depreciation method influences to the project profitability index

Table E.2 Cash flow of a TWP production project (Based on Path 1 when wood pellet selling price is 140$/t) (continued)

CASHFLOW.ICS (Cashflow)	Year	0	1	2	3	4	5	6	7	8	9	10
Sales												
S (Total Sales)	$/year	0	0	11398154	12965400	13613670	14294354	15009071	15759525	16547501	17374876	18243620
Expenses												
CAP (Capital Costs)	$/year	0	13506276									
Unescalated Cumulative Capital Cost	$/year	0	12250590	12250590	12250590	12250590	12250590	12250590	12250590	12250590	12250590	12250590
Capital Cost	$/year	0	12863120									
Cumulative Capital Cost	$/year	0	12863120	12863120	12863120	12863120	12863120	12863120	12863120	12863120	12863120	12863120
Working Capital	$/year		643156									
OP (Operating Costs)	$/year	0	1735428	5822134	6010033	6204032	6404331	6611135	6824657	7045116	7272739	7507760
Raw Materials	$/year	0	728640	2450963	2536747	2625533	2717426	2812536	2910975	3012859	3118309	3227450
Operating Labor Cost	$/year	0	291569	976028	1005309	1035468	1066532	1098528	1131484	1165428	1200391	1236403
Maintenance Cost	$/year	0	39932	133673	137684	141814	146069	150451	154964	159613	164401	169333
Utilities	$/year	0	308093	1031342	1062283	1094151	1126976	1160785	1195609	1231477	1268421	1306474
Operating Charges	$/year	0	72892	244007	251327	258867	266633	274632	282871	291357	300098	309101
Plant Overhead	$/year	0	165751	554851	571496	588641	606300	624489	643224	662521	682396	702868
Subtotal Operating Costs	$/year	0	1606878	5390864	5564845	5744474	5929936	6121421	6319127	6523255	6734017	6951629
G and A Costs	$/year	0	128550	431269	445188	459558	474395	489714	505530	521860	538721	556130
R Revenue)	$/year	0	-15241704	5576020	6955367	7409638	7890023	8397936	8934868	9502385	10102137	10735860
DEP (Depreciation Expense)	$/year	0	490024	490024	490024	490024	490024	490024	490024	490024	490024	490024
E (Earnings Before Taxes)	$/year	0	-15731728	5085997	6465344	6919614	7399999	7907913	8444844	9012362	9612114	10245837
TAX (Taxes)	$/year	0	0	1373219	1745643	1868296	1998000	2135136	2280108	2433338	2595271	2766376
NE (Net Earnings)	$/year	0	-15731728	3712778	4719701	5051318	5401999	5772776	6164736	6579024	7016843	7479461
TED (Total Earnings)	$/year	0	-15241704	4202801	5209724	5541342	5892023	6262800	6654760	7069048	7506867	7969484
TEX (Total Expenses (Excludes Taxes and Depreciation))	$/year	0	15241704	5822134	6010033	6204032	6404331	6611135	6824657	7045116	7272739	7507760
CF (CashFlow for Project)	$/year	0	-15241704	4202801	5209724	5541342	5892023	6262800	6654760	7069048	7506867	7969484
FVI (Future Value of Cumulative Cash Inflows)	$/year	0	0	11398154	25503369	41667376	60128467	81150385	105024948	132074944	162657315	197166666
PVI (Present Value of Cumulative Cash Inflows)	$/year	0	0	9419962	19161059	28459379	37335047	45807277	53894405	61613936	68982580	76016285
PVOS (Present Value of Cumulative Cash Outflows, Sales)	$/year	0	0	0	0	0	0	0	0	0	0	0
PVOP (Present Value of Cumulative Cash Outfows, Products)	$/year	0	13856095	19802667	25629621	31143130	36360316	41297358	45969542	50391310	54576310	58537434
PVO (Present Value of Cumulative Cash Outfows)		0	13856095	19802667	25629621	31143130	36360316	41297358	45969542	50391310	54576310	58537434
PV (Present Value of Cash Flows)	$/year	0	-13856095	3473389	3914143	3784811	3658483	3535187	3414944	3297763	3183644	3072581
NPV (Net Present Value)	$/year	0	-13856095	-10382705	-6468562	-2683751	974732	4509919	7924863	11222626	14406270	17478851
IRR (Internal Rate of Return)	%	37.16										
MIRR (Modified Internal Rate of Return)	%	12.2										
NRR (Net Return Rate)	%	48.98		-52.43	-25.24	-8.62	2.68	10.92	17.24	22.27	26.40	29.86
PO (Payout Period)	Year	4.73					4.73					
ARR (Accounting Rate of Return)	%	97.21										
PI (Profitability Index)		1.48	0	0.476	0.748	0.914	1.027	1.109	1.172	1.223	1.264	1.299

CASHFLOW.ICS (Cashflow)	Year	11	12	13	14	15	16	17	18	19	20
Sales											
S (Total Sales)	$/year	19155801	20113591	21119270	22175234	23283996	24448195	25670605	26954135	28301842	29716934
Expenses											
CAP Capital Costs)	$/year										
Unescalated Cumulative Capital Cost	$/year	12250590	12250590	12250590	12250590	12250590	12250590	12250590	12250590	12250590	12250590
Capital Cost	$/year										
Cumulative Capital Cost	$/year	12863120	12863120	12863120	12863120	12863120	12863120	12863120	12863120	12863120	12863120
Working Capital	$/year										
OP Operating Costs)	$/year	7750421	8000972	8259670	8526783	8802586	9087363	9381408	9685023	9998524	10322232
Raw Materials	$/year	3340411	3457325	3578331	3703573	3833198	3967360	4106218	4249935	4398683	4552637

Operating Labor Cost	$/year	1273495	1311700	1351051	1391583	1433330	1476330	1520620	1566238	1613226	1661622
Maintenance Cost	$/year	174413	179646	185035	190586	196304	202193	208259	214507	220942	227570
Utilities	$/year	1345668	1386038	1427619	1470448	1514561	1559998	1606798	1655002	1704652	1755792
Operating Charges	$/year	318374	327925	337763	347896	358333	369082	380155	391560	403306	415406
Plant Overhead	$/year	723954	745673	768043	791084	814817	839261	864439	890372	917084	944596
Subtotal Operating Costs	$/year	7176315	7408307	7647843	7895170	8150543	8414225	8686489	8967614	9257892	9557623
G and A Costs	$/year	574105	592665	611827	631614	652043	673138	694919	717409	740631	764610
R (Revenue)	$/year	11405380	12112619	12859600	13648451	14481409	15360832	16289198	17269112	18303318	19394702
DEP (Depreciation Expense)	$/year	490024	490024	490024	490024	490024	490024	490024	490024	490024	490024
E (Earnings Before Taxes)	$/year	10915357	11622596	12369577	13158427	13991386	14870809	15799174	16779088	17813295	18904678
TAX (Taxes)	$/year	2947146	3138101	3339786	3552775	3777674	4015118	4265777	4530354	4809590	5104263
NE (Net Earnings)	$/year	7968210	8484495	9029791	9605652	10213712	10855690	11533397	12248735	13003705	13800415
TED (Total Earnings)	$/year	8458234	8974518	9519815	10095675	10703735	11345714	12023421	12738758	13493729	14290439
TEX (Total Expenses (Excludes Taxes and Depreciation))	$/year	7750421	8000972	8259670	8526783	8802586	9087363	9381408	9685023	9998524	10322232
CF (CashFlow for Project)	$/year	8458234	8974518	9519815	10095675	10703735	11345714	12023421	12738758	13493729	17353086
FVI (Future Value of Cumulative Cash Inflows)	$/year	236039133	279756638	328851572	383911963	445587155	514594066	591724077	677850620	773937525	881048211
PVI (Present Value of Cumulative Cash Inflows)	$/year	82730276	89139086	95256587	101096019	106670022	111990662	117069454	121917392	126544970	130962203
PVOS (Present Value of Cumulative Cash Outflows, Sales)	$/year	0	0	0	0	0	0	0	0	0	0
PVOP (Present Value of Cumulative Cash Outfows, Products)	$/year	62286866	65836117	69196067	72376992	75388606	78240088	80940111	83496871	85918116	88211166
PVO (Present Value of Cumulative Cash Outfows)		62286866	65836117	69196067	72376992	75388606	78240088	80940111	83496871	85918116	88211166
PV (Present Value of Cash Flows)	$/year	2964559	2859558	2757551	2658507	2562389	2469158	2378770	2291178	2206332	2124183
NPV (Net Present Value)	$/year	20443411	23302969	26060520	28719027	31281416	33750574	36129344	38420521	40626854	43206279
IRR (Internal Rate of Return)	%										37.16
MIRR (Modified Internal Rate of Return)	%										12.2
NRR (Net Return Rate)	%	32.82	35.40	37.66	39.68	41.49	43.14	44.64	46.01	47.29	48.98
PO (Payout Period)	Year										
ARR (Accounting Rate of Return)	%										97.21
PI (Profitability Index)		1.328	1.354	1.377	1.397	1.415	1.431	1.446	1.460	1.473	1.485

R (revenue) =Sales-TEX
DEP (Depreciation Expense)
E (Earnings before Taxes) =R-DEP
NE (Net Earnings) =E-TAX
TEX (Total Expenses (Excludes Taxes and Depreciation)) =CAP+OP
CF (Cash Flow for Project) =TED= Sales –TEX -TAX
DCF (Discounted Cash Flow) =CF/ $(1+IRR)^n$
FVI (Future Value of Cumulative Cash Inflows) = PVI*$(1+ROR)^n$
PVI (Present Value of Cumulative Cash Inflows) = $\sum_i^n Sales/(1+ROR)^n$
PVOP (Present Value of Cumulative Cash Outflows, Products) = $\sum_i^n (TEX+TAX)/(1+ROR)^n$
PV (Present Value of Cash Flows) = CF/ $(1+ROR)^n$
NPV (Net Present Value) = $\sum_i^n PV_i$
IRR (Internal Rate of Return): $NPV(r) = \sum_{j=0}^{N=10} \frac{CF_j}{(1+r)^j} = 0$
NRR (Net Return Rate) = NPV/PVO (at 10th year)
PO (Payout Period): $PO =$ Years with negative $NPV + |NPV|/PV$
PI (Profitability Index) = PVI/PVO (at 10th year

Table E.3 Capital depreciation based on different methods (continued)

DEPRECIATION CALCULATIONS	Year	0	1	2	3	4	5	6	7	8	9	10
Depreciation Calculations using the Straight-Line Method												
Depreciation Factor												
Depreciation Expense	$/year		490,024	490,024	490,024	490,024	490,024	490,024	490,024	490,024	490,024	490,024
			9,800,472									
Depreciation Calculations using the Sum of the Digits Method												
Sum of the Digits			210									
Depreciation Expense	$/year		933,378	886,709	840,040	793,372	746,703	700,034	653,365	606,696	560,027	513,358
			9,800,472									
Depreciation Calculations using the Double Declining Balance Method												
Depreciation Factor			0.1									
Straight Line Depreciation	$/year		612,530	580,291	551,277	525,334	502,351	482,257	465,033	450,725	439,456	431,466
	$/year		1,225,059	1,102,553	992,298	893,068	803,761	723,385	651,047	585,942	527,348	474,613
	$/year	12,250,590	11,025,531	9,922,978	8,930,680	8,037,612	7,233,851	6,510,466	5,859,419	5,273,477	4,746,130	4,271,517
	$/year		1,225,059	1,102,553	992,298	893,068	803,761	723,385	651,047	585,942	527,348	474,613
			12,250,590									
Depreciation Calculations using the Accelerated Cost Recovery System												
Total Percent Depreciated				0.05	0.15	0.23	0.31	0.38	0.44	0.5	0.55	0.59
Depreciation Factor	0.1		0.05	0.1	0.09	0.08	0.07	0.06	0.06	0.05	0.05	0.04
Straight Line Depreciation	$/year		612,530	596,824	566,176	538,676	514,191	492,628	473,942	458,144	445,316	435,635
	$/year		612,530	1,163,806	1,047,425	942,683	848,415	763,573	687,216	618,494	556,645	500,980
	$/year	12,250,590	11,638,061	10,474,255	9,426,829	8,484,146	7,635,732	6,872,159	6,184,943	5,566,448	5,009,804	4,508,823
	$/year		612,530	1,163,806	1,047,425	942,683	848,415	763,573	687,216	618,494	556,645	500,980
			12,037,015									

DEPRECIATION CALCULATIONS	Year	11	12	13	14	15	16	17	18	19	20
Depreciation Calculations using the Straight-Line Method											
Depreciation Factor											
	$/year	490,024	490,024	490,024	490,024	490,024	490,024	490,024	490,024	490,024	490,024
Depreciation Calculations using the Sum of the Digits Method											
Sum of the Digits											
	$/year	466,689	420,020	373,351	326,682	280,014	233,345	186,676	140,007	93,338	46,669
Depreciation Calculations using the Double Declining Balance Method											
Depreciation Factor											
	$/year	427,152	427,152	427,152	427,152	427,152	427,152	427,152	427,152	427,152	427,152
	$/year	427,152	384,437	345,993	311,394	280,254	252,229	227,006	204,305	183,875	165,487
	$/year	3,844,365	3,459,929	3,113,936	2,802,542	2,522,288	2,270,059	2,043,053	1,838,748	1,654,873	1,489,386
	$/year	427,152	427,152	427,152	427,152	427,152	427,152	427,152	427,152	427,152	427,152
Depreciation Calculations using the Accelerated Cost Recovery System											
Total Percent Depreciated		0.63	0.67	0.7	0.73	0.76	0.76	0.76	0.76	0.76	0.76
Depreciation Factor	0.1	0.04	0.03	0.03	0.03						
	$/year	429,412	427,152	427,152	427,152	427,152	427,152	427,152	427,152	427,152	427,152
	$/year	450,882	405,794	365,215	328,693	0	0	0	0	0	0
	$/year	4,057,941	3,652,147	3,286,932	2,958,239	2,958,239	2,958,239	2,958,239	2,958,239	2,958,239	2,958,239
	$/year	450,882	427,152	427,152	427,152	427,152	427,152	427,152	427,152	427,152	427,152

Appendix F Life cycle inventory data and emission factors

This file contains the inventory data of BC wood pellet supply chains to different destinations, including Drax power plant in UK, Kochi power plant in Japan, Atikokan power plant in Ontario, and Genesee power plant in Alberta. Stages include biomass harvesting, sawmilling, storage, port operation and transportation. Production and end-use are discussed in Chapter 4 and Chapter 5, respectively.

F.1 Harvesting

Biomass resources are initially harvested in the forest site near Prince George. The harvesting energy consumptions are calculated as Eq. (F.1).

$$E_{ene_{H,p}} = \left[E_{ene_{H,fuel}} \cdot \left(\frac{1}{\rho_{wood,w}} \right) \cdot \underbrace{\dot{m}_{WC.p} \cdot \left(\frac{1}{\vartheta_{sawmill,wc}} \right)}_{\substack{\text{t logs to} \\ \text{produce 1 tonne pellet}}} \right] \cdot \vartheta_{harvest,wc} / HHV_{pellet} \quad \text{(F.1)}$$

Where $E_{ene_{H,p}}$ is the energy consumption to produce per GJ of wood pellet for different pathways in GJ/GJ, p indicate pathways 0-4, $E_{ene_{H,fuel}}$ is liter of diesel consumed to harvest per m^3 of logs (Liter diesel/m^3 logs), and $\rho_{wood,w}$ is the density of harvested green logs equal to 0.84 t/m^3 [201]. $\dot{m}_{WC.p}$ is the t of wood chips required to produce one tonne of wood pellet, which is different for different pathways as presented in Table F.1. $\vartheta_{sawmill,wc}$ is the allocation of the wood chips in the sawmill, considered as t of logs needed to generate per t of wood chips residue In BC, sawmill operations on harvested logs would on average yield 8% bark, 1% hog fuel, 7% sawdust, 27% chips, and 57% lumber on a mass basis [202]. $\vartheta_{harvest,wc}$ is the allocation of wood chips in the harvesting process, considered as t of logs in

the harvesting process that yield one t of wood chips. HHV of the conventional and the torrefied wood pellet are calculated as 17 GJ/t and 21 GJ/t, respectively. The allocations are mass based in this study. Thus, $\vartheta_{\mathrm{harvest,wc}} = \vartheta_{\mathrm{sawmill,wc}}$, and Eq. (F.1) is reduced to Eq. (F.2).

$$\mathrm{E}_{\mathrm{ene}_{\mathrm{H,p}}} = \mathrm{E}_{\mathrm{ene}_{\mathrm{H,fuel}}} \cdot \left(\frac{1}{\rho_{\mathrm{wood,w}}}\right) \cdot \dot{m}_{\mathrm{WC.p}} \,/\mathrm{HHV}_{\mathrm{pellet}} \qquad \text{(F.2)}$$

Values involved in Eq. (F.2) are summarized in Table F.1.

Sambo et al. [126] carried out a travel survey of thirty-seven interviews to quantify fuel usage rates associated harvesting per m^3 of wood log in western Canada (covering North and Central Alberta forest region, Saskatchewan forest region, Foothills forest region, Nelson forest region, Kamloops forest region, Prince Rupert forest region, Prince George forest region, and Cariboo forest region). Seven phases are included in their traveled survey, including planning & layout, road construction, right-of-way logging, logging, hauling, camp, and silviculture. Only tasks involving fossil fuel consumptions were considered. A weighted average value of fuel needed to harvest one cubic meter of wood was determined to be 7.1 L of diesel fuel per m^3 of wood harvested, and within which hauling accounts for 51% of the energy consumption [126]. In the current study, we group the hauling process to the truck transportation (T-T-1) in order to perform sensitivity analysis. Then the energy consumption of the rest phases of harvesting, including planning & layout, road construction, right-of-way logging, logging, camp and silviculture, is considered to be 3.48 L of diesel fuel per m^3 of wood harvested.

Table F.1 Parameters to calculate harvesting energy for different pathways

	$E_{H,fuel}$ [1] ($L/m3$)	$\rho_{wood,w}$ [2] (t/m^3)	$\dot{m}_{WC.p}$ [3] (t wood chips/t wood pellet)	HHV_{pellet} [4] (GJ/t)
Path 0	3.48	0.84	1.56	17
Path 1	3.48	0.84	1.716	21
Path 2	3.48	0.84	1.716	21
Path 3	3.48	0.84	1.716	21
Path 4	3.48	0.84	1.865	21

1: data source Sambo et al. (2002) [126] (Considered as 49% of the total harvesting energy consumption, which is 7.1L diesel/ m^3 harvested wood. The other 51% is the hauling of the harvested wood. The rest phases of harvesting include planning & layout, road construction, right-of-way logging, logging, camp and silviculture. Only the tasks related to fossil fuel consumption are included in the analysis.
2: data source [201]
3: value based on mass balances refer to Table 4.5
4: value calculated based on Mott and Spooner's correlation

F.2 Sawmill

Energy use of the sawmill operation process is mainly electricity, its consumption is 0.186 GJ electricity/t wood pellet produced adopted from [127]. Costs of sawmill operations are grouped to the raw material costs in the pellet production processes.

F.3 Port Operation

It is assumed the pellets are exported via Vancouver port in this study. When the wood pellets arrive the Vancouver port, they are unloaded, stored, waiting for the available shipping schedule. Usually, it takes 34 days to ship to UK and 17 days to Japan. When a shipping vessel arrives at import ports, it is moored dockside. A gantry crane equipped with a grapple unloads pellets from each ship hold. Pellets are dropped into a long storage building with a retractable roof [203]. The bulk wood pellets are eventually loaded into large hoppers that are fixed to high capacity traveling cranes to feed railway wagons, trucks or conveyor belts [204], and then transported to the power plant.

In the current study, we adopted the general air emissions data of bulk handling associated with activities at the Port of Vancouver [125]. The report was prepared in

collaboration with government and industry stakeholders every five years, estimating air emissions and energy usage associated with fuel and electricity from marine shipping, use of rail, on-road and non-road equipment, and administrative activities associated with Port of Vancouver. Emission sources and energy consumptions associated with up/downstream with production or consumption of cargoes, heavy industrial processes on or adjacent to port lands, e.g. chemical or cement manufacturing, are not covered.

In 2015, it was reported that about 9.62 million t of the bulk is handled by Port of Vancouver [205]. Thus, the GHGs and the primary energy consumptions of each tonne of the bulk cargo is calculated by dividing the total emissions with the total bulk weight, being 5.246 gCO_2eq/t pellet and 0.073 GJ/t pellet. Detail categories are summarized in Table F.2. The same value is applied to the port operations at UK (Selby port) and Japan (Kochi port).

Table F.2 2015 Vancouver port Bulk sector GHG emissions [125]

Source	GHG emissions ($mgCO_2eq$ /t bulk cargo)	Energy consumption GJ/t bulk cargo
Marine	3483	0.046
Rail	1468	0.019
On-road	161	0.002
Non-road	94	0.004
Administrative	39	0.001
Total	5246	0.073

Marine: Emissions source group that includes ocean-going vessels, harbor tugs, and dredging vessels.
Rail: Emission source group that includes locomotives that move trains as part of port operations.
On-road: Emission source group that includes container trucks, heavy duty trucks, terminal support vehicles, and passenger transportation.
Non-road: Emission source group of equipment not intended for transportation on public roads, includes cranes, container stackers, loaders, terminal tractors, and forklifts.
Administrative: Emissions source group associated with heating and electricity for buildings on port lands and lighting terminals.

F.4 Storage

Storage is a major process over the wood pellet life cycle: after production at the pellet plant, the wood pellets are stored in a silo to wait for the market demand and

transportation schedule; similar situations happen at the export port and import port. The storage periods in silos and in ships may last several months. In a confined space, the wood pellet may rapidly release high levels of CO, CO_2, CH_4 and create an oxygen-deficient atmosphere. Those spontaneous gas emissions are named as off-gassing that may cause injuries and fatality [128]. Several accidents have occurred because of exposure to off-gassing combined with poor ventilation [129]. Off-gassing has also been associated with self-healing and spontaneous ignition of wood pellets [130]. Several experimental works have been carried out at UBC by the Biomass and Bioenergy Research Group (BBRG) to evaluate different biomass materials' off-gassing behavior under different storage periods, temperature, head-space, and relative humidity etc. [129] , [130], [132], [133], [134]. Storage temperature has been found to have the most significant impact on the off-gas emissions, followed by the effect of relative humidity and head-space volume. Kuang et al. (2009) [128] and Guo et al. (2013) [130] indicated that the off-gas emissions approximately follow a first order reaction kinetics and they provided the kinetic correlations under different conditions (temperature, head-space, storage time etc.). Off-gassing studies of conventional wood chips and torrefied wood chips revealed that CO_2 off-gassing from torrefied wood chips was about 15% to 20% lower than that of untreated wood chips when stored at 20°C to 40°C. Summary and comparison of those works are presented in Table F.3. In the current study, we assumed the off-gas emission factors of 8600 gCO_2eq/t pellet and 7000 gCO_2eq/MM pellet for the conventional and the torrefied wood pellets, respectively.

Table F.3 literature review of biomass off-gassing at storage

Reference	Biomass	Storage time (Days)	T (°C)	CO_2 (mg/kg pellets)	CO (mg/kg pellets)	CH4 (mg/kg pellets)	CO_2eq (mg/kg pellets)
[128]	Switchgrass	56	20	1878	367	3	1953
			40	43104	8914	17	43529
	Fines of BC CWP	56	20	5434	7662	169	9659
			40	38327	15086	1665	79952
	BC CWP	56	20	5128	5510	138	8578
			40	36210	14334	1029	61935
	EU CWP	42	20	2156	335	7	2331
			40	30547	13973	310	38297
	EU TWC	27	20	12446	259	3	12521
			40	25084	4833	7	25259
[130]	CWP	70	20	27.3	16.7	0.8	47.3
[132]	Ground switchgrass	11	20	55.45	0.38		55.45
			40	318.72	2.68		318.72
	CWP	11	20	19.98	1.81		19.98
			40	123.5	6.96		123.5
	TWC	11	20	9.39	0.85		9.39
			40	118.68	4.85	0.0104	118.94
	CWP	11	20	3.86	1.43		3.86
			40	55.45	10.6	0.76	74.45
[129]	CWP	63	25	48.5	19.1	0.9	71
[134]	CWC	56	20	750	500	240	6750
	CWC		40	2500	650	70	4250
	TWC (260°C)		20	150	300	30	900
			40	600	350	150	4350
	TWC (290°C)		20	250	100	120	3250
			40	700	130	230	6450
	SWC (195°C)		20	9000	250	90	11250
			40	7000	300	280	14000
	SWC (215°C)		20	2500	280	280	9500
			40	4000	390	320	12000
This	CWP						8600

Reference	Biomass	Storage time (Days)	T (°C)	CO_2 (mg/kg pellets)	CO (mg/kg pellets)	CH4 (mg/kg pellets)	CO_2eq (mg/kg pellets)
work	TWP						6900

CH4=25*CO_2eq (100-year GWP)
CWC: conventional wood chips
TWC: torrefied wood chips
CWP: conventional wood pellet
TWP: torrefied wood pellet
SWC: steamed wood chips

F.5 Transportation

Transportation emission factors are summarized in Table F.4.

Table F.4 Transportation emission factors (Data source: GHGenius 4.3. 2018 BC)

Freight Emissions gCO_2eq/t_km	Marine General Cargo and Containers						Rail			Heavy Duty Truck		
	Panamax 80,000 DWT			Handymax 45,000 DWT								
General fuel-->	Fuel Oil	Marine diesel	Diesel mix	Fuel Oil	Marine diesel	Diesel mix	Rail	Diesel mix	Diesel mix	Petrol diesel	Diesel mix	Diesel mix
Fuel spec-->	0.002 % S	0.002% S	D95/T D5	0.002 % S	0.002% S	D95/T D5	0.002 % S	D95/T D5	D80/B20	0.0015 % S	D95/T D5	D80/B20
Feedstock-->	crude oil	Crude oil	oil, tallow	crude oil	Crude oil	oil, tallow	crude oil	oil, tallow	oil, Canola Oil	crude oil	oil, tallow	oil, Canola Oil
Active Energy Intensity (kJ/t_km)	93	93	93	124	124	124	220	220	220	1963	1963	1963
Total emission factor (gCO_2eq/t_km)	9.7	10.3	9.9	12.9	13.7	13.1	23.8	22.8	19.2	189.5	176.8	152

Total emission factor include: (a) vehicle operation, (b) vehicle material & Assembly, and (c) fuel upstream which including fuel dispensing, fuel distribution and storage, fuel production, feedstock transmission, feedstock recovery, feedstock upgrading, land-use changes, cultivation, fertilizer manufacture, gas leaks and flares, CO2 H2S removed from NG, emissions displaced categories.

Appendix G Transportation cost model

Transportation is divided into three major segments: heavy-duty truck (HDT) transportation (T-T), rail transportation (T-R), and ocean transportation (T-S). The transportation cost models are developed based on quoted price and regression: truck transportation costs are based on BC heavy duty truck rental price in 2018 [206]; rail transportation costs are adopted from CN rail "Carload Price Tool", 2018 [207]; and marine transportation costs are quoted from SEARATES [208]. The development of the transportation cost models goes through five steps as shown in Figure G.1.

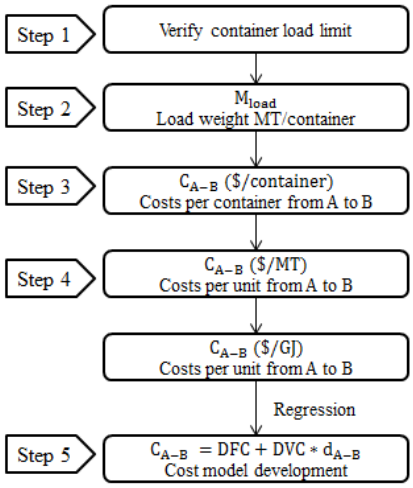

Figure G.1 Wood pellet transportation costs model development stages

(1) Step 1 Verify container load limit

In practice, wood pellets sold to power stations are transported in bulk. The transportation costs are charged in $/container (e.g. HDT, hopper, and ship vessel etc.). To normalize the costs to $/t or $/GJ, the load of the bulk wood pellet needs to be known. The load is considered to be the same as the container's limit to save transportation costs. Thus,

the first step is to identify the load limit of wood pellets by using different containers. Eq. (G.1) and (G.2) are used to verify the limitation of the container load of the pellet, either weight limited or volume limited.

$$M_{t,max} = V_{t,lim} \cdot \rho_{pellet} \quad (G.1)$$

$$V_{t,max} = M_{t,lim}/\rho_{pellet} \quad (G.2)$$

Where $V_{t,lim}$ is the volume limit of the vessel, t indicates the ways of transportation e.g. heavy duty truck, railway and marine transportations. ρ_{pellet} is the bulk density of the pellet, $M_{t,max}$ is the maximum weight load of the wood pellet according to volume limitation; $M_{t,lim}$ is the weight limit of the vessel, and $V_{t,max}$ is the maximum volume load of the container according to weight limitation.

(2) Step 2 Determine container load $M_{t,load}$

The container maximum load is either limited by volume or weight limitations.

$$\text{If } M_{t,max} > M_{t,lim}, \text{ then } M_{t,load} = M_{t,lim} \quad (G.3)$$

$$\text{If } V_{t,max} > V_{t,lim}, \text{ then } M_{t,load} = M_{t,max} \quad (G.4)$$

Where $M_{t,load}$ is the weight load of the container in t/container.

(3) Step 3 Container costs

The transportation cost of per container of wood pellets is cited from reliable website for different transportation mode: i.e. truck transportation from car rental company, railway transportation from CN rail, “Carload Price Tool”, and marine transportation from SEARATES.COM.

(4) Step 4 Transportation costs $C_t\left(\frac{\$}{t}\right)$ and $C_t\left(\frac{\$}{GJ}\right)$

When the container load and the cost of per container are known, the transportation cost per unit of wood pellets is calculated according to Eq.s (G.5) and (G.6).

$$C_t\left(\frac{\$}{t}\right) = C_{t,A-B}/M_{t,load} \quad (G.5)$$

$$C_t\left(\frac{\$}{GJ}\right) = C_{t,A-B}/(M_{t,load} * HHV_{pellet}) \quad (G.6)$$

Where $C_{t,A-B}$ ($/container) is the cost per container load of transportation way t from location A to B, with t indicating truck, railway, or marine transportation. $M_{t,load}$ is the weight load of the container (t/container). HHV_{pellet} is the high heating value of the wood pellet (GJ/t).

(5) Step 5 transportation costs model development

The transportation costs models are developed by regression of relationship of the costs in $/t and $/GJ to the transportation distance.

G.1 Truck transportation

Truck transportation cost is usually divided into distance fixed cost (DFC) and distance variable cost (DVC). Table G.1 shows the reported truck transportation cost correlations based on Eq. (G.7).

$$C_{truck} = DFC + DVC \cdot d_{distance} \quad (G.7)$$

Table G.1 Literature review of truck transportation rate of biomass

Reference	Item transported	DFC ($/t)	DVC ($/t-km)	Region/Country	Year
[209]	straw/stover	4.39	0.12	Alberta	2004
[209]	woodchips	3.01	0.07	US	
[210]		15.458	0.08		
[211]	corn stover	5.7	0.1367	Alberta	2005

Reference	Item transported	DFC ($/t)	DVC ($/t-km)	Region/Country	Year
[212]	woodchips	3.04	0.037	European and Latin American	2005
[213]	woodchips	4.32	0.134	US	2015
[213]	Pellet	3.05	0.088	US	2015

Verification of the B-train double trailer (Step 1- 2) is presented in Table G.3. At present work, we adopted the method based on Eq. (G.8) [214] to quantify the truck transportation costs per load (Step 3). It should be noticed that the truck rental is usually counted as a round trip.

$$C_{truck,A-B} = H * (t_t + t_w) \quad (G.8)$$

$$t_t = d_{A-B} * 2/v_{truck} \quad (G.9)$$

Where $C_{truck,A-B}$ is the truck transportation cost, H is the transportation hourly rate including truck rental cost and labor cost, t_t is the transportation time, which is calculated by Eq. (G.9). It should be notices that round trip is accounted for the truck rental, thus transportation cost is multiplied by 2. v_{truck} is the speed of the truck. t_w is the waiting time for loading and unloading. Assumptions of those parameters are presented in Table G.4.

Truck transportation of per unit of wood pellet is calculated by to Eq. (G.5) and Eq. (G.6) (Step 4-5) Based on the assumptions of transportation and calculated transportation costs, we carried out regressions between the transportation distance and the transportation costs of CWP and the TWP according to Table G.4. The transportation costs are found to be linearly to the transportation distances. Thus, DFC and DVC can be obtained according to the linear relations as summarized in Table G.2.

Table G.2 BC truck transportation costs based on regression

		DFC	DVC	R2
$/t	CWP	3.9	0.0325	1
	TWP	3.9	0.0325	1
$/GJ	CWP	0.2294	0.0019	1
	TWP	0.1857	0.0015	1

Table G.3 Canadian truck load of CWP and TWP

				CWP					TWP				
Truck type	Maximum weight (t)	$M_{truck,lim}$ (t)	$V_{truck,lim}$ (m^3)	ρ_{pellet} (t/m^3)	$M_{truck,max}$ (t)	$V_{truck,max}$ (m^3)	Limit	$M_{truckload}$ car (t)	ρ_{pellet} (t/m^3)	$M_{truck,max}$ (t)	$V_{truck,max}$ (m^3)	Limit	$M_{truckload}$ (t)
B-train double trailer	62.5[a]	40[a]	160	0.65	104.0	96.2	weight	40	0.7	112.0	89.3	weight	40

[a]https://www.todaystrucking.com/why-mackinnons-b-trains-are-heavyweight-champs/

Table G.4 Truck transportation assumptions and costs of CWP and TWP

							CWP		TWP	
Waiting hour (hr)	Distance (hr)	Speed (km/hr)	Total hour (hr)	Rental rate (CAD/hr)	Costs per load	per load t/load	$/t	$/GJ	$/t	$/GJ
2	10	60	2.2	50	169	40	4.23	0.25	4.23	0.20
2	20	60	2.3	50	182	40	4.55	0.27	4.55	0.22
2	30	60	2.5	50	195	40	4.88	0.29	4.88	0.23
2	40	60	2.7	50	208	40	5.20	0.31	5.20	0.25
2	50	60	2.8	50	221	40	5.53	0.33	5.53	0.26
2	60	60	3.0	50	234	40	5.85	0.34	5.85	0.28
2	70	60	3.2	50	247	40	6.18	0.36	6.18	0.29
2	80	60	3.3	50	260	40	6.50	0.38	6.50	0.31
2	90	60	3.5	50	273	40	6.83	0.40	6.83	0.33
2	100	60	3.7	50	286	40	7.15	0.42	7.15	0.34

G.2 Rail transportation

Similar to the truck transportation costs, rail transportation costs are usually divided into distance fixed cost (DFC) and distance variable cost (DVC) as shown by Eq. (G.10). Table G.5 lists the rail transportation costs reported in literature.

$$C_{rail} = DFC + DVC * d_{A-B} \quad (G.10)$$

Table G.5 Literature review of the rail transportation costs of biomass

Reference	Item transported	DFC ($/t)	DVC ($/t-km)	Region/Country	Year
[209]	straw/stover	14.15	0.023	Alberta	2004
[209]	woodchips	5.48	0.017	Alberta	
[215]	wood pellet	17.1	0.0277	US	2010
[213]	woodchips	44.68	0.046	US	
[213]	wood pellet	17.91	0.017	US	

The verification of the railway containers (step 3-4) is presented in Table G.6. The costs of delivering per rail car of cargo from A to B by using different rail cars, as well as the costs per unit that calculated according to Eq. (G.5) and Eq. (G.6) are shown in Table G.7 (Data source: CN rail, "Carload Price Tool", 2018. (Online) (Accessed: May 25th 2018).

Table G.6 Rail car description and load capacity of CWP and TWP

				CWP					TWP				
Car description	Car series	$M_{rail,lim}$ (t)	$V_{rail,lim}$ (m^3)	ρ_{pellet} (t/m^3)	$M_{rail,max}$ (t)	$V_{rail,max}$ (m^3)	Limit	$M_{railload}$ (t)	ρ_{pellet} (t/m^3)	$M_{rail,max}$ (t)	V_{max} (m^3)	limit	$M_{railload}$ (t)
Wood chip Gondola	CN 873600-873673	88	170	0.65	110.5	135.4	weight	88.0	0.7	119	125.7	weight	88
Open hopper	CC 40000-40219	92	113	0.65	73.5	141.5	volume	73.5	0.7	79.1	131.4	volume	79.1
Covered hopper	CC 475036-488706	91-93	135	0.65	87.8	140	volume	87.8	0.7	94.5	130	weight	94.5

$M_{rail,lim}$: weight load limit of the rail car
$V_{rail,lim}$: volume load limit of the rail car
$M_{rail,max}$: maximum weight according to volume capacity
$V_{rail,max}$: maximum volume according to weight capacity
$M_{railload}$: maximum weight of CWP per rail car

Table G.7 Rail transportation of wood pellet from Prince George to different destinations by using different rail cars (CAD=0.78USD)

Freight	Origin	Destination		Distance (km)[a]	$C_{rail,A-B}$ (CAD/railcar)[a]	CWP C_{rail} ($/t)	TWP C_{rail} ($/t)	CWP C_{rail} ($/GJ)	TWP C_{rail} ($/GJ)
Open hopper [a]	Prince George, BC	Region1	Prince Rupert, BC	747	3357	35.6	33.1	2.10	1.58
(CN code 2991152)			Vancouver, BC	766	3427	36.4	33.8	2.14	1.61
		Region 2	Edmonton, AB	781	5566	59.1	54.9	3.47	2.61
			Calgary, AB	1143	7652	81.2	75.5	4.78	3.59
			Saskatoon, SK	1298	8533	90.6	84.1	5.33	4.01
			Regina, SK	1752	11146	118.3	109.9	6.96	5.23
			Winnipeg, MB	2056	12886	136.7	127.1	8.04	6.05
		Region3	Atikokan, ON	2531	7808	82.9	77.0	4.87	3.67
			Hearst, ON	3214	9769	103.7	96.3	6.10	4.59

Freight	Origin	Destination		Distance (km)[a]	$C_{rail,A-B}$ (CAD/railcar)[a]	CWP C_{rail} ($/t)	TWP C_{rail} ($/t)	CWP C_{rail} ($/GJ)	TWP C_{rail} ($/GJ)
			Toronto, ON	3993	12005	127.4	118.4	7.49	5.64
		Region4	Montreal, QC	4498	26915	285.6	265.4	16.80	12.64
			Quebec, QC	4766	28449	301.9	280.5	17.76	13.36
			Moncton, NB	5416	32188	341.6	317.4	20.09	15.11
Covered hopper[a]	Prince George, BC	Region1	Prince Rupert, BC	747	3525	37.4	34.8	2.20	1.66
(CN code 2991152)			Vancouver, BC	766	3599	38.2	35.5	2.25	1.69
		Region2	Edmonton, AB	781	5844	62.0	57.6	3.65	2.74
			Calgary, AB	1143	8035	85.3	79.2	5.02	3.77
			Saskatoon, SK	1298	8960	95.1	88.4	5.59	4.21
			Regina, SK	1752	11704	124.2	115.4	7.31	5.50
			Winnipeg, MB	2056	13531	143.6	133.4	8.45	6.35
		Region3	Atikokan, ON	2531	8197	87.0	80.8	5.12	3.85
			Hearst, ON	3214	10257	108.8	101.1	6.40	4.82
			Toronto, ON	3993	12605	133.8	124.3	7.87	5.92
		Region4	Montreal, QC	4498	28260	299.9	278.7	17.64	13.27
			Quebec, QC	4766	29871	317.0	294.6	18.65	14.03
			Moncton, NB	5416	33797	358.7	333.3	21.10	15.87

[a]: Data source: CN rail, "Carload Price Tool", 2018. (Online) Available at: (Accessed: May 25th 2018)

Figure G.2 shows the rail transportation costs of per railcar of wood pellets from Prince George to different destinations using open hopper. Cost in each region follows a linear relationship to the transportation distance. DFC and DVC of the rail transportation are thus obtained through regression as summarized in Table G.8 in $/t and Table G.9 in $/GJ, respectively.

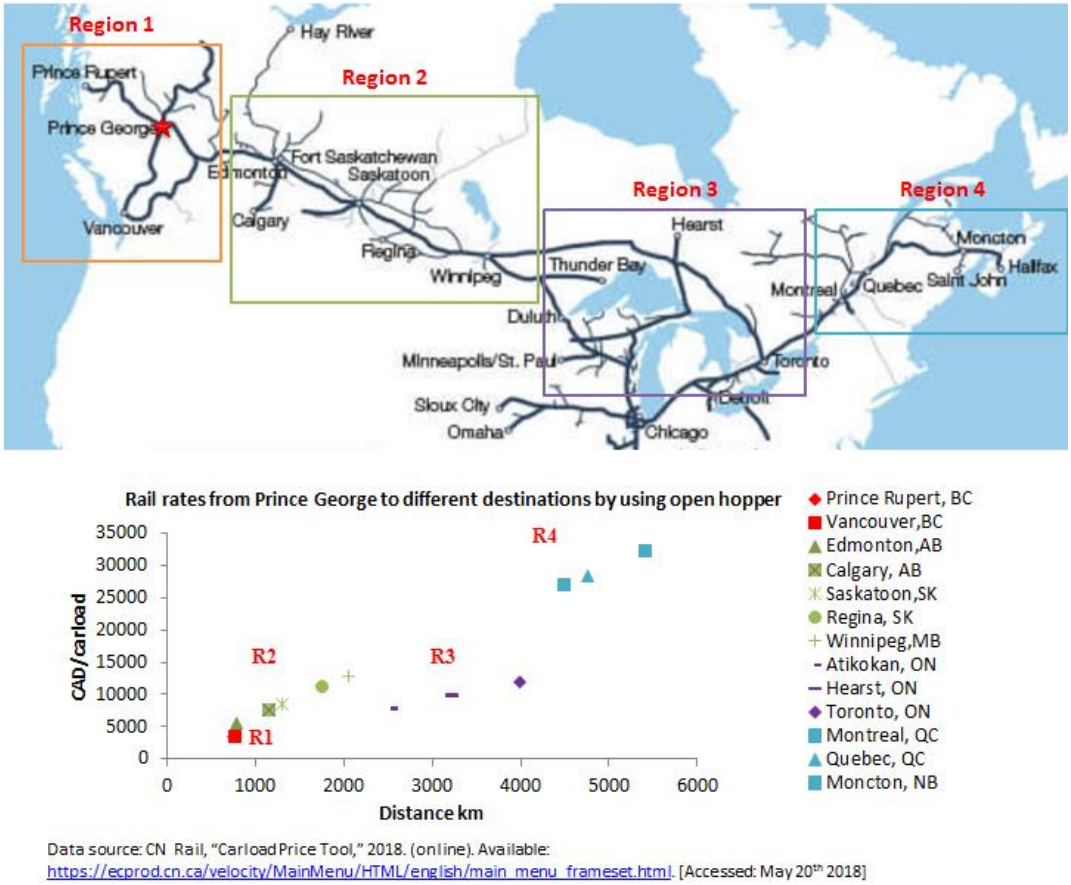

Data source: CN Rail, "Carload Price Tool," 2018. (online). Available: https://ecprod.cn.ca/velocity/MainMenu/HTML/english/main_menu_frameset.html. [Accessed: May 20th 2018]

Region 1: from Prince George railhead to the railway station in BC, Vancouver and Prince Rupert;
Region 2:from Prince George railway station to the railhead in provinces of Alberta, Sastatchewan, and Manitoba;
Region 3: from Prince George railway station to the railhead in the province of Ontario
Region 4: from Prince George railway station to the railhead in Quebec, and Newfoundland and Labrador areas

Figure G.2 Rail transportation costs from Prince George to different destinations using open hopper

Table G.8 Canadian railway transportation costs in $/t

		CWP			TWP		
		DFC($/t)	DVC ($/t_km)	R2	DFC($/t)	DVC ($/t_km)	R2
Open hopper	Region 1	6.90	0.0385	1	6.41	0.0357	1
	Region 2	11.52	0.0609	1	10.70	0.0566	1
	Region 3	5.76	0.0305	1	5.35	0.0283	1
	Region 4	11.30	0.061	1	10.50	0.0567	1
Covered hopper	Region 1	7.04	0.0406	1	6.54	0.0378	1
	Region 2	12.09	0.064	1	11.23	0.0595	1
	Region 3	6.01	0.032	1	5.58	0.0297	1
	Region 4	11.85	0.064	1	11.01	0.0595	1
Gondola	Region 1	7.74	0.0445	1	7.19	0.0413	1
	Region 2	13.24	0.0701	1	12.31	0.0651	1
	Region 3	6.60	0.035	1	6.13	0.0362	1
	Region 4	12.99	0.0701	1	12.07	0.0652	1

Table G.9 Canadian rail transportation costs in $/GJ

		CWP			TWP		
		DFC($/GJ)	DVC ($/GJ_km)	R2	DFC($/GJ)	DVC ($/GJ_km)	R2
Open hopper	Region 1	0.41	0.0024	1	0.31	0.0017	1
	Region 2	0.71	0.0038	1	0.51	0.0027	1
	Region 3	0.34	0.0018	1	0.25	0.0013	1
	Region 4	0.66	0.0036	1	0.50	0.0027	1
Covered hopper	Region 1	0.41	0.0024	1	0.31	0.0018	1
	Region 2	0.71	0.0038	1	0.53	0.0028	1
	Region 3	0.35	0.0019	1	0.27	0.0014	1
	Region 4	0.70	0.0038	1	0.52	0.0028	1
Gondola	Region 1	0.46	0.0026	1	0.34	0.002	1
	Region 2	0.78	0.0041	1	0.59	0.0031	1
	Region 3	0.39	0.0021	1	0.29	0.0016	1
	Region 4	0.76	0.0041	1	0.57	0.0031	1

G.3 Marine transportation

Table G.10 presents the literature reported DFC and DVC of the shipping transportation costs.

Table G.10 Literature review of shipping rate of biomass

	Item transported	DFC ($/t)	DVC ($/t-km)	Region/Country	Year
[209]	straw/stover	34.01	0.01	US	2004
[209]	woodchips	11.15	0.01		
[209]		17.353	0.016		
[213]	woodchips	33.34	0.025		
[213]	wood pellet	13.98	0.01		
[216]	white pellets	1.388	0.0014	Ontario	2017
[216]	Torrefied pellets	1.289	0.0013	Ontario	2017
[216]	Q' pellets	1.11	0.0011	Ontario	2017

Ship vessel load limit and the ship load (step 1-2) are verified as shown in Table G.11. Similar to rail transportation, to determine the sea transportation costs of per t or per GJ of wood pellet delivered from A to B, one needs to know the costs of per vessel $C_{sea,A-B}$, and the load weight of the ship vessel $M_{shipload}$. The costs of delivering per vessel of cargo from A to B by using different ships are shown in Table G.12 (SEARATES).

Table G.11 Ship vessel information and load capacity of CWP and TWP

			CWP					TWP				
Vessel type	$M_{ship,lim}$ (DWT)	$V_{ship,lim}$ (m^3)	ρ_{pellet} (t/m^3)	$M_{ship,max}$ (t)	$V_{ship,max}$ (m^3)	Limit	$M_{shipload}$ (t)	ρ_{pellet} (t/m^3)	M_{max} (t)	V_{max} (m^3)	Limit	$M_{shipload}$ (t)
Panamax	80,000	100,000	0.65	65000	123077	volume	65000	0.7	70000	114286	volume	70000
Handymax	45,000	56,250	0.65	36563	69231	volume	36563	0.7	39375	64286	volume	39375

$M_{ship,lim}$: weight limitation of the ship load
$V_{ship,lim}$: volume limitation of the ship load
$M_{ship,max}$: maximum weight of wood pellet per ship according to ship volume limitation
$V_{ship,max}$: maximum volume of wood pellet per ship according to ship weight limiation
ρ_{pellet}: bulk density of pellet
$M_{shipload}$: weight of ship load

Table G.12 Shipping transportation rate of wood pellet from Vancouver port to different destinations (data source: SEARATES)

Freight	Origin	Destination ports	Distance (km)	Ocean rate C_{sea} [a] ($/vessel)	CWP C_{sea} ($/t)	CWP C_{sea} ($/GJ)	TWP C_{sea} ($/t)	TWP C_{sea} ($/GJ)
Handymax	Vancouver port	Kobe, Japan	8272	1385602	38	2.23	35	1.65
45000DWT		Kisarazu, Japan	7751	1298323	36	2.09	32	1.55
		Samcheok, South Korea	8837	1396908	38	2.25	35	1.66
		Shanghai, China	9261	1551566	43	2.50	39	1.85
		Tianjing, China	9663	1618947	44	2.61	40	1.93
		Hongkong, China	10504	1759588	48	2.84	44	2.09
		Bekapai, Indonesia	12380	2074333	57	3.34	52	2.47
		Hull, UK	16597	2943952	81	4.74	74	3.50
		Rotterdam, NL	16480	2921793	80	4.71	73	3.48
		Figueira Da Foz, Portugal	15425	2735931	75	4.41	68	3.26
		Cannes, France	17021	3019020	83	4.87	75	3.59

Freight	Origin	Destination ports	Distance (km)	Ocean rate C_{sea} [a] ($/vessel)	CWP C_{sea} ($/t)	CWP C_{sea} ($/GJ)	TWP C_{sea} ($/t)	TWP C_{sea} ($/GJ)
Panamax	Vancouver port	Kobe, Japan	8271	1455908	22	1.32	21	0.99
80000DWT		Kisarazu, Japan	7751	1363813	21	1.23	19	0.93
		Samcheok, South Korea	8837	1467120	23	1.33	21	1.00
		Shanghai, China	9261	1492747	23	1.35	21	1.02
		Tianjing, China	9663	1700962	26	1.54	24	1.16
		Hongkong, China	10504	1692954	26	1.53	24	1.15
		Bekapai, Indonesia	12380	1995668	31	1.81	29	1.36
		Hull, UK	16597	3861602	59	3.49	55	2.63
		Rotterdam, NL	16480	3832772	59	3.47	55	2.61
		Figueira Da Foz, Portugal	15425	3589320	55	3.25	51	2.44
		Cannes, France	17021	3960104	61	3.58	57	2.69

According to the freight rates of delivering wood pellet from Vancouver port to the ports in Asia and Europe, as summarized in Table G.12, it is clear, as shown in Figure G.3, that the sea rates follow a linear relationship with distance, as expressed by Eq. (G.11). The coefficients of a and b are summarized in Table G.13 in $/t and Table G.14 in $/GJ.

$$C_{marine} = a * d_{A-B} + b \quad (G.11)$$

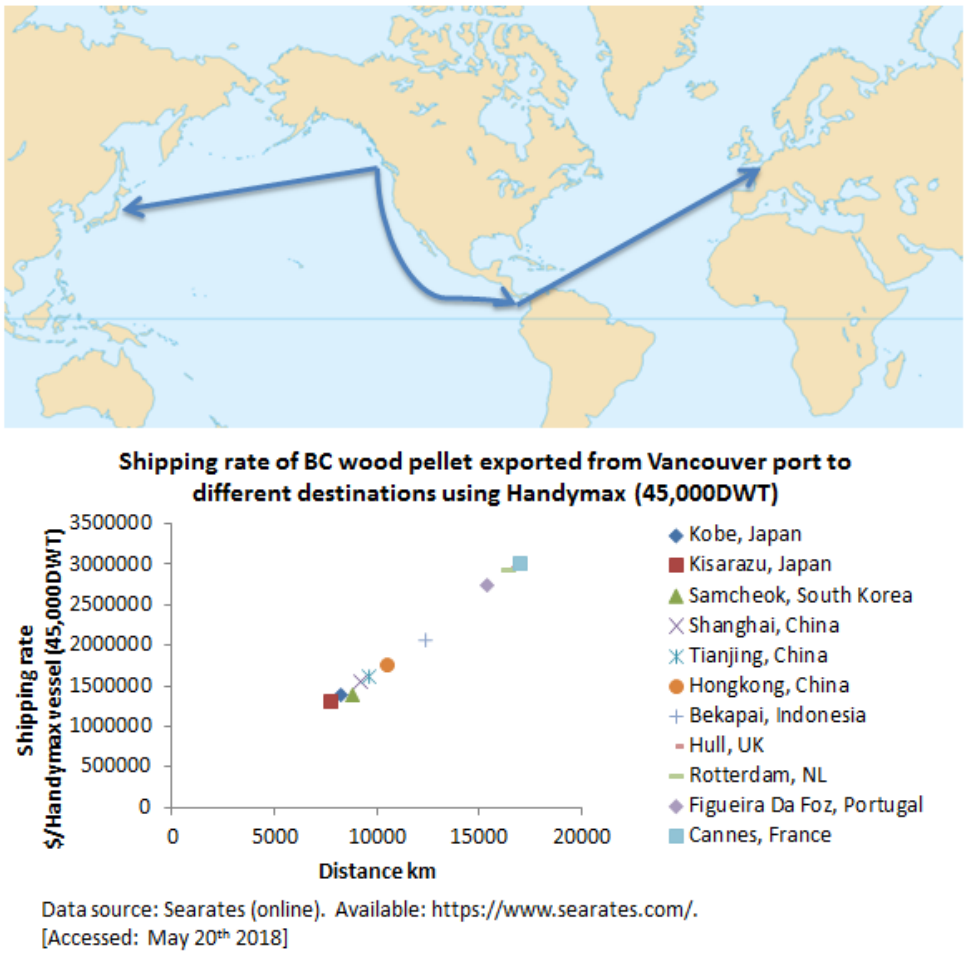

Figure G.3 Shipping transportation costs from Vancouver port to Asia and Europe (Data source: SEARATES, accessed on May 25th 2018)

Table G.13 Sea shipping rates parameters in $/t

		a ($/t_km)	b ($/t)	R2
CWP	Handymax	0.0052	-6.1145	0.9976
	Panamax	0.0047	-18.94	0.9632
TWP	Handymax	0.0048	-5.5795	0.9976
	Panamax	0.0043	-17.588	0.9632

Table G.14 Sea shipping rates parameters in $/GJ

		a ($/GJ_km)	b ($/GJ)	R2
CWP	Handymax	0.0003	-0.3597	0.9976
	Panamax	0.0003	-1.1141	0.9632
TWP	Handymax	0.0002	-0.2657	0.9976
	Panamax	0.0002	-0.8375	0.9632